Crude oil and oil brine seeps: sources, detection and environmental effects in soil and water, Kirkuk NE Iraq

Dissertation

Zur Erlangung des akademischen Grades eines Doktors der Naturwissenschaften (Dr. rer. nat.)

vorgelegt von

Layth Y. Sahib (M.Sc.)

geboren 1977 in Baghdad, Iraq

Tag der Einreichung: 3.12.2018
Tag der mündlichen Prüfung: 15.01.2019

Referent: Prof. Dr. Christoph Schüth
Korreferent: Prof. Dr. Andreas Henk
Prufer: Prof. Dr. Matthias Becker
Prufer: Prof. Dr. Matthias Hinderer

TECHNISCHE UNIVERSITÄT DARMSTADT

Source: Library of Congress

Sahib, Layth: Crude oil and oil brine seeps: sources, detection and environmental effects in soil and water, Kirkuk NE Iraq
Darmstadt, Technische Universität Darmstadt,
Year thesis published in TUprints 2019
Date of the viva voce 15.01.19

Statement of Originality

I hereby certify that all of the work described within this thesis is the original work of the author and this Ph.D. thesis

"Crude oil and oil brine seeps: the source, detection and environmental effects in soil and water, Kirkuk NE Iraq"

Any published (or unpublished) ideas and/or techniques from the work of others are fully acknowledged in accordance with the standard referencing practices.

Darmstadt on the 03 December 2018

Layth Y. Sahib

Abstract

Natural hydrocarbons have extensively contaminated both the hydro-lithospheres, damaging the environment and the health of the people living in the Kirkuk region of North-East Iraq, which is an area with a world´s significant crude oil reserves as well as various hydrocarbon seeps and brines. The study area is located in the Zagros fold-thrust belt, within the Low Folded Zone in the northeast of the Mesopotamia basin. Complex fracture systems and faults frequently cut across the Eocene, and middle Oligocene limestone reservoirs and the evaporates Miocene cap rock. High-density maps of the detected faults and lineaments within Fatha Formation have interpreted as potential seepage locations, even for seeps that are not exposed on the surface.

The present thesis aims to investigate hydrocarbon seeps, and oil brine seeps contamination impact on the surface, groundwater as well as the soil's physical and chemical properties. Therefore, various methods were used starting by identifying the origin of the seeps as a base to assess the source and ending by estimating the contamination level of hydrocarbons and related brines in water and soil directly or remotely. The essential concept of the present thesis is based on the known hydrocarbon seepage sits – which were recorded for hundreds of meters on the surface – and the sub-surface properties of the stratigraphy and hydrogeology conditions. In addition to the several reports and studies, the primary data source was based on the wide variation of the collected samples, i.e., crude oil and brine water samples from the selected oil reservoir to define the reservoir characterization and migration level.

Moreover, the reservoir oil types were used to compare them with surface crude oil seeps samples. The surface and groundwater from the selected location and different aquifers beside soil and rock samples explained the aquifer's recharge and led to the appropriate speculation of the hydrodynamic and hydrogeological conditions. The measurements included: a) oil density, organic and inorganic components and biomarkers for crude oil samples, and polycyclic aromatic hydrocarbon PAHs; b) hydrochemistry, stable isotopes; and c) the spectral reflectance behavior of crude oil and different contaminated soil samples, organic components (organic carbon (OC) and total petroleum hydrocarbons (TPHs)) and x-ray diffraction to explain the chemical composition of the soil samples.

The multiple data were transformed into one database, and the results were used to complete the final hypotheses in a conceptual model, which explains the mixing mechanism of crude oil and brine seeps with the surrounding environment. The strontium isotopes ($^{87}Sr/^{86}Sr$) showed the mixing processes between shallow groundwater resources, uprising oil field brines and differentiates it from the dissolution of gypsum and halite from the Fatha Formation.

The final discussion and conclusions connect all of the results and try to simulate the sub-surface hydraulic conductivity and highlight the contamination zones that were explained in the final comprehensive conceptual model, enriching our knowledge of the petroleum and the hydrogeology

systems of the selected fields within the Zagros fold-thrust belt. The obtained results mainly highlight the reasons behind the environmental consequences that can be a threat to the human health. The conclusion of this study opens the door to compare the findings with other locations within the study region, which contains similar complex stratigraphy and structures.

Zusammenfassung

In der Region Kirkuk im Nordosten Iraks haben natürliche vorkommende Kohlenwasserstoffe sowohl Böden und Wasserressourcen stark verunreinigt als auch die Umwelt und die Gesundheit der Menschen geschädigt. Kirkuk ist ein Gebiet mit weltweit bedeutenden Rohölreserven die stellenweise oberflächlich zu Tage treten. Das Untersuchungsgebiet befindet sich im Zagros Falten- und Überschiebungsgürtel innerhalb der schwach gefalteten Zone im Nordosten des Mesopotamienbeckens. Komplexe Bruchsysteme und Verwerfungen durchqueren häufig die Reservoire in den Kalksteinen des Eozäns und mittleren Oligozäns, sowie die Evaporite der miozänen Deckgesteine. Dichtekarten der bekannten Verwerfungen und Lineamente innerhalb der Fatha-Formation wurden als potenzielle Ölaustrittsstellen interpretiert, wobei dies auch für Austrittsstellen gilt die nicht an der Oberfläche freiliegen.

Die vorliegende Arbeit zielt darauf ab, Kohlenwasserstoffaustritte und Austritte von Solen zu untersuchen, die Auswirkungen auf das Grundwasser sowie die physikalisch/chemischen Eigenschaften des Bodens haben. Dazu wurden verschiedene Methoden angewandt, beginnend mit der Identifizierung der Herkunft der Sickerwässer als Grundlage für die Quellenbeurteilung und endend mit der direkten Bestimmung von Kohlenwasserstoffen Wässern und Böden. Die wesentlichen Ansätze der vorliegenden Arbeit basieren auf bekannten Kohlenwasserstoff-Austritten, die über Hunderte von Metern an der Oberfläche nachgewiesen werden können, sowie auf den stratigraphischen Kenntnissen des Untergrundes und den verknüpften hydrogeologischen Bedingungen. Neben einer Auswertung von vorhandenen Publikationen und Berichten wurde eine große Vielfalt von Proben aus dem Untersuchungsgebiet untersucht, d.h. Rohöl- und Soleproben aus ausgewählten Ölreservoiren, die zur Charakterisierung der Reservoire und des Migrationsverhaltens verwendet wurden.

Desweiteren wurden die Öltypen der unterschiedlichen Reservoire bestimmt, um sie mit oberirdischen Rohölsickerproben zu vergleichen. Die Analyse von Oberflächen- und Grundwasserproben aus den verschiedenen Grundwasserleitern im Untersuchungsgebiet diente zur Ermittlung der dortigen hydrodynamischen und hydrogeologischen Bedingungen. Die Messungen umfassten: a) Öldichte sowie organische und anorganische Komponenten und Biomarker in Rohölproben inklusive polyzyklische aromatische Kohlenwasserstoff-PAKs, b) anorganische Parameter (Haupt-Anionen und –Kationen sowie stabile Isotope des Wassers) in Wasserproben, und c) das spektrale Reflexionsverhalten von Rohöl und von kontaminierten Bodenproben, sowie eine Charakterisierung der Bodenproben auf den organischen Kohlenstoffgehalt (OC) und Erdölkohlenwasserstoffe (TPHs)), sowie und Röntgendiffraktometrie zur Ermittlung der chemischen Zusammensetzung der Bodenproben.

Die verschiedenen Daten wurden in einer zusammengeführt um eine konzeptionelle Vorstellung zur Entstehung der Rohöl- und Solekontaminationen im Arbeitsgebiet zu entwickeln. So konnte durch Messungen der Strontiumisotope ($^{87}Sr/^{86}Sr$) in Grundwässern gezeigt werden, dass Mischungsprozesse zwischen flachen Grundwässern und Solen aus Ölreservoiren an lokal wahrscheinlich sind und sich diese

von salinaren Wässern die aus der Gips- und Halitlösungen in der Fatha-Formation resultieren unterscheiden lassen.

Abschließend wurden die Ergebnisse in einem konzeptionellen geologisch/hydrogeologischen Modell der relevanten Entwicklungen im Falten- und Überschiebungsgürtels von Zagros zusammengefaßt. Die in dieser Studie verfolgten Ansätze können auch auf andere Bereiche mit ähnlich komplexer Stratigraphie und Tektonik in der Umgebung des Untersuchungsgebietes übertragen werden.

Acknowledgements

What inspires people to get into science? The reason is to know more, and the passion for increasing the understanding to the world, which optimizes the efficiency for the natural resources and enhances the environment protection. As scientists, we are a part of great history. We did not begin it, but we still writing it and hope our chapter will stay bright until the very end. All the ways are showing our destinations to reach the optimal goals.

The present research work has been conducted at Chair of natural sciences, Technische Universität Darmstadt between June 2012 and December 2018. Therefore, my sincerest thanks to my supervisor Prof. Dr. Christoph Schüth, the vice dean of the earth science department and Chair of Hydrogeology for his, guidance, support, inspiration, fruitful suggestions, and multiple efforts.

A special thank goes to Dr. Andres Marandi for his continued help, valuable comments and discussions to enhance this work. Many thanks to Prof. Dr.-Ing. Matthias Becker, Dr.-Ing. Damian Bargiel, Dr. Safaa Alkhagani, Dr. Paul Königer. Many thanks to Dr. rer. nat. Ralf Littke, Prof. Dr. Rafael Ferreiro Mählmann and Dr. Thanh Lan Nguyen for their support to analyses selected samples from the study area.

Thanks to all colleagues of hydrogeology group at the earth science faculty for the nice time and productive discussions: Dr. Thomas Schiedek, Dr. Stephan Schulz, Dr. Annette Wefer-Roehl. Also, Nils Michelsen, Suraiya Fatema, Abidur Khan, Aili Li, Zahra Neumann, Claudia Cosma, Rainer Brannolte, Berhane Asfaw, Tsegaye Checkol, Sahand Darehshouri, Christoph Kludt, Inga Schreiter, Anja Tögl, Matthew Silver. I would like to thank Dr. Angela Lausch and her team from Helmholtz Centre for Environmental Research – UFZ Department of Landscape Ecology in Leipzig for their support during the reflectance measurement and the spectral analysis. Many thanks go to my wonderful students, Stefanie Schmidt, Mareike Jenne and Daniel Finken who join this project in several stages. Very special gratitude goes out to Dr. Jürgen Born, and Dr. Katrin Kohler and all the Spatial Business Integration colleagues, for their continuous support. It is my pleasure to join all of you and thanks for much knowledge I gain from you all. Special thanks go to my best teachers and friends in Baghdad university Dr. Ali Maki Al-Rahim, Madeha Shakir, Fitian AL- Rawi, Dr. Deaa Al- Rawi, Dr. Moaid Rasheed, Dr. Mahmood Salman, Dr. Janan Korel and Dr. Zainab Hasan.

The author wishes to express his special thanks and gratitude to the German Academic Exchange Service (Deutscher Akademischer Austausch Dienst – DAAD) for the financial Support. The author thanks the Iraqi Ministry of Defense for ensuring the safety in field work and oil sampling despite the unsafe situation in the study area. Thank goes to the Iraqi Ministry of Oil for their permission to use the available seismic database, and seismic interpretation, as well as the North Oil Company (NOC) for using their internal data.

Big thanks to the lovely uncle Majed Jassim and my great mother and wise father, my sister Shaymaa, brothers Ghaith and Harith, last not least my lovely wife and her family.

Table of content

List of figures

List of tables

List of abbreviation

API	American Petroleum Institute
ASD	Analytical Spectral Devices
BD	Band Depth
BNH	Bisnorhopane
CPI	Carbon preference index
CRDS	Cavity Ring Down Spectrometer
CAS	Chemical Abstracts Service
DL	Detection Limit
DCM	Dichloromethane
DRS	Diffuse reflectance spectroscopy
DEM	Digital elevation model
EC	Electrical Conductivity
Emb	Embayment
EnMAP	Environmental Mapping and Analysis Program
EWH	Equivalent Water Height
FID	Flame Ionization Detector
GC	Gas-Chromatography
DAAD	German Exchange Academic Service
GMWL	Global meteoric water line
GPS	Global Positioning System
GRACE	Gravity Recovery and Climate Experiment
HTO	High Temperature Oxidation
HHI	Homohopane Index
HI	Hydrocarbon Index
IC	Inorganic Carbon
LMWL	Local Meteoric Water Line
MS	Mass Spectrometry
MCS	Metrohm CO_2 Suppressor
MSM	Metrohm Suppressor Module
NSO	Nitrogen, sulfur and oxygen
NDVI	Normalized Difference Vegetation Index
NOC	North Oil Company
OEP	Odd even predominance
OC	Organic Carbon

Ph	Phytane
PAHs	Polycyclic Aromatic Hydrocarbon
pH	Potential of Hydrogen
Pr	Pristane
RTKB	Rotary table Kelly bushing
SIM	Selected Ion Monitoring
SWIR	Short Wave Infrared
SLAP	Standard Light Antarctic Precipitation
TAR	Terrigenous/Aquatic Ratio
TLC	Thin-Layer Chromatography
TPH	Total Petroleum Hydrocarbon
TNH	Trisnorhopane
Tm	Trisnorneohopane
USGS	United States Geological Survey
UAV	Unmanned Aerial Vehicle
UCM	Unresolved Complex Mixture
VSMOW	Vienna Standard Mean Ocean Water
VNIR	Visible-Near InfraRed
Wt	Weight
WHO	World Health Organization
XRD	X-Ray Diffraction

1. General Introduction

1.1. Context

The topic of this Ph.D. thesis was created based on the results of various studies in the Kirkuk area as well as surrounding areas of north-east Iraq. In addition to the cooperation between the Deutscher Akademischer Austauschdienst (DAAD) and the Ministry of Higher Education (Baghdad, Iraq), the Technical University of Darmstadt TUD strongly supports this Ph.D. financially and logistically. Kirkuk is the focus of the Iraqi oil production as a result of sizable oil reserves. Kirkuk oil field – as one of the international super giant fields – contains different types of crude oil seeps and surface springs. Meanwhile, the surface and groundwater resources were mainly used for human activities and irrigation for agricultural purposes. Although Iraq was among the first places where scientists started surveying for oil, studies are still minimal concerning the dangers of the contamination of surface and groundwater resulting from the vast oil reserves in Iraq. Three-quarters of the land in Iraq relies on groundwater, the flow of which is limited (Jassim & Goff, 2006).

The crude oil seepage study included a careful assessment of the different components of the hydrocarbon contamination in soil, springs with direct and indirect influence in the surface and groundwater. All of the crude oil samples, water and soil samples were collected from my own personal surveys in the Kirkuk area. The samples were used with existing data to evaluate the additional effect of different aquifer rocks, reservoirs rock, faults, and fractures dimensions. The final finding of this Ph.D. thesis was actively contributed by essential scientific questions regarding the natural hydrocarbon environmental sources and their reflectance in the hydro-lithospheres in the Kirkuk area, as well as establishing a conceptual model for groundwater flow and crude oil migration trend towards the surface.

1.2. Aims

The aims of this Ph.D. thesis are as follows:

1- Determine the characterization of crude oils samples from selected boreholes and surface crude oil seeps based on the geochemical, organic chemical analysis and the stratigraphic features of the geological layers, which can help to characterize the potential source reservoirs of the surface seeps.

2- A better understanding of the groundwater quality and salinity source based on the hydrochemistry and stable isotope to evaluate the source effect of oil brine springs, and/or lithological layers within a new interpretation of aquifer's hydrodynamics of the groundwater.

3- Identify the spectral patterns of Iraqi crude oil by using a remote sensing technique and highlight the effect of the differences in the physical, chemical properties, as well as determining the seeps contamination level in the soil.

1.3. Concept and thesis outline

The major concepts of this Ph.D. thesis are based on the understanding of several studies of the hydrocarbon analyses in the term of the natural crude oil seeps and evaluating the effects of the environment. This concept is highly applicable in the North of Iraq, where the Kirkuk area is located. The large area of Fatha Formation outcrops – as the shallowest exposed cap rock – shows a wide variation of crude oil seeps, where the effects on the soil and water were recorded and sampled. The field survey and the collecting of samples lasted around five months. The sample analyses and measurements were conducted in different laboratories in Germany. In this thesis, various studies were applied. As shown in Figure 1, the chapters are organized to introduce the study area from many aspects, i.e., the geology, the lithology of the selected formations, the petroleum system, and the hydrogeology conditions, as well as highlighting related topics within previous studies (see chapter 2).

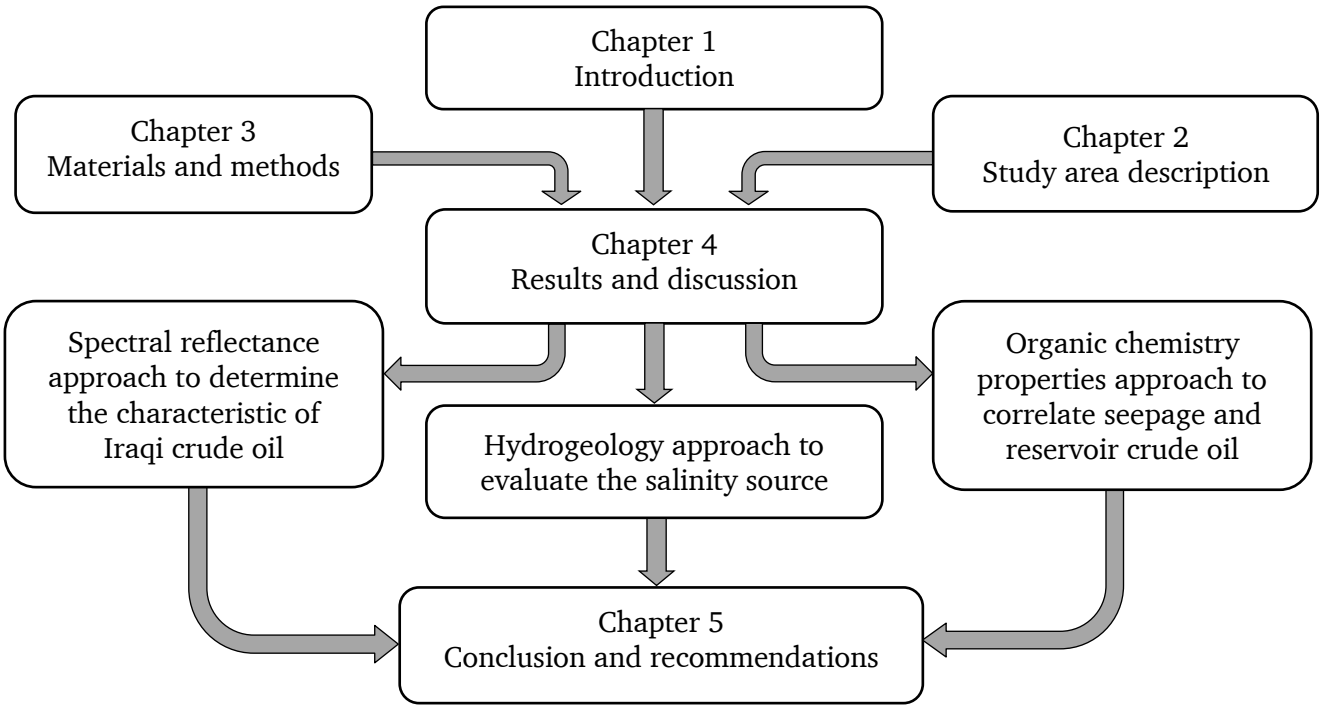

Figure 1: Network diagram showing the relationship between the chapters in this thesis

The materials and methods of the origin definition of the surface seeps, groundwater's contamination source and the hydrocarbon accumulation on the surface using remote tools were the subjects of chapter 3. Furthermore, several batch experiments were conducted, and its results were added and explained in chapter 4, where the results are discussed in detail. The obtained results were the base of the conclusion to understand the seeps occurrence within a larger scale by displaying a conceptual schematic model. Several parts of this thesis have been published and submitted to international journals as well as conference proceedings.

2. Study area, conditions and description

2.1. Location

The study area is located in Northern Iraq at 35°28'N and 44° 24'E, and it covers an area of 8500 km^2 within the Kirkuk and Erbil governments (Figure 2). To the south of the Kurdistan region, Kirkuk is the largest city in the study area and one of the largest centers of Iraq's oil industry, with a population of about 1 million. Agriculture is widespread in the region, with mainly wheat and barley production and it strongly relies on irrigation using water from shallow aquifers. The study area is geologically located around the Kirkuk anticline structure as part of the Low Folded Zone within the Zagros basin. The Zagros fold and thrust belt stretch across a length of about 2000 km, which is commonly considered as an active tectonic area.

Generally, the study area contains outcropping sedimentary rocks from Tertiary and Late Cretaceous sedimentary rocks (Jassim et al., 1986; Jassim and Buday, 2006c). With elevations ranging between 50 and 994 m above sea level, it includes several anticlines that represent known oil and oil-gas mixed fields with stratigraphic oil traps.

2.2. Tectonic and structure

Iraq – as also located to the north of the Arabian Plate – formed part of the northern margin of Gondwana with the Palaeo-Tethys. The Kirkuk Embayment represents the intermediate region between the shelf-margin prism extending from the basement of the Arabian Shield in the west of Saudi Arabia to the frontal thrust belt of the Zagros Mountains in the east of the Arabian Plate, as in its present configuration (Al Ajmi, 2013). Therefore, it is necessary to take into consideration data from surrounding regions including north-eastern Saudi Arabia, eastern Turkey, and western Iran. The Infra-Cambrian Hormuz complex represents the first deposition of a mega sequence, which is variably evaporitic or siliciclastic along the strike of the Zagros Orogen (Sharland et al., 2001; Zebari and Burberry, 2015). The potentially transtensional grabens and tilted fault blocks of the Zagros area were characterized by north-south trending during the Late Ordovician – Early Devonian. This trend results from the east-west extension of Caledonian orogeny (Sharland et al., 2001). The meander trace line between the Foothill zone and Zagros fold zone delineating the Kirkuk Embayment, the Lurestan arc and the Dezful Embayment can be related to the Hormuz salt distribution (Figure 2), which acts as a decoupling level, as well as the tilted fault blocks (Kent, 1979; Sharland et al., 2001; Bahroudi & Koyi, 2004; Casciello et al., 2009; Munt et al., 2012). By focusing on the late Mesozoic and Cenozoic ages, the later closure of Neo-Tethys was marked along the line of the Zagros (Figure 3), as the Arabian part of the Afro-Arabian Plate was subducted below Eurasia (Sharland et al., 2001, Jassim and Goff. 2006).

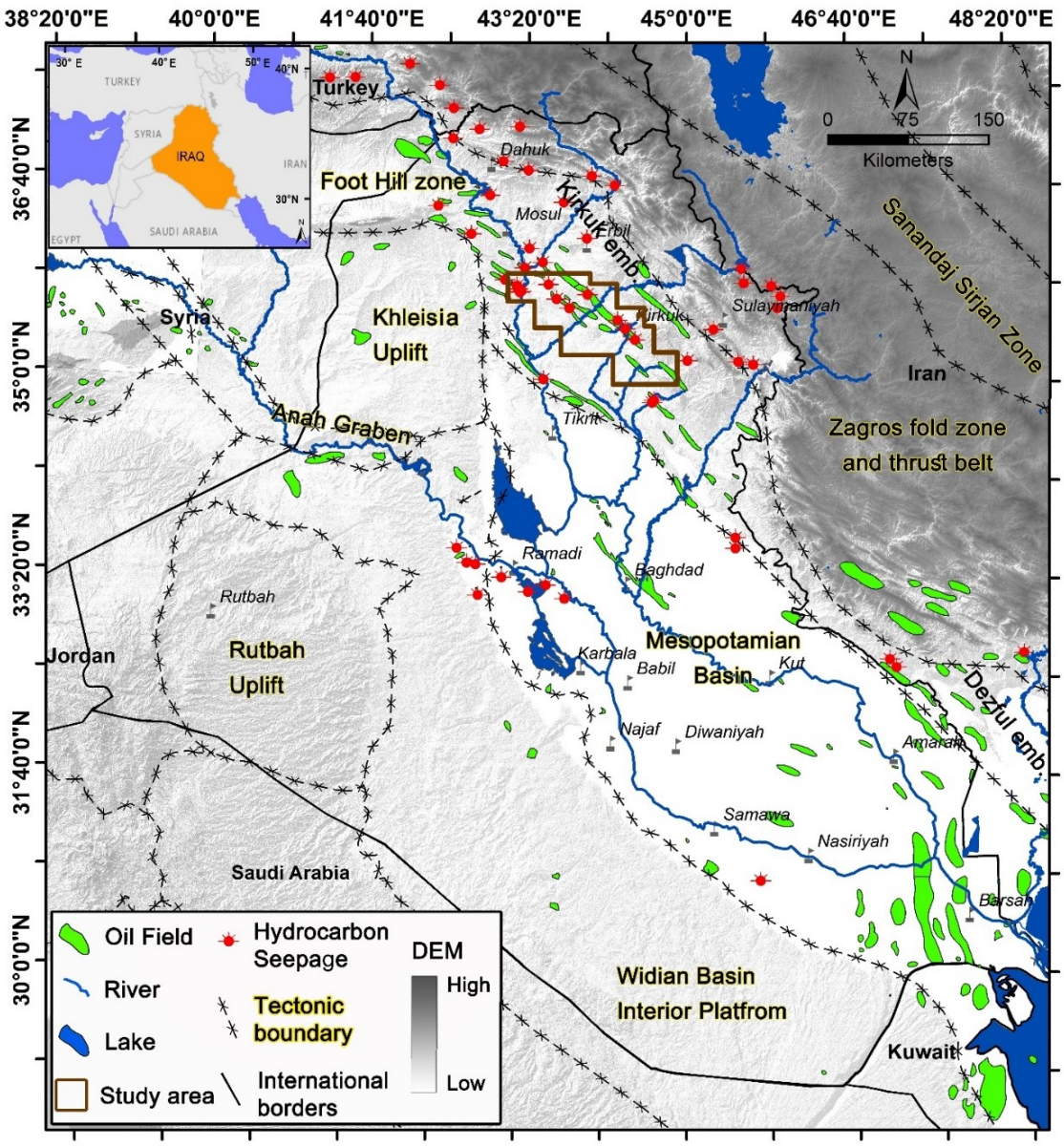

Figure 2: The location of the study area within the tectonic classification (Aqrawi,1998; Munt et al., 2012) with significant hydrocarbon reservoirs (Al-Gailani, 1996) and crude oil seeps (field survey in this study and modified after Forbes, 1955) based on digital elevation model 90m (srtm.csi.cgiar.org)

Subtle structural growth was controlled by the movement on basement strike-slip faults, which began in the late Albian (Sadooni and Aqrawi, 2000), where NE is one of the fundamental fault's orientations (Ameen, 1992). The opening of the Red Sea at the end of the Oligocene era was accompanied by an uplift of the south-west and south-east margins of Arabia, meanwhile the final Zagros collision started at the end of Pliocene, causing wide thrusting and folding of earlier sediments and inversion of foreland structures (Sharland at al., 2001). The uplift of the Zagros Mountains and its related structures are a result of the collision of the continental Eurasian and Arabian plate during the separation of the continental Arabian and African plates. The relatively straight westwards movement of the plate boundary between the Anatolian and Arabian Plate was showing direction cross the Taurus Mountains range (McClusky et al., 2003).

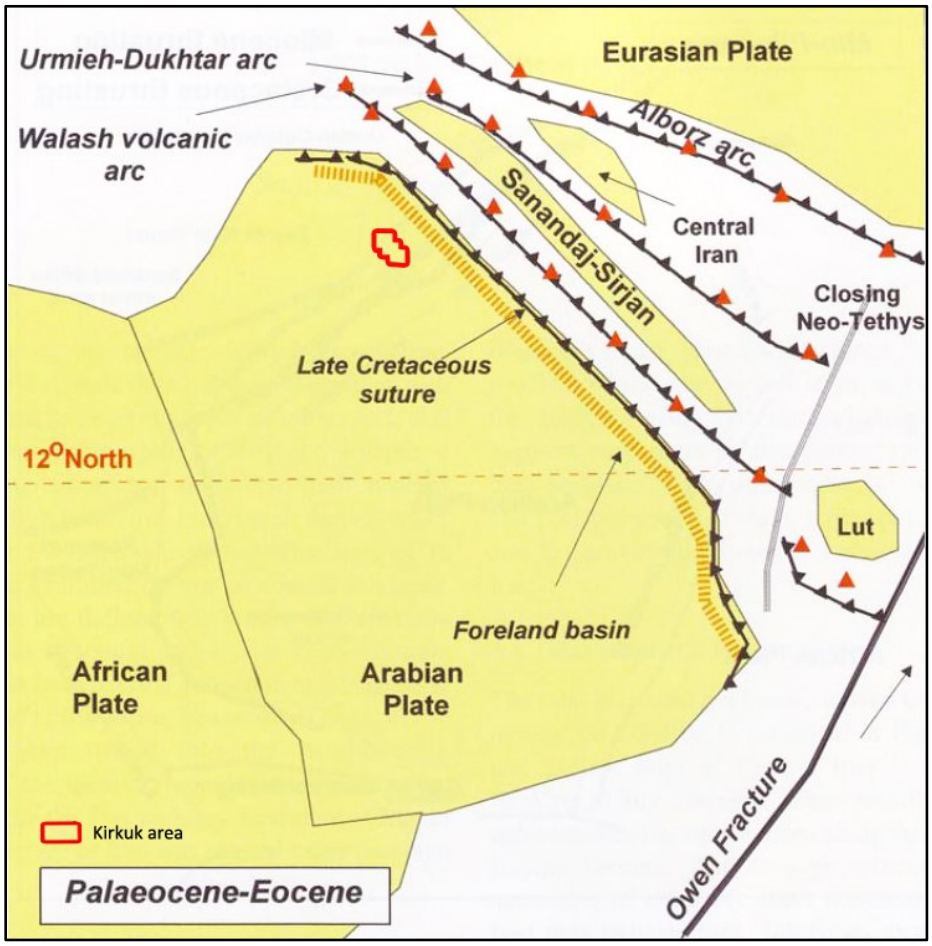

Figure 3: Tectonic plates situation during the Early Palaeocene to Latest Eocene (63-34 Ma) Mild compression and closure of Neo- Tethys (After Jassim and Goff, 2006)

The late Miocene was considered as a time when the culmination of the collision between the Eurasian and Afro-Arabian plates occurred, which also can be seen as a part of the Alpine orogeny (Falcon, 1969; Jahani et al., 2009). Up to 12 km, the thick section from Early Cambrian to Pliocene layers was recognized, which was affected stratigraphy by the uplift of the Zagros fold zone (McQuarrie, 2004; Csontos et al., 2012). The burial of the source rocks was recorded during this event makes the depth the source rocks is favorable for the generation of oil and gas (Bordenave and Hegre, 2005). Additionally, the hydrocarbon plays of Kirkuk and surrounding oil reservoirs with Miocene evaporates caprock were entirely affected by the built up complex anticlinal structures, which can be count as primary and secondary migration pathways (Al-Ameri & Zumberge, 2012). Therefore, it was essential to understand the potential hydrocarbon source rocks and the large-scale limestone reservoirs in the selected anticlines. Parallel to the Iraqi-Iranian borders, anticlinal structures, and many related oil fields are extending from the north of Iraq to the south-west of Iran have an NW trend elongation, which can be clearly observed from satellite images (Figure 1). This trend meets the Taurus and Sinjar mountains (NW of Iraq) with an E-W trend along northern Iraq, Syria and south-eastern Turkey. As well as this part is considered a transition zone between the Mesopotamian foredeep in the south and anticlinal structures in the north

of Iraq, which define as the beginning of the Zagros fold and thrust belt zone (Csontos et al., 2012). The changes in the structural strike of the mountain belt are an additional distinguishing feature of the area. In the direction of the south of Turkey, the strike line changes by around 25°-30°, from an NW-SE strike towards an E-W strike (Csontos et al., 2012). Therefore, in this area, every feature will be affected and also the distribution and the orientation of the all related oil fields.

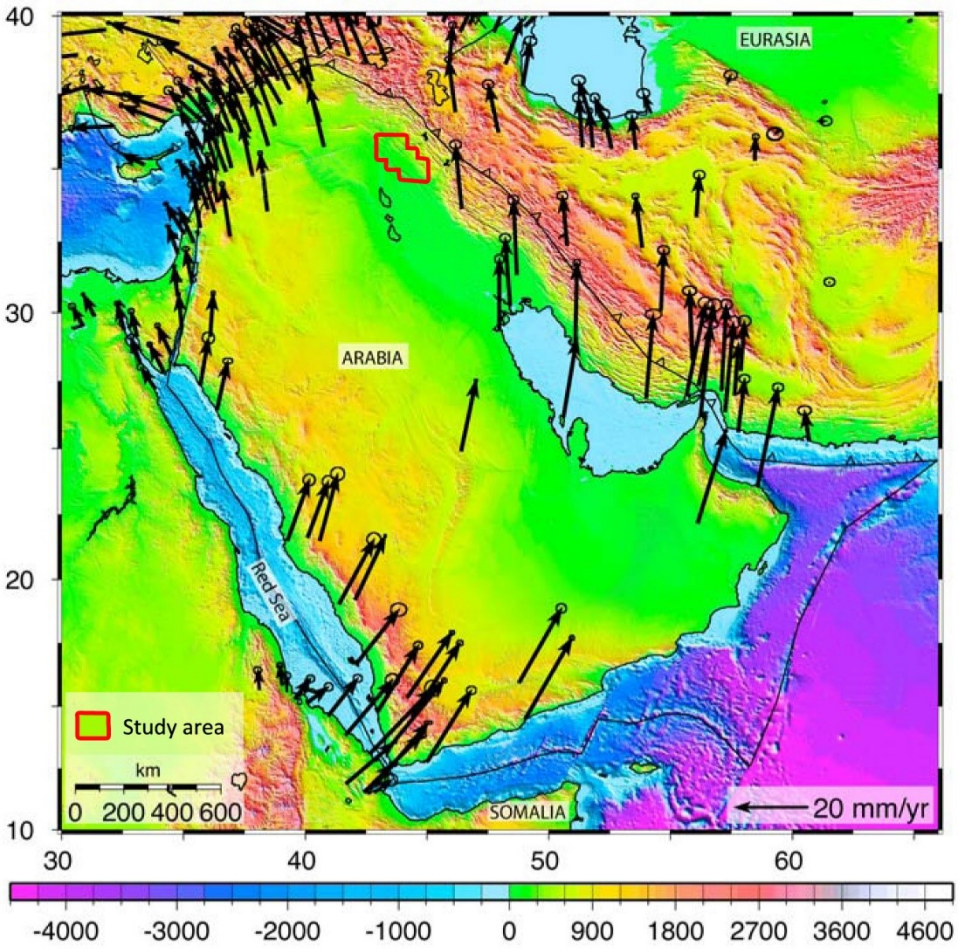

Figure 4: Velocities the Arabian plate were based on GPS with 1-sigma confidence ellipses in a Eurasia-fixed reference frame (ArRajehi, et. Al., 2010)

Earthquakes in northern and north-eastern Iraq have focal mechanisms showing both thrust and strike-slip movement (Zebari and Burberry, 2015), as listed in the online USGS database (earthquake.usgs.gov). The global positioning system (GPS) calculates the annual moving off the northern part of the Arabian Plate towards the NNE direction at a rate of about 15 mm per year. Meanwhile, the Turkish plate is moving towards the west at a rate of about 21 mm, and the Iranian plate is moving towards the NNW at a rate of about 16 mm (Reilinger et al., 2006; Abdulnaby et al., 2014) see Figure 4. The continuous tectonic activity has recently presented infrequent high magnitude earthquakes. For example, in the Halabja area (155 km to the east of Kirkuk city), a major 7.3 magnitude earthquake occurred in November 2017 (USGS 2017).

2.3. Stratigraphy and Geological description

The surface geology of Iraq nearly reflects its morphology. According to (Jassim and Goff, 2006) basement tectonic caused major faults zones with NW-SE orientation and NE-SW transversal faults, which used as a base to identify five major blocks starting from Basra block (The upper boundary is defined by Takhadid-Qurna Fault) until Sinjar-Abdul Aziz block (The lower edge is defined by Sinjar-Herki Fault) (Figure 5). Moreover within the central Iraq block and Deir Al Zor- Erbil block, the major faults with an NE - SW trend are transverse, reaching the basement rocks and dividing the Kirkuk and Mosel to smaller blocks. Kirkuk and Mosul blocks show significant differences in their level shape and relative arrangement (Ameen, 1992). Besides, within every single block, the synorogenic differential movement on longitudinal basement faults (fault stacking) affected hydrocarbon generation, migration, and entrapment.

As described in paragraph 2.2, the tectonic activity is the main reason for the high fault system in the area, which can be found within the reservoirs and in the cap rock formations exposed at the surface. Due to the tectonic activities in the region, the whole sequence of sediments is extensively fractured. These faults and other lineaments can be defined as simple linear or brittle geologic structures (faults, fractures, joints, etc.) of a surface that can be mapped. Their parts are aligned in a rectilinear or slightly curvilinear way, and they differ distinctly from the patterns of adjacent features and presumably reflect a sub-surface phenomenon (O`Leary, 1976). Since the 1950s, numerous studies have analyzed the effects of fault systems on an oil reservoir. Frequent joints and minor breaks may cut across the reservoir complex in all directions (Daniel, 1954). Consequently, the lineaments can be the most influential factor in understanding the migration processes of the reservoir fluids, as well as evaluating their impacts when coupled with other factors like bedding, hydraulic properties, and erosion in formations sealing hydrocarbon zones.

Most prominent fractures and thrust faults are oriented parallel to the anticline axes and cut deep into the sediments reaching the oil reservoirs, e.g., the Kirkuk anticline major thrust fault – as the leading case example – is acknowledged as the longest thrust fault in the area, with an approximate length of 110 km (Sissakian, 1993). Several faults that do not reach the surface have been identified in drilling logs and by geophysical investigations (Daniel, 1954). Regarding the geological situation, the youngest sediments (Quaternary and Neocene) lie within the central depression (Mesopotamian basin), while the flanks expose older strata of a Paleocene to Paleozoic age with respect to the south-west part, where the Arabian Gulf is located (Figure 5). In the north-east – where the study area is located – a series of ridges and depressions appear in anticlines. However, the geology of the study area shows a wide variety of marine and non-marine sedimentology rocks outcrops, while the dominant rock units in the study area are carbonate-sedimentary rocks (Table 1).

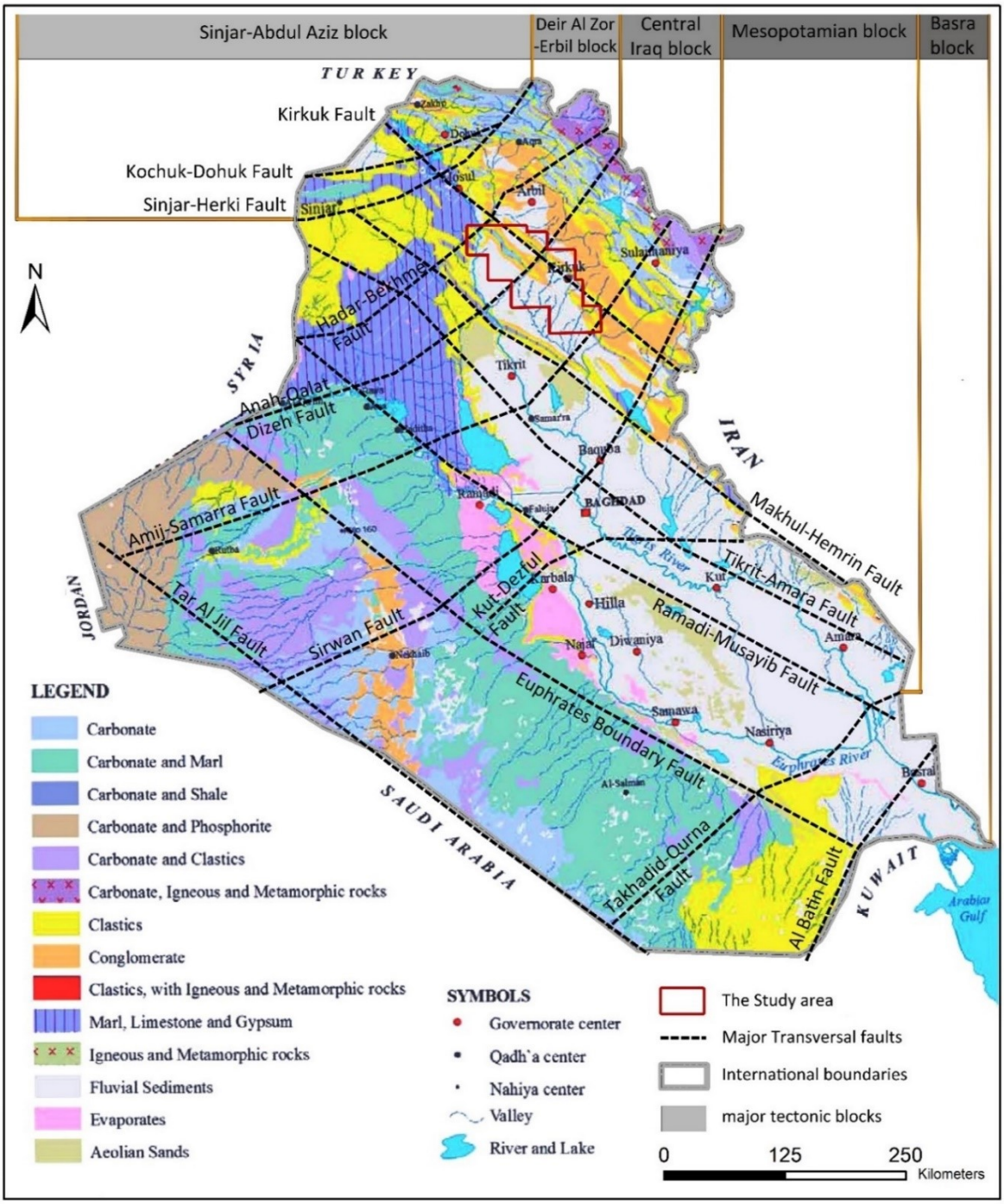

Figure 5: The distribution of the major fault system and their identified blocks (Jassim & Goff, 2006) placed on a lithological map of the exposed formation of Iraq (Sissakian and Fouad, 2015)

The lithology of the surface shows outcrops of the cap rock Fatha Formation to the Oligocene - Eocene reservoir. Due to the tectonic activates and the erosion, various outcrops can be found, and thus the age of sedimentary rocks covering study area includes Quaternary and Tertiary (Figure 6). The most significant part of the surface geology of the study area is covered by the various thickness of Quaternary deposits represented by sheet runoff deposits, river terraces polygenic deposits, slope deposits, depression fill deposits, floodplain, valley fill deposits Sabkha and sand dunes (Sissakian, 1993). Tertiary deposits with a second broad class of the area were exposed mostly across anticlines, synclines and faults

represented by the oldest Fatha Formation (Early to middle. Miocene), surrounded by the rocks of the youngest Injana Formation (Late Miocene), Mukdadia Formation (Early Pliocene) and Bai Hassan Formation (Late Pliocene).

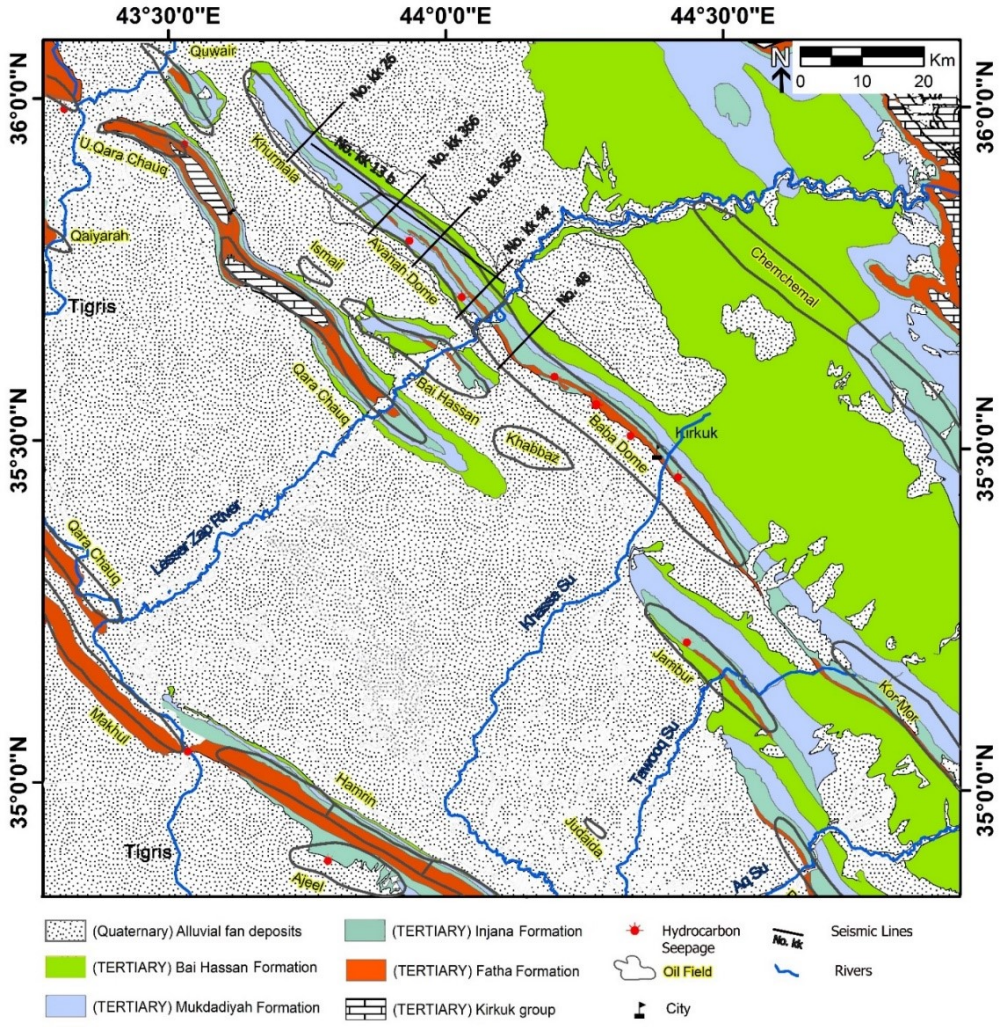

Figure 6: The surface geological map of the study area and the location of the seismic sections (modified after Sahib et al., 2016)

The cores of the anticlines are mainly formed by fractured limestone of Late Cretaceous to Tertiary age, being the host rocks of abundant oil and gas accumulations. They originate from Jurassic and Early Cretaceous source formations below (Pitman et al., 2004; Sahib et al., 2016). As the outcrops comprise Neogene sedimentary rocks, the cores of anticlines may expose Eocene limestone or Late Cretaceous sedimentary rocks (Jassim et al., 1986). As discriped in Chapter (2.4), Several formations in the geological column can be considered as reservoirs, but in the frame of the present study, the most important reservoir formation is the Kirkuk Group, which is represented by a complex of back/reef/fore reef and basinal units (Jassim and Buday, 2006c). The Fatha Formation with age of Miocene represents a cap rock formation. This formation is characterized by anhydrite, gypsum, and salt, interbedded with limestone, marl and fine-grained clastic (Buday, 1980).

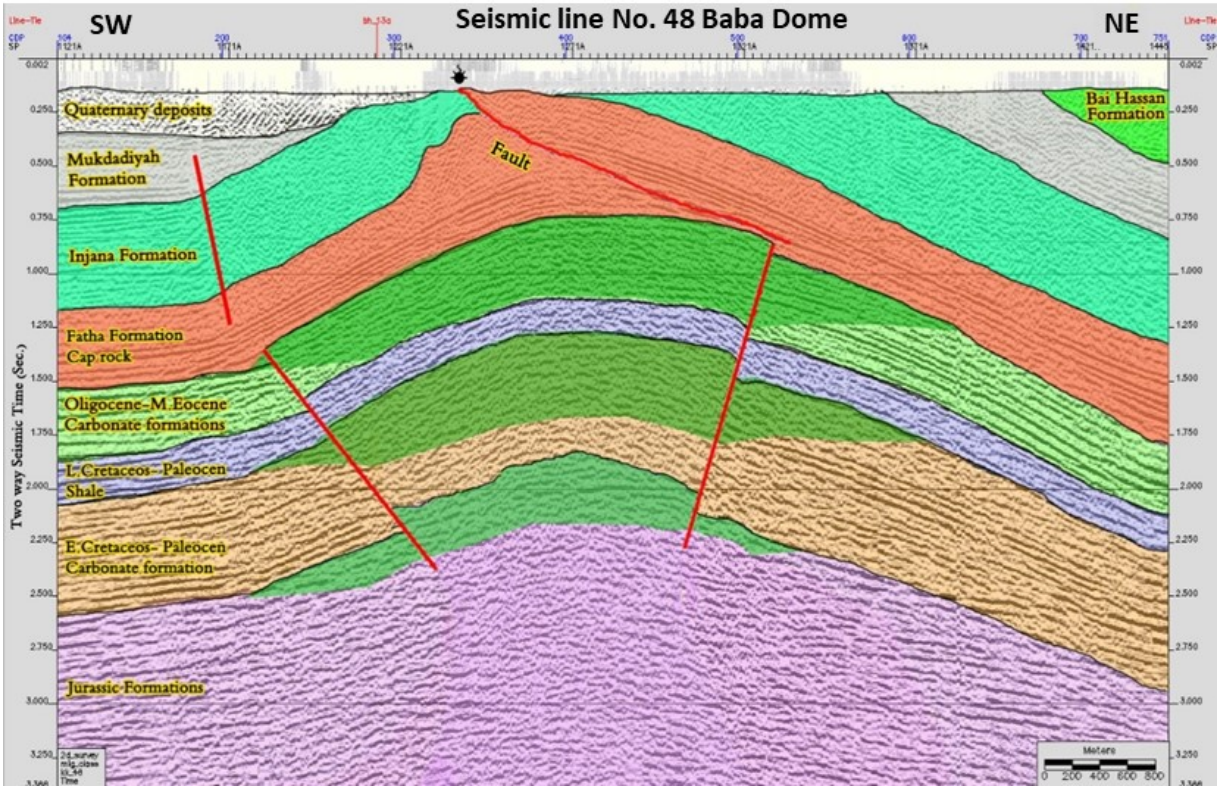

Figure 7: Seismic section (No. 48) for Baba area explain the major reservoir, geological formations, and detectable thrust faults. Seismic section and well logs database of the North Oil Company (NOC)

The field survey and seismic sections locations (Figure 6) show the thrust fault of the Kirkuk fold, which is overlapped by the NE flank. Seismic sections and their interpretations were further illustrated and confirmed the geological and tectonic setting and the location of seeps from another point of view; Figure 7 for example, is a seismic interpretation of the section No. 48 of Baba Dome (Kirkuk and its domes are explained in paragraph 2.5.3.1). Two significant oil resources and several faults were defined, the location and the sequence of the geological column - including hydrocarbon reservoir and their caps rocks - within Cretaceous and Tertiary were explained in a paragraph (2.4).

Five projected 2D sections representing Avanah and Khurmala domes close to the Lesser Zap river show two sets of thrust fault systems on each flank, dipping towards the center of the structure (Figure 8). Such fault systems can be considered as potential seeps paths to the surface. The record drill logs of the related wells explain major effects on the shallow formations like Fatha Formation – which have outcrops on the surface – as well as the older layers reaching to the late Jurassic formations. The seismic sections (No. 44 and 386) of Avanah Dome show similar effects of the faults with the direction to NW (Khurmala Dome). The highest shift of the thrust faults was recorded mainly on the older layers comparing to the other layers (No. 386 and 26). One section with an orientation parallel to the Kirkuk anticline (No. 18B) shows the main fault, which divides Baba and Avanah Domes. Seismic, significant correlations between remote sensing data and sub-surface studies were made.

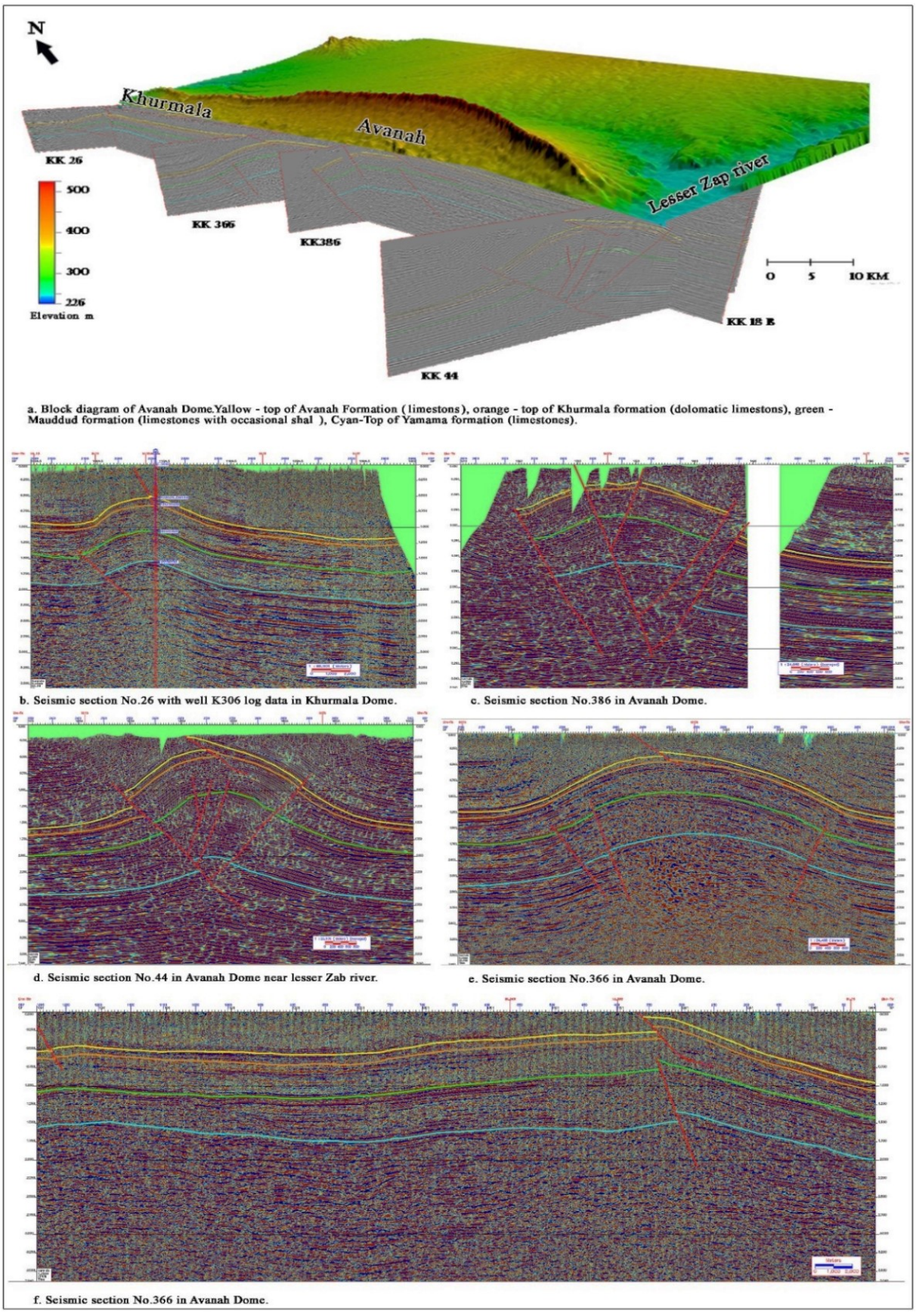

Figure 8: Block diagram and five seismic sections for Avanah area explain the major reservoir, geological formations and detectable thrust faults (five seismic sections). Seismic sections and well logs database of the North Oil Company (NOC)

2.4. The geological Formations

2.4.1. Jurassic Period

The Middle-late Jurassic formations contain one of the world's most essential hydrocarbon systems (Aqrawi et al., 2010). However, in Iraq, the few studies cannot explain this mega sequence in an entirely successful way (Alsharhan and Nairn, 2003; Jassim & Goff, 2006). This study focuses more on the shallow formation, although the author described the late Jurassic layers (hydrocarbon source rocks) shortly. Starting from the Najmah, Chia Gara and Barsarin formations, Bellen et al., (1959) descript the main lithology is based on marine deposits like limestone, dolomitic limestone and marly limestone (Table 1). Naokelekan Formation is showing bituminous dolomites and limestone interbedded with black, bituminous shale (Buday, 1980). The late Jurassic Karima Formation, showing a sequence of monotonous, dark-colored, calcareous mudstone Bellen et al., (1959).

2.4.2. Cretaceous Period

As one of the most important periods, Cretaceous formations have been the focus of several studies. However, the mid-Cretaceous formations in the Foothills Zone of the Zagros in north-eastern Iraq were challenging to relate to each other (Alsharhan and Nairn, 2003). Most descriptions of the Albian-Turonian formations in the Foothills Zone are based on the studies conducted by Bellen et al., (1959) and Buday (1980). In general, the age's boundaries are poorly defined or with wide-ranging interrelationships (Alsharhan and Nairn, 2003). The main Cretaceous formations in the study area are also described by dominant limestone as marine deposit lithology like Sarmord, Qamchuqe, Dokan, Komitan and Musharah formations (Table. 1). In Garagu Formation, the primary layers comprised of sandy, oolitic limestone with marl and sandstone(Bellen et al., 1959).

The Gulneri Formation was deposited in a basinal, euxinic environment and it is comprising black, bituminous and calcareous shale with some glauconite and collophane in the lower part (Buday, 1980). The most widely developed formation within the High Folded Zone is Shiranish Formation. With total thickness up to 400 m, it consists thinly-bedded, marly limestone overlain by blue, pelagic marl and occasional marly limestone beds. The marl sometimes is dolomitic and it rich with microfauna (Owen and Nasr, 1958; Bellen et al., 1959; Alsharhan and Nairn, 2003).

2.4.3. Tertiary Period

In Iraq, the foreland basin is known as Mesopotamian Basin, which developed in the Cenozoic time. A slightly progradational carbonate shelf developed on the passive SW margin of Mesopotamian basin in Paleocene - Eocene time, and a more aggradational shelf expanded on the active NE margin (Aqrawi, 2010). The main Tertiary formations can be listed as the following:

Table 1: Lithostratigraphy and hydrocarbon potential (Source rocks, reservoirs and caprocks) distribution of Cenozoic and Mesozoic (except Triassic) sediments of study area Northern Iraq. Kirkuk group consist of: Anah, Azkand, Ibrahim, Baba, Bajawan, Tarjil, Shura, Sheik Alas formations. Source data: Boreholes records NOC. Verma et al., 2004; Alsharhan and Nairn, 2003; Sissakian and Fouad, 2014; Al - Ameri & Zumberge, 2012; Jassim and Buday, 2006c; Ziegler, 2001

Period	Epoch	Age		(Ma)	Foramtion	Lithology	Thick (m)	Reservoir/Type	Source Rock	Seal	Comments	
Tertiary	Neogene	Pliocene	Placenzian	3.6	Bai Hassan (U.Bakhtiari)							fold and thrust development
			Zanclean	5.3	Mukdadiyah (L. Bakhtiari)							
		Miocene L.	Tortonian - Messinian	11.2	Injana (Late. Fars)		Up to 2000					
		Miocene M.	Langhian - Serravallian	16.4	Fatha (Early. Fars)		200 - 2500	X..?		X	Regional seal, Seeps & considered a reservoir in south of Iraq and Iran	
		Miocene E.	Burdigalian	20.5	Jeribe		10 - 204	X /Gas & Oil				Zagros Orogeny
			Aquitanian - Burdigalian		Dhiban		10 - 150			X	Seal in Jambur and Qaiyarah field	
			Aquitanian	23.8	Euphrates		up to 100	X / Oil				
		Oligocene L.	Chattian	28.5	Serikagni		up to 150	X / Oil			Reservoir in Jambur field	
	Paleogene	Oligocene E.	Rupelian - Chattian	33.7	Kirkuk Group+Palani		Up to 500	X /Oil		X	Reservoir in Kirkuk (Baba dome) and Bai Hassan fields	
		Eocene	Lutetian - Bartonian	54.8	Jaddala/Avanah		25 - 450	X /Gas	X..?	X	Reservoir in Kirkuk (Avanah dome) and Bai Hassan fields	
		Paleocene	Thanetian - Ypresian	65.0	Aaliji		Up to 180	X /Oil	X..?	X		
Cretaceous	Late	Senonian	L. Campanian - Maastrichtian	85.8	Shiranish		Up tp 2800	X /Gas & Oil	X	X		
			Coniacian - E. Campanian	89.0	Mushorah		85 - 300	X /Oil			Reservoir in Qaiyarah field	
	Middle	Turonian		93.5	Kometan		100 - 300	X /Oil				
		E.Turonian			Gulneri		Up to 14		X			
		Cenomanian		98.9	Dokan		4 - 150	X /Oil			Reservoir in Bai Hassan field	
	Early	Albian		112.2	Qamchuqa/Mauddud		50 - 550	X /Oil		X..?	The top layers of Qamchuqa are consist of marl, marly limestone especially when Bekhme (L. Cretaceous) formation is present	
		Valanginian - Aptian		137.0	Sarmord/ Balambo*		Up to 3800	X /Oil	X*	X	* When present, Balambo formation can act as source rock	Neo –Tethys extension
		Valanginian - Hauterivian			Garagu		Up to 230	X /Oil				
		L.Tithonian - Berriasian		150.7	Karimia		Up to 610					
Jurassic	Late	M.Tithonian			Chia Gara		Up to 230		X			
		E.Tithonian?		154.1	Barsarin		Up to 20					
		L.Oxfordian - E.Kimmeridgian		159.4	Naokelekan		Up to 30		X	X..?		
		Callovian? - E.Oxfordian		164.4	Najmah		Up to 330	X /Oil				
	Middle	Bajocian - Bathonian?		176.5	Sargelu		Up to 500	X /Oil	X			
	Early	L.Toarcian?			Alan		Up to 60			X	Regional seal	
		E.Toarcian		189.6	Mus		Up to 40	X /Gas & Oil				
		M.L.Pliensbachian?		195.3	Adaiyah		Up to 100			X	Regional seal	
		Hettangian – L.Pliensbachian		205.7	Butmah		Up to 500	X /Oil			Reservoir in the limestone lower part only	

2.4.3.1. Aaliji and Jaddala/Avanah formations

In the type section in well Kirkuk-109 a sequence of about 150 m of gray and light-brown, argillaceous marl, marly limestone, and shale with fine-grained chert and associated rare glauconite were definite (Alsharhan and Nairn, 2003). The formation was interpreted by Buday (1980) as typical offshore marine sediments containing a series of marginal uplifts with reefs in north-eastern North. As deep-water deposits, Aaliji and Jadala/Avanah were interpreted including a 350 m of marly and microporous (chalky) limestone and marl with occasional thin intercalations of oolitic, peloidal grainstone (Bellen et al.,1959; AI-Kufaishi and AI-Rubaie, 1986).

2.4.3.2. Kirkuk Group formations

In northern Iraq, Oligocene sediments have been assigned to the Kirkuk Group divided into numerous formations with relatively restricted distribution and thickness. The individual formations are showing a progression from the reef and back-reef facies into offshore and basinal conditions (Alsharhan and Nairn, 2003). The most remarkable formations were identified in presumed stratigraphic order as the following:

- Palani Formation (Early Oligocene).
- Shurau Limestone Formation (Early Oligocene).
- Sheikh Alas Formation (Early Oligocene).
- Tarjil Formation (Early Oligocene).
- Bajawan Formation (Middle Oligocene).
- Baba Formation (Middle Oligocene-early Late Oligocene).
- Anah Formation (Late Oligocene).
- Azkand Formation (Late Oligocene).
- Ibrahim Formation (Late Oligocene).

According to (Aqrawi, 2010), In the Anah, Bajawan and Shurau formations, reef-zone facies appear. Heterolithic embedded limestones with colonial corals and algae are comprised. Additionally, the Anah, Bajawan and Shurau Formations are a forming part of Back-reef (lagoonal) facies. Azkand, Baba and Sheikh Alas formations were assigned to the fore-reef to slope facies of the Kirkuk Group (Bellen et al.,1959).

2.4.3.3. Serikagni Formations

With mainly globigerinal chalky limestones with a few layers of limestones representing the basinal facies, (Bellen et al.,1959) was the first who intorduced the Serikagni Formation in 1955. These Facias is unconformable in several locations and overlay the basinal Oligocene formations or Jaddala Formation (Alsharhan and Nairn, 2003).

2.4.3.4. Euphrates Formation

The Euphrates Formation lies under the Fatha Formation (Miocene) in the north-west part of the study area and extends eastward. It mostly contains chalky limestone with thin layers of marl and gypsum, these indicate a shallow marine environment of sedimentation. The Euphrates Formation can consider as oil reservoir in northern Iraq (Hammoshi, 1972; AL-Mamuri, 2005). This formation lies unconformably under the Al-Fatha Formation and has thickness until 33 m.

2.4.3.5. Dhiban Formation

In this formation, gypsum layers, thin beds of marl and brecciated recrystallized limestones were recorded. Such layers represent the final evaporitic sediments of the Late Early Miocene subcycle (Buday, 1980). The depositional environment was not fully formed by lagoon evaporitic conditions or basin-centered Sabkhas and saline environments (Jassim and Goof,2006). (Hammoshi, 1972).

2.4.3.6. Jeribe Formation

The Jeribe Formation is mainly characterized by limestone, albeit with more recrystallized and dolomitic conditions similar to the Euphrates Formation (Alsharhan and Nairn, 2003). The lower contact between the Serrikagni Formation and the Jeribe Formation is unconformable. In many locations, when the Dhiban Formation is not present, it is may be replaced by the Euphrates Formation (Bellen et al., 1959). In this case, the Euphrates Formation underlies the Jeribe Formation. In the study area, the Jeribe Formation separates the Euphrates Formation from the Dhiban Formation.

2.4.3.7. Fatha Formation (Early Fars)

Fatha is one of the most important geological formations in this study. The first records of this formation were introduced in the Agha Jari oil field from the south-west of Iran (Bellen et al., 1959). In Iraq, the typical sections of this formation were recorded in the Makhol area to the south-west of Kirkuk. However, the Fatha Formation is considered as a reservoir in the south of Iraq and Iran. The exact age of deposition is a matter of controversy. Sayyab and Kureshy (1967) also Mahdi (2007) assign the formation to the Early Miocene and Bellen et al., (1959) to the Middle Miocene. Majid and Veizer (1986) mark the occurrence boundary of the Fatha Formation from Oligocene to Miocene.
With age of 20 M, the environment of sedimentation is a shallow marine. According to Bellen at al. (1959), The formation was divided into four irregular units: upper red beds (Figure – App. 1), seepage beds (Figure – App. 2), saliferous and transition beds. The oil wells data in the Area of Interest (AOI) showed that the thinness can reach more than 900 m. However, the thickness of the formation is variable from one location to another, where it reaches 305 m thick on the NW (Khurmala) Dome of the Kirkuk structure, and 610 m thick on the SE (Baba) Dome (Aqrawi et al., 1989; Aqrawi, 1993). Generally,

Buday, (1980) and Aqrawi (1993) describe the Fatha Formation as comprising anhydrite, gypsum and salt, interbedded with limestone and marl, forming an important cap rock layer to numerous oil reservoirs in the north of Iraq (Hammoshi, 1972).

The outcrops of the Fatha Formation can be mostly found on the NE flank of the Kirkuk, Bai Hassan and Jambur anticlines, while the SW flanks mostly lie below the alluvium. The Fatha Formation outcrops cover the majority of the Qaiyarah oil field. Meanwhile, this layer lies under thick column alluvial deposited in the Khabbaz oil field. The out croup of the Fatha layout is limited near the folded anticlines axis, which results from the tectonic folding process. The Injana, Mukdadia and Bai Hassan formations, as well as Quaternary deposits, can be found in both limbs of all anticlines especially, in the north-east from the study area. Finally, it is important to highlight that most of the recorded seeps in the AOI were recorded within the outcrops of the Fatha Formation.

2.4.3.8. Injana Formation (Late Fars)

The Injana is the most dominated formation on the sides of the Kirkuk, Jambur, Qara Chauq, and Bai Hassan structures. The formation is characterized by consecutive beds of gray sandstone and red siltstone, a few lenses of limestone and gypsum, which appear on the lower part of the formation. The environment of sedimentation is mostly continental. The maximum thickness of the formation is 900 m near Kirkuk (Jassim and Goff, 2006). The appearance of a gravel layer above the Injana Formation indicates the beginning of the Mukdadia Formation (Al-Jaboury, 2009).

2.4.3.9. Mukdadia Formation

This formation is described as Early Bakhtiari Formation in Iran by Busk and Mayo (1918). The lithology is mainly formed through a cyclic repetition of sandstone, claystone, and siltstone (Jassim et al., 1984 and Al-Rawi et al., 1992). The gradient of the grain size starts from sandstone beds in the lower part ending to claystone in the upper part (Sissakian and Al-Jibouri, 2012). The Mukdadia Formation rests conformably over the beds of the Injana Formation, although it can be found with angular unconformity (Figure – App. 3).

2.4.3.10. Bai Hassan Formation (Late Bakhtiari)

The outcrops of this formation are found around the major structures in the AOI. With almost entirely comprises terrigenous clastic from silt to boulder conglomerates, Bai Hassan Formation occupies an enormous area to the north-east of the Kirkuk anticline (Buday, 1980). However, the grain size of the classics increases generally upwards and is interbedded with sandstone siltstone and claystone. The environment of sedimentation is continental, resulting from the erosion of the high mountains. Its total thickness reaches up to 750m, where it is difficult to diagnose the separation limit with the overlying

Quaternary sediments (Jassim and Goof, 2006). The appearance of the first layer of conglomerates marks the boundary between this layer and the underlying Mukdadia Formation (Buday, 1980).

2.4.4. Quaternary Deposits

Most of the recent Quaternary deposits are formed by diverse sediments from Pleistocene and Holocene reaching to the recent deposits. The wide variation of different morphologic and lithological features can be explained by different sediment layers within a relatively short time (Jassim and Goof, 2006).
Due to the good porous and permeability, the Quaternary deposits are considered as a good media for the good quantity of groundwater availability. However, limited permeability in some locations was referred to the recent deposits comprise fine-grained sand and gravel, silty clay and gypsum (Al-Hamdani, 2009). According to (Sissakian and Al-Jibouri, 2012), a briefly describe the most important types of Quaternary deposits can be shown as the following:

2.4.4.1. River traces. Pleistocene-Holocene

Close to main rivers of the area, the deposits of multi layer represent multi seasons events with high and low precipitation. The calcareous, sandy and gypsiferous are the main cementing materials for the sediment gradients. In general, river traces is shown cross-bedding, graded bedding and channeling sedimentary structures.

2.4.4.2. Polygenetic deposits. Pleistocene-Holocene

The major composite of this deposits is silt, clay, sand and a mix of gypsum and iron, although the cementing materials are also from different sources. The average thickness is bigger than 1 m and most of these sediments are used for agricultural activities.

2.4.4.3. Slope deposits and alluvial fans. Pleistocene-Holocene

The source of these deposits is mainly from the mechanical erosion of the Bai Hassan Formation. Deposits can be found with the spatial distribution of slope deposits around the anticlines. A clear example of the alluvial fan can be found in the Qara Chauq anticline. With thickness varying from 1-8 m, this fan covering the surrounding area can be calculated as 15 km^2 based on the spatial resolution of satellite data.

2.4.4.4. Gypcrete. Pleistocene-Holocene

These sediments can be found in small locations, and they are representing high interaction with Ca-SO4. 2H2O especially close to the Fatha Formation deposits.

2.4.4.5. Residual soil. Holocene

Residual soil sediments can be found close to the main river areas, similar river traces sediment. The main component is mixed soil with calcareous, gypsiferous, sandy, silty and clayey sediments.

2.4.4.6. Sabkha deposits. Holocene

Mostly located to the south-west of the Kirkuk anticline. With a maximum thickness of 1-2 meters, the major components are clay and high salty.

2.4.4.7. Floodplain and valley-fill deposits. Holocene

These deposits are located close to the main rivers and their tributaries. It can be found as sand and silt eroded from the Bai Hassan Formation. Valley dropsies are formed mainly formed by gravels, sand and clay with 0.5- 3 meters as conglomerate accumulations. These deposits are located within the major rivers and their tributaries. It is found as eroded sand and silt from the Bai Hassan Formation. Valley deposits accumulate as conglomerate formed by gravels, sand, and clay with a thickness of 0.5- 3 m.

2.5. Crude oil and petroleum system in the north of Iraq

2.5.1. History and Finding

Iraq has the recent name of Mesopotamia, which means “the land between two rivers” in Greek. This location hosted several ancient civilizations like the Sumerian, the Akkadian, the Assyrian, the Babylonian and the Chaldean (Neo-Babylonian). The Eternal Fire is a gas seep that has burned for at least 4,000 years until now (Figure 9). Great cities were built with developing industries and agriculture. The use of oil and bitumen were known for various purposes, like building to resist erosion and for mortar, wars as well as art (Das, P.K., and Baruah, H.,1997). According to Connan, (1999), this usage can be considered as proving the presence of numerous seeps in Iraq (Figure 9).

At the beginning of this century, the seeps locations were the first evidence of underlining oil fields. Surface indications of natural oil and gas seeps are often recognized by local names such as naft, which is Arabic for oil; for example, NaftKhaneh (170 km south-east of Kirkuk city), NaftShahr and Masjed-Soleyman in western Iran, Ain Nafat, west of Baghdad, as well as Kirkuk and Qaiyarah. These areas were the reason behind the decision to drill the first exploration wells. The most important and largest single reservoir in Iraq is the Kirkuk oil field in the north-eastern part of the country. The early findings – such as the Baba Dome in the Kirkuk field and the Qaiyarah field – were enabled by the occurrence of hydrocarbon seepage at the land surface, indicating the potential for an underlying reservoir. The biodegraded petroleum seepage has long been recognized as an essential indicator in oil exploration (Link, 1952).

Figure 9: A left photo showing baked bricks and bitumen mortar of the ziggurat at Ur. 2100 B.C.E (Bible and Spade.2004). The picture to the right, Kirkuk Eternal Fire in Baba Dome 2015 (photographed by the author)

One of the first comments regarding the oil seeps was from the Austrian geologist Emil Tietze. In the year 1879, he noted in his paper: "*Near Kirkuk, TuzKurmatti and Kifri, one of the most important areas of the Old World is waiting for future exploration; once those areas, at present, still much too remote, will be made more accessible to European skill*." The first drilling took place in 1902 (Jassim and Goof,2006). The discovery well was drilled by the Turkish Petroleum Company. The Baba Gurgur-1 discovery well blew out with a column of oil some 40 m in height in October 1927 (Aqrawi et al., 2010). Seven hundred tribesmen were recruited to build a levee around the well to contain the oil, which created the river of oil (Figure 10). The well was finally brought under control after eight and a half days, flowing at a rate of 95,000 barrels of oil a day. Most of the other known oil fields in Iraq were discovered rather late, in the 1970s (Jassim and Goof,2006).

Figure 10: River of oil resulted from blowing out of the well in Baba gurgur area in 1935. The first discovery well was drilled by the Turkish Petroleum Company on October 15th, 1927 (Library of Congress)

2.5.2. Petroleum System

Iraq's oil fields together form a mega-reservoir that comprises about 10.4% (143 billion barrels) of the known oil resources worldwide (OPEC, 2015). According to (Al-Gailani, 1996), 526 structures have been classified as potential hydrocarbon prospects, which mostly concerned as elongated anticlines with length range from 1 to 110 km. The most essential petroleum systems in the north of Iraq are the Jurassic, Cretaceous, and Tertiary (Jassim and Al-Gailani, 2006) and significant source rocks in the basin occur in the Jurassic. The Middle Jurassic Sargelu Formation is one of the primary source rocks and has a good to excellent hydrocarbon generation potential.

The Kirkuk, Jambur, Bai Hassan, Khabbaz and Qaiyarah oil fields are located in the Foot Hill Zone (Figure 11). According to the Al-Ameri et al., (2006), the source rock has reached the oil window with a maximum temperature between 432 and 450°C. Beside Sargelu Formation, the Chia Gara and Naokelekan formations are described in the Kirkuk and Jambur fields as significant source rocks (Al-Ameri et al., 2006; Mohialdeen et al., 2013). The Chia Gara and Naokelekan formations were deposited after the Sargelu formation (Late Jurassic), therefore have seen less temperatures and maturity conditions (Al-Ameri & Zumberge, 2012).

Most of the reservoirs in northern Iraq are formed by limestone, as well as the selected oil field, which contains three main pay zones, i.e., Cenozoic limestone, fractured Late Cretaceous marls and limestone and the Middle Cretaceous limestone (Aqrawi et al., 2010). The Cretaceous and Tertiary oil and gas accumulations in the Mesopotamian Basin and Zagros fold belt are overlying mature Jurassic and Early Cretaceous source rocks, emphasizing the importance of vertical migration (Pitman et al., 2004). Beside Fatha Formation as most important caprock, in the basin center overlaying the fractured Late Cretaceous reservoirs, the main caprock formations are Aaliji, and parts of Jaddala Formations (Hart and Hay, 1974; El Zarka, 1993). Meanwhile, Jaddala Formations may also have reservoir potential in particular in the fractured parts (Aqrawi.2010).

2.5.3. Studied Oil Fields

The most prominent features in the study area are Kirkuk, Qara Chauq, Bai Hassan and Jambur anticlines. Accordingly, a brief explanation of these fields is provided in the following:

2.5.3.1. Kirkuk Field

The Kirkuk oil field is an anticlinal type and structure, covering an area of around 100 km in length and 4 – 6 km in width (Al-Rawi, 2015), making it the largest in Iraq and one of the world's ten largest oil fields (Kulke, 1994; OPEC, 2015). The Kirkuk field has a reserve of around 2.2 billion tons (Kulke, 1994), which is equivalent to 16 billion barrels when assuming an average density of 0.86 t/m^3.

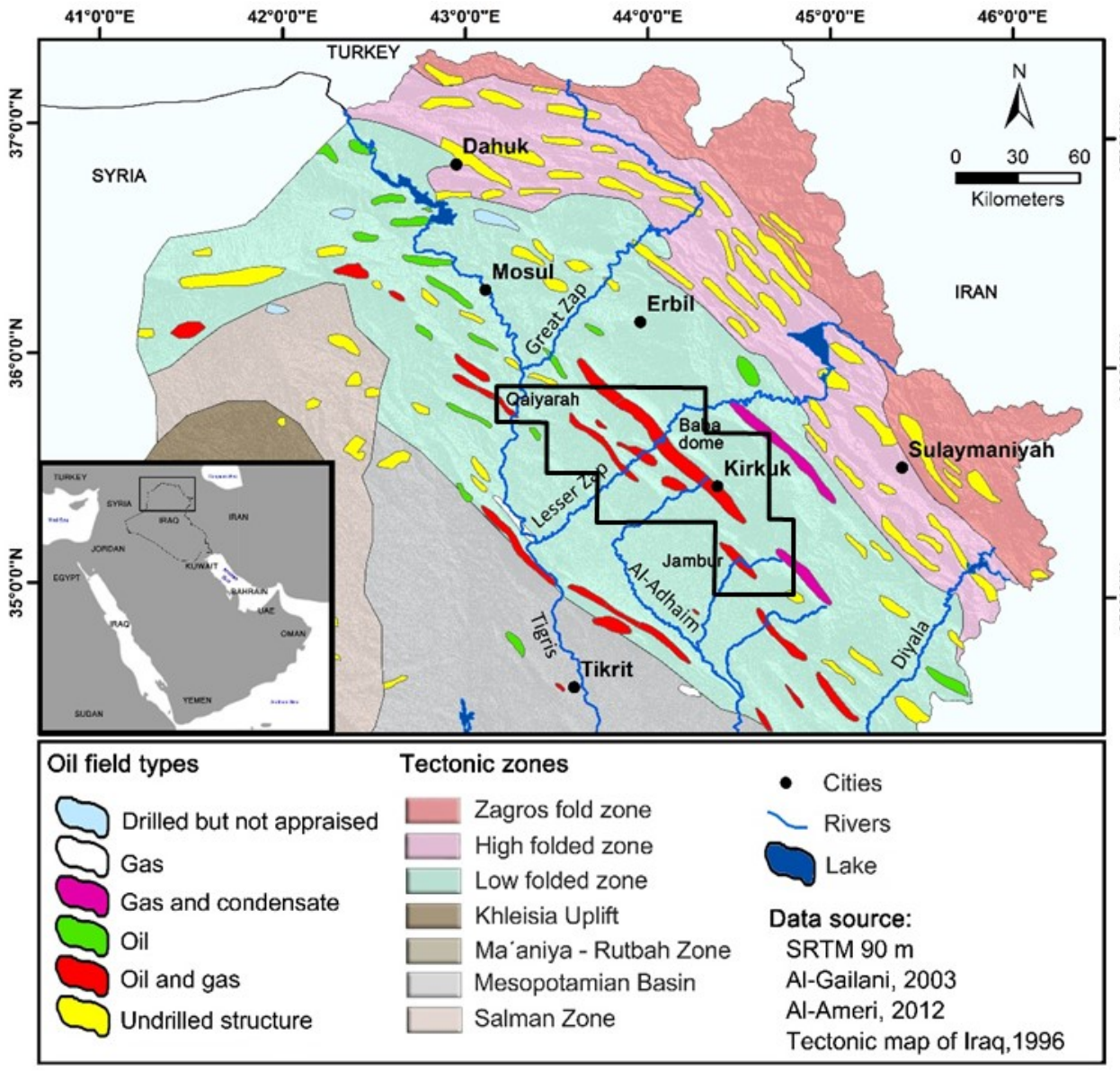

Figure 11: The location of the study area shown relative to the structural classes and oil field classifications in northern Iraq. The south-east of the Kirkuk -Baba Dome is shown in the satellite image

The Kirkuk oil field contains three main pay zones (Figure 12): Cenozoic limestone, fractured Late Cretaceous marls with limestone of Shiranish Formation, and the Middle Cretaceous limestone (Dunnington, 1958). Beside the Tertiary Reservoir, two smaller reservoirs from the Late and Middle Cretaceous exist. In contrast to the large Tertiary Reservoir, these two produces less (Al-Rawi, 2015). The producing Tertiary and Mesozoic reservoir lithologies of the are quite fractured carbonate rocks. Based on the seismic data, drilling records and many studies, the fractures are generally perpendicular to bedding (Majid &Veizer, 1986; Sorkhabi, 2009).

In general, Kirkuk anticline – with a northwest-southeast trending – is divided by two prominent saddles (Dibega and Amsha), which form three major domes (Figure 6): Khurmala, Avanah, and Baba (Majid and Veizer, 1986). With a length of 54 km, the oil reserve of the Baba Dome has a shallow depth, which

can reach 350 m from the base point of the Rotary table Kelly bushing (RTKB). With a length of around 27 km, the Avanah Dome can consider as a second largest hydrocarbon bearing dome in the Kirkuk field. The sampled depth in this structure starts at 400 m and ends at 1650 m RTKB. The final part of the Kirkuk anticline ends with the Khurmala Dome, with a length of around 18 km. The porosity and permeability of the surrounding carbonate rocks produce appropriate conditions for exploration (Jassim and Goof,2006). However, the water injection had been started in 1962 from different locations in the Kirkuk field to increase the production, which caused a rise of the oil/water contact (Al-Rawi, 2015).

According to geochemical analyses of Al-Ameri and Zumberge (2012) and Al-Ameri (2014), the oils in Kirkuk Embayment can be classified to three distinct families, which corresponding to a Triassic source rock, a Jurassic source rock and a mixed Jurassic-Cretaceous source system. Triassic oil family can be identified from Jurassic-Cretaceous oils due to the lower $\delta^{13}C$ values of Triassic oil (Naqishbandi et al., in press).

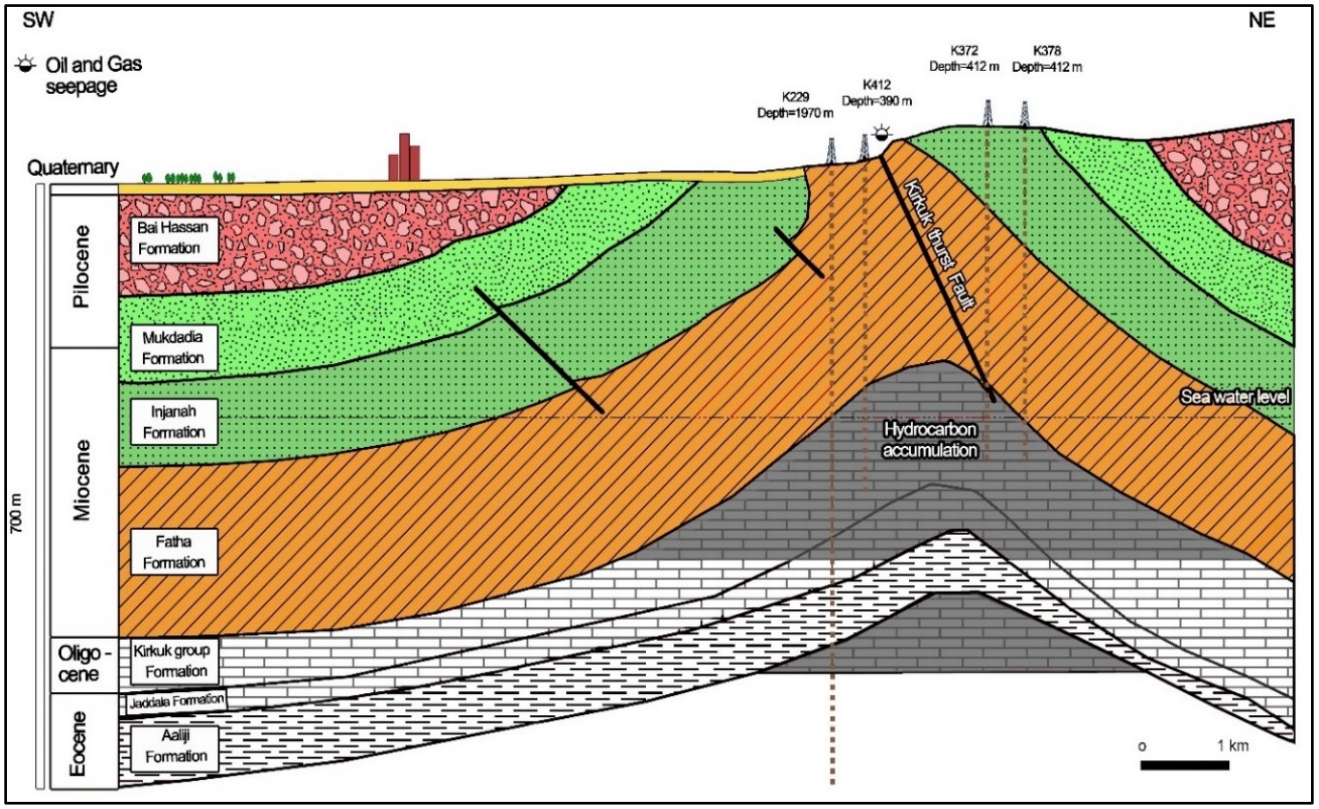

Figure 12: A geological cross section for Kirkuk anticline (Baba Dome). Modified after Dunnington (1958) with the using two seismic sections and well records (K 229, K 412, K 372 and K 378) provided by the North Oil Company, Ministry of Oil, Iraq. In this section, unconformity is found between Fatha and Kirkuk group formations (Sahib et al., 2016)

2.5.3.2. Bai Hassan Field

From the size dimension, The Bai Hassan oil field is the second place after Kirkuk field in the study area. It is located within 35 km SW of Kirkuk city. Similar to Kirkuk oil filed, the main producing horizons is the folded anticline of the Tertiary and Mesozoic carbonates (Al-Shahristani& Al-Atyia, 1972). The

sampled layers showed thickness range was between 1500 – 2000 m RTKB. The Garagu Formation – a lateral and facies equivalent of the Yamama Formation – is reported to contain oil in the Bai Hassan and Jambur fields in northern Iraq (Dunnington, 1967a; Al-Rawi et al., 1980).

2.5.3.3. Qaiyarah Field

The Qaiyarah oil field is located around 100 km NW of Kirkuk city and to the west of the Tigris river to the south of Mosul city. The main producing layers are also from a fractured Tertiary carbonate formation under the caprock (Fatha) Formation (Al-Ahmed, 2011). In this study, only seep samples were used for comparison purposes.

2.5.3.4. Jambur Field

To the south of Kirkuk field, The Jambur field is located. With depth between 1982 m to 3531 m RTKB, the sampling reaches to the deepest extent comparing to the other fields. Similar to the Kirkuk structure, the Bai Hassan and Jambur structures have an evaporite cap layer. The Jambur anticline located in parallel to the Kirkuk structure with 10-15 km away to the south-west (Kulke, 1994).

2.5.3.5. Khabbaz Field

The Khabbaz oil field is located to the east of the Kirkuk field (Fig. 6). Generally, the primary producing layer sequence is the dominant dolomites, limestones Late and Early Qamchuqa Formation, which is present in a 125 and 175-meter-thick column respectively (Al-Qayim et al., 2010). The sampled depth range in Khabbaz is from 2350 – 3050 m RTKB and comprises the whole reservoir sequence.

2.5.4. Crude Oil Seeps, Types and Mechanism

Worldwide, many hydrocarbon reserves have been identified on- and offshore. Anaerobic transformation processes produced oil in sub-surface rocks millions of years ago (Tissot and Welte, 1984). Natural oil leakages or hydrocarbon seeps were recorded on the surface. Due to pressure and geological pathways like fractures, faults and cap rock erosion, oil can find its way (vertical migration) to the surface naturally (Schlumberger, 2015). Furthermore, anthropogenic oil exploration processes result in seeps.

The source of natural hydrocarbon contamination of soil and water goes back to macro-seepage, which refers to visible (outflow) oil and gas seeps (Link,1952; Etiope, 2009) and micro-seepage, which can be described as invisible seeps caused by gas or less commonly a crude oil source (Macgregor, 1993). Based on geological controls, Link (1952) classified seeps into five groups: (1) seeps arising from the ends of homoclinal beds; (2) seeps associated with the beds and formations in which the oil was formed; (3) seeps from large petroleum accumulations that have been uncovered by erosion or from reservoirs ruptured by faulting and folding; (4) seeps at the outcrops of unconformities; and (5) seeps associated with intrusions such as mud volcanoes, igneous intrusions, and piercing of salt domes (Figure 13). In Iraq, many locations present very famous seeps, whereby the most dominant seeps types are 2 and 3.

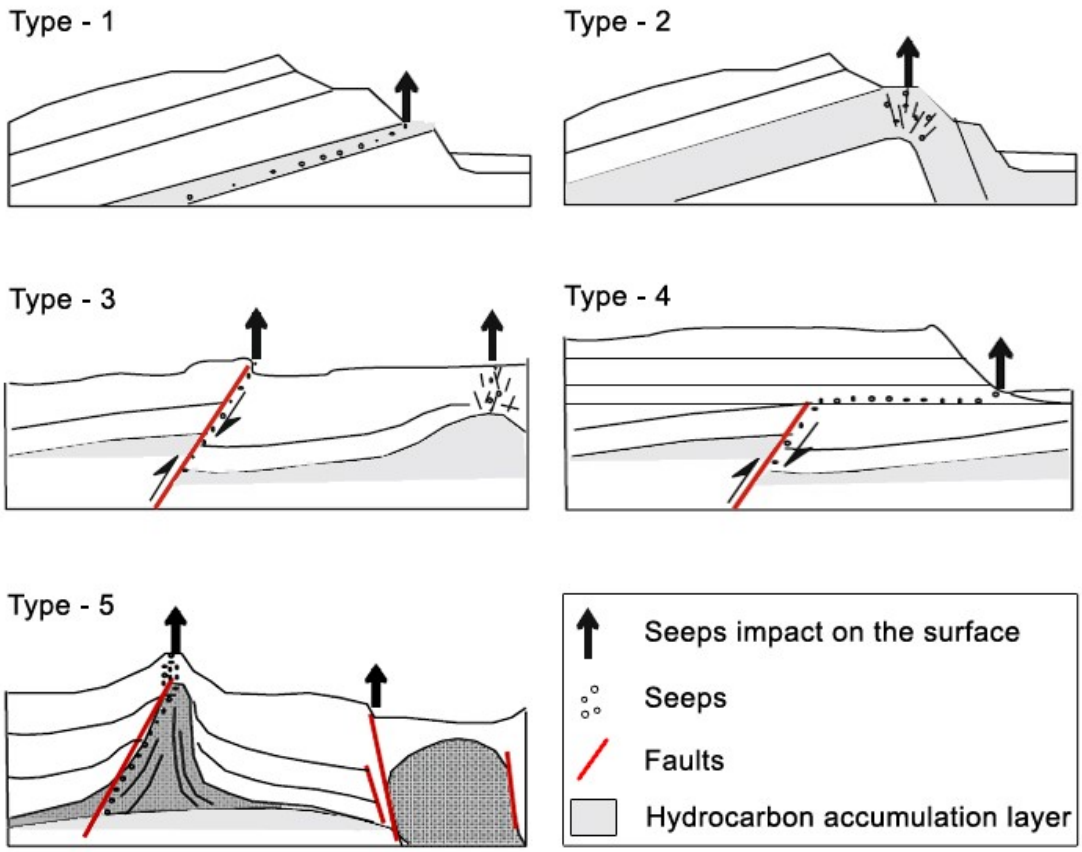

Figure 13: seeps types according to Link 1952 classification (Modified after Etiope, 2015)

The Kirkuk area as an AOI presents a good example of these natural crude types in addition to industrial seeps from pipes leakage or production. The rocks and soil alteration are the additional product of micro seeps, which represents an association of oxidizing petroleum seep, gypsum, jarosite, sulfuric acid and sulfur (Thomas, 1952; Clarke and Cleverly, 1991; Salati et al., 2013). The Baba area can be considered as a perfect location for many kinds of terrestrial hydrocarbon seeps. The outcrops of the Fatha Formation comprise gypsum, marble and limestone layers. Macro and micro seeps at the different locations were recorded as crude oil, heavy oil, asphalt, bitumen and sulfur springs (Figure 14). In addition, mineral alteration and bleaching of red beds are visible near gas seeps from field observation (Figure 15).
Hydrocarbons such as oil and gas are sensitive to field pressure and they respond by moving to areas of lower pressure horizontally, obliquely or vertically, according to the nature of the structure and permeability. With respect to the water injection for production purposes, the water content in an oil field also influences oil movement or migration due to oil density (Al-Banaa, 2012). The shallow depths of hydrocarbon accumulations and cap rock erosion of the Kirkuk and Qaiyarah – for example – can play a essential role in seep concurrency, where the production zone is less than 400 m from the surface for wells K 412 and K 378 in the Baba Dome (Figure 12). It is uncertain when the seeps first occurred, although Jassim and Goff (2006) speculated that the seepage activity began in the Middle Miocene and a substantial volume of oil has since been lost to the surface.

Figure 14: Macro Seeps examples, A and B in Qaiyarah. C and D in Baba Dome

Figure 15: Bleaching of red beds close gas seeps in Baba Dome, Kirkuk oil field

The seeps in the AOI appear to be mostly controlled by major north-south faults, by faults that cut to the surface in major anticlines (Pitman et al., 2004; Jassim and Al- Gailani 2006; Aqrawi 2010). Faults and other lineaments can be an important factor that increases the possibility of formation water, brine and hydrocarbon seepage to reach the shallow aquifer or even the surface. During the field survey along the Kirkuk anticline, various magnitudes of natural and industrial crude oil seepage have been recorded (Figure 16).

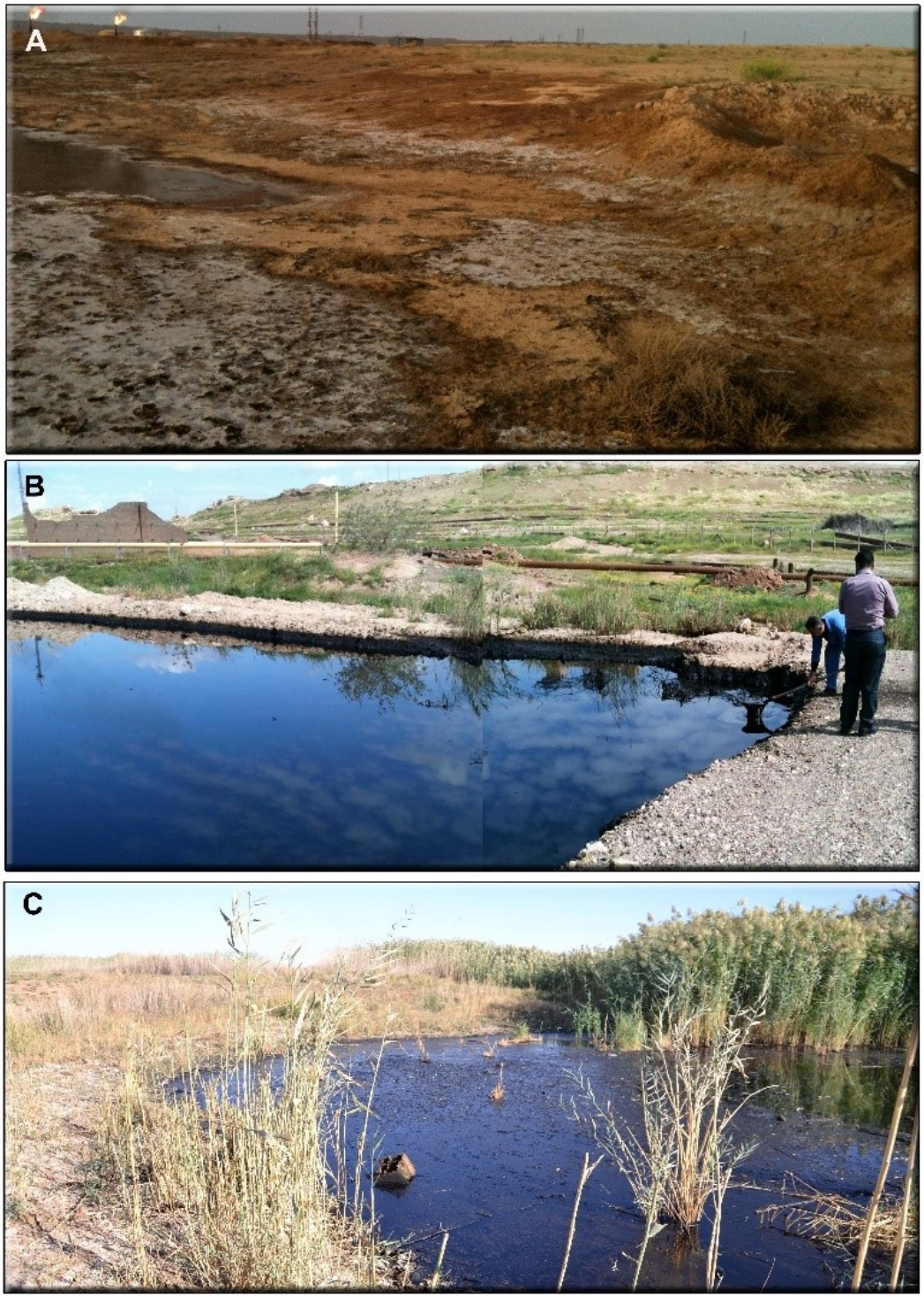

Figure 16: Industrial crude oil seepage examples (a) South-east of Jambur Field (B, C) Baba Dome

2.5.5. Polycyclic Aromatic Hydrocarbons (PAHs)

Crude oil is a complex mixture of hydrocarbons containing more than 17,000 compounds and the compositions of different oils have a high variety (Marshall and Rodgers 2004). According to varying properties of the hydrocarbon compounds, certain elements remain in the oil itself, some become air-borne vapors, while others form concentrations in soil and are dissolved in water. PAHs are relatively persistent in the environment, solid, non-polar, lipophilic and neutral (Manahan, 2010). As much as 10% of PAHs are covered by the organic compounds in crude oil (Vinas et al., 2010). Organic substances comprise a minimum of least two cyclic conjugated aromatic rings of carbon and hydrogen atoms. The basis of these aromatic rings is formed on the molecular composition of benzene, which is fused on at least one common edge (Table 2). The PAHs dissolving rate in water is from 0.00026 to 31.7 mg/l at 25°C. The decrease the water solubility level will happen when the number of rings increases. Additionally, the Solubility becomes more achievable at higher temperatures (Schwarzenbach et al., 2003). PAHs usually enter oceans and seas as a result of oil seeps and oil production processes despite their comparatively reduced ability to dissolve in water (Tedesco, 1985). Under the Chemical Abstracts Service (CAS) number 130498-29-2, hundreds of PAHs are registered and categorized as being pyrogenic or petrogenic PAHs. Petrogenic PAHs naturally occur in crude oil, while combustion processes (shared processes) of organic material form pyrogenic PAH, which occurs everywhere (Jacob, 2004; Feng et al., 2009). There are two categories of PAH, which classified as low molecular weight PAHs with fewer than four aromatic rings, and high molecular weight PAHs with four or more rings (Deutsche BP AG (1989). A number of PAHs demonstrates cancer-causing properties. Benzo[a]pyrene works as the primary substance of the cancer-causing effect of PAH mixtures (Jacob, 2004) and it is the most detailed common- studied PAH (Manahan, 2010). The high molecular weight of PAHs is particularly well-known toxins, carcinogens, and mutagens (White, 1986). Benz[a]anthracene, Chrysene, Dibenz[a,h]anthracene, Benzo[a]pyrene, Benzo[b]fluoranthene, Benzo[k]fluoranthene and Indeno[1,2,3- cd]pyrene have proven to cause cancer in tests conducted on animals (ASTM, 1998). The United States Environmental Protection Agency has recorded sixteen PAHs as priority pollutants, known as EPA PAHs (Keith & Telliard, 1979). In this part, twenty PAHs were investigated, including the EPA list (Table 2).

In 2001, a study published by Kerr et al., (2001) tested how many PAHs were contained in crude oils from 60 countries across the globe. The outcomes showed that in over 97% of the tested oil samples, the presence of Naphthalene, Phenanthrene, Fluorene, Chrysene, Pyrene, and Benzo[b]fluoranthene was recorded (Table 3). However, Acenaphthylene was not present in any of the 60 tested crude oils. It can thus be understood that low molecular weight PAHs will usually be detected in water that has been contaminated by oil. The anticipated amount of C for each PAH in the water was calculated using Raoult's law (Loyek, 1998; Schwarzenbach et al., 2003) (Eq. 1).

Table 2: List of all tested PAHs and their properties (in cooperation with Jenne, 2015)

Name	Acronym	Structure	Water Solubility (mg/L)	Molecular Weight (g/mol)	EPA PAH
Naphthalene	Nap	 a)	31.7 c)	128	Yes
2-methyl- Naphthalene	2-methyl-Nap	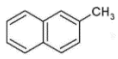 a)	25.4 c)	142	No
1-methyl- Naphthalene	1-methyl-Nap	 b)	28.5 c)	142	No
Acenaphthylene	Any	 a)	3.93 d)	152	Yes
Acenaphthene	Ace	 a)	3.93 c)	154	Yes
Fluorene	Fln	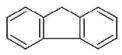 a)	1.98 c)	166	Yes
Phenanthrene	Phe	 a)	1.29 c)	178	Yes
Anthracene	Ant	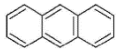 a)	0.07 c)	178	Yes
Fluoranthene	Fth	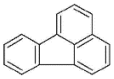 a)	0.26 c)	202	Yes
Pyrene	Pyr	 a)	0.14 c)	202	Yes
Benz[a] anthracene	BaA	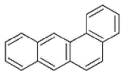 a)	0.014 c)	228	Yes
Chrysene	Chr	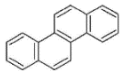 a)	0.002 c)	228	Yes
Benzo[b] fluoranthene	BbF	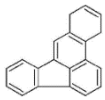 a)	0.0012 d)	252	Yes
Benzo[k] fluoranthene	BkF	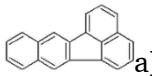 a)	0.00055 d)	252	Yes
Benzo[e] pyrene	BeP	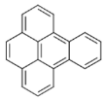 b)	0.0063 e)	252	No
Benzo[a] pyrene	BaP	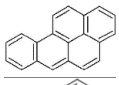 a)	0.038 c)	252	Yes
Perylene	Per	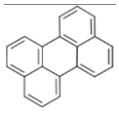 a)	0.0004 c)	252	No
Indeno [1,2,3 cd] pyrene	Indeno	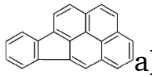 a)	0.062 d)	276	Yes
Dibenz[a,h] anthracene	DahA	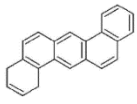 a)	0.005 d)	278	Yes
Benzo[ghi] perylene	BghiP	 a)	0.00026 c)	276	Yes

a) Palm, 2002; b) U.S. National Library of Medicine (2013); c) Mackay & Shiu, 1977; d) Sims & Overcash, 1983; e) Pearlman et al., 1984

C= χ. γ. S……. (Equation 1)

According to (Lane & Loehr, 1992), (Lee et al.,1992 a,b), the activity coefficient in the organic mixture γ was simplified as 1. Meanwhile, the mole fraction χ was calculated with the molecular weight M and mass m of each PAH and crude oil (Eq. 2).

X= m (PAH). M (oil) / M (PAH). m (oil).....(Equation 2)

Based on the literature, the molecular weights for the PAHs were taken. The molecular weight of the crude oils samples was not calculated and an overall value for each oil type was given that oil types have varying properties, where the light oil was set as 92.7 g/mol, medium oil as 108 g/mol and heavy and extra heavy oil as 135.5 g/mol (Loyek, 1998). Water solubility (S) – as a subcooled liquid – is valid for complex mixtures with solved solids. S is the water solubility and the temperature, which was not known. Therefore, the literature values for S were used for these calculations (Loyek., 1998).

Table 3: Results of a study dealing with the PAH content in oils by Kerr et al., (2001) (in cooperation with Jenne, 2015)

PAH	Minimum (mg/kg)	Maximum (mg/kg)	Mean (mg/kg)	Detection Frequency (%)
Naphthalene	1.2	3700	422.9	100
Acenaphthylene	ND	ND	ND	0
Acenaphthene	ND	58	13.9	80
Anthracene	ND	17	3.4	40
Phenanthrene	ND	916	176.7	98
Fluorene	1.4	380	73.6	100
Benz[a]anthracene	ND	38	5.5	67
Fluoranthene	ND	26	3.9	40
Chrysene	4	120	28.5	100
Pyrene	ND	82	15.5	97
Dibenz [a, h] anthracene	ND	9.2	1	47
Benzo[a]pyrene	ND	7.7	2	75
Benzo[b]fluoranthene	ND	14	3.9	100
Benzo[k]fluoranthene	ND	7	0.46	93
Indeno[1,2,3-cd] pyrene	ND	1.7	0.06	7
Benzo[ghi]perylene	ND	9.6	1.53	63

ND: Not Detectable

2.6.Hydrological description

Iraq has two main rivers, the Tigris and Euphrates. However, a tiny percentage of the agricultural areas of Iraq have utilized the water of these rivers and their tributaries, which represent river valleys in the north part of Iraq as well as the central and south part from the Mesopotamian Basin (Jassim & Goff, 2006). Several global and regional factors lead to reduced water resources, e.g., global warming and numerous recent dams on the Tigris and Euphrates in Turkey and Iran.

2.6.1. Hydrology

The study area is located in general to the east of the Tigris river between the Great Zap and Diyala rivers from the north and south, respectively (Figure 11). The catchment of the Lesser Zab river is located at an altitude of around 3,000 m asl on the eastern part of the Iranian Zagros Mountains. The Lesser Zab river flows in Iraq for approximately 402km before joining with the Tigris river north of Beji city in the Saladin governate. The Lesser Zap river and three other streams – Khassa Su, Tawooq Su and Aq Su – are the main surface water channels in the study area, which cut Kirkuk, Bai Hassan, Qara Chauq and Jambur anticlines at an almost perpendicular angle. Khassa Su is a seasonal river (stream) that springs from the mountains in the Chemchamal areas (Figure 6). It is the only river that crosses Kirkuk city, although this river has become dry with only occasional flow depending on precipitation events. Additional to the groundwater wells, the irrigation projects partly use the Lesser Zab river by pumping through different types of channels (Al-Hamdani, 2009).

2.6.2. Hydrogeology

Only 25% of the need for fresh water for domestic use and irrigation is provided by the main two rivers in Iraq, namely the Tigris and Euphrates. Meanwhile, the other 75% of the country's need comes from groundwater (Krasny et al., 2006). Major rivers such as the Al-Adhaim and Lesser Zab flow through the Foothill areas and contribute significantly to direct and indirect groundwater recharge, especially during dry periods (May to October). The joint aquifer system is present in the Tertiary and Quaternary deposits which are often hydraulically connected to the carbonates rocks (Jassim and Goff, 2006). In the same time, the groundwater and surface water are connected in many locations, especially in the upper catchment area. Based on UN-ESCWA and BGR (2013) such connection can be determined through the discharge of groundwater from aquifers carbonate formations and the shallow aquifers.

In general, and due to the porous and permeable rock types, the main aquifers in the study area are Bai Hassan, Mukdadia and Quaternary aquifer systems (Table 4). Mukdadia and Quaternary aquifer were recorded as confined in some locations where the groundwater flows under artesian pressure to the surface in some wells (Lopez-Geta, 2006). With an estimated 22%-25% of rainfall infiltrates, 90% of the

2,000-3,000 wells in the area are explaining the depth of Bai Hassan system around 200 m from the surface (UN-ESCWA and BGR., 2013).

Table 4: The characteristics of the main formations and aquafers in the Kirkuk area

Formation name	Age	The range of thickness. [a b, d, f]	Hydraulic conductivity	Hydrocarbon reservoirs
Recent deposits	Quaternary	10–100	Low	No
Bai Hassan	Pliocene	30–1100	High	No
Mukdadia	L. Miocene-Pliocene	50–500	High	No
Injana	L. Miocene	20–350	Medium	No
Fatha	E-M. Miocene	100–500	Low	Low Local accumulation
Kirkuk group	E-M. Oligocene	18–100	High [c]	Yes
Jaddala/ Avanah	Eocene	350	-	Yes

a. NOC drilling reports, b. Sissakian and Fouad (2014) & (UN-ESCWA and BGR., (2013), c. Aqrawi et al., (2010), d. Jassim and Goff (2006), f. Alsharhan and Nairn (2003).

The crude oil seeps are a severe contamination threat to the groundwater resources located between the oil reservoirs and the surface. Therefore, seeps may contain high concentrations of hydrocarbons, heavy metals or salts, making the groundwater unusable. Such contamination of groundwater by oil field brines has been shown at various hydrocarbon reservoirs worldwide (Mast, 1985; Dutton et al., 1989; Zhang et al., 2009; Gleason and Tangen, 2014; Heston, 2015). On the other hand, the detection of trace elements in groundwater can indicate or verify the presence of pathways between the reservoirs and the surface. The groundwater has high salinity in shallow groundwater aquifers in the Kirkuk region, which are used for irrigation and domestic water supply. As one from the main aims in this study, the challenge is to distinguish between contamination from uprising oil field brines and from brines derived from water-rock interaction in the Fatha cap rock Formation, as suggested earlier (Sadiq, 2008; Saud, 2009; Khanaqa and Al-Manmi, 2011). Both can contribute to increase the salinity and thus make the groundwater unsuitable for use.

The exploitable saturated thickness of the Bai Hassan and Mukdadia aquifer systems is estimated up to 1100 m and 500 m, respectively, while the thickness of Injana and recent Quaternary deposits can reach 350 m and 100 m, respectively (Table 4). The transmissivity range of the Mukdadia, Bai Hasan, and Quaternary aquifers is between 3 - 728 m^2\day (Saud, 2009). Generally, it is difficult to define unconfined, semi-confined and confined conditions between the studied aquifers due to lithology differences. However, additional variable permeability and lateral/horizontal changes in the lithology of basin deposits often result in highly variable productivity.

Depending on the geology, structure and topography of the area, groundwater aquifers have shown some differences in depth, flow direction as well as water types. The Baba Dome and the Kirkuk anticline in

general, divide the area into two sub-basins (Saud, 2009). The first basin is located to the north-west of the Kirkuk anticline and the second basin to the south-west. Both basins are cut by the Lesser Zab river ,and different water types are found in intergranular aquifers with medium to high productivity (Bai Hassan, Mukdadia, and Quaternary deposits). According to (Araim 1990), the groundwater is defined by two types. The water type of the first basin is 87% Ca-HCO_3 and 13% Ca-So_4 and Na-So_4. The second basin contains Na-So_4 as dominant water with 78% and 22% Ca-So_4 & Mg-So_4, respectively. The water variations refer to the effects of evaporates dissolving from the Fatha Formation, especially near the Baba Dome where many sulfur springs can be found.

The data of Gravity Recovery and Climate Experiment (GRACE) was used to monitor the equivalent water height (EWH) of the shallow groundwater with millimeter scale (Mulder et al.,2015). NASA and the German Aerospace center introduced GRACE as a joint mission measuring earth gravity and mass exchanging of the earth's surface. Monthly repeat cycle for an optimal solution was used to GRACE data from March 2004 to 2016. Figure 17 shows the equivalent water height of the groundwater, which explains the mass decline in the groundwater storage starting from 2007. This depletion can be demonstrated due to the growth in dam numbers in Turkey, which provide less surface water to Iraq and the AOI. The other important factor refers to the upper groundwater aquifers of the area, which mainly depend on the sustained groundwater pumping and less on precipitation, which recorded drought years especially between 2007 and 2009.

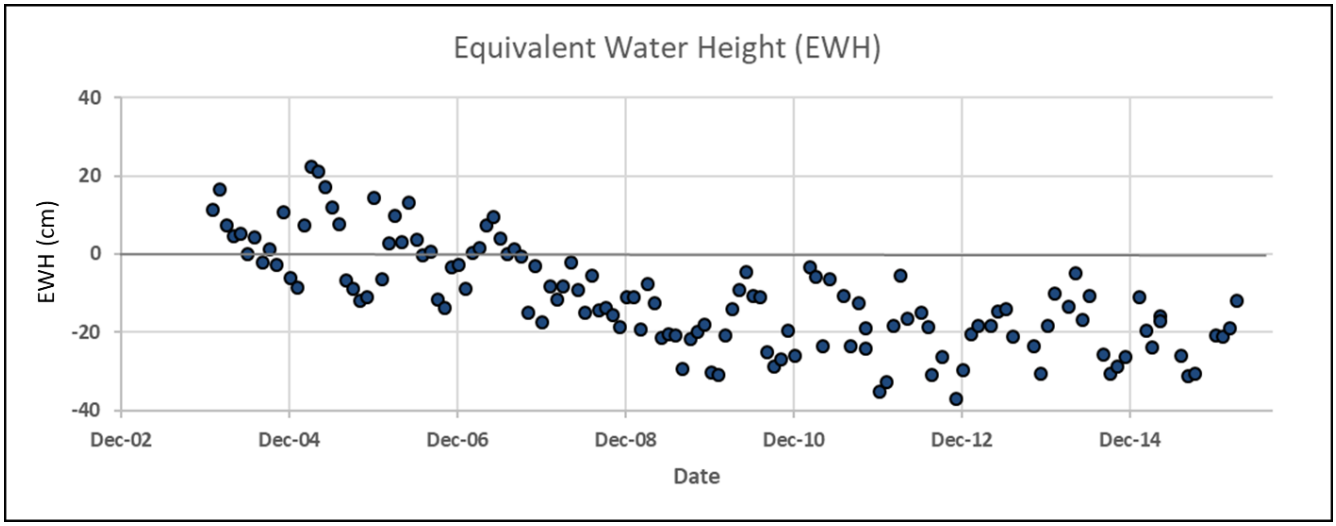

Figure 17: GRACE data, showing the equivalent water height of the groundwater in Kirkuk area starting from 2004 – 2016

2.7. Climate conditions

The climate plays a vital role in the hydrological cycle, where the intensity and long duration of precipitation influence water infiltration downward to groundwater aquifers and fill surface water basins. Historical data series of precipitation from the country base between 1960 to 2015 explains the average rain depleted during this period (Figure 18). On the other hand, the historical temperature from

1960 to 2015 explains notable increases in temperature (Figure 19). The summer temperature – from June to September – reaches 50°C to the south of Iraq and decreases towards the higher elevation in the north. The winter months record (between November and April) shows an average temperature of around 8°C, and it decreases to below zero to the north part of Iraq.

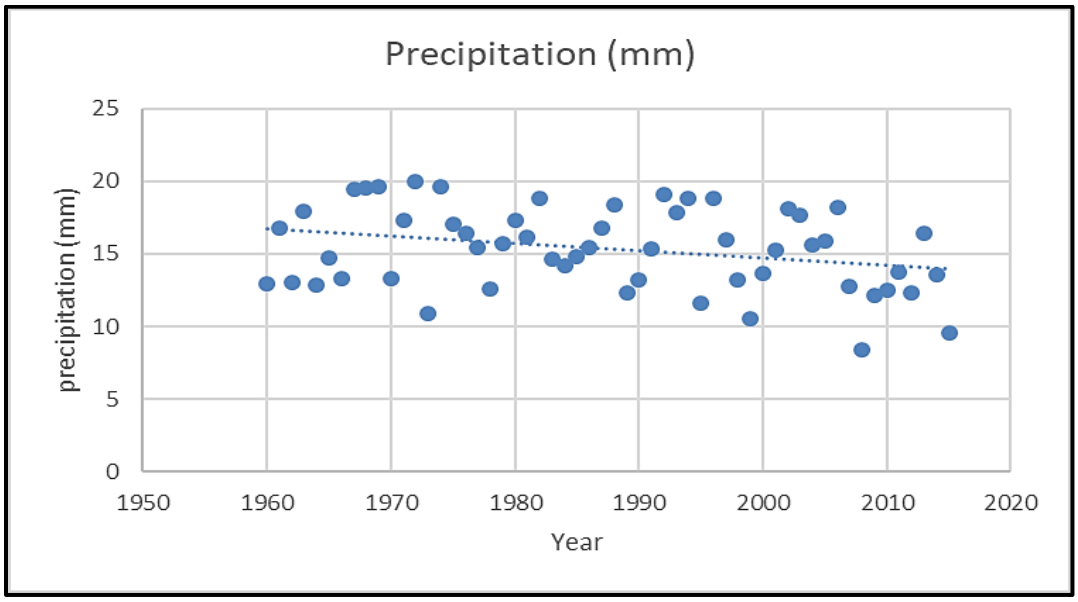

Figure 18: The historical average monthly (1960-2015) precipitation (NOAA's National Climatic Data Center)

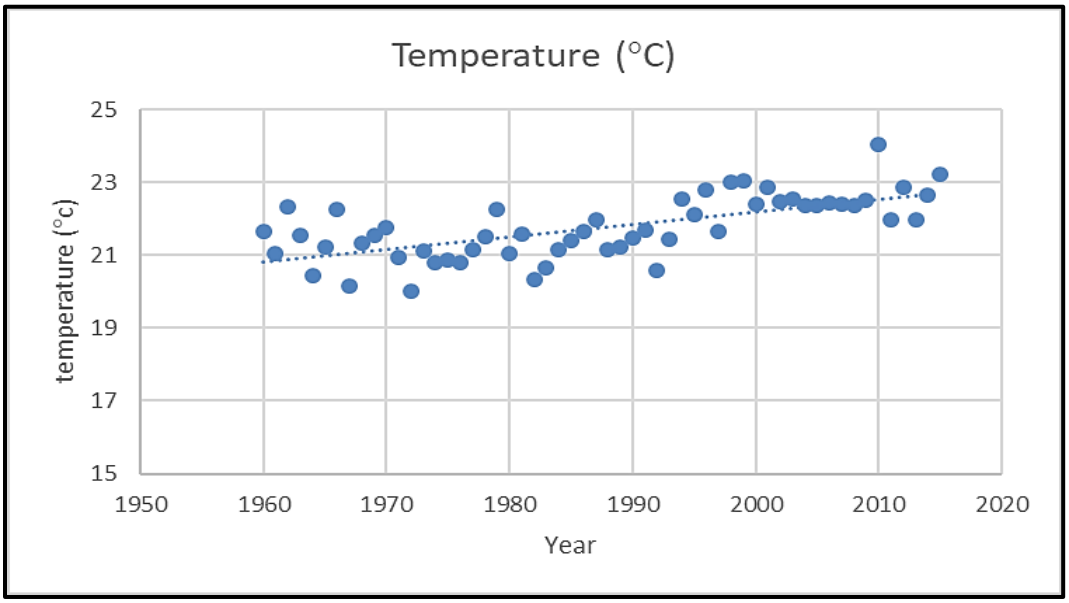

Figure 19: The historical average monthly (1960-2015) temperature (NOAA's National Climatic Data Center)

According to the last update of the Köppen-Geiger classification (Kottek et al., 2006) and data from the Kirkuk meteorology station as well as data of NOAA, the climate in the region is categorized as very hot and semi-arid (BSh). To identify the seasonal variations and linkage of these variables in the study area, the Kirkuk climate station was used to determine the climatic situation of the region as the closest climatic stations to the study area, which is characterized by accurate detailed data for long periods of

time. The average annual rainfall is 360 mm, and rain falls mostly in the winter months (Jassim & Goff, 2006). Meanwhile, the wettest months with an average annual rainfall of 45 mm are in the winter months between November and March, with a minimum temperature of around 5°C (Figure 20).

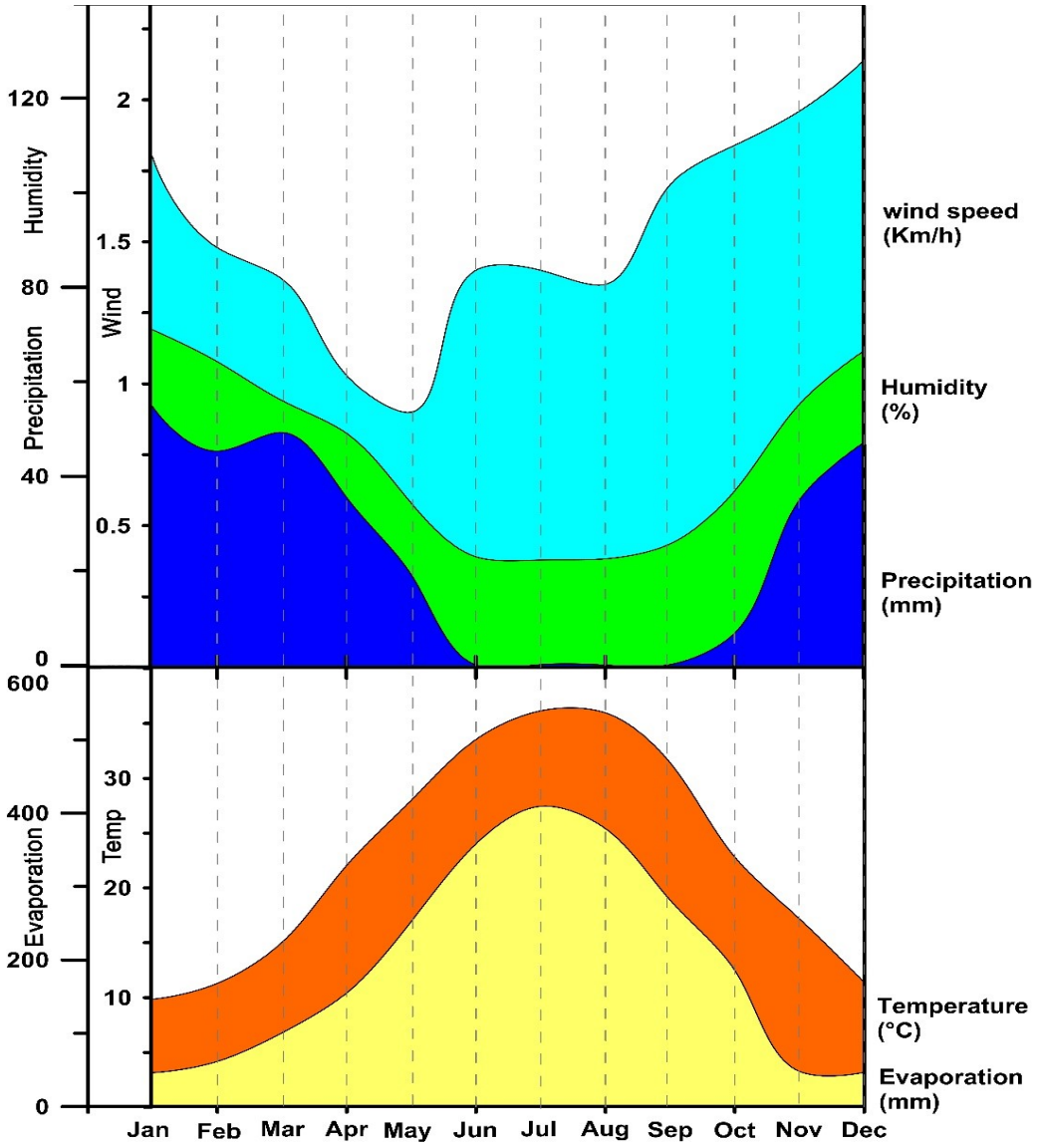

Figure 20: The monthly average of weather data of Kirkuk area (2002-2018)

Within the summer period, the mean annual precipitation is almost zero. The mean annual temperature is 21.6°C, and the potential evapotranspiration often exceeds 450 mm in summer. In the same months, the average air temperature reaches a maximum level of around 39°C. The average monthly rate of evaporation is the highest in July and August (403 mm a-1). The wind speed averages around 1.6 m/s, while the dominant wind directions are north-east and west (Kirkuk weather station).

2.8. Remote sensing applications in the identification of hydrocarbon contamination

Remote sensing has been a common technique to identify petroleum contamination offshore and onshore on a large scale for many years (Salem et al., 2005; lamoglia and Filho, 2011). Reflectance spectroscopy and statistical models have been used to investigate the spectral properties of hydrocarbons and quantify element concentrations on land from spectra absorption features (Wendlandt and Hecht, 1966, Kortum, 1969).

Various models have been used to analyze absorption features for water, black carbon and tar sand (Charette, 1976; Clark and Roush, 1984; Short et al., 2006). Cloutis (1989) identified several absorption features in the near-infrared reflectance as hydrocarbon spectra. Several studies with different techniques explain a widely-varying detection limit (DL) of 0.1-4 % of organic compounds in soils or sand (Schneider et al., 1995, Zwanziger and Heidrun, 1998) and bitumen in tar sand (Cloutis, 1989), while grain size seems to have a significant impact on the DL. When diesel and gasoline are used as a contaminant, the DL is around 0.1-0.5 % (Zwanziger and Heidrun, 1998).

Hyperspectral sensors – e.g., HYMap – were successfully applied to detect hydrocarbons and oil-contaminated soils with more than 2.5% (Hörig et al., (2001). Kühn et al., (2004) developed a simple hydrocarbon index (HI) from the absorption of the reflectance of spectral wavelengths. Additional studies have found a positive correlation between HI and total petroleum hydrocarbons (TPH) in soil (Kvenvolden and Cooper, 2003). Clark et al., (2009) used hyperspectral spectroscopy data (0.35-15.5 μm) to characterize and quantify hydrocarbons (Alkanes). Clark et al.'s (2009) study explained the absorption peaks including the absorption bands within 1.2, 1.7 and 2.31 μm considering that hydrocarbon compounds from oil generally increase the carbon concentration in soil and thus the total organic carbon (OC) concentration, whereby measuring the OC can reveal oil contamination in soil. However, determining the source of OC (as a crude oil origin or not) using remote spectral methods is complicated, because: i) the soil OC can be associated with a complex mixture of compounds with different polarities (Schwartz et al., 2012); ii) the soil mineral composition and various moisture levels can influence the hydrocarbon absorption; and iii) the HI can be calculated with different models, which may deliver different results. Therefore, during this current study, all of these compounds are covered.

Lineaments features in the cap rock over the oil fields may create pathways for formation water, brines and hydrocarbons to the shallow aquifer systems and the surface. Therefore, the detection of such features can be an essential addition to understand the seeps mechanism in the AOI. However, very few publications discuss the issue of hydrocarbon contamination sources and their effects in this area because the available studies were concerned more with detecting the rocks alteration over the oil fields in the study area to locate spectral anomalies associated with hydrocarbon leakage in rocks or sediments (Perry and Kruse,2011; Al-Banaa, 2012).

3. Materials and methods

3.1. Organic chemistry properties approach to correlate seepage and reservoir crude oil

3.1.1. Crude oil samples

Sixty-nine crude oil samples from the Kirkuk, Bai Hassan, Khabbaz and Jambur oil fields have been collected to study the Tertiary and Cretaceous petroleum systems (Figure 21). With various visible density levels, the seeps oil samples have been collected in outcrops of the E. Fars Formation to study their origin and migration path and link them to the neighboring fields. The samples were stored in a cool and dark place during the shipping until they were processed. At the Institute of Geology and Geochemistry of Petroleum and Coal, RWTH Aachen University, Germany the samples tests were conducted and prepared.

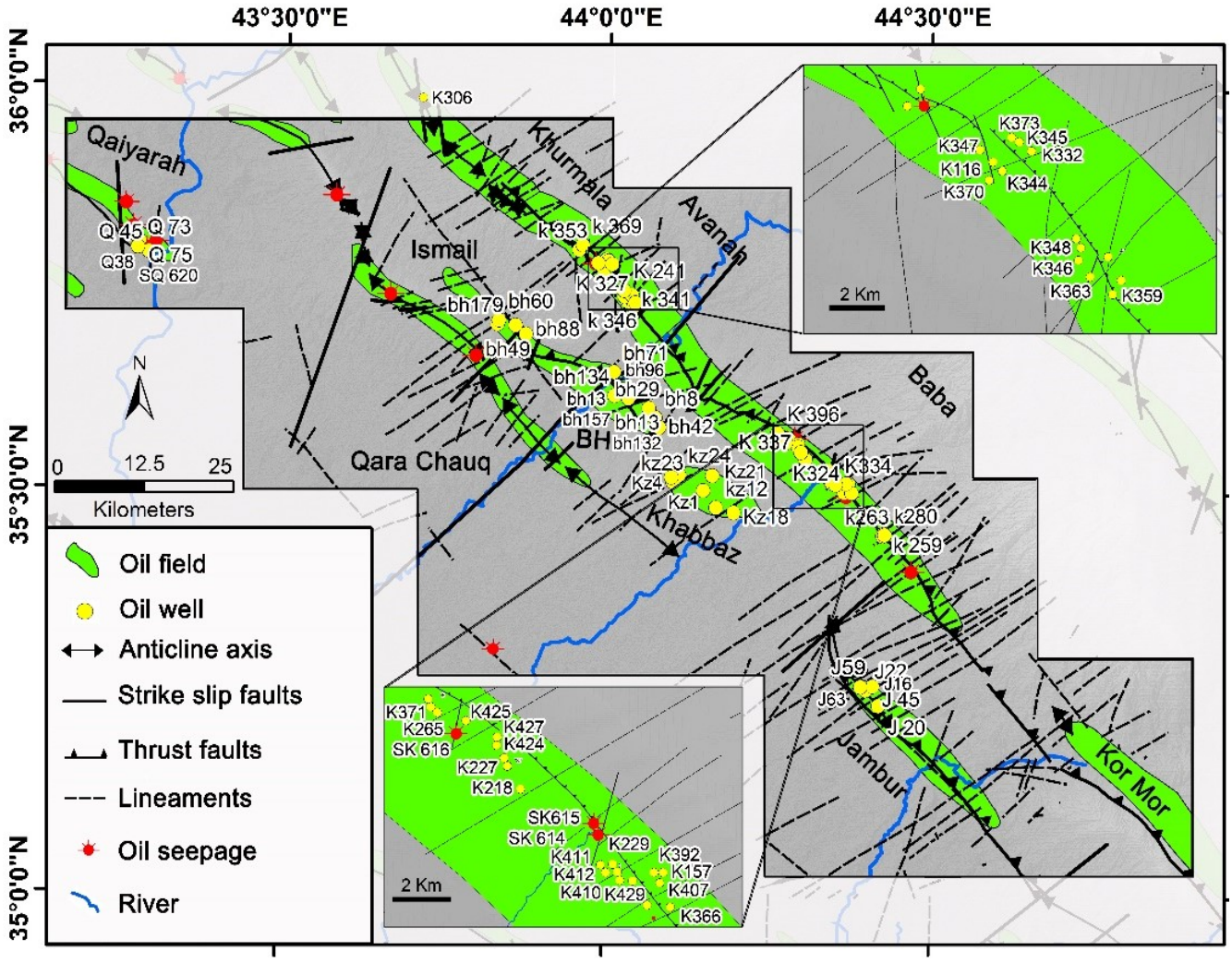

Figure 21: The distribution of the selected oil fields and recorded surface seeps with the main faults and lineaments

3.1.2. API gravity and density

The American Petroleum Institute (API) gravity shows the density of crude oil compared to water. It can be calculated in a pycnometer by density determination of cooled samples (ASTM D287 – 92, 2006). The pycnometer gets filled with sample materials of a given volume. With the using a water bath, the pycnometer will be warmed up until reaching a stable temperature of 15.6 °C for 30 minutes (Hunt, 1996). After removing the pycnometer, it gets be closed with a glass stopper. The included oil rises until it reaches the top leakage point. The pycnometer weight was measured a second time and the API gravity get calculated according to Eq. 3-5 over the sample density (Eq. 3-5).

$$\rho = \text{massofsample}[g]/\text{volume}\ [cm^3] \quad \text{(Equation 3)}$$

$$SG = (\rho - 0.001205)/(\rho(H_2O) - 0.001205) \quad (SG = \text{specific gravity}) \quad \text{(Equation 4)}$$

$$\text{APIgravity} = 141.5/SG - 131.5 \quad \text{(Equation 5)}$$

According to the following rules the oil was classified: API gravity > 31.1 = light oil; API gravity between 22.3 and 31.1 = medium oil; heavy oils have an API gravity between 22.3 and 10; and extra heavy oils have an API gravity < 10.0, which is also the API gravity of water.

3.1.3. Sulfur content

The sulfur content was analyzed with a SPECTRO X-Lab 2000 Sulfur Determinator. By burning the sample in the combustion chamber a flow of oxygen, oxidize the sulfur to SO_2. The resulting SO_2 content can be calculated by IR absorption and is correlating to the sample weight.

3.1.4. Thin-Layer Chromatography-Flame Ionization Detection (TLC–FID)

The relative composition of each crude oil sample was measured simultaneously - as a set of 10 chromarods - with a TLC-FID IATROSCAN (MK-5) and comprise spotting, production and heating. According to Abeed et al., (2012), Schwarzbauer et al., (2000) and Amijaya et al., (2006), the elution procedure was conducted by filling with *n*-Hexane and the set remains in the solvent for 35 min to mobilize the saturated hydrocarbons (*n*-alkanes, iso-alkanes and cycloalkanes).

After being air dried for 2 min, the toluene was used for 14 min to separate aromatic hydrocarbons (mono-, di- and poly-aromatic). Meanwhile, the third container with a mixture of dichloromethane (DCM) and methanol of 93:7 v/v mobilizes the polar components, especially molecules that contain nitrogen, sulfur and oxygen (NSO) and asphaltenes. However, an IATROSCAN analysis was not possible for some seepage samples due to the high viscosity of some samples. Each IATROSCAN run contained five samples, which were measured simultaneously. Therefore, to ensure comparability, the first sample

was measured in every process and gives a failure of +/- 5 %, with single outbursts of up to 9 %. Furthermore, each sample was analyzed twice.

3.1.5. Compound fractionation, Gas-Chromatography (GC), GC–Mass Spectrometry (GC–MS) and GC– Flame Ionization Detector (GC-FID)

Liquid saturated fractions of the samples were analyzed in a sector field mass spectrometer. The analyzer comprises an electrostatic sector field, which speeds up the emitted ions in a magnetic sector field, to separate the ions by their m/z (mass/charge) ratio. The divided ions with a necessary degree of m/z can pass the magnetic field and can be analyzed by spectrum detectors. In order to analyze every common m/z ratios, the internal magnetic field changed its force in a regular pattern. The electrostatic, as well as the magnetic field set up, are located in a vacuum, that let the ions to react only to the field within the mass spectrometer and according to their chemo-physical behavior, which is triggered by the electrostatic and magnetic fields.

Finally, the flame ionization detector (FID) with an including Gas Chromatograph (GC) analyze the organic components of a liquid sample. To guarantee the comparability for each measurement 1 μl sample liquid was used. The first fraction – which represents the aliphatic compounds – of selected samples was measured. Programmed for the temperature steps was a 60 to 300 °C at a rate of 3 °C/min, with a 20 min isothermal over 300 °C.

3.1.6. Carbon preference index (CPI), Odd-even-predominance (OEP) and the terrigenous/aquatic ratio (TAR)

A combination of OEP and CPI - up to five odd- and even-numbered *n*-alkanes - gives a good overview of odd/even *n*-alkane predominance. CPI is sensitive to the maturity, biodegradation and the petroleum source, depending on which alkanes have entered into the petroleum and in which relative quantity (Eq. 6). Organic matter input can influence a preference for odd- or even-numbered *n*-alkanes. Several options can control single parameters, but only one combination of several parameters can give a clear statement about thermal maturity (Peters et al., 2005).

$$CPI = \frac{2\,x\,(nC23 + nC25)}{2\,x\,nC24 + 2\,x\,nC26} \quad \text{(Equation 6)}$$

Another indicator for thermal maturity is the OEP, but – similar to CPI- it depends on the organic matter input. OEP is further flexible than the CPI because any n-alkanes can be used separately, without concern to the chain length (Eq. 7). The OEP values can be interpreted in the same way as the CPI dataset (Peters et al., 2005).

$$OEP = \frac{\sum_{8}^{34} nCx+1}{\sum_{8}^{34} nCx+2} \quad \text{(Equation 7)}$$

TAR contains three odd-numbered abundant biomolecules, which can be mostly deducted from algal and higher land plants. Low values of TAR can be interpreted as marine-derived organic matter. Influences on the parameters can occur from thermal maturation and biodegradation. Disproportionate weight assignment is created by a higher input of land-plant organisms too. Therefore, a favoring ratio of an aquatic milieu is even more remarkable (Peters et al., 2005) (Eq. 8).

$$TAR = \frac{nC27+nC29+nC31}{nC15+nC17+nC19} \quad \text{(Equation 8)}$$

3.1.7. Polycyclic Aromatic Hydrocarbons (PAHs) in natural crude oil and seeps

External and internal standards hold a significant position in controlling the quality of batch experiments. External standards were tested with the different concentrations ranging between 1.667 $\mu g/l$ and 161.391 $\mu g/l$ for 1-Methyl-Naphthalene. To make the quantitative analyses without knowledge about the exact injection volume, internal standards were used. With each sample, an internal standard with the deuterated PAHs Naphthalene d8, Acenaphthene d10, Phenanthrene d10, Chrysene d12, and Perylene d12 were added. Nine oil samples were chosen based on a variety of API gravity differences. Among these samples, three samples were representing the seeps oils from the Baba and Qaiyarah areas.

3.1.7.1. Determination of PAHs in the crude oils

By using cyclohexane, PAHs can be solved directly from the oil to its hydrophobic and organic solvent properties (Loyek, 1998). Pre-tests have found the most favorable ratio of oil and cyclohexane, which was 1:100. 0.1 ml of the internal standard was added to the oil-cyclohexane mixture, enabling the quantitative analysis. All mixtures were stored in a dark place after having been in the ultrasonic cleaner for five minutes. No remaining oil particles were obvious in any sample once the oil had been solved. After a number of days (6-12 days), the mixtures were made ready for the aromatics to be separated from the oil-cyclohexane solution. The supposed high levels of other oil components that could contaminate the GC-MS column required the separation of the aromatics from the oil-cyclohexane mixture. The aliphatic and aromatic compounds were separated using a 10 ml burette. The column was packed with 3g of silica gel, 1g of sodium sulfate (Na_2SO_4) and mineral wool. Four methods with various solvents had their differences evaluated in the pre-tests. In the chosen procedure, the column was moistened with 10 ml *n*-heptane. The burette stopcock of was opened to a point where only 1 ml of *n*-heptane remained above the layer of Na_2SO_4. 1 ml of the oil-cyclohexane mixture was subsequently added to the face of the filter. 10 ml of *n*-heptane were used as transportation fluid to separate the aliphatic compounds. Then, 10 ml of dichloromethane were added to dissolve the aromatics and transport them through the column. A DryVap Concentrator System tested the concentration of the outflow and it was tested with the GC-MS.

The procedure for the separation was founded on demonstrated separation processes for crude oils and it was altered (compare Priemon-Storer & Cornillot, 1985; Speight, 1999). In this study, the dichloromethane was used as a solvent for the aromatics. The dichloromethane has good solvent properties and it is less toxic than benzene. However, such a procedure is not similar to the literature. A comparison of the color of an oil sample before and after the separation is shown in Figure 22.

Figure 22: Oil sample Q 73 before separation, picture to the left, and after the separation right picture. (in cooperation with Jenne, 2015)

3.1.7.2. PAHs Gas Chromatography-Mass Spectrometry

The assessment of all samples and external standards was conducted by gas chromatography-mass spectrometry (GC-MS) operated in the Selected Ion Monitoring (SIM) mode. The target PAHs in the samples were recognized by comparing their retention time correlated to that of the standards. In Table 5, the details and conditions of the GC-MS analysis are outlined.

The software Agilent Technologies Enhanced MSD ChemStation E.02.02.1431 was used for the assessment and all PAHs peaks of the samples and standards were integrated manually in an identical manner. The mass of a specific PAH in a sample was calculated using the external and internal standards equations (9-10):

$$m(PAH) = \frac{A(PAH).m\ (internal\ standard)}{A(deuterated\ PAH).rf} \quad \text{(Equation 9)}$$

$$rf = \frac{A\ (PAH\ in\ external\ standard).c\ (deuterated\ PAH)}{c(PAH\ in\ external\ standard).A\ (deuterated\ PAH)} \quad \text{(Equation 10)}$$

m(i) mass of the compound I, A(i) peak area of the compound I, c(i) concentration of the compound i

The observation of PAH levels in crude oil differed from how many PAHs were in oil, as cyclohexane does not solve all PAHs. Thus, the actual PAH content in the oil to calculate the concentration by Raoult's law is not known. Nevertheless, the results were suitable for contrasting the structure of the crude oils with each other. For similar tests, it is recommended that all mixtures are prepared three times to ensure that potential inaccuracies are as low as possible.

Table 5: The used GC-MS setup and condition for PAHs analyses (in cooperation with Jenne, 2015)

Gas chromatograph	**Agilent Technologies 7890A**
Column	ZB-5MS (phenomenex), 30 m (+10 m) x 0.25 mm x 0.25 μm
Oven program	75°C (3 min), ramp 20°C/min to 235°C hold 18 min, ramp 15°C/min to 300°C hold 10 min, ramp 10°C/min to 320°C hold 2 min. Total time: 47 min
Detector	Mass Spectrometry: Agilent Technologies 5975C VL MSD with Triple Axis Detector
Inlet	320 °C
Carrier gas	Helium, constant flow 1 ml/min
Analytic software	Agilent Technologies Enhanced MSD ChemStation E.02.02.1431

3.2. Hydrogeology approach to evaluating the salinity source

3.2.1. Water samples

Sixty-five water samples from surface water (Lesser Zab river, springs) and groundwater (Bai Hassan, Mukdadia and Quaternary aquifer) as well as brine (formation water) from the Kirkuk and Bai Hassan oil fields (wells K 396 and BH 175 as M. Oligocene-Eocene), respectively, were collected in the study area around the Kirkuk anticline. Sampling locations were chosen based on the geographic location, e.g., distance to faults, elevation and defined screened intervals of the wells (Figure 23).

Surface water samples were taken from the Lesser Zab river and directly at the discharge points of the springs. Groundwater samples were collected at operating groundwater wells (Figure 24). The Iraqi North Oil Company provided the oil field brine samples. Before sampling, field parameters like the potential of Hydrogen (pH), electrical conductivity (EC) and bicarbonate) were obtained. At each location, two samples were collected in polyethylene bottles (250 ml). One of the two samples were filtered and acidified with HNO_3 to preserve cations. In addition, isotope samples were collected in 100 ml glass bottles sealed with Teflon caps. Samples were stored in a cooler before transported to the laboratory.

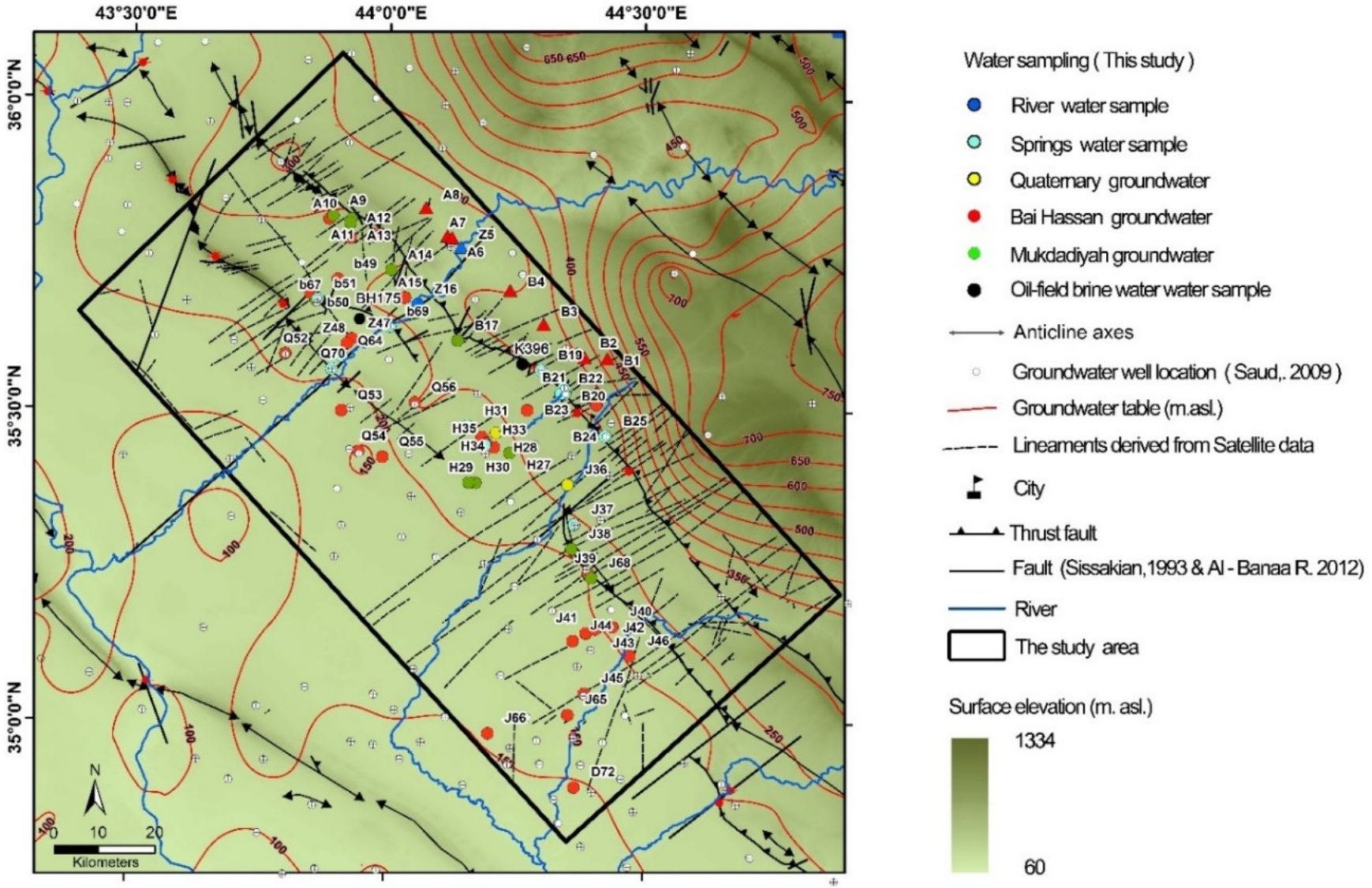

Figure 23: Map of contour lines indicates groundwater (m. asl). Triangles refer to the samples from the upstream basin, circles represent samples from the downstream basin (Sahib et al., 2016)

3.2.2. Methods

3.2.2.1. Hydrochemistry analyses

Acidified water samples were analyzed in the laboratory of TU Darmstadt (Germany) by Ion chromatography Metrohm 882 compact IC plus were used for detecting the major cation, anion, and Sr concentrations. The concentrations were determined after dilution of the sample in pure water and filtering. A compact IC plus instrument equipped with a high-pressure pump, sequential Metrohm CO_2 Suppressor (MCS) – which removes the CO_2 from the eluent flow to reduce the background conductivity – improves the detection sensitivity and minimizes the injection and carbonate peaks. The Metrohm Suppressor Module (MSM) was used for chemical suppression in anion analysis with conductivity detection. For cations, the standard eluent was used, comprising 1.7 mmol/L nitric acid (HNO_3) and 0.7 mmol/L dipicolinic acid (DPA). The relative standard deviation was 3 %. The limit of quantification of strontium was 0.1 mg/l.

Figure 24: Water sampling from the surface and groundwater (picture A). Picture (B) is showing methane seeps mixed with water stream and traces of sulfur were recorded in different locations in Fatha Formation Baba Dome Kirkuk

3.2.2.2. Stable isotopes analyses

Stable water isotopes (δ^2H and $\delta^{18}O$) were analyzed using a Picarro L2130-i Cavity Ring Down Spectrometer (CRDS) connected to a Picarro A0211 high precision vaporizer. All values are expressed in the standard delta notation in per mil against Vienna Standard Mean Ocean Water (VSMOW) according to Coplen (1996) (Eq. 11).

$$\delta_{sample}\ (permil) = (R_{sample} / R_{reference} - 1) * 1000 \quad \text{.....(Equation 11)}$$

First, raw data was corrected for memory effect and machine drift, then it was normalized to the VSMOW/ Standard Light Antarctic Precipitation (SLAP) scale. Normalization was conducted according to Gonfiantini's (1984) method, where the values between 0 to - 428 per mil for δ^2H and between 0 to - 55.5 per mil for $\delta^{18}O$ were assigned to VSMOW and SLAP. For this purpose, two laboratory standards – which were calibrated directly against VSMOW and SLAP – were measured in each run. External reproducibility – defined as standard deviation of a control standard during all runs – was 0.63 per mil and 0.15 per mil for δ^2H and $\delta^{18}O$, respectively. The cryogenic vacuum distillation method was used with the high salinity samples to reduce the isotope salt effect (Ingraham and Shadel, 1992).

According to Peterman (2012), the Sr isotopic ratio can change by further water-rock interaction during the sub-surface residence of the water (McNutt, 2001) and by mixing with other waters that differ in $^{87}Sr/^{86}Sr$ ratio and Sr concentrations (Shand et al., 2009). Overall, for 22 water samples, strontium isotope ratios were determined based on the EC and strontium concentration, including the assumed end members of the geochemical analysis, i.e., the oil field brines, river water and springs located in the Fatha outcrop areas. Therefore, Sr isotopes were measured using a Finnigan MAT 262 TIMS at the Isotope Geochemistry Group of the University of Tübingen (Germany).

Sample material was pipetted into Savillex c Teflon beakers and dried down. Subsequently, the samples were re-dissolved in 2.5M HCl for the separation of Sr by conventional ion exchange chromatography using quartz glass columns filled with BioRad AG 50W-X12 (200- 400 mesh). Subsequent purification of Sr was achieved in micro-columns filled with Eichrom © Sr-spec resin. Sr separates were loaded with a Ta-activator on Re single filaments and isotope ratio measurements were performed in dynamic mode. Analytical mass fractionation was corrected using an $^{88}Sr/^{86}Sr$ ratio of 8.375209 and exponential law. External reproducibility for NBS SRM 987 ($n = 3$) is 0.710239 ± 0.000017 for the $^{87}Sr/^{86}Sr$ ratio. Total procedural blank (chemistry and loading) was ≤ 96 pg for Sr.

3.3.Spectral reflectance approach to determine the characteristic of Iraqi crude oil

3.3.1. Material

Oil and soil samples were collected in the vicinity of Kirkuk, to investigate the spectral effects of soils with different properties and various states of oil contamination. Following the methodology plan (Figure 25), one set of the samples comprises pure crude oil from different oil fields with different densities, while the other set comprises oil-contaminated soil samples from selected seepage NW of Kirkuk.

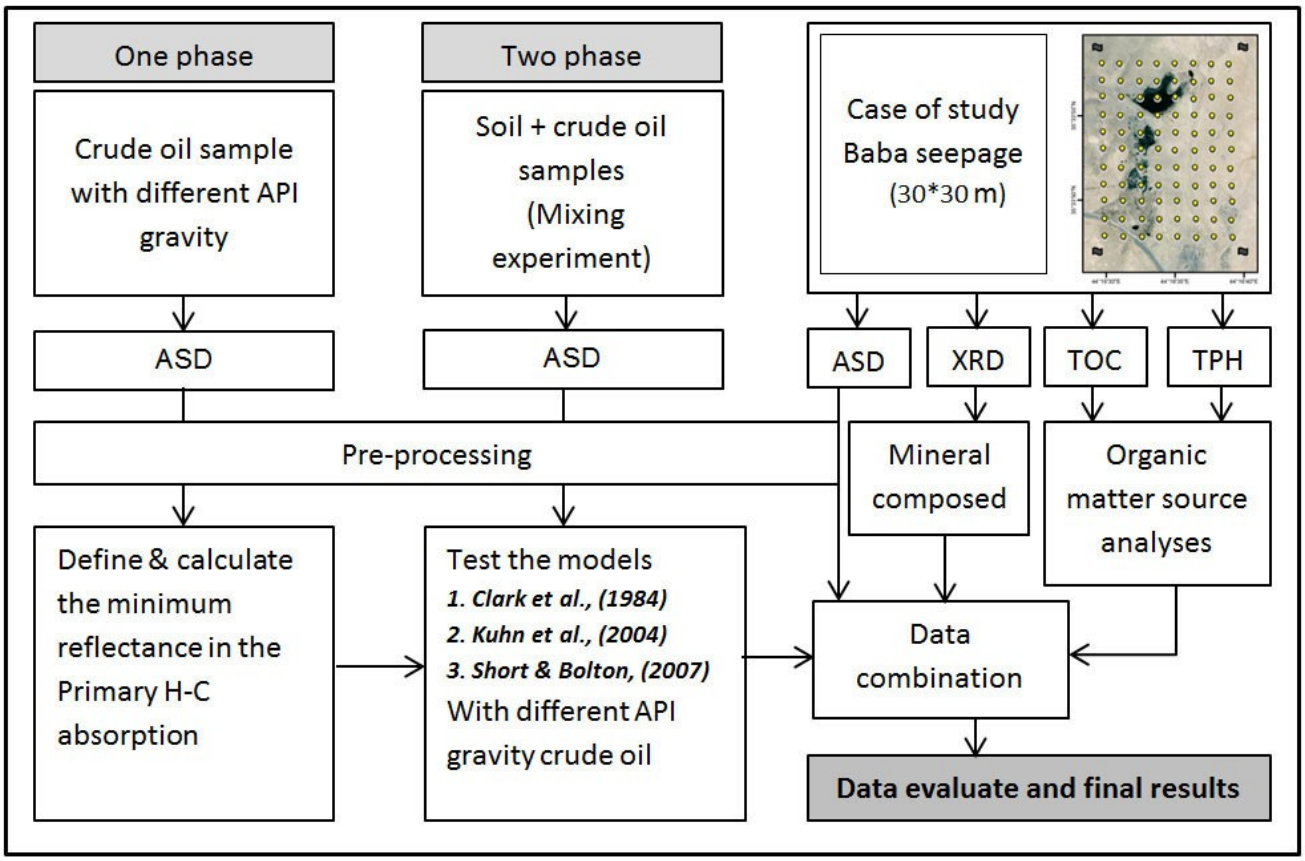

Figure 25: The workflow of spectral reflectance approach to determine the characteristic of crude oil

3.3.1.1. Crude Oil Samples

Four crude oil samples, with different viscosities, were collected to represent different oil fields. The samples are 551,571, 612 and 628 from the wells K 359, Q 45, J 22 and Jambur condensing gas respectively. The results from the API, as well as the total sulfur concentration (which will be discussed in chapter 4), were the basis to select these samples, e.g., very light condensed oil from natural gas from Jambur field and Qaiyarah's heavy crude oils (Figure 26). For one phase (one material) input in a batch experiment, all samples were collected and stored in commercially pre-cleaned glass jars with Teflon caps.

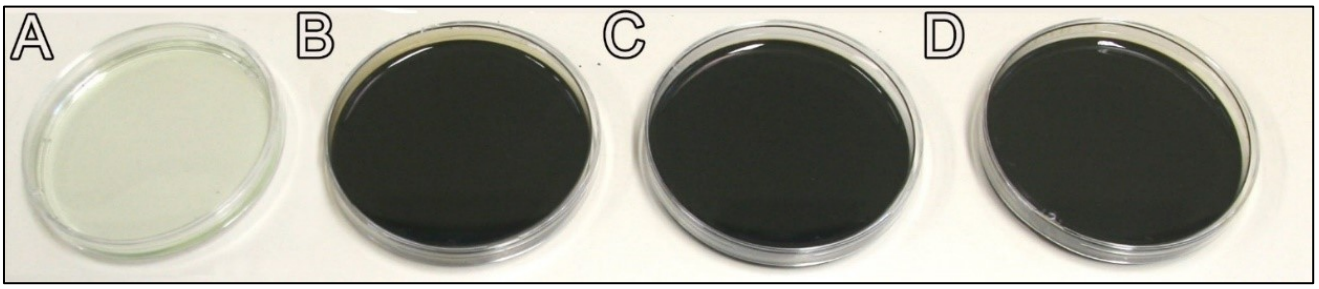

Figure 26: 20 ml of four selected oil samples in glass Petri dishes. A: natural condensing gas from Jambur oil field (No. 628), B: Qaiyarah oil sample (No. 571), C: Jambur oil sample (No. 612), D: Kirkuk oil sample (No. 551)

3.3.1.2. Soil Samples with Artificial Oil Contamination

To investigate the reflectance spectra of oil-contaminated soils, sand and loamy soils from a clean reference location close to Kirkuk. These soil samples were artificially contaminated with different amounts of oil by using an oil injector following the method of Andreoli et al., (2007) and Tian (2012). Three selected oil samples were chosen according to API classes 628, 551 and 571. As a two-phase experiment (soil and oil), these crude oil samples were progressively added to Fatha Formation soil samples from 0.1 to 11 % weight (wt) and the reflectance of the resulting contaminated sample was measured. The oil percentage in the samples was determined by weight and oil covered surface area (Figure 27).

Figure 27: The preparation of the soil sample from Fatha Formation with the controlled amount from crude oil sample in UFZ Department of Landscape Ecology. By using diffuse reflectance spectroscopy, the reflectance measurement was performed after each oil concentration (two-phase experiment)

3.3.1.3. Seepage Soil Samples

Detailed soil studies were conducted in the Baba seepage area, ca. 15 km NW of the city of Kirkuk (35°33'55.82"N, 44°16'33.33"E). The selected seepage was located to the south-west of the Baba Dome area within the limits of the Fatha Formation, covering an area of ca. 4732 m^2 of crude oil.

The location was divided into 88 parcels with an area of 30*30 m^2 each parcel (Figure 28). From every single parcel, five samples were taken from the center and the four corners and were mixed later to receive preferably representative samples. Although sampling was conducted during October, the vegetation cover was limited to very few Alhagi Maurorum and other dry plants. The samples were crushed, air dried and sieved with a 2 mm sieve (Chakraborty et al., 2012) to reduce spectra effects of soil particles and dry vegetation debris.

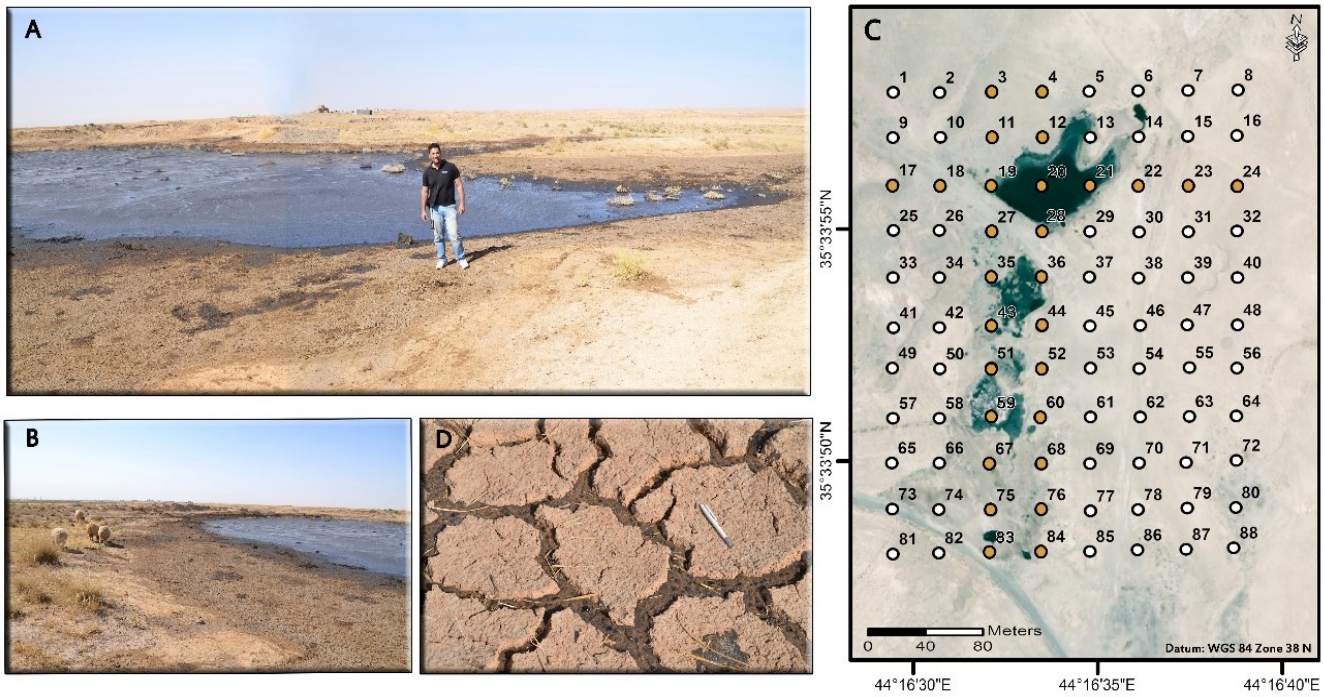

Figure 28: The selected seepage. A and B: field photos of point No. 20 with surrounding points. C: Sampling locations around seepage Baba center labeled with location number. The orange points indicate samples selected for the organic laboratory (HTO and GC/FID) and remote sensing. D: A crude oil filling the mud cracks

3.3.2. Methodology

3.3.2.1. Visible-Near InfraRed (VNIR) Scanning method

Diffuse reflectance spectroscopy (DRS) for the spectra range VNIR (350-2500 nm) is a rapid, cost-effective sensing method to characterize petroleum contaminated soils (e.g., Chakraborty et al., 2012). All of the soil samples were scanned in the laboratory with a FieldSpec Pro FR3 spectrometer, Analytical Spectral Devices (ASD). The measurements were conducted using an incandescent quartz halogen lamp for illumination relative to a spectralon plate. A FieldSpec Pro FR3 spectrometer has three wavelength detectors: a visible-near infrared (VNIR) detector (350-1000 nm), the first short wave infrared (SWIR)

detector (1000-1800 nm) and 2nd SWIR detector (1800-2500 nm). The spectral resolution of the FieldSpec Pro FR3 spectrometer is between 3 nm (350-1050 nm, sampling interval 1.4 nm) and 10 nm (1000-2500 nm, sampling interval 2 nm), with a field of view of 25. The fiber optic sensor was fixed at a nadir above the sample at a distance of 7 cm with a light angle of 30 (Moreira and Teixeira, 2014). The final reflectance spectra were calculated as the mean value from the six measurements with a 10 s - time interval (Figure 29). This signal was corrected to an absolute reflectance using a splice correction to adjust the signal step occurring when the detector changes at 1000 and 1800 nm. Four crude oil samples with a volume of 20 ml were filled in glass Petri dishes with a depth of 11 mm and a radius of 43.99 mm. A glass rod was used to remove any air bubbles on the surface. Spectral scanning was first conducted on clean (no artificial contamination) soil samples to record the natural, uncontaminated spectral signature. DRS was recorded for each contamination level (0.1-11% wt). The soil samples from the seepage area and the two-phase samples were measured in four positions, with a difference of 90 C to increase the precision of the measurements (following the method Amare et al.,2013). From these four measurements the average value was calculated.

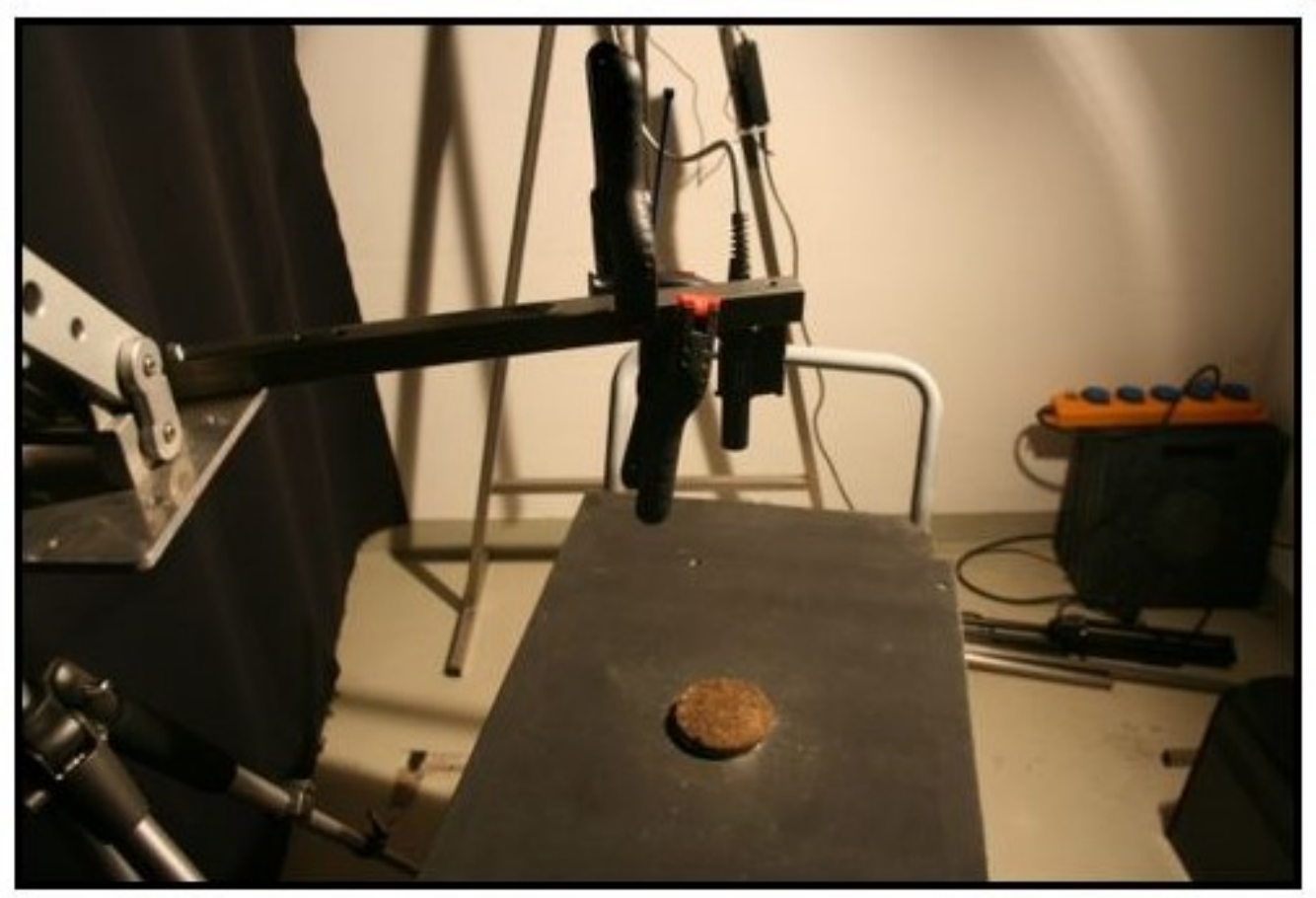

Figure 29: The preparation of the reflectance measurements using diffuse reflectance spectroscopy (DRS) in UFZ Department of Landscape Ecology in Leipzig

3.3.2.2. Calculation of the Hydrocarbon Index HI

According to Clark and Roush, (1984), the apparent continuum in a reflectance spectrum is modeled as a mathematical function used to isolate a particular absorption feature for analysis. It is also shown that a continuum should be removed by dividing it by the reflectance spectrum or subtracting it from the apparent absorption. Therefore, three models were tested for calculating the hydrocarbon index, which was chosen to obtain the best match with the concentration as well as identifying the sensitivity of each model. A three-band-ratio equation and the absorption depth were used to explore the presence of hydrocarbons. Within the spectral range 350-2500 nm, three primary absorption features were defined at 1.2, 1.7 and 2.31 μm (Cloutis, 1989). In order to calculate the hydrocarbon index (HI), the continuum was used as a mathematical function to isolate a particulate absorption feature that is indicative of the hydrocarbons (Clark et al., 2009). The model I is based on Clark and Roush's (1984) calculation of band depth (BD), which we consider here for possible use as the HI (Eq. 12):

$$DB = HI = (R_D - R_B)/ R_D \quad \text{(Equation 12)}$$

Where R_B is the reflectance at the minimum band center and R_D is the reflectance of the continuum at the band center (Figure 30). This method measures the vertical line length on DB. The model I is still widely used to calculate the band depth (Moreira and Teixeira, 2014). Model II also defines the HI with a vertical line between the minimum absorption reflectance and the continuum line at the known hydrocarbon absorption features. This method was able to detect oil concentrations corresponding to a volume of 25 ml within a 4 x 4 m soil area using Hymap hyperspectral images (Kühn et al., 2004). In Model II, the HI was calculated as follows (Eq. 13):

$$HI = 2/3 * (R_C - R_A) + (R_A - R_B) \quad \text{(Equation 13)}$$

Where R_A and R_C represent the start and end shoulders of the absorption feature and R_B is the minimum band center (Figure 30). Model III is an analogous equation for the 2310 nm absorption feature, which was tested for bitumen in tar sand, and is described in a NASA Remote Sensing Tutorial (Short et al., 2006). The ratio of two reflectance values on absorption feature shoulders was obtained by dividing by the minimum value of the reduced reflectance in the spectral curve as follows (Eq. 14):

$$HI = (R_A+R_C) / 2R_B \quad \text{(Equation 14)}$$

In Models I and II, hydrocarbons are present when the results are higher than zero, while in Model III hydrocarbons are present when HI > 1. For all of these models, it has to be considered that the HI value is strongly affected by the chosen starting point R_A and ending point R_C of the maximum amplitude R_B of the absorption continuum. To identify the hydrocarbon contamination levels and sources in the Baba seepage samples and compare the real TPH soil concentration with HI results, Wayne et al., (2001)

mention that OC or TPH is the most widely-used parameters. In this study, both methods were applied and compared the results with the HI.

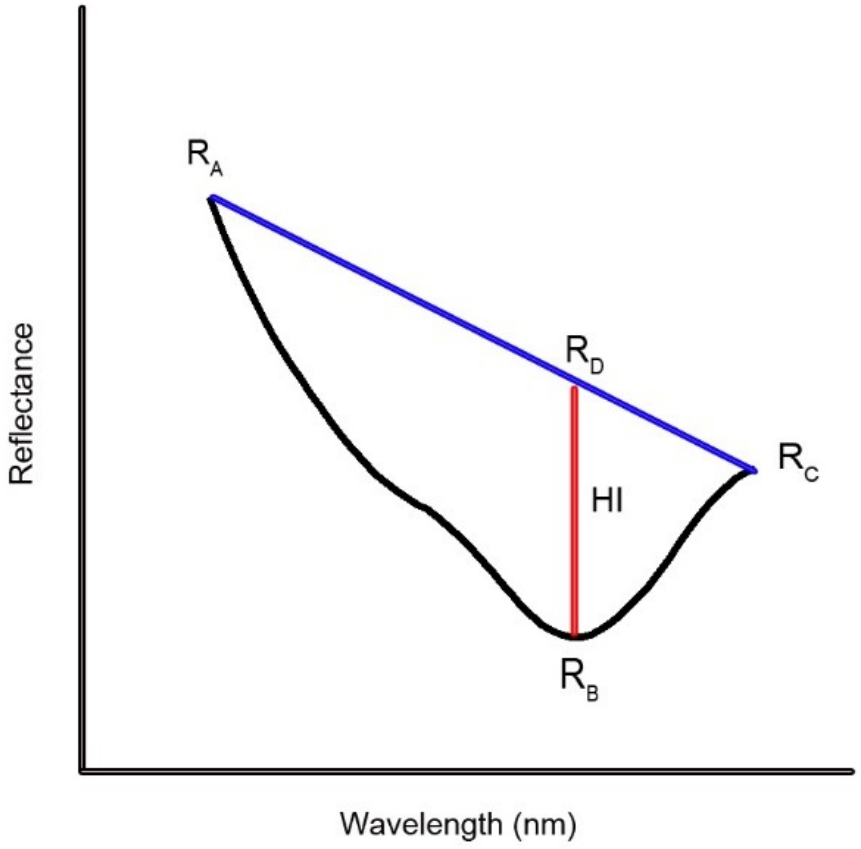

Figure 30: An absorption feature with peak shoulders RA, RC (continuum boundaries). RB is the minimum reflectance and continuum center RD, which is used with the three models (modified after Kühn et al., 2004)

3.3.2.3. High-Temperature Oxidation (HTO) method

OC originates from the decomposition of plants and animals and it can range from fresh (leaves, twigs) to highly decomposed forms such as humus (e.g., Schumacher, 2002). Additionally, spills of anthropogenic contaminants and naturally-occurring oil seepage can increase the total organic carbon content in soils and sediments. A LiquiTOC IIR (manufacturer: Elementar Analysen Systems GmbH, Germany) is able to distinguish between organic carbon (OC), inorganic carbon (IC) and elemental carbon (EC) in solid matter using a temperature ramp method, where OC is first analyzed at 450 _C with N_2 as the carrier gas. The reactor is then heated to 850 _C to measure IC in the same manner. In order to determine organic carbon in the soil samples, 5 to 10 mg of soil was weighed in a silica glass crucible. All 88 samples were measured with this technique. Calibration was done using a soil standard (1.6 % of both OC and IC) provided by Elementary Analysen Systems GmbH. The limit of detection (mean of noise + 3x standard deviation) at 20 mg sample mass was 0.06 %, using baked (organic free) quartz sand as a blank medium (Table 6).

Table 6: Summary of the used methods to determine the organic contents in the samples (modified after Okparanma and Mouazen, 2013)

Measuring technique and samples Qty.	Capability	Detection Limit % (DL) sample	Estimated analysis time	Measure target	Limitation
GC/FID, 30	High sensitivity, oil source identification	0.003	lab-based GC cycle time may be 40 min	TPHs in total and PAHs	Laboratory-based GCs are not for compounds < C_{10} and based on the standards. The samples need to be treated with solvent extraction.
HTO, 88	High sensitivity, carbon type identification.	0.06	lab-based, the one cycle time between 15 to 20 min	Organic, inorganic, elemental carbons	Combine the organic matters from petroleum and vegetation.
DRS, 88	Rapid, simple, inexpensive, portable, zero solvent extraction, noninvasive, little or no sample preparation	0.1- 0. 4	0.1 to < 1 min	Organic carbon (this study)	Matrix effect (water, soil, and nature of oil), overlapping spectra.

3.3.2.4. Total Petroleum Hydrocarbon (TPH) method

Among the different methods, gas chromatography with a flame ionization detector (GC/FID) is the recommended method to determine the TPH in the soil (Scherr et al., 2007). Thirty soil samples from the Baba seepage area were chosen to be analyzed by GC/FID to compare with the OC results (the orange points in Figure 28 C). The extraction step is based on the harmonized DIN ISO 16703 method "soil quality determination of the content of hydrocarbon in the range C_{10} to C_{40} by gas chromatography" (ISO 16708 soil quality).

This method defines the TPH as the total amount of hydrocarbons that can be extracted from the soil with an acetone/*n*-heptane mixture (2:1) and which elutes between *n*-decane ($C_{10}H_{22}$) and tetracontane ($C_{40}H_{82}$) by using a non-polar capillary column (Figure 31). All samples were spiked with a solution of *n*-decane and tetracontane (as an internal marker) and chromatograms were integrated into between these two peaks. Although this method is very effective and sensitive, it does not include the higher organic carbon range > C_{40} that can be found in crude oil from seepages in general.

Figure 31: Sedimented soil samples after extraction (left). The soil extracts were then given into separation funnel (right), (in cooperation with Schmidt, 2014)

3.3.2.5. X-Ray Diffraction (XRD)method

The spectral signature of several minerals was tested to evaluate any similarity with a hydrocarbon (like carbonates CO_3), which can affect the absorption calculations. The spectral libraries and other studies (ENVI spectral library; Grove et al., 1992) showed that many minerals could cause a spectral interference with hydrocarbons. Therefore, XRD diffraction measurements were carried out to determine and characterize the mineral composition of bulk samples. In order to understand the general minerals of the seepage, six samples were chosen as representative of the whole area (1, 8, 27, 54, 81 and 88). X-Pert-Highscore software of PANanalytical Co. was used for analyzing the mineralogical phases. The BGMN program (Bergmann et al., 1998) – which is based on the Rietveld methodology – was used for the quantification and further characterization of each identified phase. The Rietveld method uses a least squares approach to refine a theoretical line profile until it matches the measured pattern.

3.3.2.6. Remote sensing and Satellite data

Due to the importance of understanding the impact of the structure of the rock, the lineaments detection patterns have been identified in this study by remote sensing techniques, using the satellite digital elevation model (DEM) and the auto lineament extraction method in PCI Geomatica program (Abdullah et al., 2010). In order to reveal the potential of hyperspectral remote sensing reflectance data to quantify soil hydrocarbon contamination in oil areas using the laboratory´s results like OC and TPH, the mass

content of soil samples as well as the results were compared with typical mineral absorption features from the ASTER Spectral Library (within ENVI 4.7) (Baldridge et al., 2009).

Several methods including the use of band ratios and indices from different satellites were tested to detect the hydrocarbon satellite images with different specifications (Figure 32). The Normalized Difference Vegetation Index (NDVI) was used, for example, as a primary step to classify the different vegetation types (Schumacher, 1996). The results from the satellite data will be published in the separate case study.

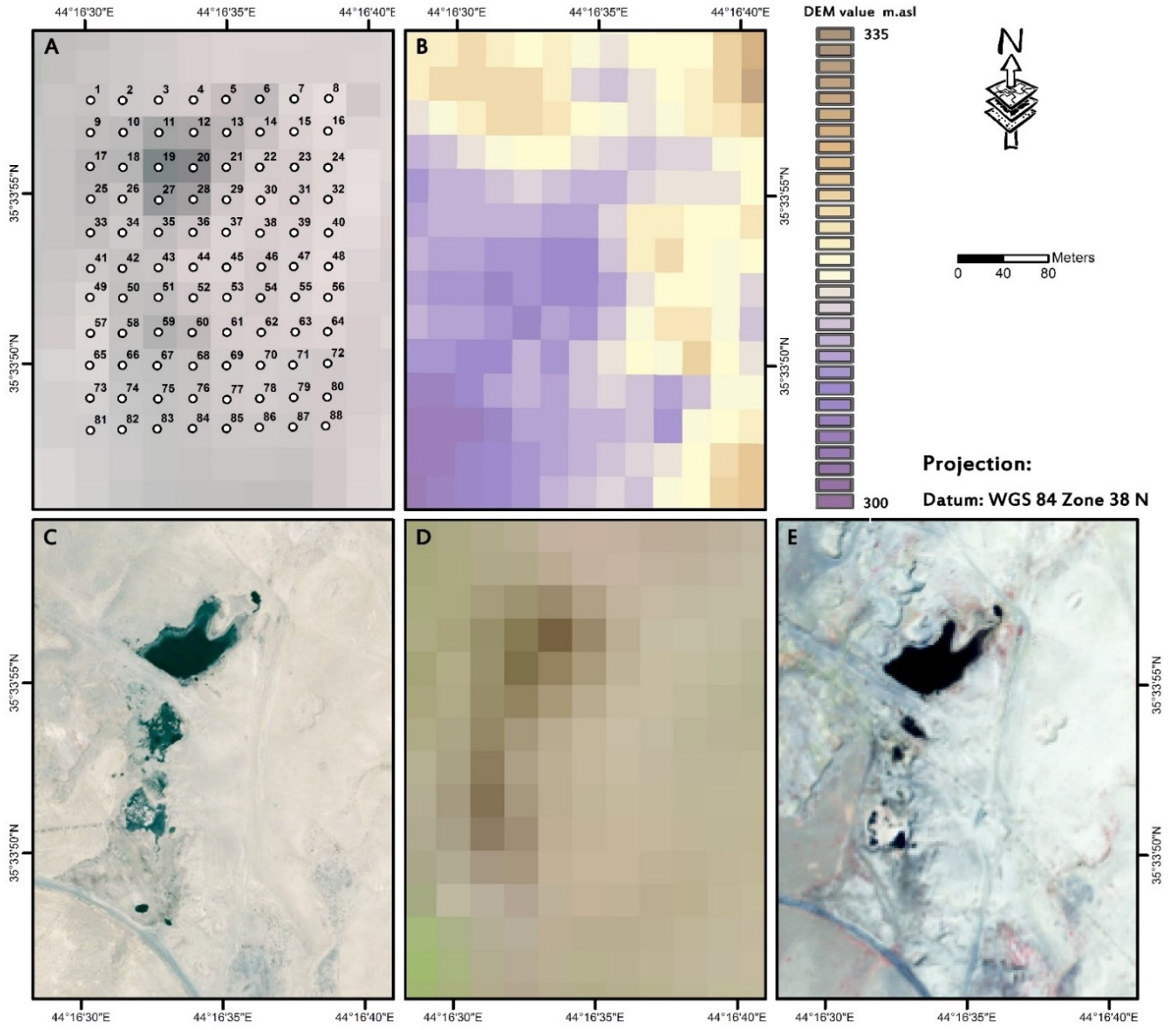

Figure 32: Satellite data (archive) with natural colors for selected seepage in Baba area. A) Hyperion image (2015) with spatial resolution (30 m). B) Digital elevation model (DEM) from Shuttle Radar Topography Mission (SRTM) with spatial resolution (30 m) https://www2.jpl.nasa.gov/srtm/ . C) QuickBird image (2006) with spatial resolution (0.6 m). D) Landsat image 7 (2013) with spatial resolution (30 m). E) GeoEye-1 image with spatial resolution (2 m)

4. Results and discussion

4.1. Organic chemistry properties approach to correlate seepage and reservoir crude oil

4.1.1. API gravity and sulfur content

The API gravity of the crude oil samples shows a wide range at 11.8 – 43.3 and for the seepage samples 8.5 – 9, which can be classified in the range of very heavy to light oils (Table App - 1). This result confirms that the Iraqi crude oil has wide variations in density API gravity values depending on the saturation of the source rocks and the age and depth of reservoir formations (Jassim and Al- Gailani 2006; Simon, 2011). Besides the type of source rocks, certain ranges can also be interpreted as different lithologies and related environmental settings. However, oil gravity decreases with decreasing reservoir age (Aqrawi et al., 2010). On a field scale, the general results from all the fields showed no clear correlation between oil reservoir age and API except Bai Hassan oil field where the oil samples from Cretaceous reservoir have slightly lower API values comparing with a Tertiary reservoir (Figure 33). The lightest oil (highest API) is from the Jambur field in the Early Cretaceous reservoir (L. Sarmord Formation), while the heaviest oil is from the Qaiyarah field in the Early Miocene (Euphrates Formation), with an average of 15.5°.

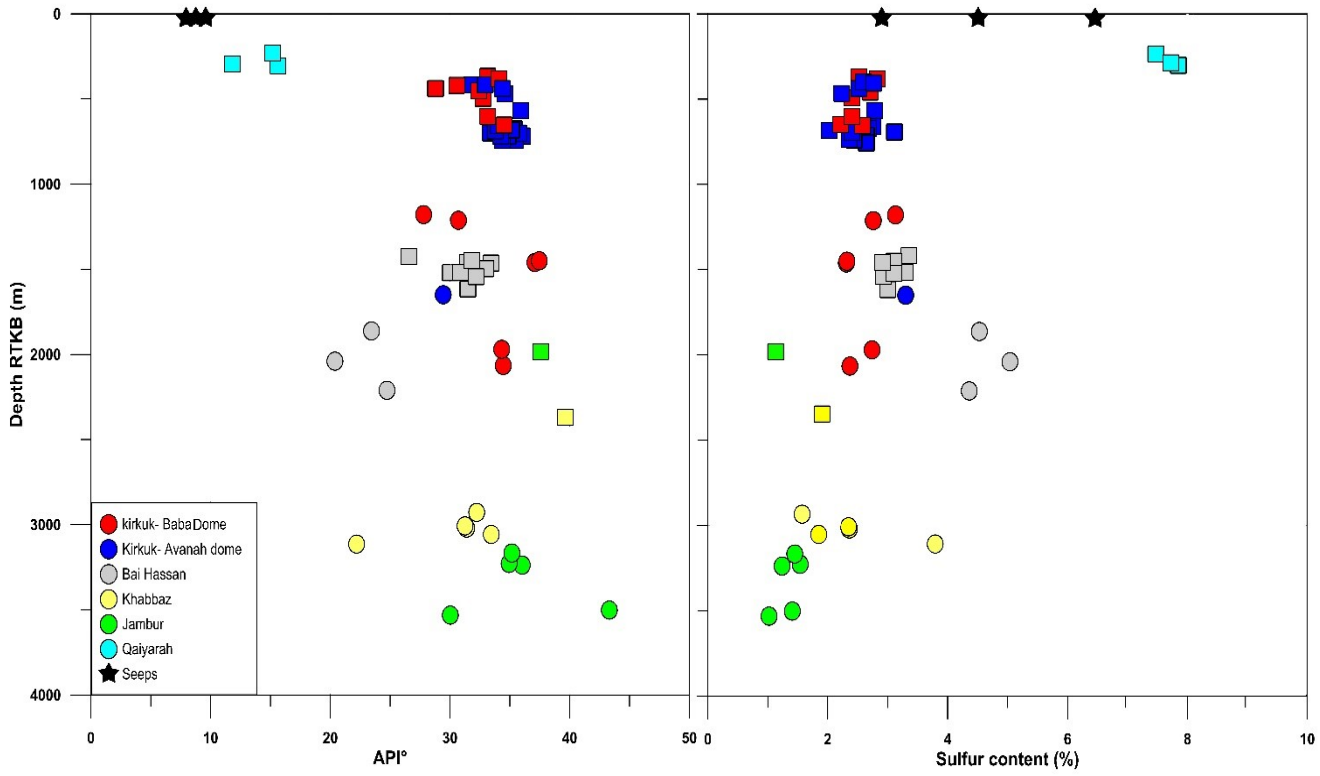

Figure 33: API gravity and sulfur content of oils vs. reservoir depth (RTKB). The circle symbol is representing the Cretaceous reservoirs, while the tertiary reservoirs are represented by a square

Due to the high concentration of the sulfur content, all oil type of the selected fields can be considered as “sour” crude oil type (>0.5 wt% S) (Duissenov, 2012). The sulfur content range is 1.02 - 7.8 and higher than 4 for the seepage samples. With respect to the Cretaceous Bai Hassan samples, the sulfur content slightly increased with increasing depth (Figure 33). The relation between the API and sulfur can be the result of maturation, with high API gravity values showing lower sulfur content (Figure 34). A general trend can be noticed between the API and sulfur content especially in the samples from Bai Hassan and Khabbaz fields.

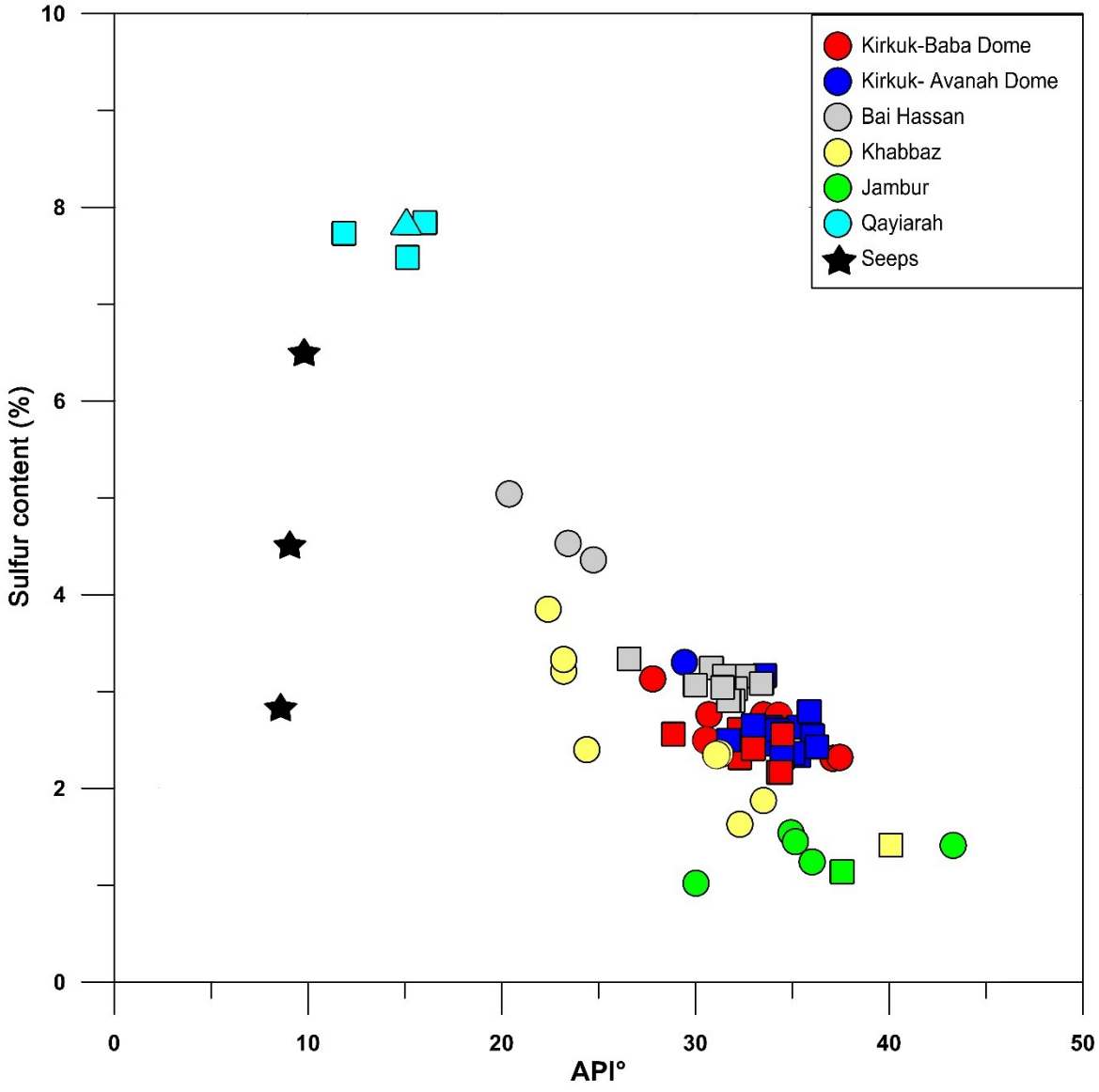

Figure 34: Sulfur content vs. API gravity allows a further characterization of the single oil field. The circle symbol represents the Cretaceous reservoirs, while the tertiary reservoirs are represented by a square. The triangle symbol refers to the unknown age samples

4.1.2. Bulk screening analysis Crude oil composition

The results from compound group separation (IATROSCAN) show a large compositional variation between the fields and even samples within the same field (Table App - 1). In contrast to this observation, samples from the Kirkuk field (Avanah and Baba) are relatively similar. Little variation around 28-30 % aliphatics, 50-25 % aromatics, 12-15 % NSO compounds and 3-5 % resins + asphaltenes are shown and asphaltenes are mobilized at last. Meanwhile, Bai Hassan samples are showing more heterogeneous of the oil composition. Three selected oil and on seepage samples were shown in Figure 35.

4.1.3. Molecular composition

The predominating characteristic of every measured sample is the paraffinic composition with a high abundance of short-chain n-alkanes and gradually decreasing peaks towards long-chain n-alkanes. The results of applying chromatogram to the selected sample are presented in Table 7, Table 8 and Table 9. CPI and OEP are changing only for the K 371from the Baba Dome, where this sample has an almost equal OEP, but a regular CPI. The *n*-alkane range has a high similarity of all analyzed samples. With a range between 2 and 13, the nC_{17} / nC_{25} (for example) have high above 1. According to (Peters et al., 2005), thermal maturity could be referred by CPI values above or below 1.0. Values close to 1.0 are showing low maturity, which is rare in general. Therefore, an odd or even *n*-alkane dominance is expected in a thermally-mature hydrocarbon system like the study area.

A certain predominance of Pristane (Pr) or Phytane (Ph) was not detected in the studied fields. The TAR (terrigenous/aquatic ratio) is representing a clear marine trend. Moreover, the values between 0 and 0.1 do not show a potential terrigenous input. Biomarker results are split into three parts, namely source, age, and maturity. The analyzed samples show a rather homogenous sterane distribution. C_{29} diasteranes were recorded in seepage sample 614. Except for Baba Dome and in the seepage samples, The C_{35} homohopane index varies in samples based on the field level. As most-useful indicators of oil maturity (Peters et al., 2005), the ratio of Trisnorhopane (Ts) & trisnorneohopane (Tm) as Ts/(Ts+Tm) and the regular sterane/17α-hopane ratio (St/H) vary slightly, especially in Jambur. Ts/(Ts+Tm) is mainly a thermal parameter, which is based on the thermal stability of C_{27} hopanes. Tm (or C_{27} 17α-trisnorhopane) is less stable than Ts (or C_{27} 18α-trisnorhopane) during catagenesis (Seifert & Moldowan, 1978).

With the most significant depth difference, the C_{35}/C_{34} (hopane ratios) were remarkable for the Bai Hassan and Khabbaz samples. Meanwhile, the Maturity and age-related parameters are similar for all fields, including for most of the seepage results. Moreover, ßß/(αα+ßß) explains also differing results for oil samples of Bai Hassan and the seepage samples.

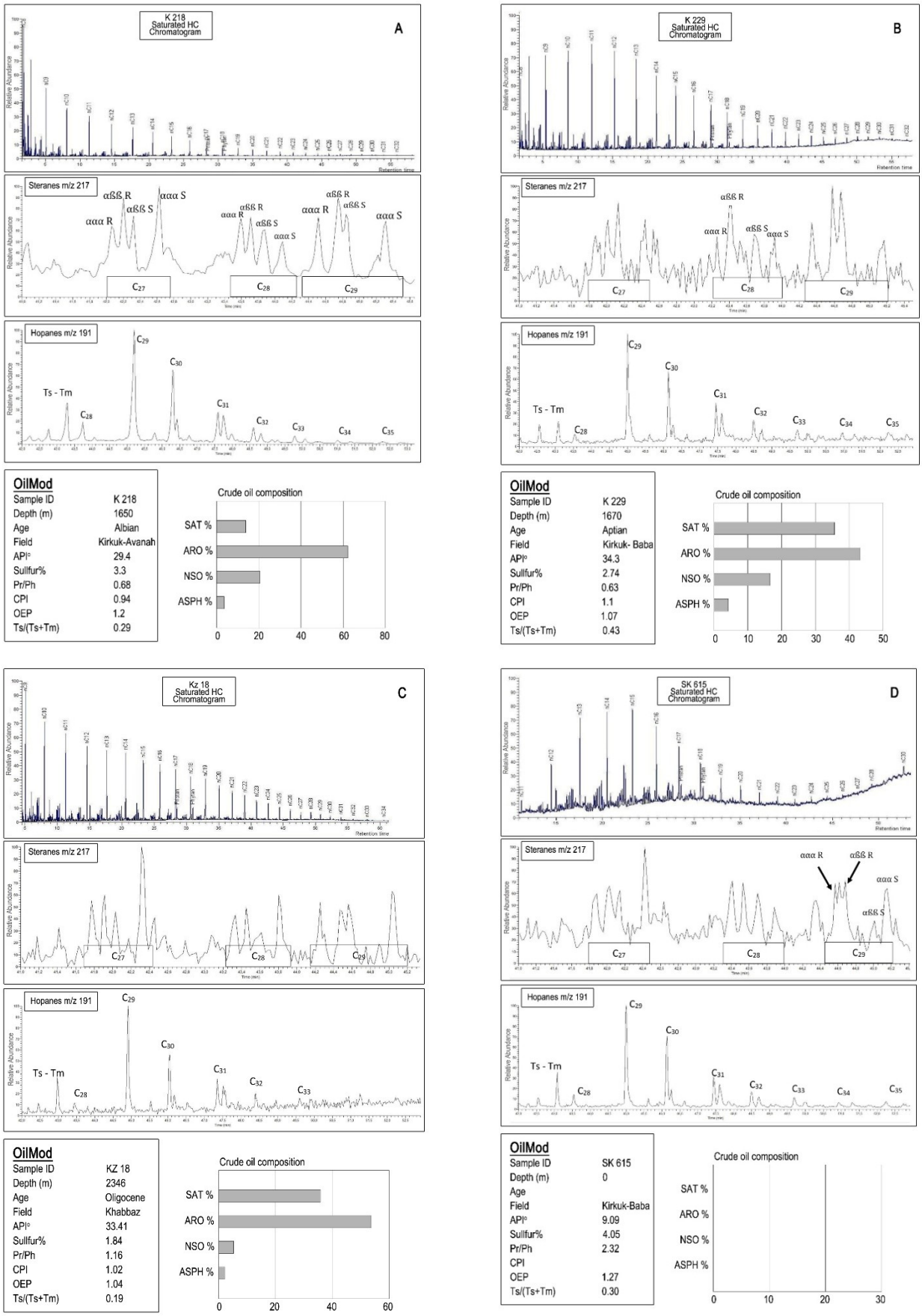

Figure 35: Bulk and molecular geochemical data for four selected oil samples K 218, K 229, Kz 18 and SK 615

Table 7: GC data for saturated hydrocarbon fraction of crude oils from Northern Iraq

Well	Pr/nC_{17}	Ph/nC_{18}	Pr/Ph	Pr + nC_{17} / Ph + nC_{18}	nC_{17}/nC_{25}	CPI	OEP	TAR
K 411	0.14	0.24	0.82					
K 407	0.24	0.30	1.15	1.35	7.58	0.95	1.04	0.09
K 429	0.11	0.26	0.57	1.14	6.52	1.00	1.1	0.08
K 229	0.11	0.23	0.63	1.12	4.75	1.10	1.07	0.1
K 324	0.22	0.34	0.80	1.12	5.23	1.35	1.12	0.06
k 348	0.25	0.29	1.23	1.38	12.66	0.97	1.16	0.05
k 346	0.25	0.29	1.18	1.34	10.77		1.19	0.1
K 347	0.22	0.28	0.92	1.12	3.90	0.87	1.1	0.08
K 332	0.25	0.30	1.16	1.32	6.41	1.19	1.31	
k 425	0.34	0.37	1.13	1.20	8.91	1.04	1.17	0.02
k 218	0.16	0.28	0.68	1.10	5.14	0.94	1.2	
K 371	0.25	0.29	1.03	1.18	5.46	1.14	0.99	0.05
K 265	0.26	0.33	0.93	1.12	4.61	1.01	1.2	0.27
K 263	0.25	0.30	1.14	1.31	7.17	1.03		
K 280	0.64	0.66	1.05	1.07	2.09	0.98	1.2	0.24
K 337	0.19	0.31	0.75	1.10	7.45	1.04	1.28	0.05
SK 614	0.33	0.33	1.31	1.33	8.70		1.04	0.07
SK 615	1.52	0.56	2.32	1.39	3.88		1.27	
K334	0.17	0.25	0.85	1.10		0.96		
bh 157	0.23	0.28	1.12	1.33	8.31	0.97	1.2	0.06
bh 96	0.13	0.25	0.75	1.25	9.39	0.96	1.06	0.03
bh 134	0.13	0.24	0.73	1.22	7.99	1.09	1	0.03
bh 8	0.36	0.34	1.28	1.26	12.13	0.96	1.19	0.03
bh 42	0.22	0.31	0.92	1.22	9.18	0.97	1.23	0.08
bh 29	0.23	0.28	1.06	1.25	6.46	1.07	1.24	0.04
bh 49	0.23	0.29	1.08	1.31	11.95	1.03	1.13	0.06
bh 71	0.23	0.36	0.92	1.31	12.25	1.04	1.17	0.05
bh 60	0.22	0.34	0.96	1.31	13.31	0.91	1.1	0.05
Kz 18	0.37	0.35	1.16	1.12	4.11	1.02	1.04	0.11
Kz 12	0.13	0.23	0.73			0.93		
Kz 23	0.13	0.13	0.81	1.26	8.49	0.9	0.99	0.05
Kz 24	0.17	0.17	0.65			0.91		
Kz 4	0.16	0.27	0.65			0.9		
Kz 1	0.13	0.23	0.6			0.91		
J22	0.37	0.36	1.18	1.17	3.26	0.97	0.99	0.18
J 16	0.25	0.32	0.99	1.19	10.34	1.07	1.08	0.07
J 63	0.22	0.25	1.16	1.30	6.15	1.00	1.09	0.02
Q 75	0.28	0.23	1.68	1.41	7.78			
Q 45	0.28	0.45	0.81	1.15	4.1			
Q 73	0.19	0.3	0.52	0.94	2.7			
Q 38	0.28	0.34	0.74	1.01	2.9			
SQ 81	0.57	0.27	1.55	1.2	3.4			

4.1.4. Source-related

For source analysis of the organic matter, the relative abundance of three sterane groups (ααα R+S & αßß R+S) was used. Characteristic of an anoxic environment is a specific sterane distribution of marine steranes (Connan et al., 1986). Specific ecosystems have particular common sterane: C_{27} dominance steranes are common in lacustrine environments and dominance of C_{28} are marine and C_{29} are terrigenous environments. Concerning the depositional environment of the organic matter, the relative

abundance of C_{27}-C_{28}-C_{29} steranes for most samples plot is in an overlap area of marine carbonate and non-marine shale, close to marine shale (Figure 36).

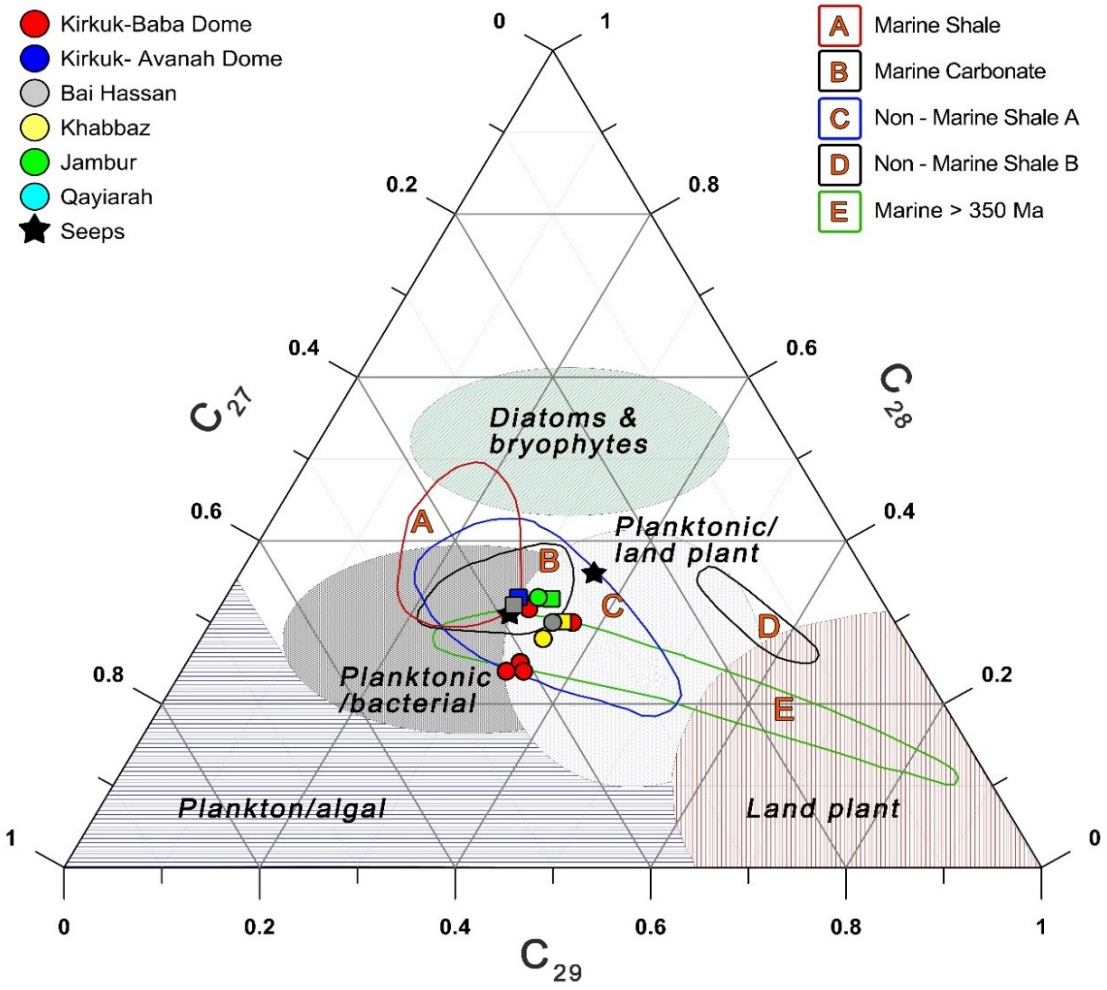

Figure 36: Distribution of regular steranes showing relative sterane abundance. Non-marine shale A: non-marine algal organic matter and B: terrigenous (higher plant) organic matter. The circle symbol represents the Cretaceous reservoirs, while the tertiary reservoirs are represented by a square. Modified after Huang and Meinschein, 1979; Peters et al., 2005

A distance of at least 200 km between the Chia-Gara Formation and the coastline - during Late Jurassic and Early Cretaceous, was calculated (Mohialdeen et al. 2013). Even it was suggested that due to the similar geochemical characteristics of Tertiary and Jurassic-Cretaceous oils propose a similar origin, probably in source rocks in the Sargelu Formation (and Naokelekan, Barsarin /Gotnia Formations) and the Chia Gara Formation (Aqrawi et al., 2010).

Regular sterane/17α-hopane (St/H) provides further information about the depositional settings. The most commonly used biomarkers are St/H distribution for source related studies. The distribution of regular steranes consist of the C_{27} - C_{29} ααα (20S + 20R), aßß (20S + 20R) and the 17α-hopanes consist of the C_{29} – C_{33} (22R + 22S) are pseudohomologs, which gives understanding about the relative input of eukaryotic (algae and higher land plants) vs. prokaryotic (bacteria) organisms (Hunt, 1996; Peters et al., 2005).

Based on the data presented above, a terrigenous input is rather unlikely, and Connan et al., (1986) have observed a high bacteria input in carbonates and anhydrite facies of a sabkha palaeoenvironment. The findings with a predominance of (C_{27} - C_{28}) hopanes occurred from high microbial input from marine deposited carbonates. As well as, two hopane based parameters, a tandem of C_{29}/C_{30} vs. C_{35}/C_{34} hopanes and the C_{35} Homohopane index (HHI) are supporting a marine depositional setting. C_{35} hopanoids in prokaryote microorganisms originate from C_{31}-C_{35} Homohopanes. Their abundance can be used to gain information regarding the redox potential during and directly after deposition.

Crude oils represent highly reducing marine source rocks with non-available free oxygen, because of a relatively high abundance of C_{33}, C_{34} or C_{35} homohopane compared to lighter homologs. In systems with free oxygen, the precursor bacteriohopanetetrol is oxidized into a C_{32} acid, or get preserved as a C_{32} homolog if the available oxygen was consumed (Peters et al., 2005).

Table 8: Analysis chart of GC and GC-MS oil biomarkers data for selected oil samples representing Cretaceous and Tertiary formations

Field	Well	C_{27}	C_{28}	C_{29}	C_{35}-HHI	Ts/(Ts+Tm)	Reg. sterane/17 a hopane (St/H)	C_{29}/C_{30}	C_{35}/C_{34}	C_{28}/C_{29}
Kirkuk - Avanah	K 218	32	32	37	5.08	0.29	0.32	1.58	0.74	0.86
	K 371	30	33	37	8.79	0.27	0.52	1.38	1.09	0.89
	K 429	37	30	33	18.54	0.32	0.52	1.24	1.28	0.90
	K 229	35	24	41	15.52	0.43	0.24	1.27	0.90	0.58
Bai Hassan	bh 42	30	32	38	18.48	0.23	0.47	1.57	1.34	0.84
	bh 96	35	30	35	3.10	0.23	0.26	1.26	0.23	0.85
Khabbaz	KZ 18	36	30	34	7.24	0.19	0.37	1.56	0.61	0.88
	KZ 23	35	28	37	20.40	0.20	0.31	1.53	1.07	0.75
Jambur	J 16	32	33	35	7.78	0.27	0.45	1.33	1.07	0.94
	J 45	33	33	34	13.47	0.34	0.71	1.17	1.07	0.97
Seepage	SK 614	36	36	28	12.64	0.25	0.33	1.44	1.07	1.27
	SK 615	30	31	39	13.78	0.30	0.27	1.48	1.20	0.79

*: C_{29} diasterane. C_{27}-C_{29}: steranes, HHI = Homohopane index, C_{29}/C_{30} and C_{35}/C_{34} =

A characteristic C_{35}/C_{34} ratio of > 0.6 is common for Marine source rocks and mainly the crude oil of marine carbonate source rocks has values of > 0.8, combined with high C_{29}/C_{30} ratios (>0.6) (Peters and Moldowan, 1993). Low HHI results explain a dominance of C_{31} and C_{32} homohopans and indicate a dominantly suboxic environment, but due to the HHI differences between 3 and 20 % C_{35} the area of Kirkuk shows variations in its redox conditions during deposition (Table 8). Figure 37 indicates C_{29}/C_{30} and C_{35}/C_{34} ratios compared with values of the carbonate or marl source rocks. For the Khabbaz fields, a salient trend can be observed; two largely different C_{35}/C_{34} results combined with a consistent C_{29}/C_{30}. An indicator for a suboxic environment is the abstinence of C_{35} without a preservation potential for homohopane precursor molecule.

High Pristane (Pr) /Phytane (Ph) values (> 3) indicate a terrigenous input of organic matter with oxidation conditions, as well as matching with Sulfur contents (Peters et al., 2005). Thermal maturation and the numerous inputs of biomolecules are primary sources for influence on the results, whereby the Pr/Ph ratio decreases with increasing depth (Figure 38). Regarding the lithology, dominating carbonates or calcareous layers in source rocks at entire areas is supported by low Ts/(Ts+Tm) values (Table 8).

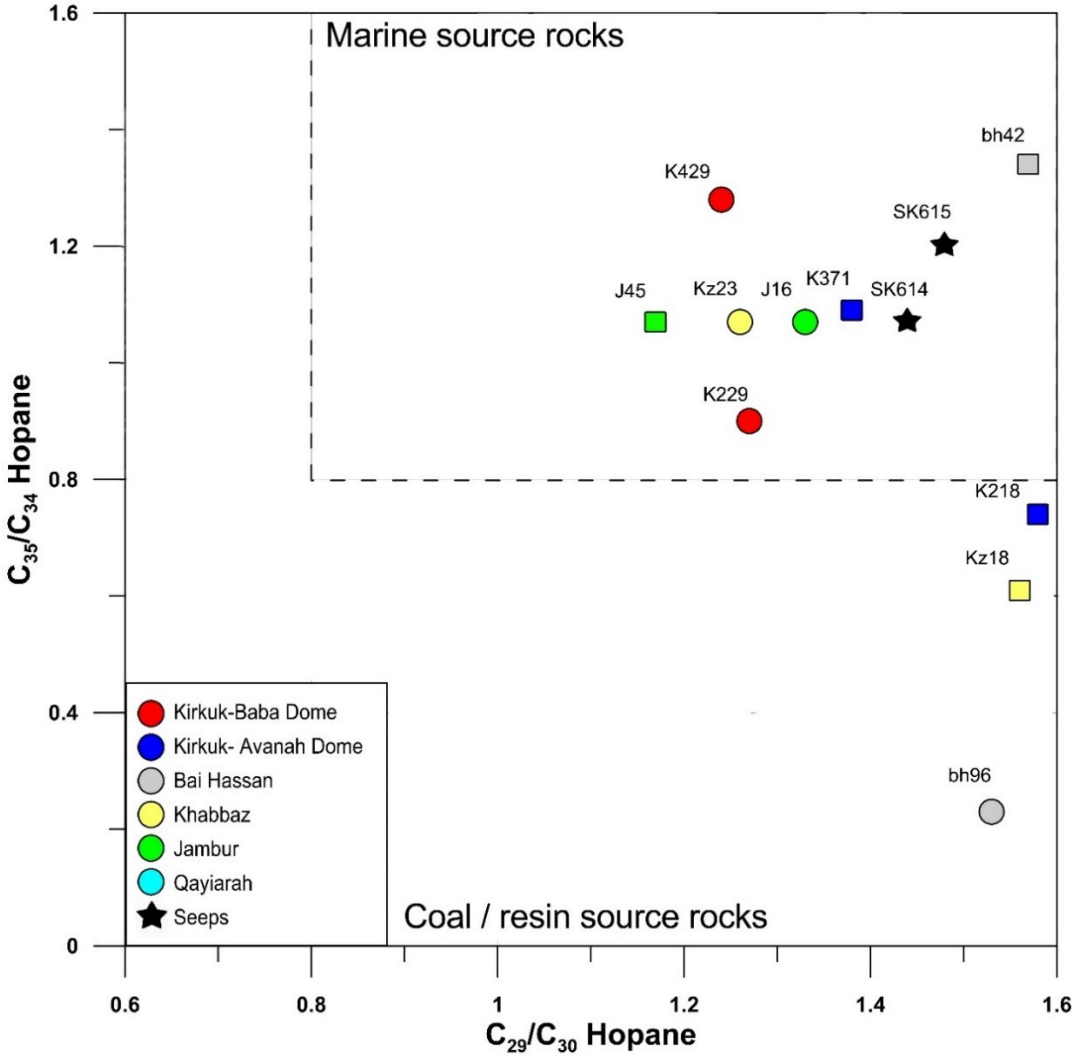

Figure 37: Hopane ratio diagram of crude oil samples from different oil fields. The highlighted corner is characteristic for marine carbonates and marl and Coal/ resin source rocks when C35/C34 Hopane lower than 0.6. The circle symbol is representing the Cretaceous reservoirs, while the tertiary reservoirs are represented by a square. Rock source after Peters et al., 2005)

The source of organic matter has a strong influence on this maturity-related parameter, whereby Ts/(Ts+Tm) gives source and maturity information (Peters et al., 2005; Seifert & Moldowan, 1978). McKirdy et al., (1983) and other case studies have proven a clear predominance of Tm over Ts for carbonates. Therefore, and due to the similar results, the organic matter from carbonate source rocks is most dominant in the area of Kirkuk area.

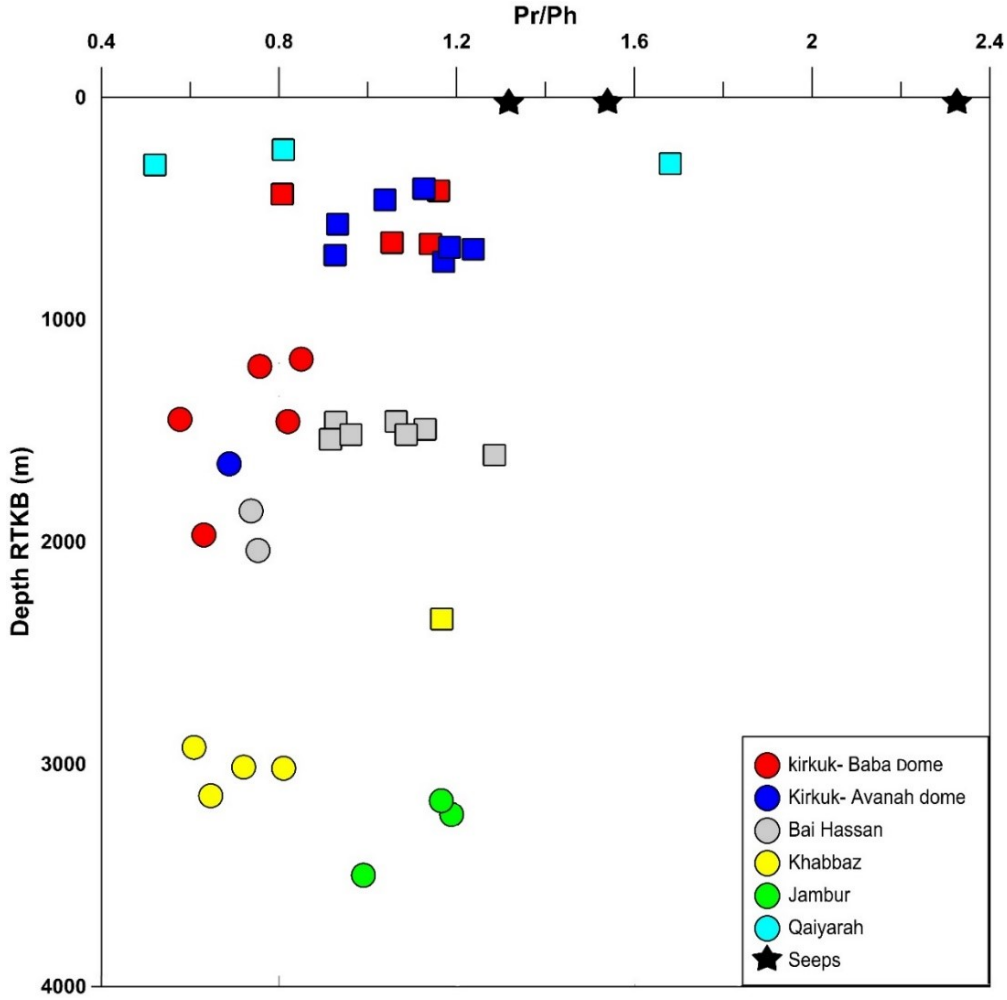

Figure 38: Pristane/Phytane ratio with depth (m) RTKB for selected oil samples in Kirkuk and Qaiyarah areas. The circle symbol is representing the Cretaceous reservoirs, while the tertiary reservoirs are represented by a square

According to the results of the oil samples, the third most abundant atomic constituent is sulfur. Values between 1 and 8 % of sulfur content are a clear indicator of shale and/or carbonate from the marine origin (Peters et al., 2005). Therefore, sulfur content can be a tool for oil fields separating, and this can observe in the fields of Qaiyarah, Bai Hassan and seeps, where a remarkably high sulfur content was found. However, more mixing starts in Avanah, Baba, and Jambur, ending with Qaiyarah (Figure 33), where separation is mainly driven by API gravity. The Bai Hassan Cretaceous reservoir, for example, has lower API gravity and higher sulfur content. High sulfur content can result from migration pathways and the difference in the source, while API gravity is also driven by depth. However, it is essential to consider that the reservoir age is representing oil specification.

The three Bai Hassan tertiary oil samples are located next to each other, and this explains similar source origin (Figure 33 & Figure 34). The analyzed dataset represents such an interpretation, with a dominance of saturated and aromatic hydrocarbons and a still high number of sulfur-bearing molecules. The migrated oils are usually rich in saturated and aromatic hydrocarbons and depleted in NSO and asphaltenes (Tissot and Welte, 1984).

4.1.5. Age-related

Without terrigenous input, the C_{28}/C_{29} regular sterane ratio offers age estimation method for oils. Over the geologic time the relative content of C_{28} steranes increases (Grantham & Wakefield,1988), without the characterized rise of specific organisms, but most with the arising diversification of phytoplankton assemble. The most intensive increase, characterized by values > 0.7 generated by Jurassic and Late Cretaceous (Figure 39). C_{29} sterane abundance decreases over time and increases the C_{28} sterane trend (Grantham & Wakefield, 1988).

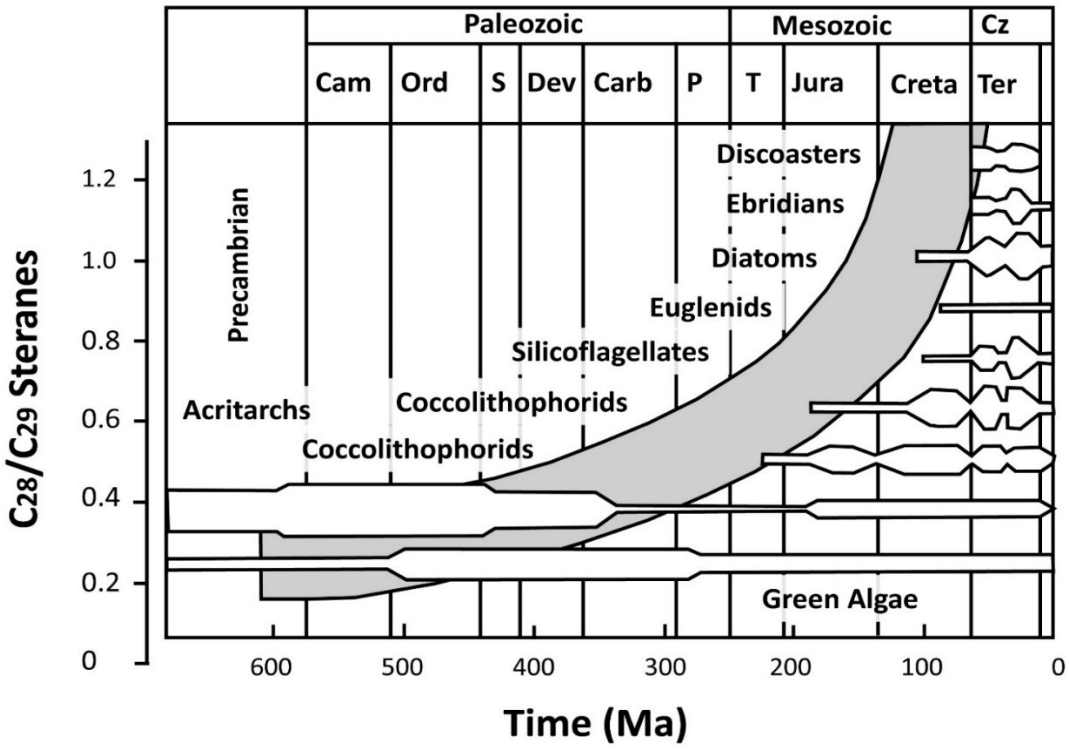

Figure 39: The geologic time and the increase of C28/C29 sterane. Peters et al., (2005), modified after Grantham & Wakefield (1988)

According to Al-Ameri and Zumberge (2012), the GeoMark Research OILS_ database and the results in Table 8, the regular sterane ratio of C_{28}/C_{29} can classify the oil samples to three types. The source of oil family type (1) is Middle and Late Jurassic age carbonate rocks Sargelu and Naokelekan formations based on the ratio of C_{28}/C_{29} = 0.56 - 0.65 from the samples K 229, K411 and K334 (the three red dashed lines with the low ratio in Figure 40). All other samples except SK614 were used to estimate the boundaries to the ratio of C_{28}/C_{29} = 0.75 to 0.94, which represent a second family type (2) from the Late Jurassic/Early Cretaceous age, mainly Chia Gara Formation (Mohialdeen et al., 2013) carbonate and marl. The seepage SK 614 explains the high ratio of C_{28}/C_{29} reaching to 1.27, which reflects more recent source rocks (as family 3). Due to the sampling location within the Fatha cap rock Formation, the source could be Late Cretaceous Shiranish Formation (Table 1) or even in the Early Tertiary Aaliji or Jaddala formations (Al-Shrhan and Naten, 2003).

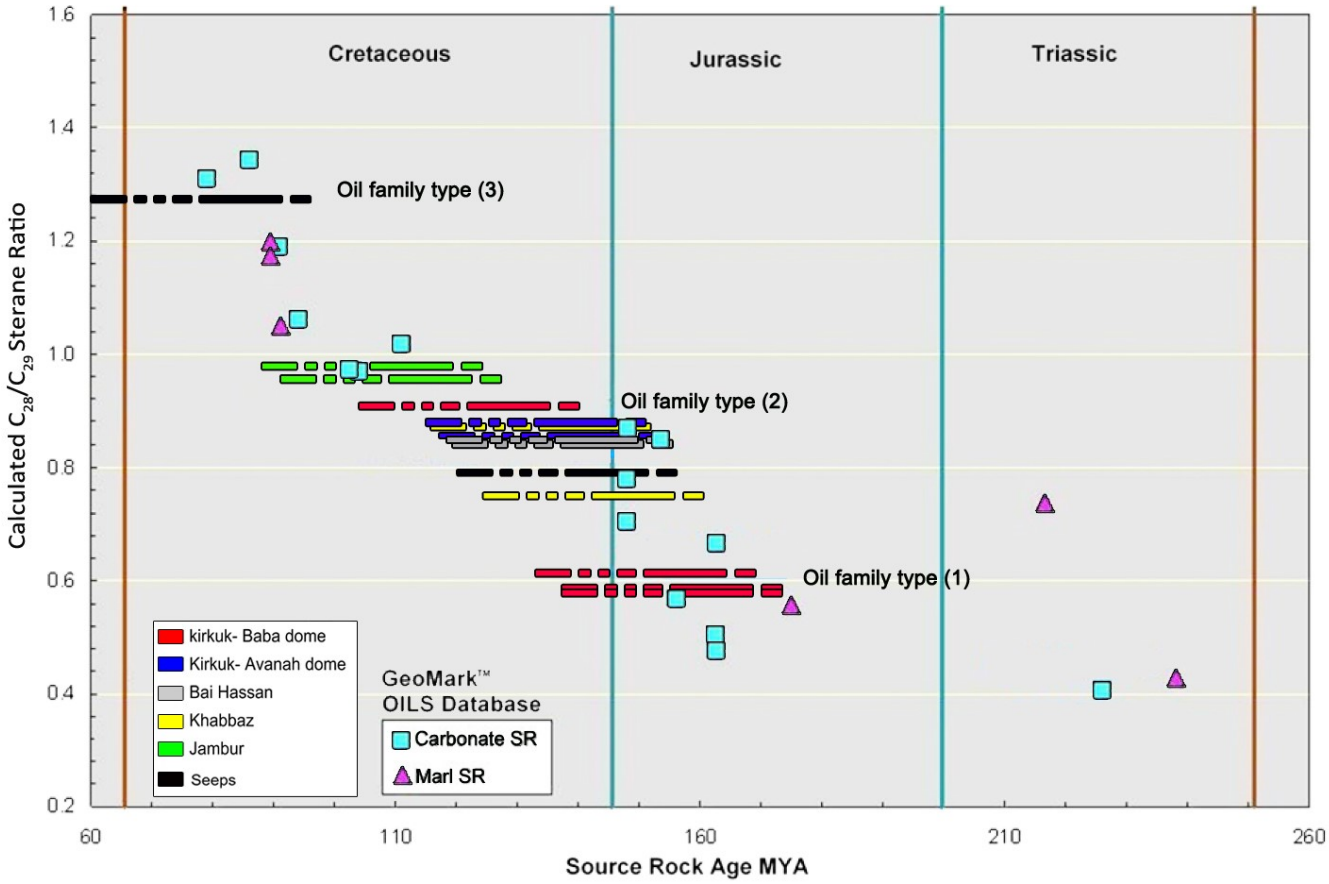

Figure 40: C28/C29 sterane increase over geologic time for selected samples (dashed lines). Both regular steranes and triaromatic steranes of Cretaceous and Tertiary reservoir oils from Northern Iraq based on from GeoMark Research OILS_ database and modified after (Al-Ameri and Zumberge, 2012)

4.1.6. Maturity-related

Basically, Thermal processes include cracking of longer chains into shorter. A tandem plot – given in Figure 41 – shows an overview of the analyzed samples. The Pr/nC$_{17}$ and Ph/nC$_{18}$ decrease with rising depth in the Kirkuk field (Avanah and Baba Domes), Khabbaz and Bai Hassan. The varying input of Pristane and Phytane, which affects the result, would indicate a higher maturity in Cretaceous reservoirs. Generally, a maturation trend can be observed in every single field. Higher maturation results of Cretaceous can be found in Baba, Khabbaz and Bai Hassan. The C$_{29}$ (20S/ (20S+20R) sterane index can define less or immature to mature samples, while C$_{29}$ ßß/ (ßß + αα) can detect the range of mature to over-mature samples (Table 9). In a tandem diagram, mature samples should plot in the central upper part, but not come to close the equilibrium line of ßß/ (ßß + αα) (Figure 42).

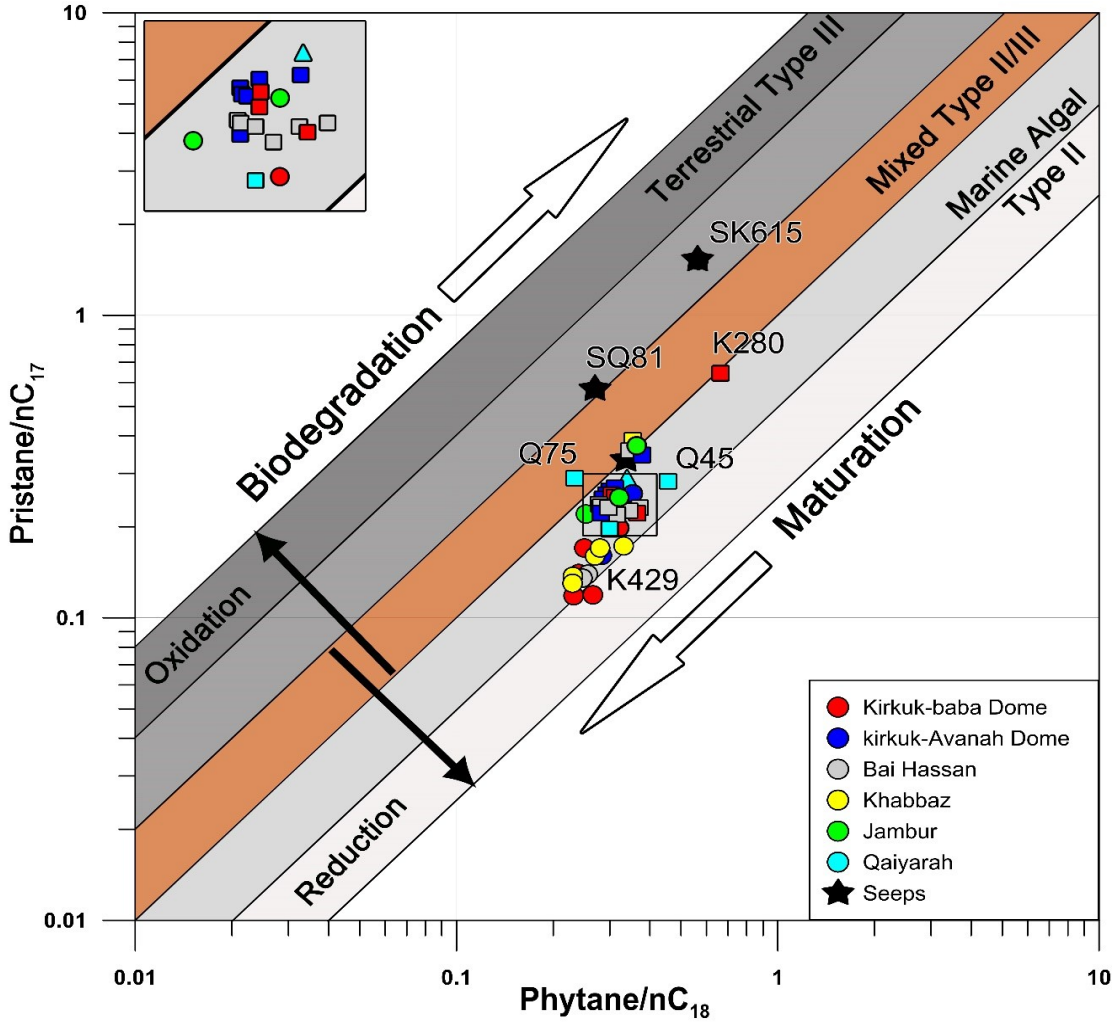

Figure 41: Relationship between Pr/n-C17 and Ph/n-C18 for oils from northern Iraq. The circle symbol is representing the Cretaceous reservoirs, while the tertiary reservoirs are represented by a square. The triangle symbol refers to unknown reservoir age samples. After Peters et al., (1999)

Table 9: Listed are the calculated GC-MS biomarkers. The relative 20S and ßß abundance are measured for the C_{29} sterane

Field	Well	20S/(20S+20R)	ßß/(αα+ßß)	BNH+TNH/hopane
Kirkuk / Avanah	K 218	0.5	0.50	0.47
	K 371	0.56	0.52	0.42
Kirkuk / Baba	K 429	0.52	0.55	0.48
	K 229	0.51	0.55	0.44
Bai Hassan	BH 42	0.45	0.46	0.35
	BH 96	0.47	0.57	0.39
Khabbaz	KZ 18	0.49	0.59	0.48
	KZ 23	0.51	0.54	0.39
Jambur	J 16	0.54	0.56	0.48
	J 45	0.52	0.48	0.60
Seepage	SK 614	0.48	0.35	0.42
	SK 615	0.46	0.53	0.40

BNH = Bisnorhopane, TNH = Trisnorhopane, hopane = C_{30} hopane + C_{29} norhopane.

According to Peters et al., (2005), Isomerization starts during burial and with the values 0.5 reaches equilibrium at thermal maturation. However, for every field and reservoir, the results of this maturity approach quite similar, again at 0.5. With values between .7 (= equilibrium) and zero, the relation based on the ßß/(ßß + αα) isomerization provides further detailed information about the occurred maturity. These samples represent mature fields, without reaching a maximum or over-maturation, defined by isomerization equilibrium for ßß + αα.

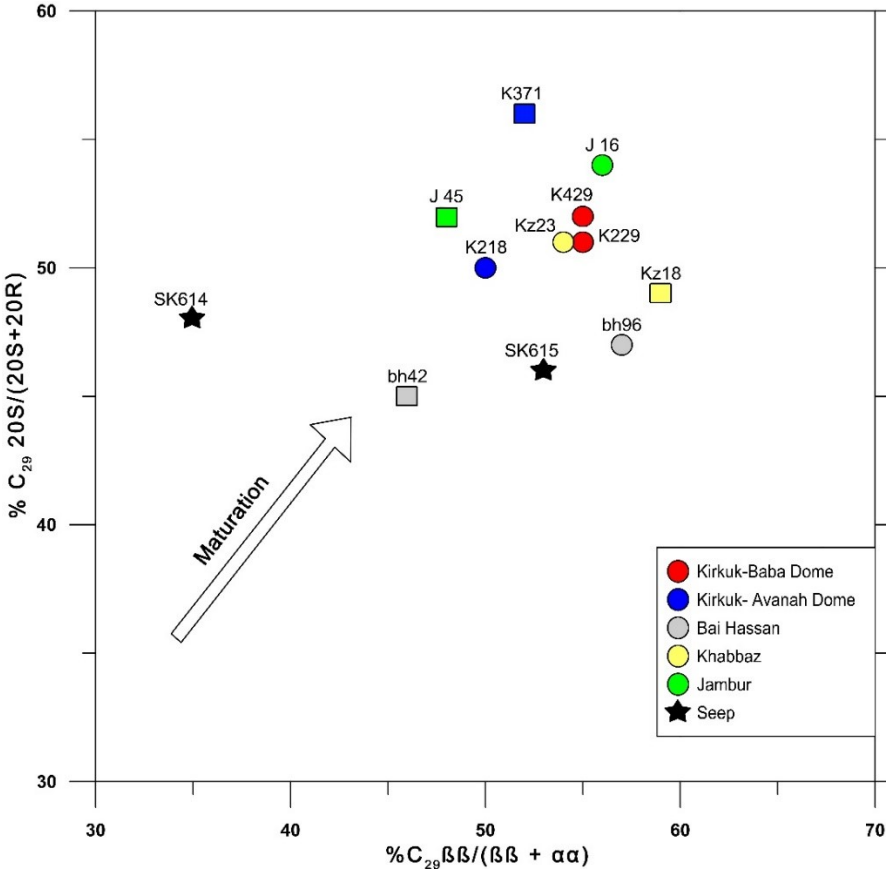

Figure 42: Correlation of C29 steranes isomerization parameters, which commonly increase with maturation. The circle symbol represents the Cretaceous reservoirs, while the tertiary reservoirs are represented by squares

4.1.7. Kirkuk Seepage samples

Regarding the different characteristics and behavior of the seepage samples, it was difficult to make the same measurement to the samples SK 614, SK 615 and SK 616. According to the Wenger et al., (2002) biodegradation quantification scale (Figure 43), and the seepage sample SK 615 show a biodegradation result of Unresolved Complex Mixture (UCM). *n*-alkanes decrease relative to iso-alkanes, they are affected by depletion without a complete elimination. Therefore, the classification of sample No. SK 615 is Moderate biodegradation. The iso-alkanes/n-alkanes ratios of 1.52 for Pr/*n*C17 support this interpretation. A Pr/Ph ratio of 2.32 is higher than in moderate samples and the API gravity represents solid material, which cannot be proven by Wenger et al., (2002). However, according to a sulfur content of 4.5 % and an API gravity of 9°, the classification of the seepage sample SK 615 would fit into heavily to severely degraded samples (Figure 43).

The C_{35} homohopane index can give a potential connection between the seeps and Baba Dome reservoir. Reducing conditions and preservation of biomolecular precursors can be interpreted from a high C_{35} homohopane index. This means the intensive biodegraded seepage sample SK 615 could not related to the water washing in an oxic environment.

Seepage sample SK 616 has no UCM signal and a peak from *n*C15 loss of light saturated hydrocarbons. It is slightly biodegraded - supported by a sulfur content of 2.87 % - with an alteration of Pristane and Phytane. Enrichment of sulfur content of both samples according to biodegradation is shown. The seepage sample SK 616 shows the enriched sulfur content of 2.87. This value is within the range of the upper reservoir of Baba Dome oil samples, which have sulfur content varies between 2 and 2.7 %.

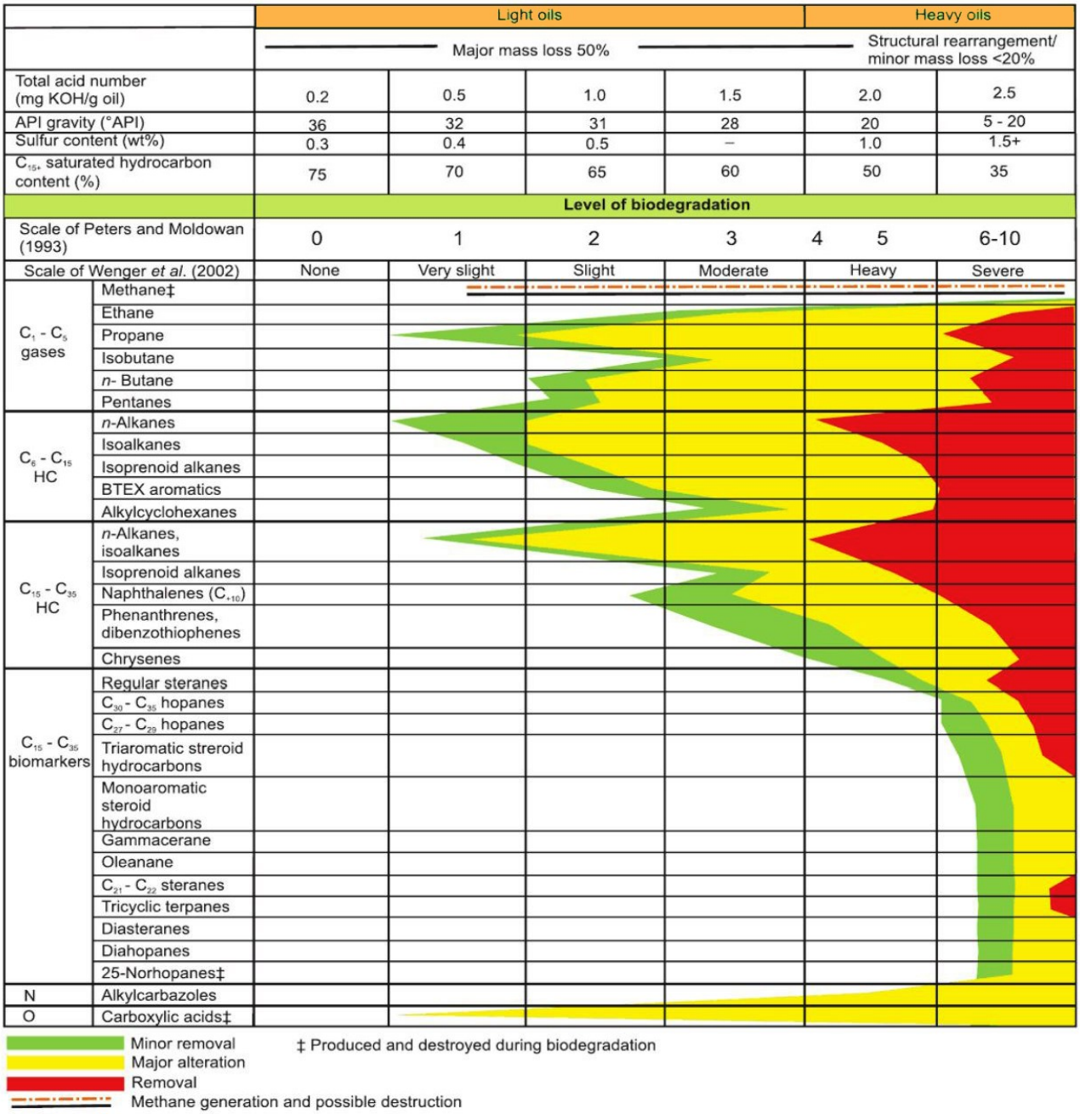

Figure 43: A scale for quantification of biodegradation. The absent of selected components at biodegradation levels modified after Littke et al., (2008); Wenger et al, (2002); Head et al., (2003)

4.1.8. PAHs in Crude and Seepage Oils

The results were established on seven oil samples (as described in 3.1.7). These samples were used based on their properties (different API gravity) and origins order (Table 10). Figure 44 contrasts the percentage of PAH dispersion of the crude oil and the seepage samples are indicated. The findings make it clear that almost all PAHs are evident in the tested oils. The structural amount of the primary elements is comparable for all tested oils, except for seepage sample 20.

Table 10: List of all oil and seepage samples and their properties

Sample name	Oil type	API (°)	Density	Sulfur wt (%)	Depth (m) RTKB	Age - Formation	Field
J 16	light	43.31	0.809	1.41	3501.5	Aptian - L. Sarmord	Jambur
K 411	light	37.10	0.84	2.31	1460	Albian - L. Qamchuqa	Baba - Kirkuk
K 324	medium	29.54	0.878	2.03	438	Oligocene – Baba	Baba - Kirkuk
bh 88	medium	26.58	0.8944	3.34	1425	Oligocene – Baba	Bai Hassan
Q 73	heavy	15.66	0.9615	7.84	304	Miocene - Euphrates	Qaiyarah
Q 75	heavy	11.86	0.9861	7.73	296	Miocene - Euphrates	Qaiyarah
SQ 81	extra heavy	9.89	1.005	6.45	0	-	Qaiyarah seepage
SQ 82	extra heavy	ND	ND	ND	0	-	Qaiyarah seepage
Seep 20	extra heavy	>7	1.028	7.97	0	-	Baba seepage

The most influential portions of the other eight oil samples are 2- methyl-Naphthalene, 1- methyl-Naphthalene and Naphthalene, which cover a minimum of 60 % of the total PAH amount (Table App – 2). According to the Figure 44, High API gravity (more than 10) of oils samples (J 16, K 411, K 324, bh 88, Q 73, Q75) have recorded higher than 80 % of these three compounds of the total of all tested PAHs. Lower than the first three PAHs, the Phenanthrene and Fluorene were detected as a relevantly high influential compound. The Acenaphthylene, Acenaphthene, Pyrene, and Chrysene were also identified with lower concentration. The PAHs were present with smaller amounts in some of the oil samples. Meanwhile, there was no traced of Anthracene and Benzo[k]fluoranthene were found in any other tested oil samples.

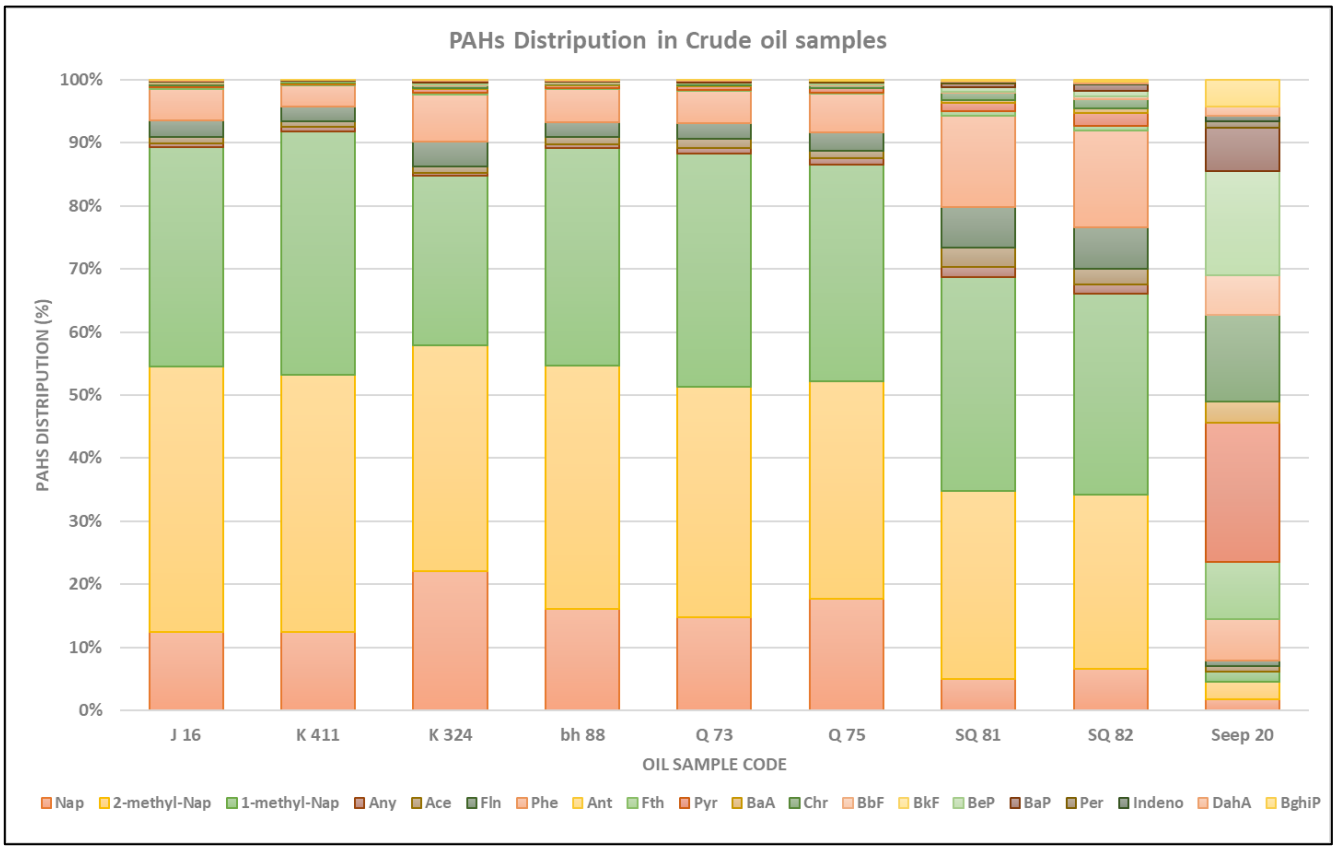

Figure 44: Percentage distribution of different oil and seepage samples

Each oil usually differs in its origin, whereby the findings of these study do not imply that Anthracene and Benzo[k]fluoranthene never occur in oil. Seepage sample No. 20 varies from the other samples (Figure 44), where small quantities of 2- methyl-Naphthalene, 1- methyl-Naphthalene and Naphthalene were noticed. The seeps samples faced an external influence such as the impact of climatic, which means that biodegradation and erosion by water can accelerate the breaking down of the low molecular weight PAHs (Pothuluri & Cerniglia, 1994). Figure 45 shows the percentage dispersion of the high molecular weight PAHs in an effort to emphasize this impact.

The low molecular weight distribution of sample Nr. 20 could have been similar to the other samples. Meanwhile, the main difference is related to the degradation of the low molecular weight. This hypothesis of the sample genesis could not be applied to seepage samples SQ 81 and SQ 82, because they were constantly leaking to the surface. In contrast, seepage Nr. 20 was for a long period exposed to the weathering process. Thus, the samples SQ 81 and SQ 82 show similarities to crude oil, not to degraded seepage oil.

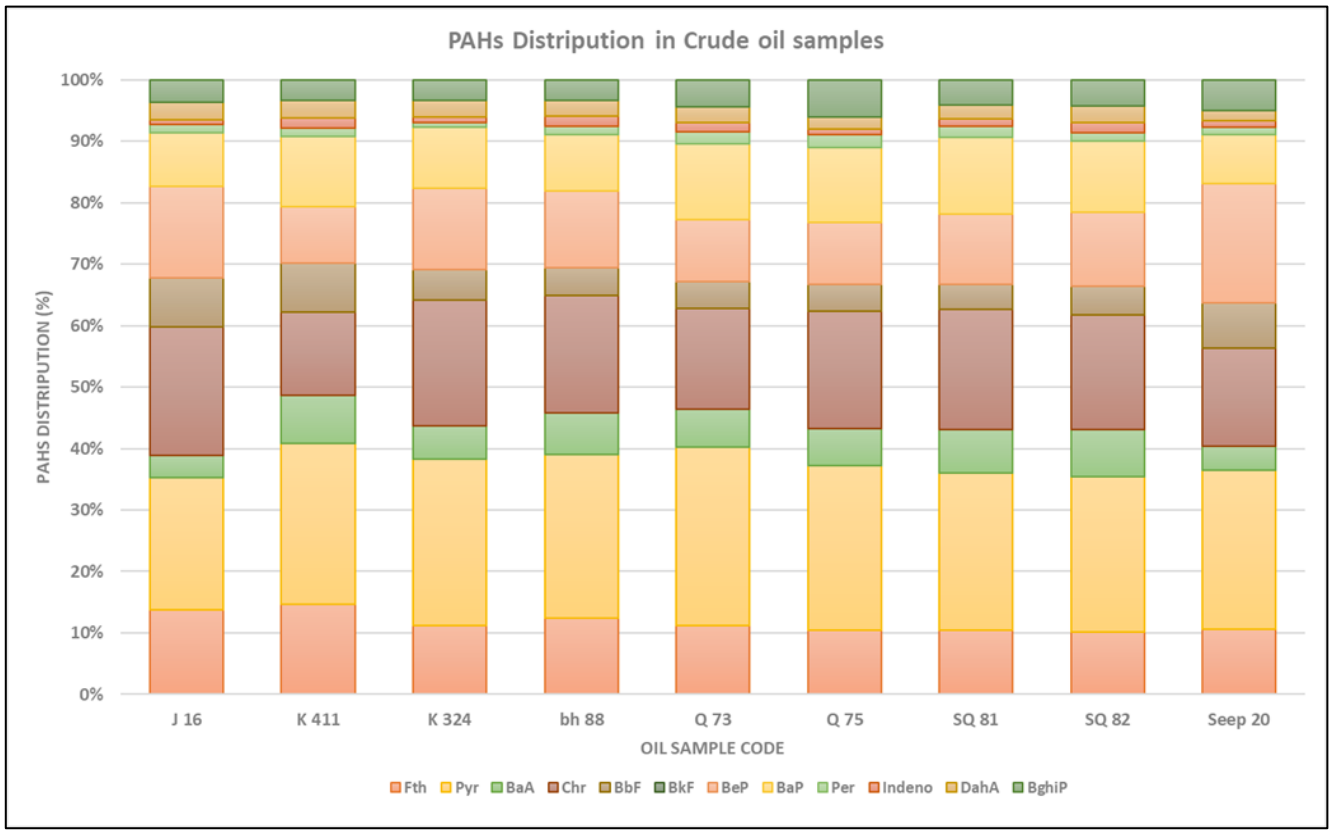

Figure 45: Percentage PAH distribution of high molecular weight PAHs in different oil and seepage samples

As described in 2.3.8, the range of the PAH concentrations of the analyzed crude oil samples was compared with the Kerr's results (Table 11). The mean of the batch experiments was calculated and compared with and without seepage sample No. 20. This comparison was made due to the remarkable composition of sample 20, which have a high impact at the mean concentration. The PAH content of the study area, beside Indeno[1,2,3-cd] pyrene, generally have lower values than the mean content of crude oil in Kerr at al., (2001) study. Furthermore, the highest content of Indeno[1,2,3-cd] pyrene in the Kirkuk crude oils is still less than the results of Kerr et al., (2001).

The result of the comparison shows significant differences in the PAH distribution of the Kirkuk oil samples and Kerr's study results. The Kirkuk crude oil in this study contains Acenaphthylene even though it was not recognized in Kerr's experiments. Anthracene and Benzo[k]fluoranthene were detected in Kerr's analysis, but they were not identified in this study. Kerr et al., (2001) found in 93% of 60 samples Benzo[k]fluoranthene. Meanwhile, the tested offshore crude oils in the North Sea did not show any Benzo[k]fluoranthene (Aas et al., 2000). The summation of PAHs is an additional important parameter to analyze the PAH contamination. The summation of PAH in all 20 oil samples is illustrated in Figure 43. The equation which was used for the calculation of the content was the following: (mass of PAHs (ng) diluted in cyclohexane (ml)) divided by the mass of oil in gram. The total PAH content clearly shows a link between the number of PAHs and the classified oils. According to this method, lighter oils (J 16) contain more PAHs than heavier oils Nr. 20.

Table 11: Comparison of the PAH content between the results of this study and other worldwide oils

PAH	Mean values (mg/kg)[1]	Mean values of experiments without sample No. 20 (mg/kg)	Mean values of experiments inclusive sample No. 20 (mg/kg)
Naphthalene	422.9	131.02	116.52
Acenaphthylene	ND	6.73	5.98
Acenaphthene	13.9	10.18	9.08
Anthracene	3.4	ND	ND
Phenanthrene	176.7	52.25	46.68
Fluorene	73.6	26.7	23.76
Benz[a]anthracene	5.5	1.04	1.05
Fluoranthene	3.9	2.02	2.12
Chrysene	28.5	3.23	3.37
Pyrene	15.5	4.44	4.75
Dibenz[ah]anthracene	1	0.44	0.44
Benzo[a]pyrene	2	1.83	1.88
Benzo[b]fluoranthene	3.9	0.93	1.06
Benzo[k]fluoranthene	0.46	ND	ND
Indeno[1,2,3-cd]pyrene	0.06	0.21	0.22
Benzo[ghi]perylene	1.53	0.67	0.75

[1] Kerr et al., 2001

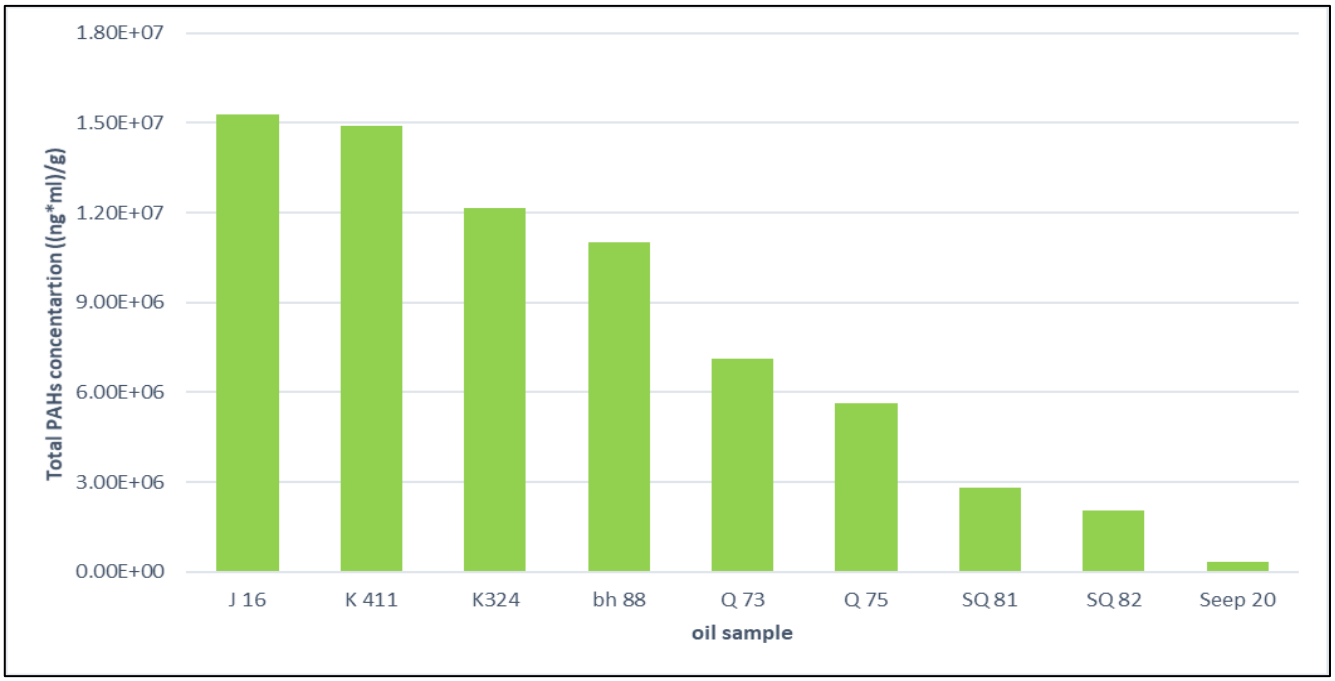

Figure 46: The total 20 PAHs concentration of the studied oil samples

4.2.Hydrogeology approach to evaluating the salinity source

Sixty-five water samples from the Kirkuk area (Figure 23) were analyzed for hydrochemical parameters, including water isotopes (D, 18O). In addition, strontium concentrations and strontium isotopes ($^{87}Sr/^{86}Sr$) were determined (Table App - 3).

4.2.1. Hydrochemistry analyses

The groundwater contour map – constructed base on hydraulic head measurements during the sampling campaign and using data from Saud (2009) – indicates regional groundwater flow direction from north-east to south-west, following the topography of the region. This shows a regional hydraulic connection between the two basins due to the fracture system of the Fatha Formation. However, the occurrence of several diffuse sulfur springs along the north-eastern outcrops of the Fatha – e.g., B23 in the Kirkuk anticline, Q64, and Q70 in the Qara Chauq anticline, and the low discharge spring J37 in the Jambur anticline – underlines that the Fatha Formation acts at least partly as a hydraulic barrier, due to the low matrix permeability.

As discussed in section 2.4.5, the north-west to south-east striking Kirkuk anticline divides the area into two sub-basins (Saud, 2009). These basins are separated by the Fatha Formation, which has a low matrix permeability and outcrops in a small band on the anticline axis (see Figure 6, Figure 7, Figure 12) and (Figure – App. 4). The hydrochemistry of the groundwater in the two basins is significantly different, as indicated by the location of the samples in the Piper diagram (Figure 47). While in the upstream basin – upstream from the Fatha Formation in the Kirkuk anticline – groundwater chemistry is mainly dominated by calcium and bicarbonate and a relatively low overall mineralization (EC from 350 μs/cm to 900 μs/cm), the groundwater hydrochemistry in the downstream basin is dominated by calcium/sodium sulfate with higher salinities (EC reaches to 6500 μs/cm). This is also reflected in the composition of the Zab river water sampled upstream (Z5) and downstream (Z16) of the anticline. The rapid change in general hydrochemistry along the flow path at the anticline axes is most likely due to the dissolution of evaporates in the Fatha Formation, especially near the Baba Dome (Araim, 1990).

Plotting the Na/Br and Cl/Br molar ratios of all samples reveals that both upstream and downstream samples plot below the halite dissolution/recrystallization line, which indicates an additional source of sodium in the water (Figure 48). The depositional setting of the Fatha Formation is assumed to be a semi-closed, arid and shallow epicontinental sea with a series of various Sabkha evaporates (Aqrawi, 1993). This can result in the formation of sodium sulfate (Shawkat, 1979) and sodium, magnesium and potassium-rich evaporates have been reported to occur in the Fatha Formation (Al-Jaboury et al., 2009). Moreover, cation exchange may contribute to the elevated sodium concentrations in the water samples.

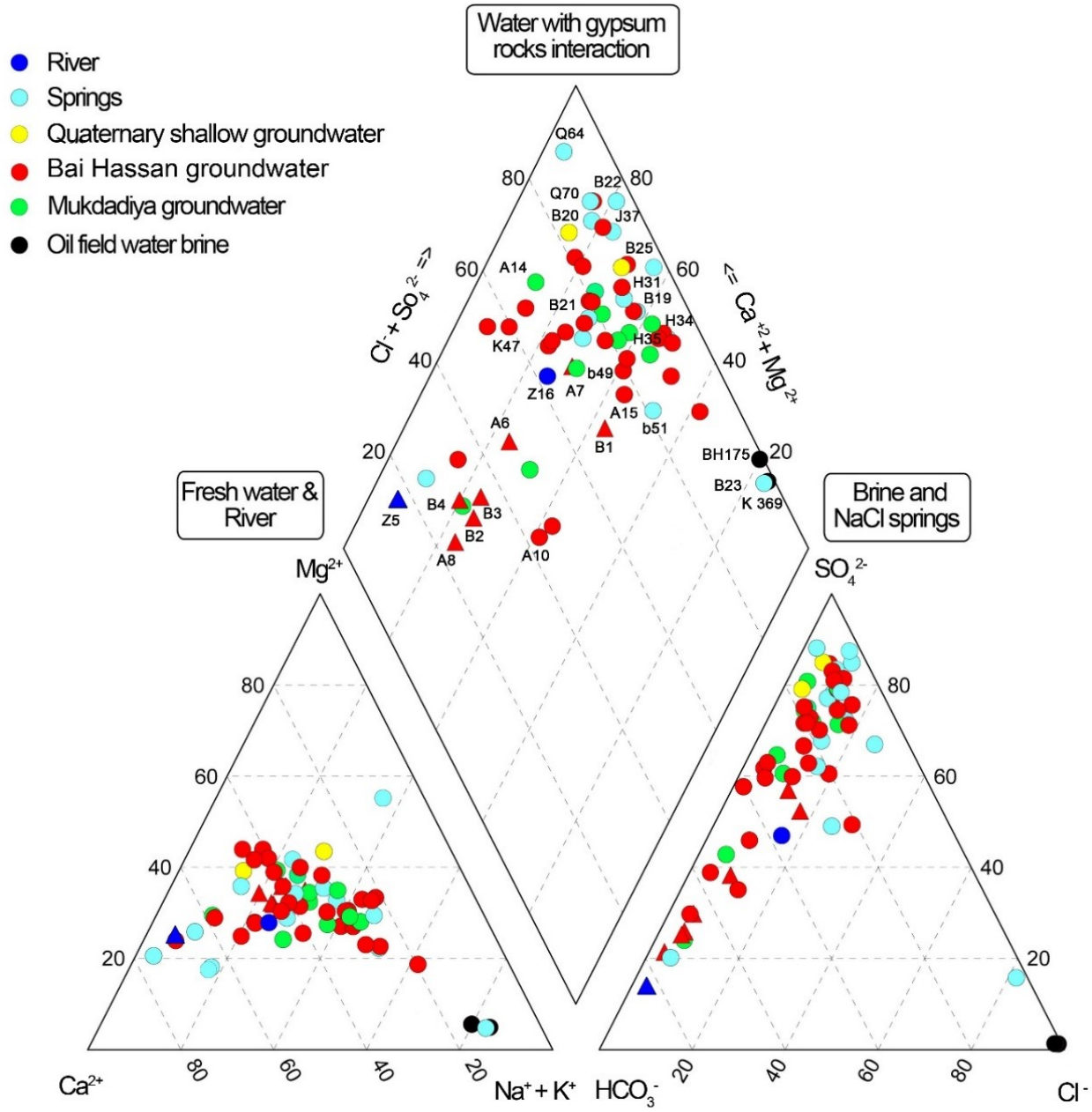

Figure 47: Piper diagram of the water samples indicating the main three end members. Triangles refer to the samples from upstream basin, circles represent samples from the downstream basin (Sahib et al., 2016)

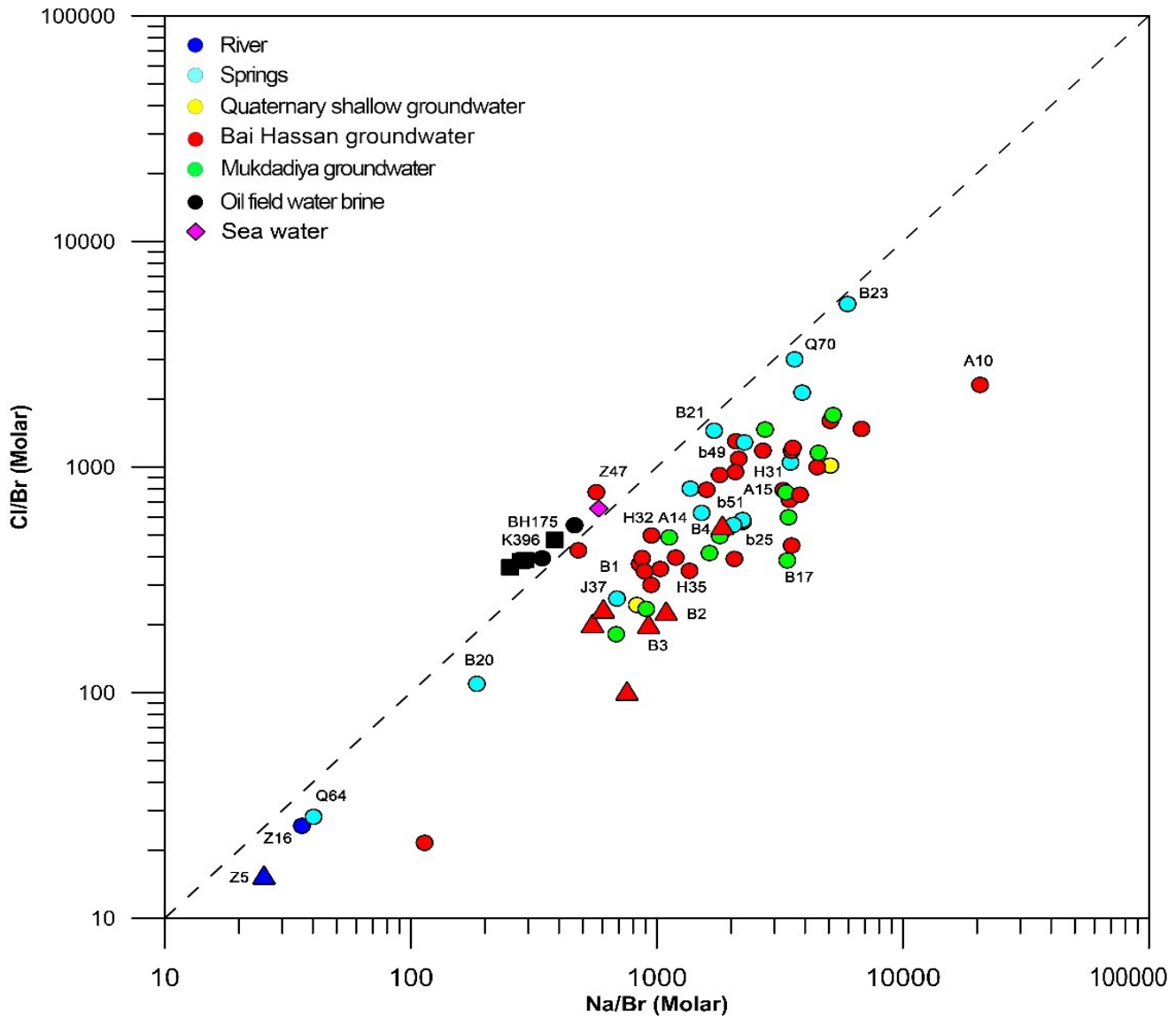

Figure 48: Relationship between Na/Br and Cl/Br molar ratio. The dashed line in halite dissolved line. For comparison, squire symbols refer to brines from Oligocene oil traps in Iran (Mirnejad et al, 2011). Triangles refer to the samples from upstream basin, circles represent samples from the downstream basin (Sahib et al., 2016)

A bivariate plot of $Ca^{2+} + Mg^{2+} - HCO^{3-} - SO_4^{2-}$ versus $Na^{+} + K^{+} - Cl^{-}$ (Figure 49) was constructed to assess the possible effects of cation exchange. Data points close to the origin of the figure indicate that no significant ion exchange occurs. Deviations from the origin can be caused by either cation exchange (Mclean et al., 2000) or the dissolution of other minerals than halite, gypsum or carbonates. Cation exchange would result in a line with a slope of -1 (ion exchange line). In our case, most samples deviate from the ion exchange line towards relatively higher sodium and potassium concentrations, indicating the dissolution of additional minerals containing these cations. This is in accordance with the assumption that sodium and potassium-rich evaporates occur in the Fatha Formation.

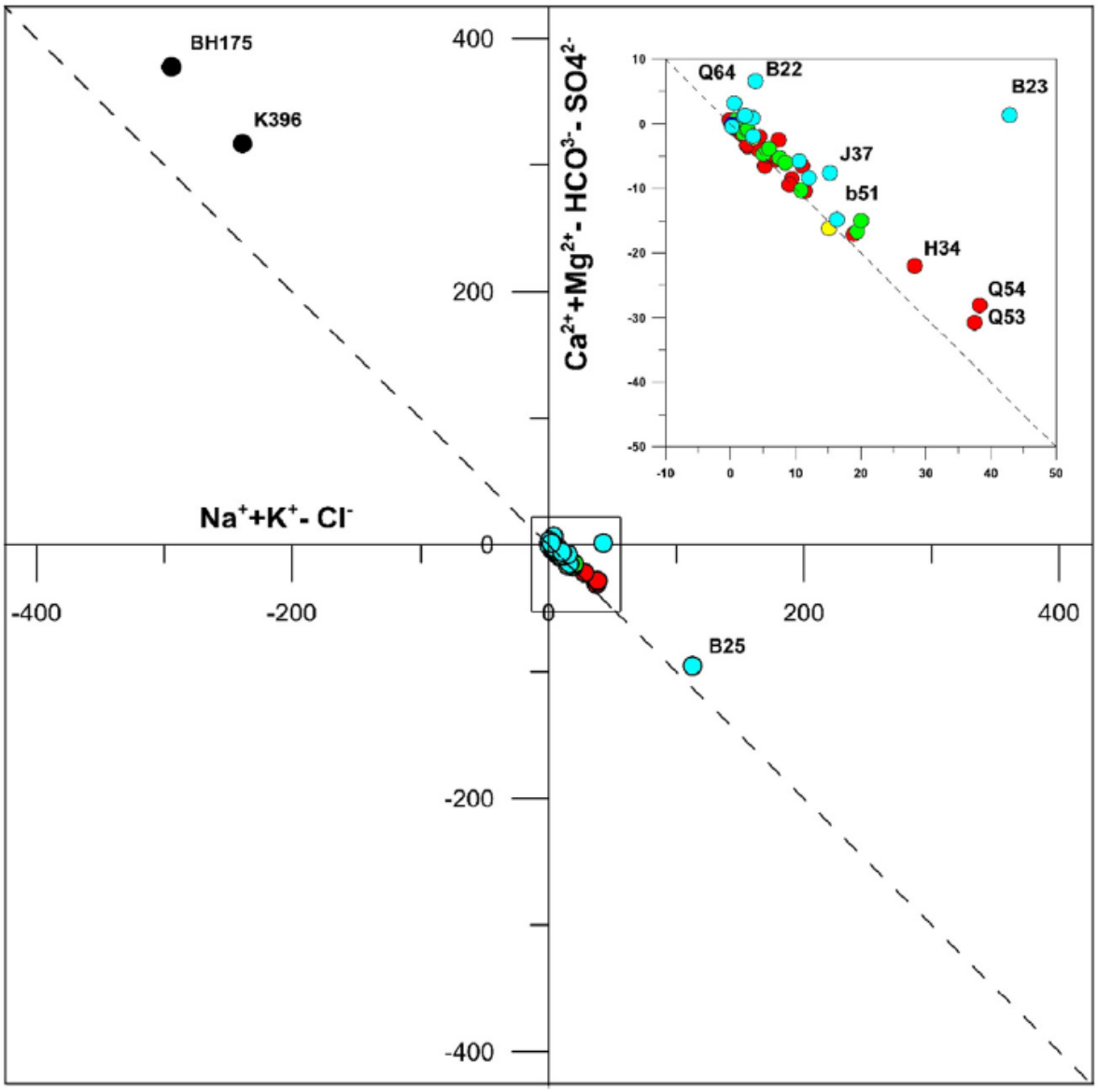

Figure 49: Ca+Mg-HCO3-SO4 versus Na+Ka-Cl plot of groundwater in the Kirkuk area. The solid black line indicates the ion exchanging line with a slope of -1 (Sahib et al., 2016)

The oil field brine samples (BH 175, K 396) are dominated by sodium and chloride and exhibit the highest mineralization with an electrical conductivity of around 155,000 μS/cm. In the Piper diagram, the oil field brine samples, the upstream river water sample (Z5) and the sulfur spring samples (e.g., Q64) indicate the potential end members of mixing between the different water sources. However, for most of the samples from the downstream basin – which are generally high in sulfate – additional mixing with oil field brine is unclear as the Fatha Formation also contains some salt (halite) layers (Jassim and Goff, 2006). Dissolution of halite would shift the location of the samples in the Piper diagram to the chloride corner where the oil field brines are located. Dissolution of halite from the Fatha Formation might even be true for sample B 23, a spring close to an oil seepage location whose chemical composition matches that of the oil field brine sample, although electrical conductivity (EC) values are much lower compared to the brine sample.

4.2.2. Strontium in groundwater

Strontium concentrations in the water samples range from less than 1 mg/l for the upstream river water sample to about 180 mg/l and 300 mg/l for the two brine samples, respectively. Plotting strontium concentrations in water samples against the distance of a sampling location from the anticline cores reveal an increased strontium concentration closer to the cores (Figure 50). Such increasing indicates that the main sources for elevated strontium concentrations in the water samples are located at the anticline axes. Strontium is an alkaline-earth element that follows calcium (Ca^{2+}) in geochemical and hydrological cycles. Strontium is specifically incorporated in marine limestone, gypsum and anhydrite during precipitation from seawater. Most likely, the high strontium concentrations in the brine samples result from dissolution and dolomitization processes in carbonates of the Kirkuk and Jaddala/Avanah formations (Majid and Veizer, 1986), as strontium often substitutes calcium in carbonates (Klimas and Malisauskas, 2008). This is especially enabled by the typically strongly acidic conditions in such reservoirs. Majid and Veizer (1986) reported strontium concentrations in the carbonates of these formations, reaching up to 1000 mg/kg.

The Fatha Formation might potentially also be a source of elevated strontium concentrations in the water samples. According to Al-Bassam and Hak (2006), the Fatha Formation contains sulfur-bearing horizons comprising secondary calcite, gypsum and aragonite that can release strontium through the dissolution of strontianite or celestite (Eq. 15).

$$SrSO_4 \leftrightarrow Sr^{2+} + SO_4^{2-} \quad \text{(Equation 15)}$$

There is ample field evidence for the dissolution of gypsum in the Fatha Formation as karstic hypogene and epigene caves are formed in gypsum-rich layers (Figure - App. 5). Due to the presence of H_2S (Fig. 24 B) in the groundwater, identified by its characteristic smell, karstification might also be due to the oxidation of hydrogen sulfide with oxygen in the groundwater (Palmer and Hill, 2012) (Eq. 16). This is supported by the occurrence of the traces of sulfur at the surface (Figure - App. 6).

$$2H_2S + O^2 \text{ --- oxidation environment --- } 2S + 2H_2O \quad \text{(Equation 16)}$$

With this, two potential sources for high strontium concentrations in groundwater can be identified: (i) dissolution of carbonates in the Kirkuk Group and Jaddala/Avanah formations and resulting enrichment of strontium in the oil field brines, and (ii) dissolution of gypsum in the Fatha Formation. Especially in the highly fractured cores of the anticlines with outcrops of the Fatha Formation, an uprise of oil field brines and dissolution of gypsum may occur at the same time, leading to elevated strontium concentrations in the water.

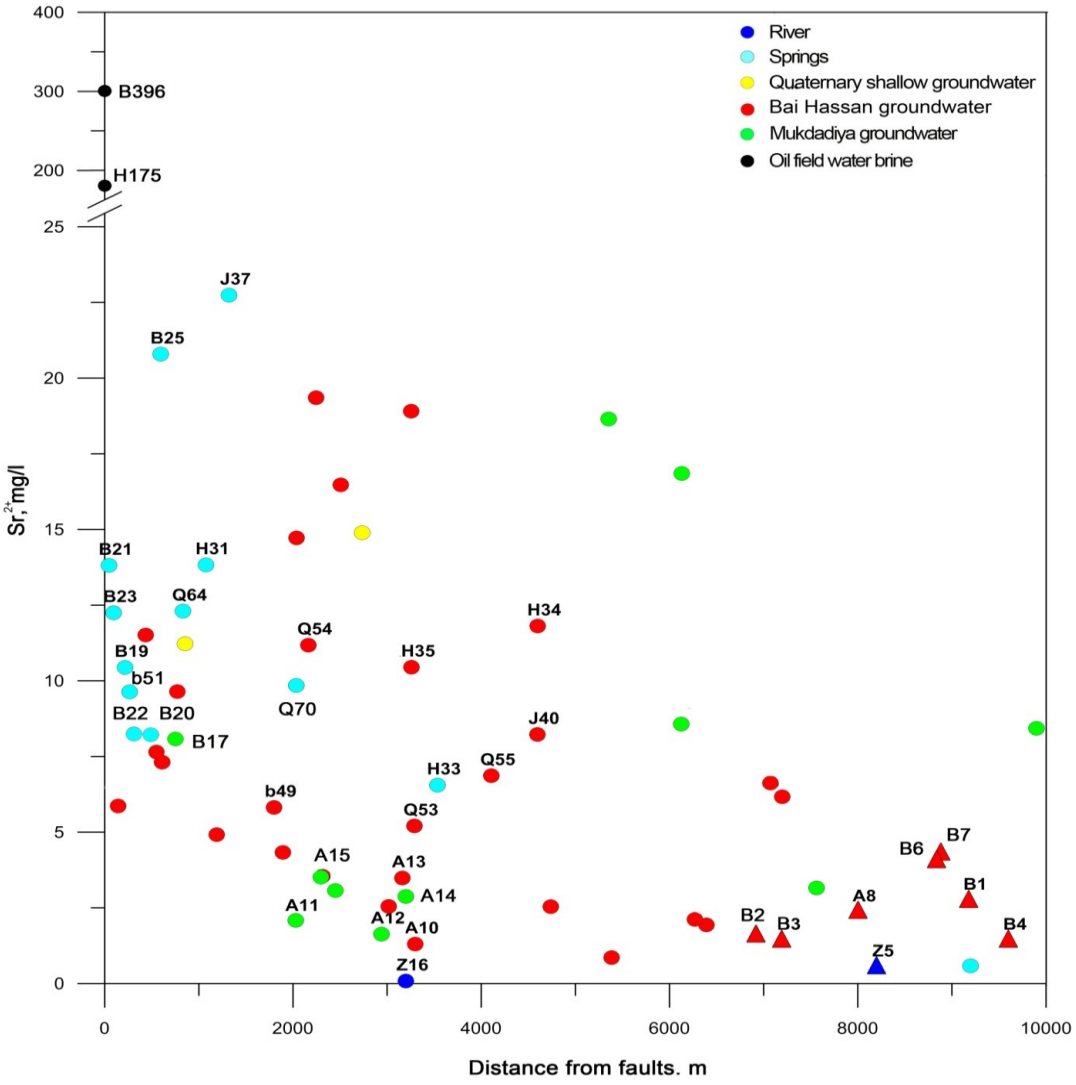

Figure 50: Relationship between Strontium concentration in water and the distance from the main faults in the Kirkuk area. Triangles refer to the samples from upstream basin, circles represent samples from the downstream basin (Sahib et al., 2016)

4.2.3. Stable Water Isotopes

4.2.3.1. Deuterium (δ ^{2}H) and Oxygen (δ^{18}O)

In order to further elucidate mixing between the oil field brines and the groundwater, stable water isotopes ($\delta^{2}H$, $\delta^{18}O$) were determined (Figure **51**). The isotopes of the spring water, surface water and groundwater samples show some variability, but plot mostly close to the Local Meteoric Water Line (LMWL; $\delta^{2}H = 7.5\ \delta^{18}O + 11.9$, Al-Paruany, 2013). For the spring samples plotting right of the LMWL, secondary evaporation can be assumed. Samples showing this trend were mainly taken from small ponds at diffuse springs with low discharge (Q70, J37 and B25). Furthermore, the elevated EC values are in line with the postulated evaporation effect. Meanwhile, the high depleted samples can refer to the recharge from the rivers that are fed with the water from the higher elevation gradient lands to the north-east after the winter season. The oil field brines show isotopic signatures that significantly differ

from those of the water samples. The positive $\delta^{18}O$ values are probably caused by an exchange of O atoms between the brine and the $CaCO_3$ in the reservoir rocks (Clayton et al., 1966; Craig, 1963, Craig et al., 1956). For the Eocene and M. Oligocene limestone of the Kirkuk oil field, Majid and Veizer (1986) report $\delta^{18}O$ values between −9 and 0‰ PDB. Converting these values into δ values on the VSMOW scale (Coplen, 1988), one obtains $\delta^{18}O$ signatures roughly ranging between 22 and 31‰VSMOW. Hence, even a limited exchange would result in a significant positive displacement or "oxygen shift" (Craig, 1963).

In the present case, this shift caused a unique isotopic fingerprint of the brines (enriched by about 5‰). Thus, the stable water isotopes can – in principle – be utilized as a mixing indicator. Nonetheless, Figure **51** does not reveal such a mixing. Even the sample B23 that shows an elevated salinity and a major ion composition resembling that of the brine samples (Fig. 47) plots close to the LMWL. However, this does not necessarily mean that no mixing occurs. Considering the EC values of the brine samples (approx. 155,000 μs/cm) and the EC values of the remaining water samples (several hundred mg/l to 20,000 μs/cm), a maximum of about 10% brine could be mixed into the water samples. This would cause a maximum$\delta^{18}O$ enrichment by 0.5‰, albeit this is in the range of $\delta^{18}O$ variations in the water samples. Therefore, the stable water isotopes are not sufficiently sensitive for detecting mixing in the present case.

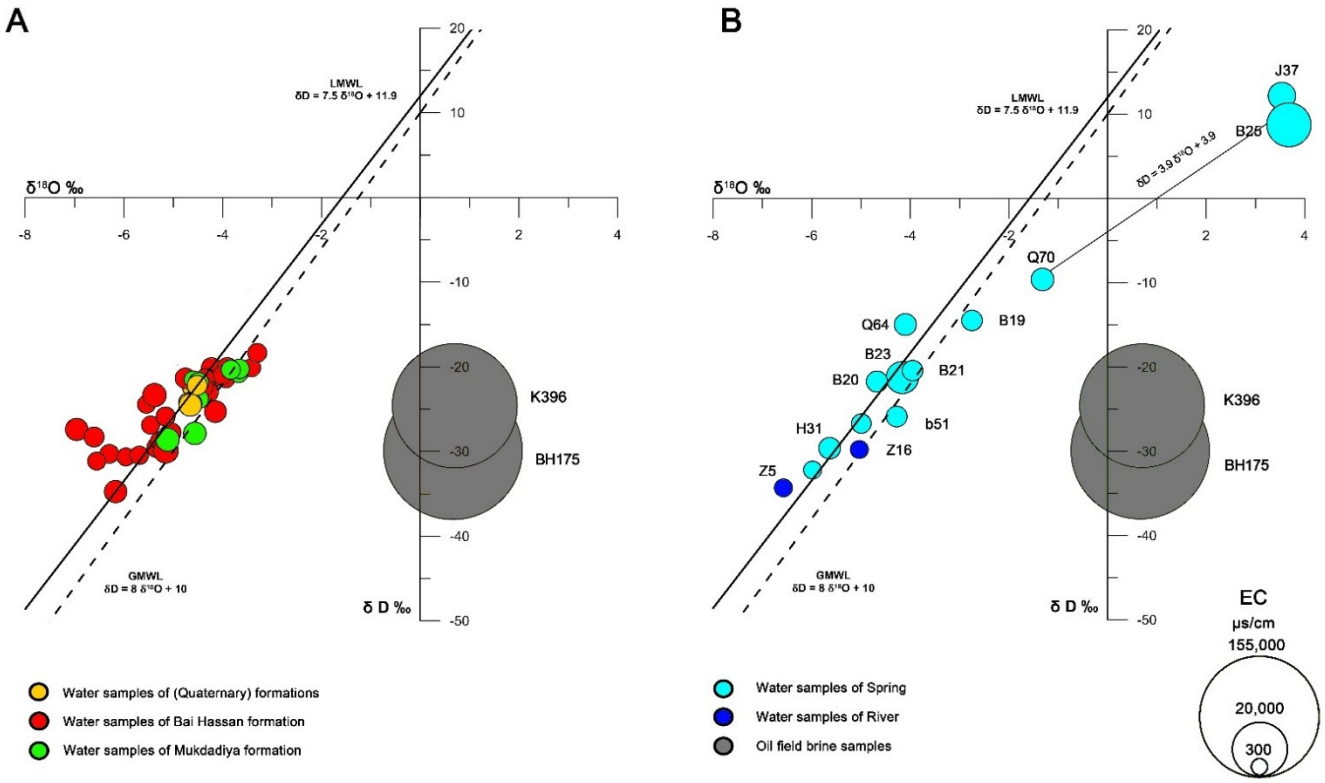

Figure 51: Cross plot of the δ D and δ18O of all water samples. Global meteoric water line (GMWL) (Craig, 1961) and LMWL (Al-Paruany, 2013). On the left groundwater samples, on the right river and spring water samples, in comparison to oil field brine samples. The symbol size indicates EC values (Sahib et al., 2016)

4.2.3.2. Sr isotopic

However, strontium concentrations in the water samples alone do not reveal the source of the strontium. Therefore, strontium isotopes were used to distinguish between the contribution of oil field brines and the Fatha Formation to the total strontium concentrations in the water samples. This approach is based on the fact that strontium isotopes can be used for dating of marine deposits (McArthur et al., 2012). Especially for tertiary deposits, the strontium isotopic signature of marine deposits shows a gradual increase in the $^{87}Sr/^{86}Sr$ isotope ratios over time (Oslick et al., 1994). As evaporation is conservative with respect to strontium isotopes (Peterman and Stuckless, 1992) dissolution of strontium from a carbonate formation will result in a unique strontium signature in the water, depending on the age of the formation. Depaolo and Ingram (1985) and Elderfield (1986) reported $^{87}Sr/^{86}Sr$ isotope ratios between 0.7081 and 0.70765 for middle Oligocene-Eocene formations (i.e., Kirkuk and Jaddala/Avanah formations), while Oslick et al., (1994) and Howarth and McArthur (1997) reported ratios between 0.70828 and 0.7090 for the Miocene formations (i.e., Fatha Formation).

In Figure 52, the results are plotted against the strontium concentrations in the water samples. Most of the water samples have an average $^{87}Sr/^{86}Sr$ ratio of about 0.70820, which is between the values expected for the middle Oligocene-Eocene formations and the Miocene formations, respectively. Moreover, the upstream river water sample (Z5) – taken at some distance (8 km) from the axes of the Kirkuk anticline and the Fatha outcrop area – and all analyzed groundwater samples from the upstream basin fall in this range. Therefore, it can be assumed that this value is indicative for samples that are likely not to be influenced by the oil field brines and by waters originating from the Fatha Formation but originate from the shallow Mukdadia and Bai Hassan aquifers. The sediments of these aquifers are mainly terrigenous, unconsolidated materials that are derived from various sources and thus generate a mixed strontium signature in the water.

The $^{87}Sr/^{86}Sr$ ratio of the brine samples (K396 and BH175) taken from production wells in the Kirkuk and Bai Hassan oil fields, respectively, show the typical signature of middle Oligocene-Eocene formations. This is expected as the brine samples are derived from the wells tapping the Kirkuk Group. There is some difference between the two samples that cannot be explained readily as the exact location of the screened sections of the wells are not known. However, the isotopic signature of both samples is significantly different compared to the signature of the waters from the upgradient basin. The spring water samples collected close to the fault zone (Q64, B20, and B21) have $^{87}Sr/^{86}Sr$ ratios typical for younger formations, which suggests that the discharging groundwater originates from the Fatha Formation. Moreover, sample B23 – which plots close to the brine sample in the Piper diagram – has an $^{87}Sr/^{86}Sr$ ratio that indicates at least some extent of dissolution of evaporates and carbonates from the Fatha Formation. In contrast to this, strontium isotope ratios of the spring water sample b51 (0.70788) – which was also taken close to the fault zone – indicates mixing with oil field brine. This is the only water sample that clearly shows this effect and indicates an uprise of brines from the Kirkuk Formation through a local fracture system. However, not all water samples were analyzed for strontium isotopes.

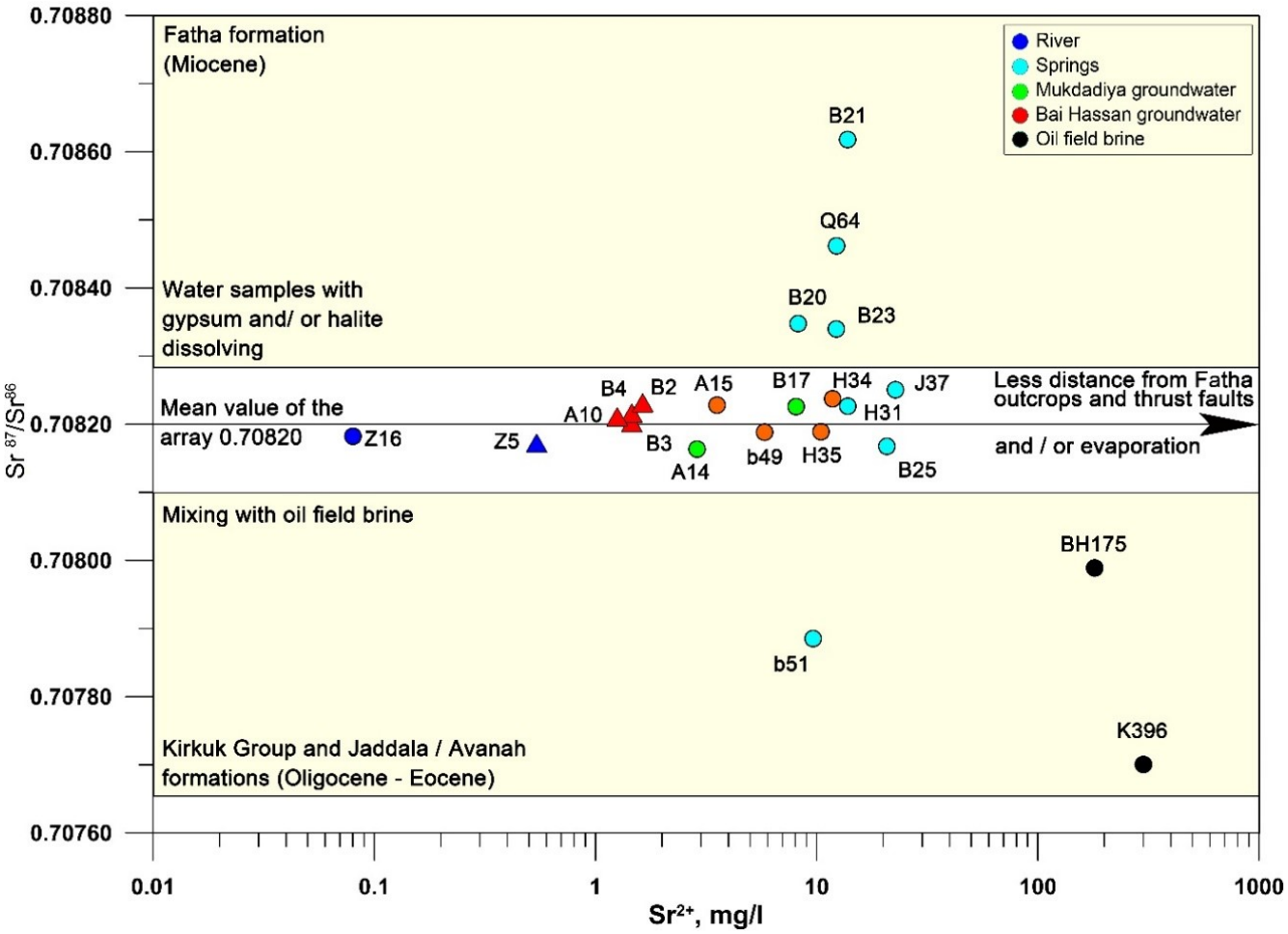

Figure 52: Cross plot of $^{87}Sr/^{86}Sr$ isotope ratio vs. Strontium concentrations of selected water samples. The two shaded areas are the $^{87}Sr/^{86}Sr$ of the rocks formed during M. Oligocene - Eocene is typically between 0.70810 and 0.70765 (Depaolo and Ingram, 1985; Elderfield, 1986). Miocene rocks have $^{87}Sr/^{86}Sr$ ratios between 0.70828 and 0.70895 (Oslick et al, 1994; Howarth and McArthur, 1997). Triangles refer to the samples from upstream basin, circles represent samples from the downstream basin (Sahib et al., 2016)

4.3. Spectral reflectance approach to determine the characteristic of Iraqi crude oil

4.3.1. Crude oil spectral absorption

As a single-phase case, the four crude oil samples from the Kirkuk oil fields were analyzed for their spectral reflectance, scanning the wavelength range of 350-2500 nm by the Analytical Spectral Devices (ASD). Figure 53 shows the reflectance versus the wavelengths. Numerous absorption features were recorded in the crude oil spectra. Due to the different selected oil types (Table 12), the higher the API oil type correlates with deeper absorption features.

The reflectance spectra of the condensate gas sample 628 show more absorption features than the other oil samples. It was noticed that sample 551 and 612 have a similar spectral pattern, which is related to the similar API gravity. For all samples, the primary absorption features of reflectance could be detected at 1720-1732 nm and 2301-2313 nm (P2 and P3 in Figure 53). A third primary absorption feature could be observed at 1200-1210 nm (P1) for all the samples except the lowest API oil sample 571.

Table 12: API gravity and sulfur content for four crude oil samples. According to the API, the samples are classified as light and heavy API oils

Sample No.	Well, No.	API	S % wt	Density	Age / Formation	Oil field	Sample type
551	K 359	34.070	2.650	0.8546	E. M Eocene / Avanah	Kirkuk	Light crude
571	Q 45	15.127	7.481	0.9650	E. Miocene / Jeribe	Qaiyarah	Heavy crude
612	J 22	34.920	1.546	0.8500	E. Eocene / Aliji	Jambur	Light crude
628	-	52.000	-	0.7470	-	Jambur	V.Light crude [1]

[1] Condensed oil from natural gas.

Secondary absorption features were also visible at 1640 and 1760 nm (S1 and S2). The different extent of the reflectance of the four samples is due to the differences in the composition of the organic compounds in the samples, i.e., alkanes that contain single carbon-carbon bonds (Clark et al., 2009), carbon-hydrogen bonds (C-H, $C-H_2$ and $C-H_3$), as well as double and triple bonds of aliphatic and aromatic compounds (Winkelmann, 2005). The other absorption features are a result of hydroxyl groups (O-H) (Pope & Fry, 1997; Yakovenko et al., 2002; Wu, 2008).

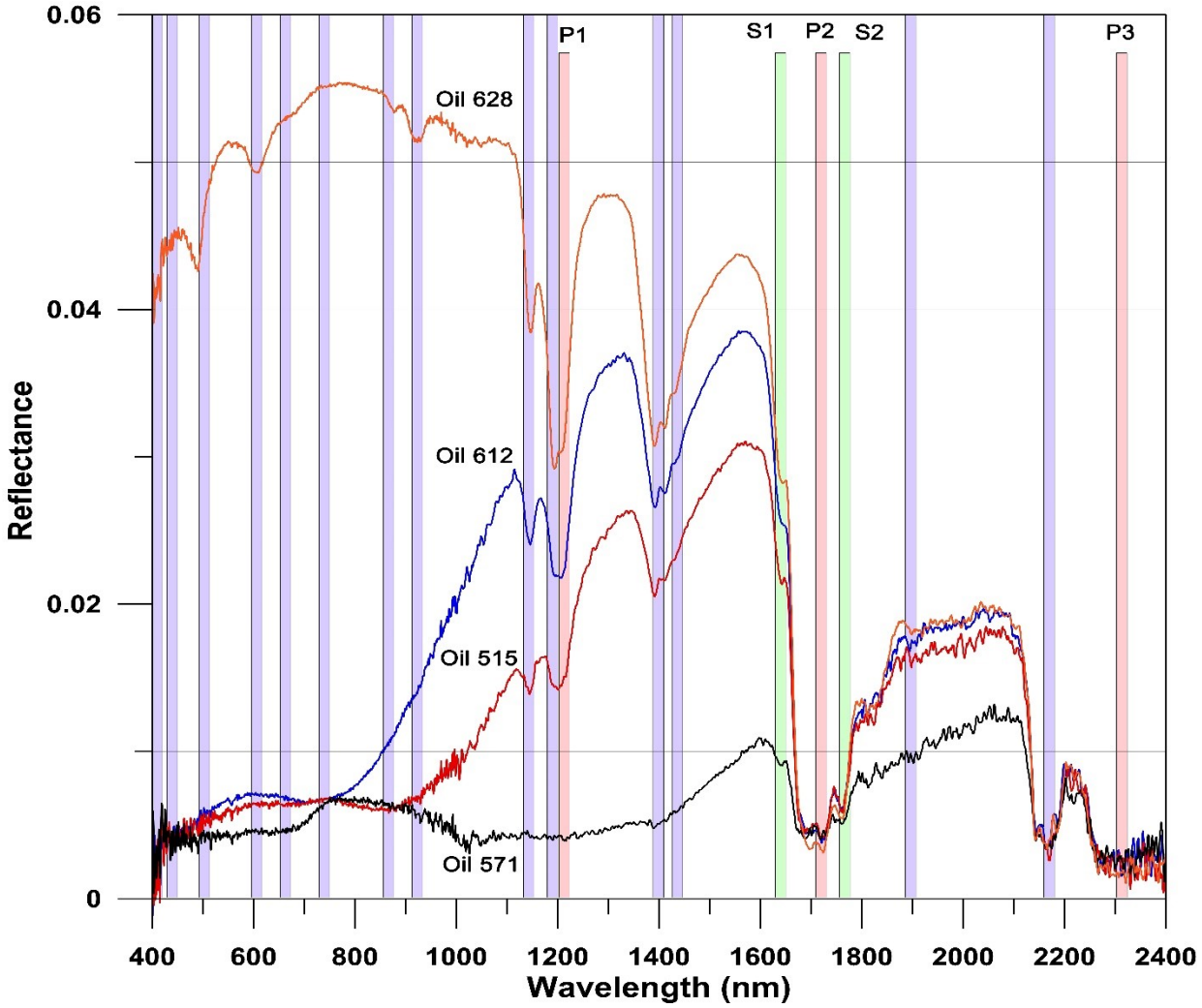

Figure 53: Raw spectral reflectance of four crude oil types with different API gravity. P1, P2, and P3 are the primary absorptions features, S1 and S2 are the secondary absorption features. The water absorption features are shown in blue lines. The spectra before 400 nm and after 2400 were removed because of the noise

4.3.2. Soil and crude oil spectral absorption (two-phase experiment)

The reflectance of soil mixed with crude oil was investigated under defined conditions. The three selected oil samples were chosen according to API classes 628, 551 and 571 (see Table 12). Figure 54 shows the reflectance of oil-spiked soil samples with an increasing oil percentage from 0.1-11%. In general, the reflectance decreases with increasing oil content. The primary absorption features showed the oil contamination at wavelengths from 1200-1210 and 1720-1732 nm. At higher oil percentages – more than ca. 2% oil in the experiments – a third absorption feature occurred at 2301-2313 nm. These findings are in agreement with the results of Cloutis (1989), even though this author used a different setup and was investigating bituminous tar sands.

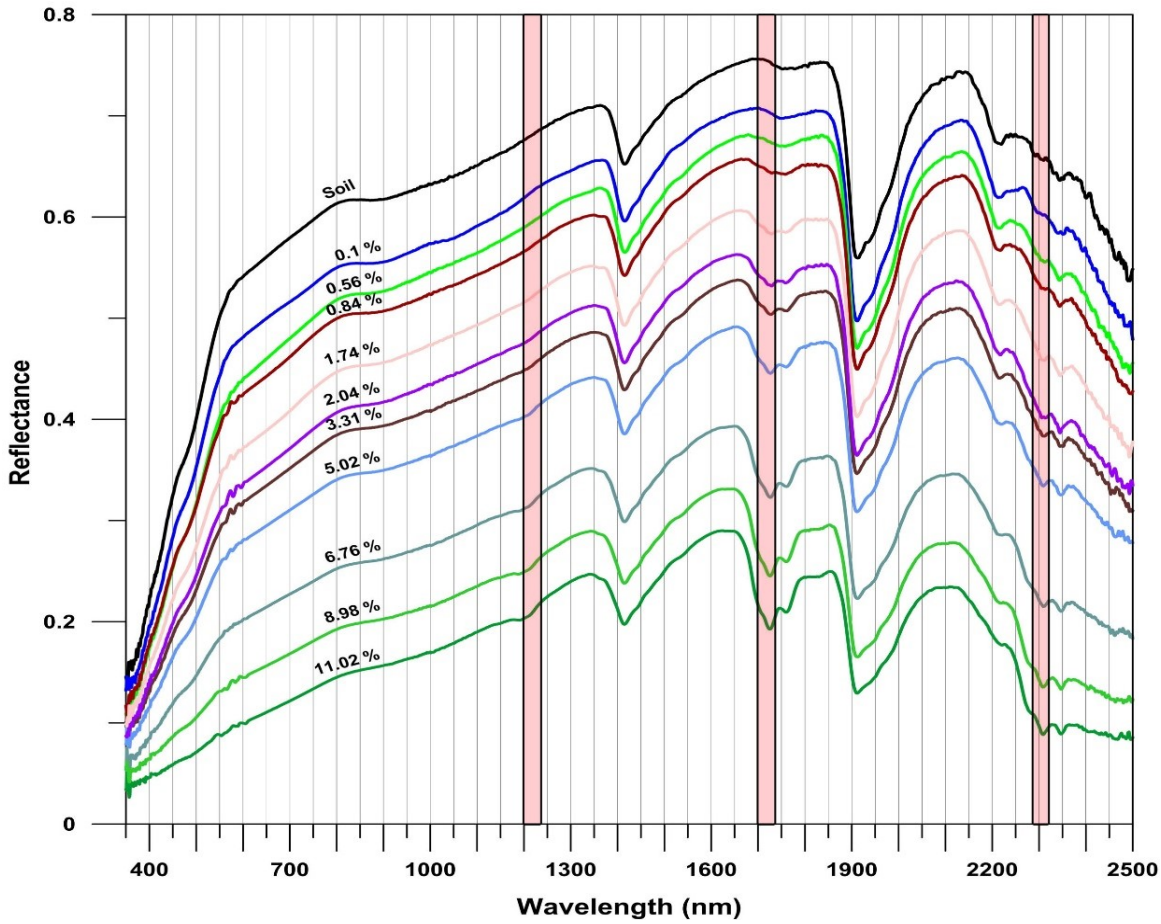

Figure 54: Reflectance spectra of different crude oil percentages in soil (sample 551). The primary absorption features are shown with shaded bands at wavelengths 1200-1210, 1720-1732 and 2301-2313 nm

For quantitative analysis, the reflectance signals were transformed to the first derivative, i.e., the rate of change of reflectance per wavelength (Owen, 1996). The variations between the positive and negative values in the inflection point define the absorption amplitude. At the primary absorption features, the signal can be explained by the hydrocarbon content in soil (Figure 55). Among the studied wavelengths, the second band at 1720-1732 nm exhibits the most sensitive signal range for organic components within the whole spectra used. This is in harmony with the findings of Kühn et al., (2004) and Hörig et al., (2001), who found that the 1730 nm wavelength is typical for hydrocarbons and is suitable to calculate the HI.

The negative peaks at ca. 1400 nm and 1900 nm are typical for water (Walrafen & Pugh, 2004), showing that even the residual water after air drying can be detected in the soil samples. In order to calculate the HI for the chosen wavelength, it was important to define the absorption peak boundaries (width and depth) by selecting the absorbance shoulders R_A and R_C and the lower reflectance values R_B (Figure 30). Different wavelengths were recommended to calculate the HI from the second absorption. In order to identify the suitable absorption components (R_A, R_B, and R_C), Kühn et al., (2004) used 1705, 1729 and 1741 nm and Tian (2012) used 1699, 1729 and 1749 nm, respectively. By comparing the second band reflectance values with the results from phase one and two experiments, the wavelength shoulders 1705-

1741 nm and 1699-1749 nm – with 1729 nm as a peak center – seems more suitable, because the minimum reflectance values for the point R_B were between 1720-1732. For the artificially-contaminated soil samples, the HI values of the three crude oils were calculated using the Models I, II and III. For each model, the HI was calculated for both continuum boundaries. The HI values within the continuum boundaries 1699 and 1749 nm show higher values for all samples for all models (Y-axes in Figure 56). This finding was expected since the defined width of the continuum boundary is wider than the definition by Kühn et al., (2004). Therefore, the continuum with boundaries 1699 and 1749 nm was used for further calculations.

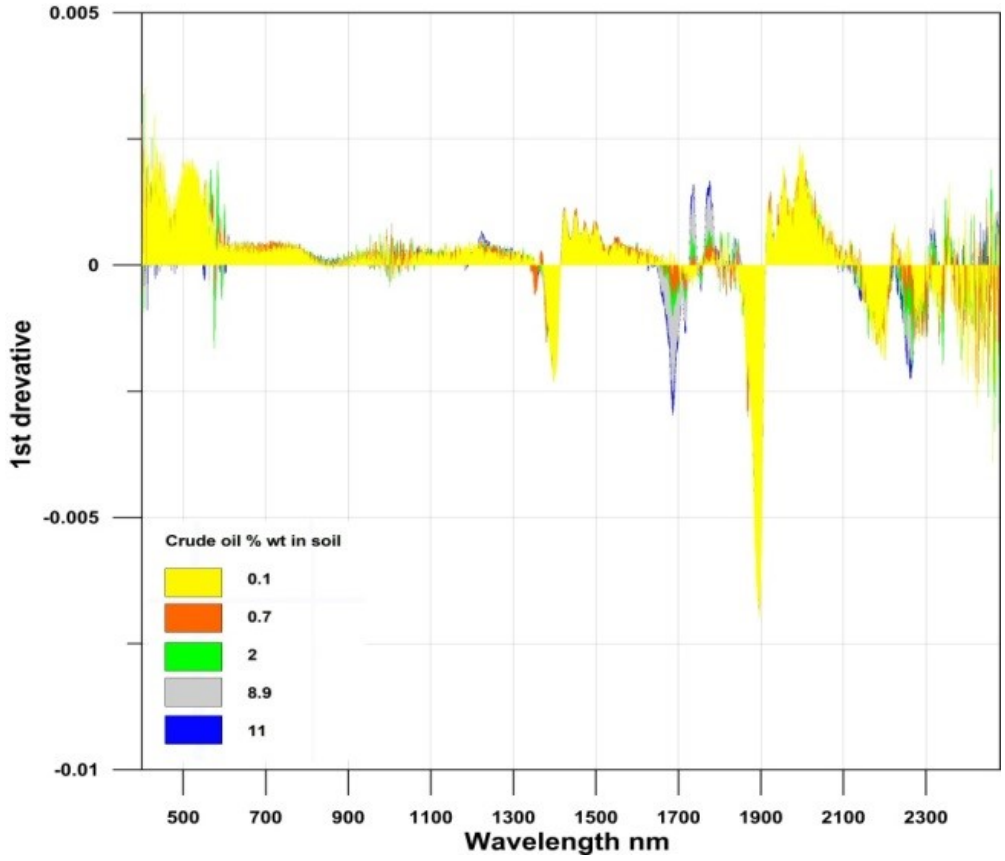

Figure 55: Comparison of the 1st derivative of raw reflectance spectra for different crude oil concentrations (sample 551) in the soil. The arrows pointing to the main three studied absorptions

The sensitivity and the Detection limit (DL) of the HI change are depending on the oil type and used model. Starting with light crude oil samples 628 and 551, Models I and II showed positive values as DL, which means the presence of oil content by HI (See: 3.3.2.2. Calculation of the Hydrocarbon Index HI). The continuum boundaries (1966-1748) presented a positive HI of the oil content in the soil starts at 0.28 % wt., and end with 0.59 % wt., which can consider as DL (Table 13). The DL showed relative similarity values of the samples 628 and 551. However, the sample 628 (as condensing natural gas) have a higher light percentage of the aromatic and aliphatic component. Meanwhile, for the heavy crude oil sample 571, both models and continuum give the same DL values.

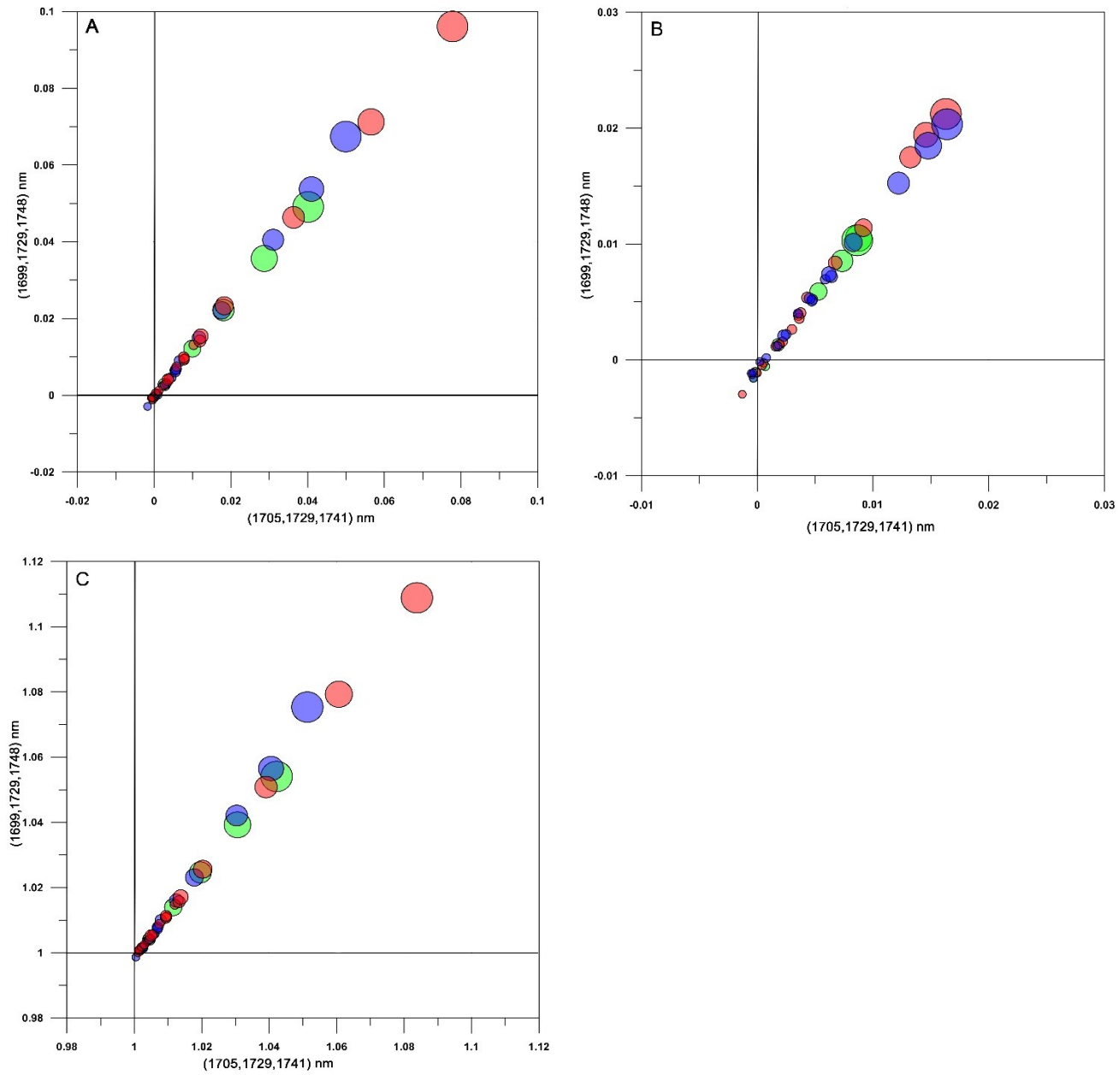

Figure 56: The HI of two continuum boundaries (1966-1748) nm and (1705-1741) nm and absorption feature center at 1729 nm for three crude oil types with known contamination limits in the soil. The red point refers to oil sample No. 551, blue points are oil samples 628 and the green points are oil samples 571. The dark lines represent the present of HI for each model. A. The model I, B. Model II, C. Model III. The circle size represents the oil content

Model III explains that the presence of oil content depends on values higher than 1. The two-phase experiment showed that this model successfully detected the minimum added (around 0.1 % wt.) of the oil samples 625 and 551. That was even clear with very low API oil sample 571, which also have about 0.4 % as DL. Comparing the DL values for all of the models for the three samples shows higher DL values for Model III compared to Models I and II. For testing the correlation with higher oil concentration, the continuum 1699-1749 nm for the three models was plotted against the three oil content types in the soil. Models I and III explain a better correlation between HI and oil content comparing with Model II (Figure 57).

Table 13: The detection limits for used methods with three selected oil content in soil (two-phase experiment). The continuum boundaries (1966-1748)

Model No.	Model I (% wt.)	Model II (% wt.)	Model III (% wt.)
DL of the HI (sample 628)	0.34	0.59	0.12
DL of the HI (sample 551)	0.28	0.42	0.10
DL of the HI (sample 571)	2.13	2.13	0.42

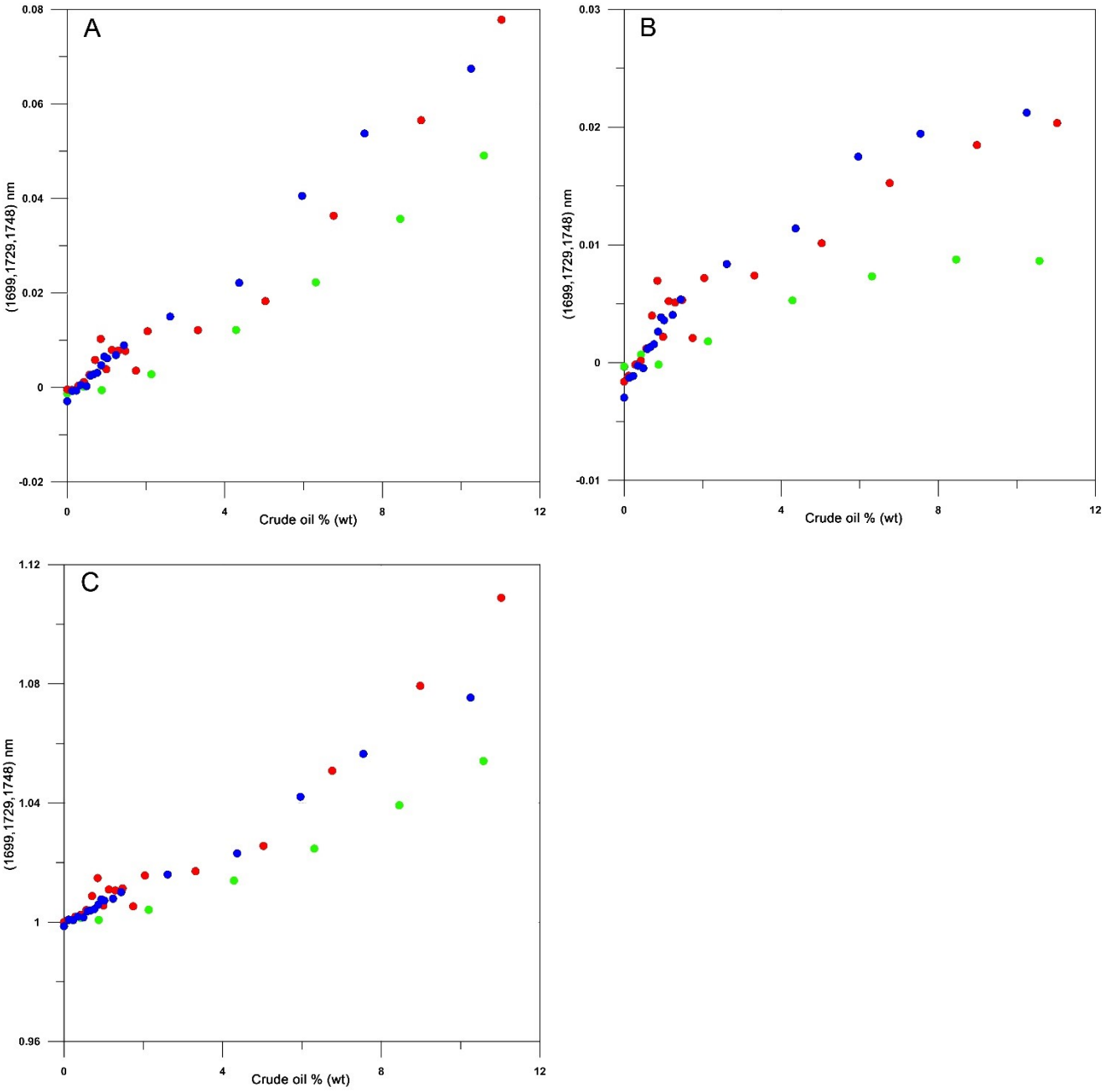

Figure 57: Hydrocarbon Index (HI) for three oil types with three models. The used continuum boundaries (1699-1748) nm, and 1729 nm as absorption minimum reflectance. The red color is oil sample No. 521, the blue color is oil sample No. 628, and the green color is oil sample No. 571. A. The model I, B. Model II, C. Model III

4.3.3. Organic Carbon (OC) and Total Petroleum Hydrocarbon (TPH) of the field Samples from the Baba seepage

Table 14 shows the OC and TPH percentage of the soil samples from the investigated seepage area. According to Hiederer and Köchy (2011), the soil organic carbon content OC for combined topsoil and subsoil layers in Iraq usually ranges from 0.01 to 1%. The plot of the samples with OC < 1% and TPH < 0.1% shows a low correlation ($R^2 = 0.57$) due to the normal background soil OC content from natural sources, e.g., vegetation other than crude oil from the seepage (Figure 58 A).

Table 14: The measured and calculated organic carbon (OC), total petroleum hydrocarbons (TPH) and hydrocarbon index (HI) to the Baba seepage samples

No.	OC [%]	TPH [%]	No.	OC [%]	TPH [%]	No.	OC [%]	TPH [%]	No.	OC [%]	TPH [%]
1	0.46	-	23	0.58	0.003	45	1.14	-	67	3.85	1.592
2	0.46	-	24	0.46	0.003	46	0.35	-	68	0.42	0.005
3	0.42	0.003	25	0.47	-	47	0.55	-	69	0.75	-
4	0.54	0.003	26	0.47	-	48	0.53	-	70	0.48	-
5	1.78	-	27	4.63	0.197	49	1.33	-	71	0.77	-
6	0.74	-	28	19.79	7.226	50	0.78	-	72	0.44	-
7	0.83	-	29	0.57	-	51	8.20	2.548	73	2.75	0.108
8	0.31	-	30	0.45	-	52	0.40	0.003	74	1.17	-
9	1.54	-	31	0.57	-	53	0.52	-	75	1.23	0.185
10	0.41	-	32	0.57	-	54	0.47	-	76	0.39	0.003
11	0.55	0.014	33	1.38	-	55	0.65	-	77	0.32	-
12	3.16	1.158	34	0.65	-	56	0.59	-	78	0.52	-
13	15.75	-	35	11.43	3.737	57	0.99	-	79	0.51	-
14	1.94	-	36	7.83	4.521	58	7.52	-	80	0.63	-
15	1.26	-	37	0.72	-	59	37.21	17.0	81	1.03	-
16	0.47	-	38	0.64	-	60	0.70	0.006	82	1.21	-
17	0.46	0.005	39	0.42	-	61	0.55	-	83	0.90	0.031
18	0.70	0.013	40	0.41	0.009	62	0.82	-	84	5.45	0.972
19	29.45	8.727	41	0.95	-	63	0.45	-	85	1.12	-
20	74.21	39.164	42	23.79	-	64	0.58	-	86	0.84	-
21	26.65	11.268	43	9.62	3.121	65	1.03	-	87	0.76	-
22	0.66	0.007	44	0.51	0.004	66	1.64	-	88	1.87	-

The TPH content values for the samples 83, 11, 18 and 40 might explain crude oil sources (Figure 58 A), while the OC values were less than 1%, which is considered as the natural OC level. Meanwhile, a high coefficient of determination ($R^2 = 0.97$) for TPH and OC was calculated for samples with a TPH content > 0.1% and an OC content > 1%. This result points to a saturated source such as the seepage (Figure 58 B) for the TPH and the OC in the soil samples. It is interesting to note that the slope of the regression line increases from 0.03 to 0.51 in the OC range of 0.01-1% and the OC range higher than 1%. This result could be an artifact that goes back to the limited integration of the FID-generated peaks between C_{10} and C_{40}.

As shown in Figure 59 for the soil chromatograms No. 67 and 73, there is still a substantial signal from hydrocarbons after the C_{40} standard, which is not integrated but will be measured and quantified by the HTO method. For example, the sample No. 20 from the center of the seepage (see Figure 28 C) shows a TPH content of ca. 39% and an OC of 74.2% (ratio of ca. 1:2). Salanitro et al., (1997) found that high concentrations of > C_{40} hydrocarbons can be a result of biological degradation processes. Higher carbon number species (C_{35} - C_{44}, degradation rate 35-60%) are more recalcitrant against biodegradation than low chain hydrocarbons (C_{11} - C_{22}, degradation rate 70-90%), which leads to an accumulation in the residual oil phase in the soil.

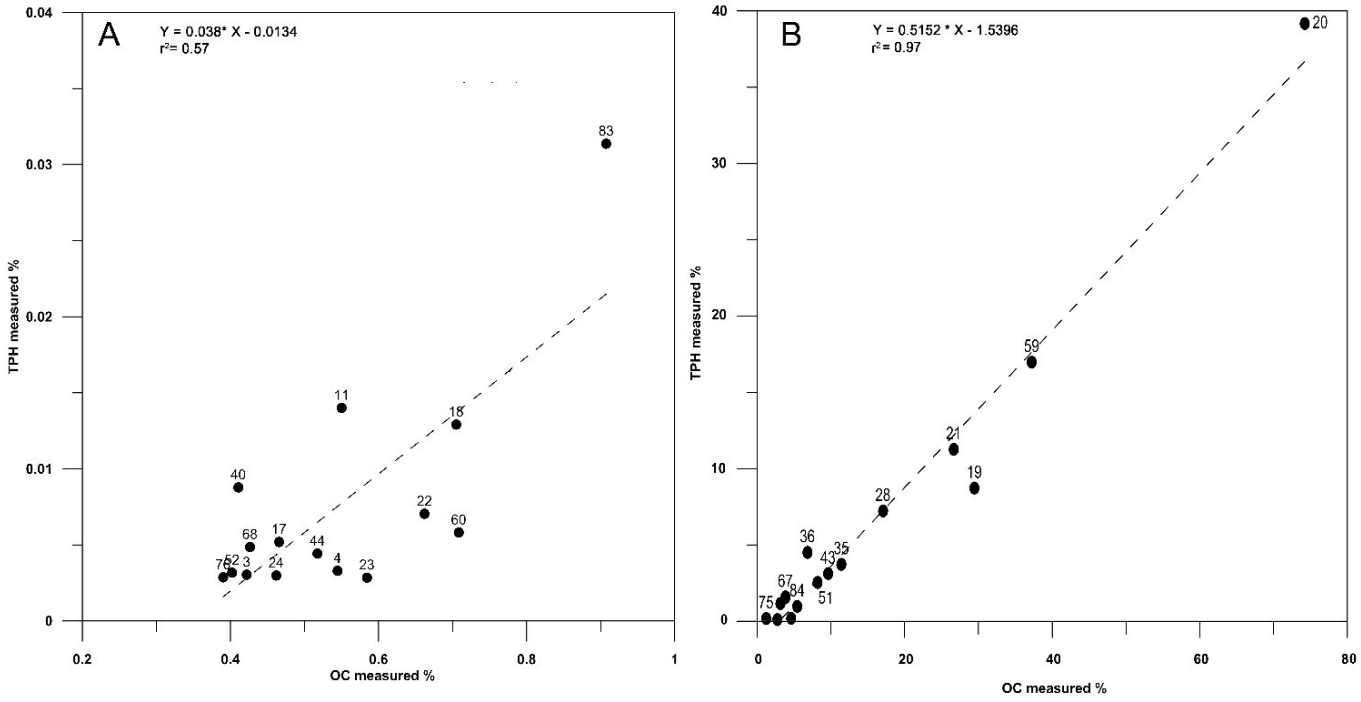

Figure 58: The relationship between TPH and OC for the selected 30 samples. A. Samples with OC < 1% and TPH < 0.1%. B. Samples with OC > 1% and TPH > 0.1%

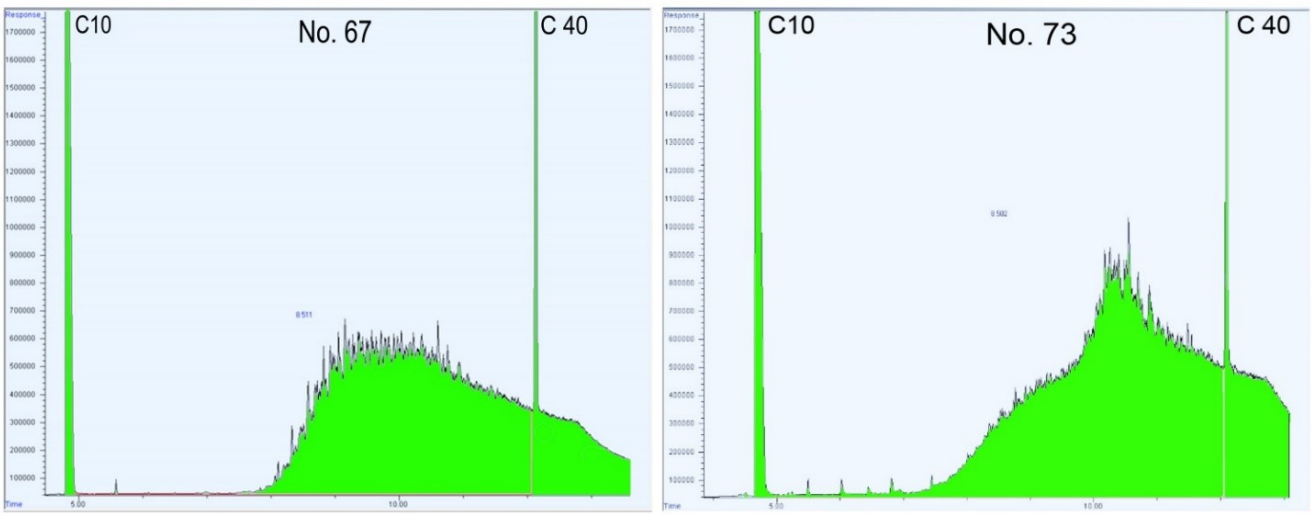

Figure 59: Integrated chromatograms of two selected soilsamples, No. 67 and No. 73. Units are a response (y-axis) and time (x-axis). Both samples show that existing higher fractions > C40 are not included in the integrated area

4.3.4. Mineral composition of the soil

The XRD results for selected samples show various minerals that normally result from the weathering and erosion processes of geological outcrops in the study area (Table 15). The minerals concentration main values indicate the high presence of calcite, quartz, and chlorite. The reflectance signature for each mineral contains different absorption features (Figure 60 & Figure 61). For example, calcite ($CaCO_3$) is present in all of the samples with high concentrations, which normally results from the erosion of limestone. Both calcite and dolomite also create an absorption feature within 2310-2315 nm.

In this range, it could be expected overlap with the third hydrocarbon feature. A similar picture can be seen in the spectrum absorption feature of gypsum and dry vegetation within 1200-1205 nm, which is close to the first hydrocarbon feature and can affect the hydrocarbon feature by the overlapping combination. The central absorption feature at 1729 nm was unique for hydrocarbon compounds (Table 15). However, the dry vegetation and gypsum have absorption features at 1750 and 1754, respectively, while all other main mineral phases do not affect the oil absorption features.

Table 15: Mineral concentrations for representative soil samples with absorption features near hydrocarbon absorption features

Sample Minerals (%wt.)	**Sample 1**	**Sample 8**	**Sample 27**	**Sample 54**	**Sample 81**	**Sample 88**	**Main (%wt.)**	**Absorption features (nm)**
Albite + Orthoclases	10.3	7.5	13.5	7.5	trace	6.6	7.5	-
Palygorskite	7.1	3.3	5.7	Trace	trace	6.7	3.8	-
Quartz	31.3	19.5	25.6	23.9	26.9	19.8	24.5	-
Chlorite	12.8	16.4	25	32.8	33.6	20.6	23.5	2325 (1)
Illite	7.7	4.1	5.6	Trace	4.4	3.9	4.2	1724 (1)
Calcite	31.4	22.1	24.6	35.7	28.7	26.9	28.2	2315 (1)
Gypsum	-	27.1	-	-	-	11.4	6.4	1205,1750 (1,2)
Dolomite	-		-	-	6.2	4	1.6	2310 (1)
Total wt	100.6	100	100	99.9	99.8	99.9		
Dry Vegetation								1200, 1754, 2316 (1)

Data source: (1) NDVI spectral library, (2) (Moreira and Teixeira, 2014)

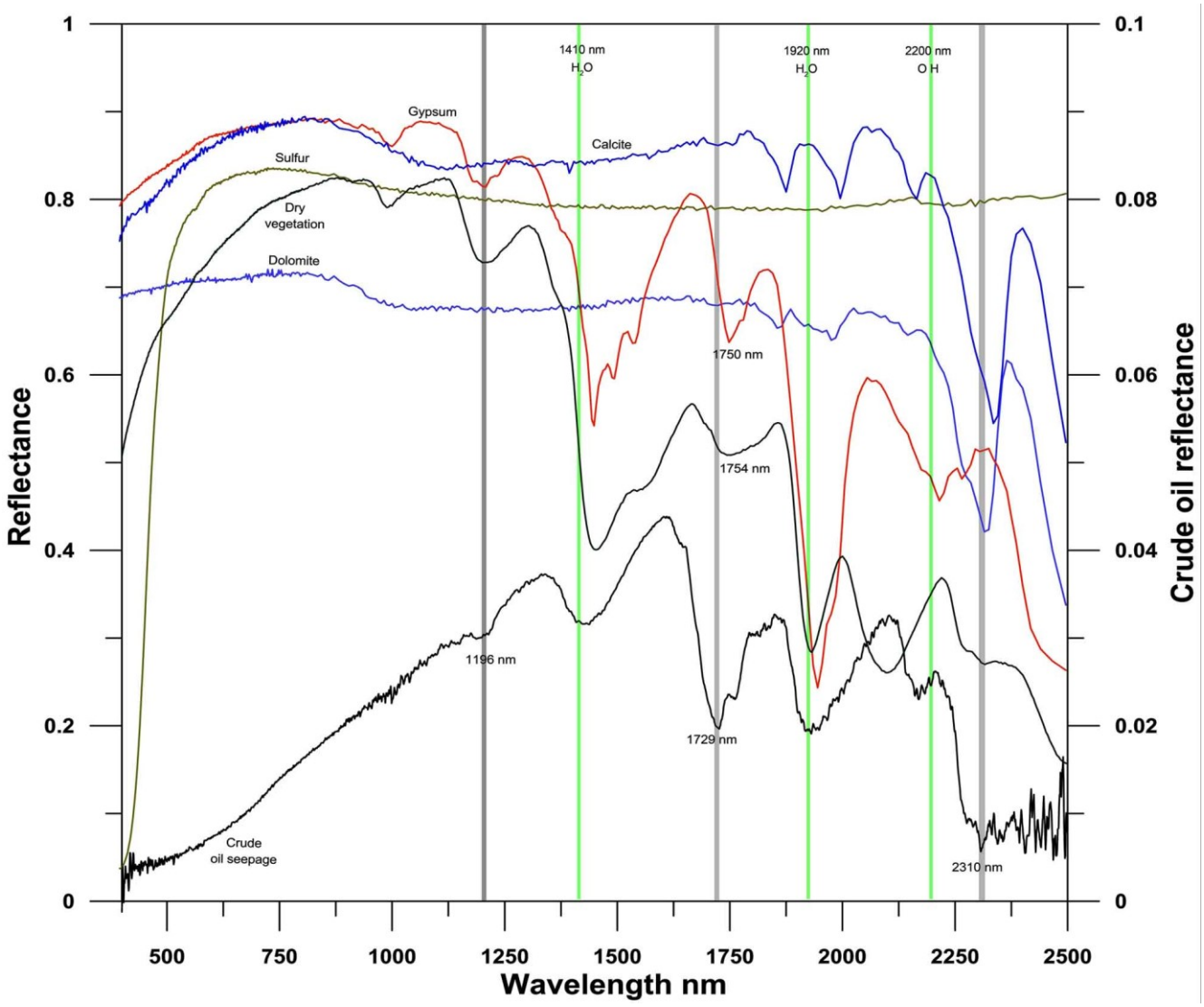

Figure 60 : The spectra of major minerals (Gypsum, Calcite, Sulfur, Dolomite) and two vegetation types in Baba seepage soil as well as the spectra for a crude oil sample. Note: The shown spectra are pure mineral spectra from the ENVI 4.7 reflectance library. The P1, P2, and P3 are the primary absorptions features of oil spectra from field sample No. 20. It can be seen that there is a potential interference with primary hydrocarbon absorption features

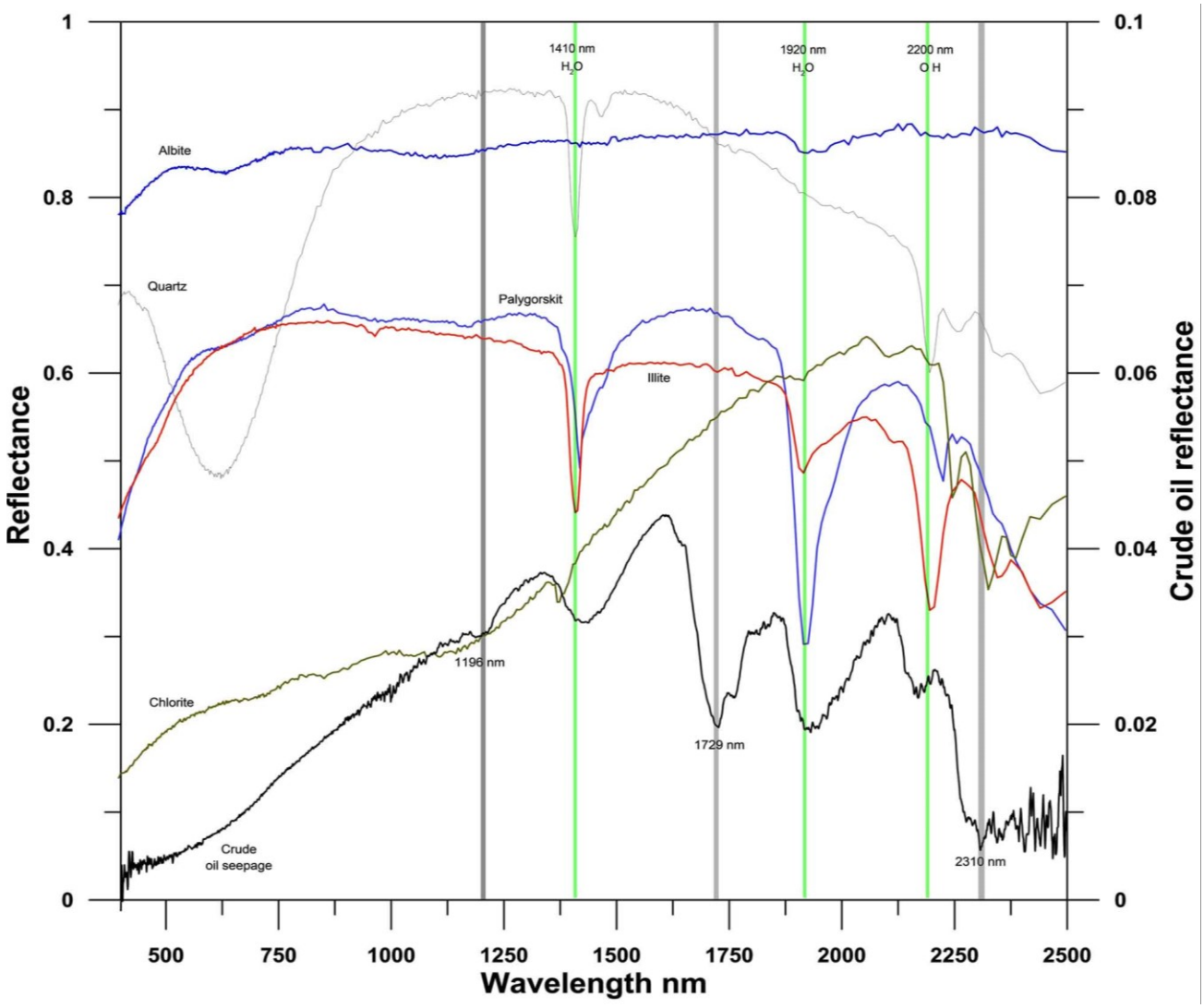

Figure 61: The spectra of major minerals (Quartz, Albite, Playgorskit, Illite, Chlorite) in Baba seepage soil as well as the spectra for a crude oil sample. Note: The shown spectra are pure mineral spectra from the ENVI 4.7 reflectance library. The P1, P2, and P3 are the primary absorptions features of oil spectra from field sample No. 20. It can be seen that there is a potential interference with primary hydrocarbon absorption features

4.3.5. Hydrocarbon index (HI) and performance of the models

The OC < 1% samples were plotted against the HI for each model. Due to the additional sources of OC besides oil, the linear regression fitting values for all of the models show no relation (
Figure **62**). However, this result confirms the low correlation between OC and TPH (Figure 58 A). The samples 83, 11 and 18 can still explain TPH higher than 0.01 (Table 14). Thus, the samples with TPH less than 0.01 illustrate the origin of OC is not a result of the crude oil source. The OC > 1% that mainly resulted from crude oil source and the HI explain the high correlation.

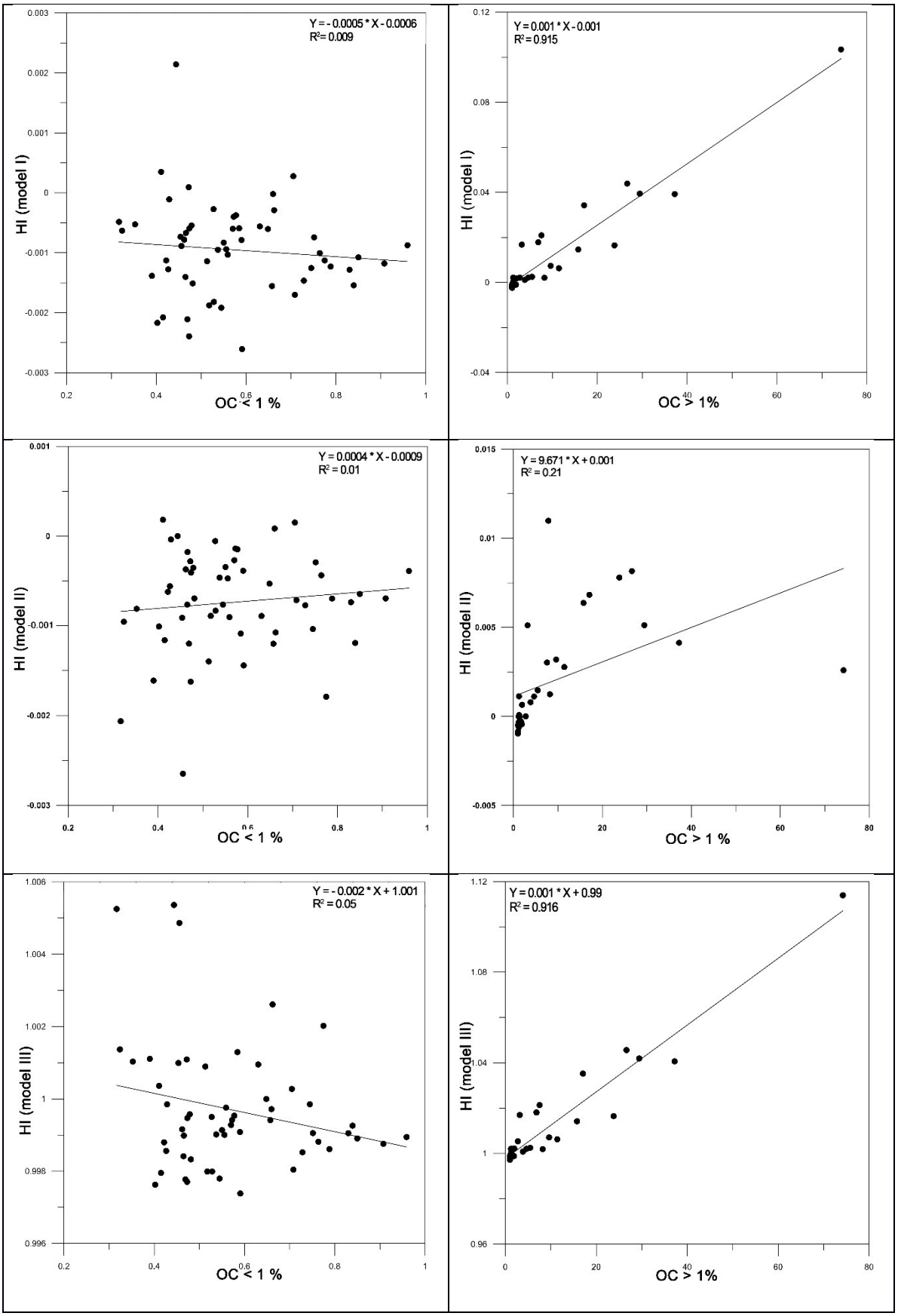

Figure 62: HI and OC with three used methods for samples of Baba seepage. The left three graphs represent OC less than 1%. The right three graphs represent OC higher than 1%

Starting with Models I and III, a good linear regression fitting was reached R^2= 0.91(
Figure **62**). Meanwhile, Model II explains weak correlation with OC%. Model II is only able to distinguish between the high OC samples and shows less DL. The Non-normalized HI values caused the week correlation in Model II. However, Model I and II results of Baba seepage explain very similar correlation with linear regression giving R^2= 0.99 (Figure 63). These models depend on different calculations, as Model I calculates the vertical line of the band depth and Model III calculates the ratio between absorption shoulders and the absorption center. In order to isolate the contaminated boundaries and according to McMillen et al., (2001), the accepted TPH limits were defined around 6.95% wt.
Within Baba seepage, the HI values from Model III were plotted to represent each parcel (Figure 64). HI values above 1.0069 show the highly contaminated locations within the Baba seepage. The HI of this seepage will be the target of the using of the satellite data to evaluate the atmosphere effect as well as the accuracy of the selected bands of each chosen satellite.

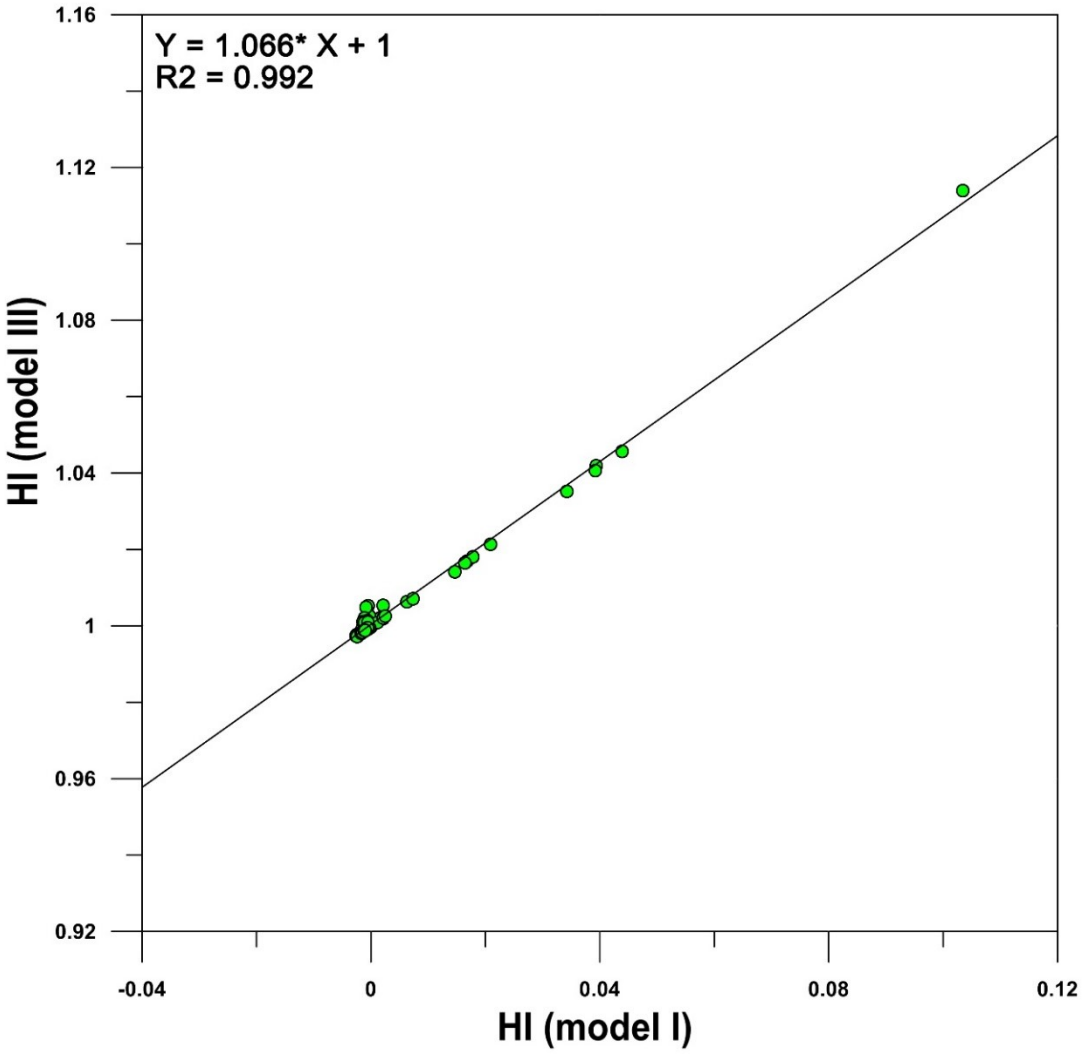

Figure 63: Cross-validation Model I vs. Model III for 88 soil samples using the continuum boundaries (1699, 1729, 1749 nm)

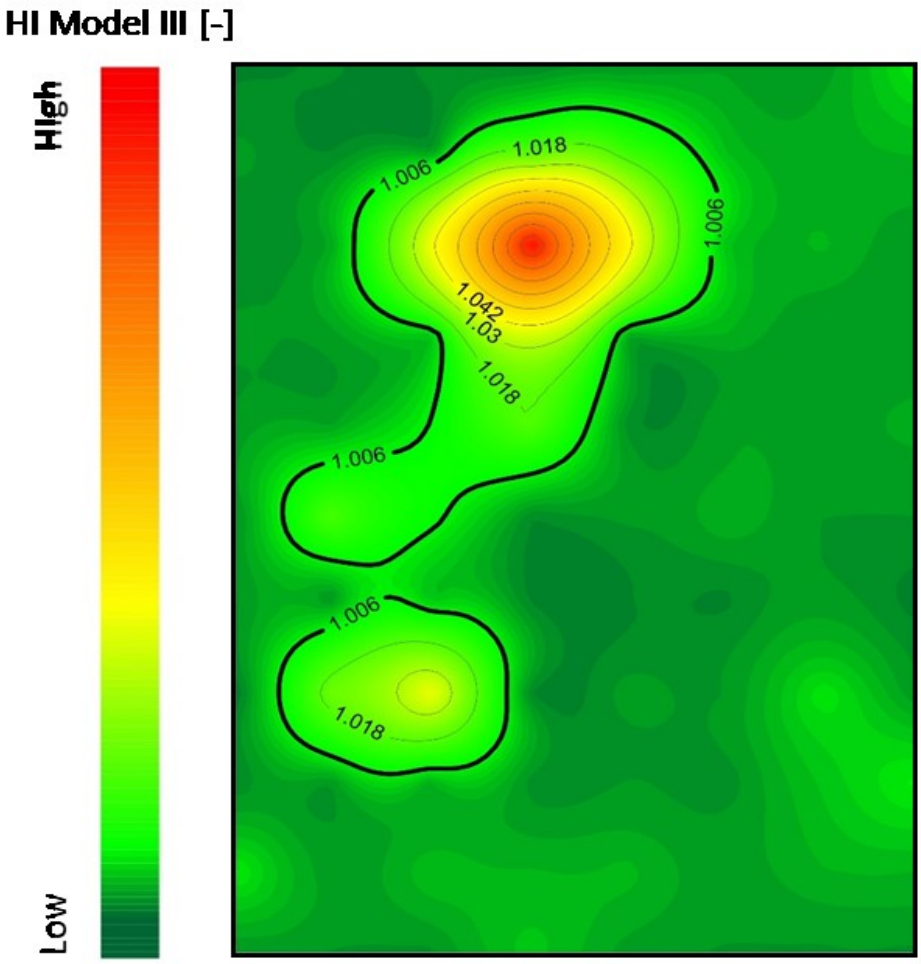

Figure 64: Organic carbon concentration map as HI values (Model III) to the Baba seepage

4.3.6. Lineaments and seeps locations

By plotting seepage and the results of the auto lineaments algorithm, many lineaments were not only found in outcrops of the Fatha cap rocks, but also in the younger formations. As demonstrated by using SRTM DEM input data, the accuracy of the resolution and the data processing methods can change the spatial characteristics of the lineaments, such as their quantity, length and direction. The auto lineaments algorithm was a valuable tool to generate multisets of lineaments for each input type with a minimum lineament length of 750 m required for detection. The use of shaded relief and aspect gradients was beneficial in detecting a high number of lineaments throughout the study area.

However, by using slope gradient maps, the number of lineaments detected was generally lower, especially in very complex topographic areas like the Qara Chauq area and the Kirkuk anticline. Within 5 km as unit area value, the result of density map for all lineament demonstrates a connection between high-density values and seepage locations, which also indicated that lineaments are the major reason for the occurrence of these seeps (Figure 65).

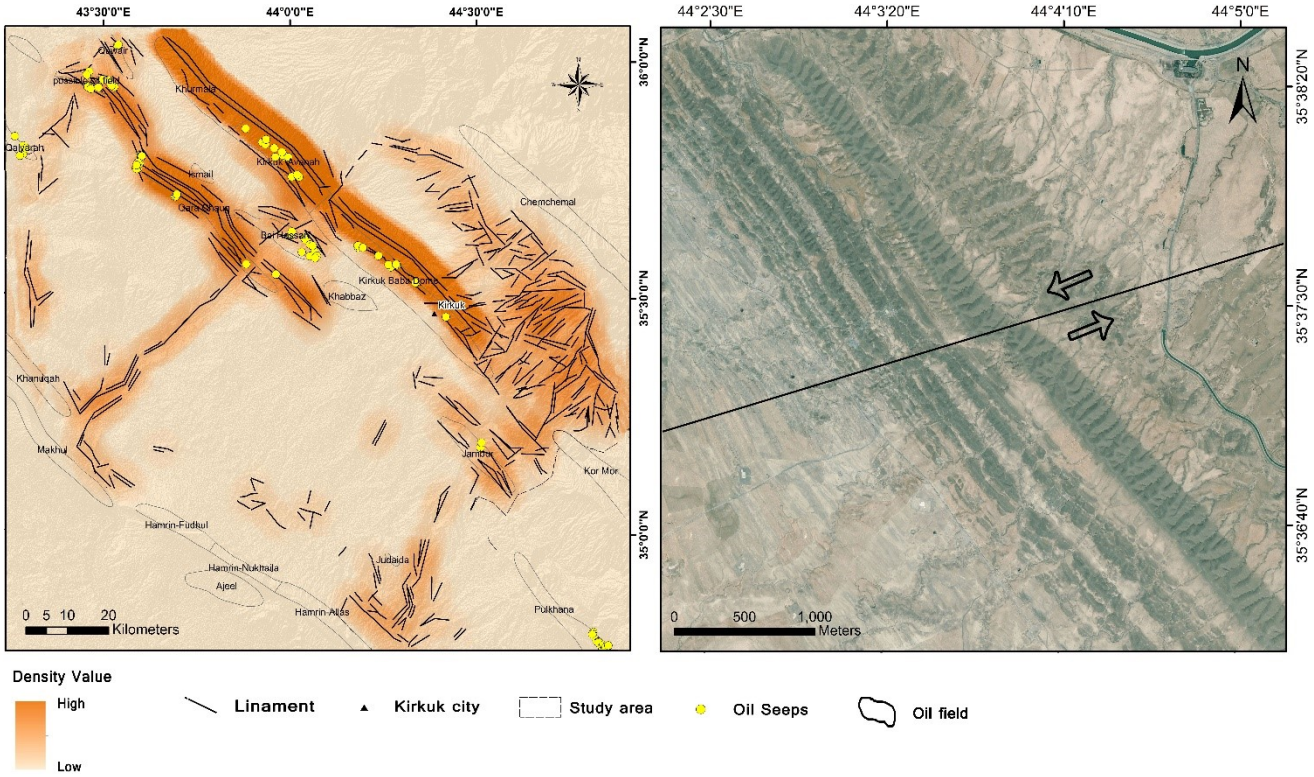

Figure 65: Lineaments and oil seeps spatial distribution based on DEM data of the AOI with their density maps in Kirkuk area (lift). Satellite image (Landsat 7) with a notified fault in the Bai Hassan field

The lineaments potentially affected the cap rock Fatha Formation and increased the impact of the major faults that reached the oil body and created migration paths. Besides, structural geological maps can provide further evidence of promising locations for exploration. The dominating lineaments trends are NE-SW and NW-SE. According to the results, the highly distinctive appearance of the NE-SW trend is more related to macro seeps than micro seeps in the study area. The seepage appears to be controlled by major north-south faults that cut the surface perpendicularly in major anticlines (Pitman et al., 2004). The DEM explains major faults with either a parallel trend of anticline axis (Bai Hassan, Jambur) or cutting the anticline axis in different angles depending on the tectonic forces like Qara Chauq. Moreover, the faults and fractures can also increase the possibility of karst phenomena in the evaporate layers in Fatha Formation.

5. Conclusions and recommendation

5.1.General conclusion

The natural crude oil fields and their surface seeps can contain a high environmental impact of the hydro and lithospheres in the area of Kirkuk. However, understanding and tracking the crude oil from the reservoir to the surface demanded numerous methods, which required the dealing with big data set and considerable efforts to extrapolate the final results. The main reason for the seepage in the AOI is the existence of many types of major faults like the Kirkuk normal fault, which was clearly marked in seismograms from the Avanah and Baba domes by the presence of many fractures and joints. The field evidence explains the effect of faults in the area by methane seepage, which migrates through these faults to the surface.

5.1.1. Organic chemistry properties approach to correlate seepage and reservoir crude oil

The source rocks are showing overlap between carbonate marine and non-marine rocks. In Kirkuk area, two main ages of the oil samples are present. The first is the carbonate or carbonate-rich shales source rocks age Jurassic – Early Cretaceous are present in the area of Kirkuk. In harmony with the C_{28}/C_{29} sterane results, the primary proven source rocks can be listed:

1. The Middle and Late Jurassic, which represented by Sargelu and Naokelekan formations.
2. The Late Jurassic - Early Cretaceous age, mainly Chia Gara Formation.

The oil samples of Cretaceous reservoirs explain low values of Pr/Ph, which propose that the oils were generated from a source rock containing mainly marine organic matter deposited under reducing conditions with an effect of biodegradation and mature stage of occurrence.

The seeps in the study area mostly occur by the fractures and the erosion of the regional anhydrite caprocks of the Fatha Formation, supported by the shallow depth of the Oligocene accumulation. Beside the seismic sections, seeps source results were shown in the C_{35} homohopane index and sulfur content. Seepage sources can explain different age, which might be Late Cretaceous as Shiranish Maastrichtian Formation or early Tertiary Aaliji or Jaddala Eocene formations. The vertical migration along faults is most likely the connection between the seepage samples and Baba Dome.

Eighteen of twenty PAHs were detected in the selected oil samples, whereby light molecular weight PAHs are the dominating fractions. Generally, the light oils contain more PAHs than heavier oils. Meanwhile, the PAH distribution in seepage oils differs based on the ecological processes like erosion and biodegradation.

5.1.2. Hydrogeology approach to evaluating the salinity source

In general, the area is subdivided into an upstream basin with high hydraulic gradients that are separated by the outcrops of the Fatha Formation in the anticline cores from a downstream basin with low relief and low hydraulic gradients. Despite being low in matrix hydraulic conductivity, the Fatha Formation is highly fractured and locally karstified with fractures generally oriented perpendicular to the anticline axis, allowing a hydraulic connection between the two basins. Springs at the upstream outcrops of the Fatha Formation indicate locally low permeability and disconnection of the basins. However, most of the springs are located close to the major fault system running in parallel to the anticline axes. These major faults – such as the Kirkuk thrust fault – reach the middle Oligocene-Eocene oil trap formations.

In the upstream basin, shallow groundwater of calcium bicarbonate type with low salinity is present in the Mukdadia and Bai Hassan formations, above the Fatha cap rock. When reaching the highly fractured anticline axis with the outcrops of the Fatha Formation, dissolution of gypsum leads to an increase in salinity. In addition, the fracture systems in parallel to the anticline axes potentially enables an uprise of oil brines and hydrocarbons. Both processes cause a release of strontium into the water, with concentrations reaching up to 25 mg/l. Due to the connection of the two basins by the perpendicular fracture system, in general higher salinities (EC reach to 6500 μS/cm) are found in the Mukdadia and Bai Hassan formations in the downstream basin. Increased concentrations of calcium indicate the dissolution of gypsum while an increase in sodium is related to the dissolution of halite or mixing with oil field brine.

Strontium isotopes proved to be a very powerful tool in distinguishing between mixing of groundwater with oil field brines or water originating from the Fatha Formation. In the study area, the latter is generally more likely, whereby groundwater results showed a strontium isotopic composition that suggests mixing with oil field brines.

5.1.3. Spectral reflectance approach to determine the characteristic of Iraqi crude oil

The results were intended for testing the capability of using the unique absorption feature for the crude oil with three different models to calculate the HI. The spectral analyses of various crude oil types define the absorption features and the feature boundary. Moreover, the controlled increase of OC in selected soil samples fits with absorption depth size. The comparison of different continuum boundaries ends with concluding the combination of 1699, 1729, 1749 nm is more usable than the other hydrocarbon primary absorptions, because it can offer higher DL and it is not affected by any absorptions resulting from water or minerals. In addition to Model III, the normalization in Model I – by dividing the results into the reflectance spectrum or subtracting them from the apparent absorption – provides more accepted results. The TPH and OC classified Baba seepage samples into two groups: OC values higher than 1% indicate the direct influence of the crude oil seepage, while in samples with OC less than 1% the OC

must originate from other sources. The absorption band 1720-1732 nm presents a good OC indicator even for heavy crude oil types, even though the band 2301-2313 nm is recommended for such crude oil types. The high concentrations of calcite in of all the samples beside the dolomite as a member of the CO_3 group makes the chosen third absorption 2301-2313 nm unsuitable due to the spectral interference. The Model III shows very good fitting between the calculated and measured organic carbon. While Model I is still wildly used to calculate the band depth (Moreira and Teixeira, 2014), Model III offers very similar results. Moreover, Model III is easily applied than Model I. This due to its use of the selected absorption values directly with no need to calculate HI from the R_D point within the continuum line. Finally, the results show the usefulness of calculating the HI from hyperspectral data to the same oil seepage and other seeps in Baba area, as well as known oil-filled locations.

Different remote sensing techniques were used to identify the correlation between faults, fractures and joints and the occurrence of hydrocarbon seeps from oil fields in the Kirkuk area. Different lineament pattern characteristics like major trending, spatial distribution and length can be used in a structural model to highlight weakness zones in selected formations. Therefore, the combining the input data and the results of the main approaches lead to a conceptual understanding of the comprehensive situation in the study area (

Figure **66**).

5.2. Recommendation

1. The historical documented field survey data referred to locations changing with some natural crude seeps during the last 30 years. Therefore, hyperspectral satellite images can be used for producing high-resolution maps of seeps locations within constant time intervals. The recommended and available hyperspectral sensors such as the EnMAP (Environmental Mapping and Analysis Program) or unmanned aerial vehicle (UAV) images will be used in future studies to classify the contamination zones as well as the concentration level the for natural and artificial seepage.
2. Several studies explain the toxic impacts of PAH mixtures on human ingestion (Rengarajan et al., 2015; Varjani et al., 2018). Thus, the PAH findings of the crude oil samples in Kirkuk area can be a basis for a similar study with soil and water samples, before subsequently comparing the results with the German Drinking Water Ordinance Guideline and the World Health Organization (WHO). However, WHO provides a guideline value for limited PAHs types like Benzo[a]pyrene.
3. The results of this study cover the time between 2012-2016, the new active tectonic developments were recorded with high frequency and amplitude earthquakes like November 2017 (USGS, 2017) with a moment magnitude of 7.3 based on the Richter scale. Such a situation highlights the role of remote sensing data to define the new lineaments as an accurate, rapid tool.

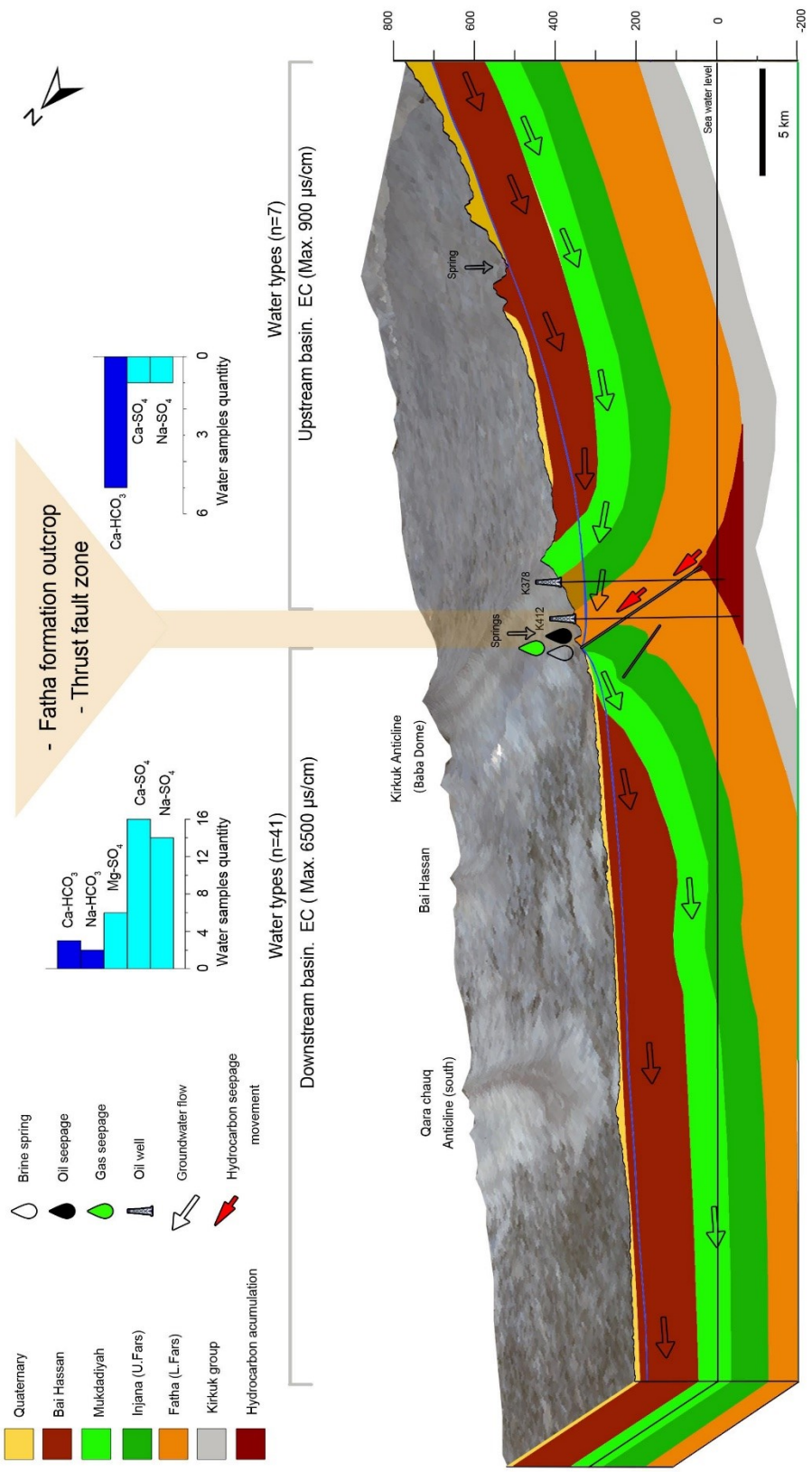

Figure 66: A schematic model for Kirkuk anticline explains the hydrogeological and hydrogeochemical between the two basins. The water type is presenting the groundwater in Mukdadia, Bai Hassan and, Quaternary formations (Sahib et al., 2016)

References

Aas E., Baussant T., Balk L., Liewenborg B., Andersen O.K., 2000: PAH metabolites in bile, cytochrome P4501A and DNA adducts as environmental risk parameters for chronic oil exposure, a laboratory experiment with Atlantic cod, Aquatic Toxicology, Volume 51, Issue 2, pp. 241-258. doi:10.1016/S0166-445X(00)00108-9

Abdullah A., Akhir J., M. Abdullah I. 2010: Automatic mapping of lineaments using shaded relief images derived from digital elevation model (DEMs) in the maran - sungi lembing area, Malaysia, The Electronic Journal of Geotechnical Engineering, Volume 15, pp 949-957.

Abdulnaby W., Mahdi H., Al-Shukri H., Numan N. M. S., 2014: Stress patterns in northern Iraq and surrounding regions from formal stress inversion of earthquake focal mechanism solutions. Pure Appl. Geophys. 171 (9), pp. 2137–2153. https://link.springer.com/article/10.1007%2Fs00024-014-0823-x

Abeed Q., Leythaeuser K., Littke R., 2012: Geochemistry, origin, and correlation of crude oils in Lower Cretaceous sedimentary sequences of the southern Mesopotamian Basin, southern. Iraq. Organic Geochemistry Volume 46, pp. 113–126.

Al Ajmi H., 2013: Sedimentology, stratigraphy and reservoir quality of the Paleozoic Wajid Sandstone in SW Saudi Arabia. PhD Thesis. Institut für Angewandte Geowissenschaften Darmstadt, pp.134.

Al Shdidi S., Thomas G., Delfaud J., 1995: Sedimentology, diagenesis and oil habitat of Lower Cretaceous Qamchuqa Group, northern Iraq: Am. Assoc. Petrol Geol. Bull., Volume 79, pp. 763-779.

Al-Ahmed A. A., 2006: Organic geochemistry, palynofacies and Hydrocarbon Potential of Sargelu Formation (Middle Jurassic), Northern Iraq. unpublished thesis the University of Baghdad, pp. 120.

AL-Ameri T. K., 2014: Oil biomarkers, isotopes and palynofacies are used for petroleum system type and migration pathway assessments of Iraqi oil fields. Arabian Journal of Geosciences doi:10.1007/s12517-014-1606-5.

Al-Ameri T. K., Najaf A. A., Zumberge J. E., Brown S. W., 2006: Petroleum potential and oil correlation of the Middle Jurassic Sargelu formation, Iraq. AAPG Houston 2006. Poster Presentation.

Al-Ameri T. K., Zumberge J., 2012: Middle and Upper Jurassic hydrocarbon potential of the Zagros Fold Belt, North Iraq. Marine and Petroleum Geology, Volume 36, pp. 13-34.

Al-Banaa R. G., 2012: Structural Control Evaluation of Hydrocarbon Seeps in Northern Iraq Using Remote Sensing Techniques. Ph.D. Thesis, College of Sciences, University of Mosul, Iraq.

Al-Bassam K., Hak K., 2006: Metallic and industrial rocks and minerals, Chapter 20,: Jassim, J. Go, J. 2006: Geology of Iraq, Prague, Czech Republic, Dolin, Prague and Moravian, Museum, Brno.

Al-Gailani M.B., 1996: Iraq´s significant hydrocarbon potential remains relatively undeveloped. Oil and Gas Journal, pp. 108-112.

Al-Gailani M.B., 2003: Assessing Iraq`s oil potential. Geotimes, October 2003, pp. 16-19.

Al-Hamdani j. A., 2009: hydrochemical effect of groundwater due to irrigation and drainage projects in tawuq sub-basin., a thesis submitted to the College of Science University of Baghdad, in partial fulfillment of the requirements for the degree of master of science in geology.

Al-Jaboury A. L., Al-Tarif A. M., Aulaiwi J. H., Al-Kaisy A., 2009: Mineralogy and Geochemistry of Meha solar salt pond, Iraq. Proceedings of the 2nd International Conference on the Ecological Importance of Solar Saltworks (CEISSA2009).

Al–Kufaishi F. A. M., Al–Rubaie N. M. Z., 1986: Petrography and Geochemistry of Jaddala formation in selected sections Northern Iraq. Journal of the Geological Society of Iraq, Volume 19, No.2, (7IGC).

AL-Mamuri N. M. L., 2005: Optimum Management of Surface & Subsurface Water of AL-Adhaim Basin , Ph. D., Thesis, College of Engineering, Uni. of Baghdad, pp. 158.

Al-Paruany K. B. N., 2013: Hydrochemical and isotopic study of water resources between Haditha dam and site of al-Baghdadi dam, Ph.D. thesis, College of Science of University of Baghdad.

Al-Qayim B., Qadir F., Al-Biaty F., 2010: Dolomitization and porosity evaluation of the Cretaceous Upper Qamchuqa (Mauddud) Formation, Khabbaz oil field, Kirkuk area, northern Iraq. GeoArabia. Volume 15, pp. 49-76.

Al-Rawi M., 2015: Kirkuk, a Silent Giant Oilfield. GeoExPro article appeared in Volume 11, No. 6 American petroleum institute, petroleum HPV testing group (2003). Test plan crude oil category. Submitted to the U.S. EPA, No 201-14858B

Al-Rawi Y. T., Sayyab A. S., Jassim J. A., Tamar-Agha M. Y., Al-Sammarai A. I., Karim S. A., Basi M. A., Dhiab S. H., Faris F. M., Anwar F., 1992: New names for some of the middle Miocene pliocene formations of Iraq, (Fatha, Injana, Makdadiya and Bai Hassan formations).; Iraq Geo. Jour., Volume 1, pp.1-18.

Al-Rawi Y., 1980: Petrology and sedimentology of the Gercus Red Beds Formation (Eocene), northeastern Iraq. Iraqi Journ. Sci., Volume 21, pp.132-188.

Al-Shahristani H., Al-Atyia, M. J., 1972: Vertical migration of oil in Iraqi oil fields: Evidence based on vanadium and nickel concentrations. Geochimica et Cosmochimica Acta, Volume 36, Issue 9, pp. 929-938. doi:10.1016/0016-7037(72)90013-0

Alsharhan A. S., & Nairn A. E. M., 2003: Sedimentary basins and petroleum geology of the Middle East (843 p.). Amsterdam, Netherlands: Elsevier Science B. V.

Amare T., Hergarten C., Hurni H., Wolfgramm B., Yitaferu B., Yihenew G., Selassie G., 2013: Prediction of Soil Organic Carbon for Ethiopian Highlands Using Soil Spectroscopy. Hindawi Publishing Corporation ISRN Soil Science, Volume 2013, Article ID 720589, pp. 11 pages. doi:10.1155/2013/720589.

Ameen M. S., 1992: Effects of Basement Tectonics on Hydrocarbon Generation, Migration and Accumulations in Northern Iraq. Bulletin of the American Association of Petroleum Geologists, Volume 76, pp. 356-370.

Amijaya H., Schwarzbauer J., Littke R., 2006: Organic geochemistry of Lower Suban coal seam, South Sumatra Basin, Indonesia: Palaeoecological and thermal metamorphism implications. Organic Geochemistry Volume 37(3), pp. 261–279.

Andreoli G., Bulgarelli B., Hosgood B., Tarchi D., 2007: Hyperspectral Analysis of Oil and Oil-Impacted Soils for Remote Sensing Purposes. Institute for the Protection and Security of the Citizen. European commission joint research center. Luxembourg: European communities. https://www.ugpti.org/smartse/research/citations/downloads/Andreoli-HSI_for_Oil_and_Spills-2007.pdf

Aqrawi A., 1993: Miocene evaporitic sequence of the southern Mesopotamian Basin. Mar. Pet. Geol. Volume 10, pp. 172–179.

Aqrawi A.A.M., Goff, J.C., Horbury, A.D., Sadooni, F.N., 2010: The Petroleum Geology of Iraq. Scientific Press, Brucks, UK, pp. 424.

Araim H., 1990: Regional Hydrological Map of Iraq. Scale 1: 1 000 000. Geosurv.

ArRajehi A., McClusky S., Reilinger R., Daoud M., Alchalbi A., Ergintav S., Gomez F., Sholan J., Bou-Rabee F., Ogubazghi G., Haileab B., Fisseha S., Asfaw L., Mahmoud S., Rayan A., Bendik R.,and Kogan L., 2010: Geodetic constraints on present-day motion of the Arabian Plate: Implications for Red Sea and Gulf of Aden rifting. TECTONICS, VOL. 29, doi:10.1029/2009TC002482.

Bahroudi A., Koyi H., 2004: Tectono-sedimentry framework of the Gachsaran Formation in the Zagros foreland basin. Marine and Petroleum Geology. Volume 21. pp. 1295-1310. doi:10.1016/j.marpetgeo.2004.09.001.

Baldridge A. M., Hook S. J., Grove C. I., and Rivera G., 2009: The ASTER Spectral Library Version 2.0. *Remote Sensing of Environment*, Vol. 113, pp. 711-715.

Bellen R. C., Dunnington H. V., Wetzel R., Morton D., 1959: Lexique Stratigraphique International Asie, Iraq. Volume 3C, 10a, pp. 333.

Bergmann J.; Friedel P.; Kleeberg R., 1998: BGMN - a new fundamental parameters-based Rietveld program for laboratory X-ray sources, it's use in quantitative analysis and structure investigations CPD. Newsletter, Commission of Powder Diffraction, International Union of Crystallography 1998, 20, pp. 5–8.

Bible and Spade, 2004: Volume 17 no.4.
http://www.biblearchaeology.org/bookstore/product.aspx?id=12

Bordenave M. L., Hegre J. A., 2005: The influence of tectonics on the entrapment of oil in the Dezful Embayment, Zagros fold belt, Iran. Journal of Petroleum Geology, Volume 28 (4), pp. 339-368.

Buday T., 1980: The Regional Geology of Iraq, Vol 1: Stratigraphy and Paleogeography. Publications of Geological Survey of Iraq, Baghdad, pp. 445.

Busk H. G., Mayo H. T., 1918: Some Notes on the Geology of the Persian Oilfields. Journal of the Institute of Petroleum Technology, Volume 5, pp. 5-26.

Casciello E., Verges J., Saura E., Casini G., Fernandez N., Blanc E., Homke S., Hunt D., 2009: Fold patterns and multilayer rheology of the lurestan Province, Zagros simply folded belt (Iran): Geological Society (London), Volume. 166, pp.1-13, doi:10.1144/0016-7649.2008-138.

Chakraborty S., Weindorf D., Zhu Y., Li B., Morgan C., Ge Y., Galbraith J., 2012: Assessing spatial variability of soil petroleum contamination using visible near-infrared diffuse reflectance spectroscopy, Journal of Environmental Monitoring, Volume: 14 (11), pp. 2886-2892. doi:10.1039/C2EM30330B

Charette M., Soderblom L. A., Adams J. B., Gaffey M. J. McCord T. B., Age – color relationships in the lunar highlands. Proc. Lunar Sci. Conf 1976, 7th, pp. 2579–2592.

Chatton M., Hart E., 1960: Revision of Tithonian- Albian stratigraphy of Iraq. Manuscript report, GEOSURV, Baghdad.

Clark R., Curchin J. M., Hoefen T. M., Swayze G. A., 2009: Reflectance spectroscopy of organic compounds: 1. Alkanes, Journal of Geophysical Research E: Planets, Volume 114 (3) doi:10.1029/2008JE003150, http://pubs.er.usgs.gov/publication/70034984

Clark, R., Roush, T., 1984: Reflectance spectroscopy - Quantitative analysis techniques for remote sensing applications. Journal of Geophysical Research, Volume 89, pp. 6329 – 6340.

Clarke R. H., Cleverly R. W., 1991: Petroleum seepage and post-accumulation migration. Geological Society, London, Special Publications, 59, 265-271, 1 January 1991, doi:10.1144/GSL.SP.1991.059.01.17

Clayton R. N., Friedman I., Graf D. L., Mayeda T. K., Meents W.F., Shimp N.F., 1966: The origin of saline formation waters 1. Isotopic composition. J. Geophys. Res. 71, pp. 3869–3882.

Cloutis E.A. 1989: Spectral Reflectance Properties of Hydrocarbons - Remote- Sensing Implications. Science 245, 2454914, pp.165–168.

Connan J., 1999: Use and trade of bitumen in antiquity and prehistory: molecular archaeology reveals secrets of past civilizations. Philosophical Transactions of the Royal Society B: Biological Sciences. doi:10.1098/rstb.1999.0358.

Connan J., Bouroullec J., Dessort D. & Albrecht P., 1986: The microbial input in carbonate-anhydrite facies of a Sabka palaeoenvironment from Guatemala: a molecular approach. In: Advances in Organic Geochemistry 1985 Volume 1, Pergamon Press pp. 29-50.

Coplen T. B. 1996: New guidelines for the reporting of stable hydrogen, carbon, and oxygen isotope ratio data, Geochimica et Cosmochimica Acta 60 (17), pp 3359-3360.

Coplen T. B., 1988: Normalization of oxygen and hydrogen isotope data. Chemical Geology, Isotope Geosciences Section 72 (4), pp 293-297. doi:10.1016/0168-9622(88)90042-5.

Craig H. Boato G. White D.1956: Isotopic geochemistry of thermal waters, in: Proceedings of the 2nd Conference on Nuclear Processes in Geologic Settings, National Research Council Publication 400, pp 29-38.

Craig H., 1961: Standards for reporting concentrations of deuterium and oxygen-18 in natural waters. Science, 133, pp1833-1834.

Craig H., 1963: The isotopic geochemistry of water and carbon in geothermal areas, in: Nuclear Geology of Geothermal Areas, Tongiorgi, E., pp 17-53.

Csontos L., Sasvari A., Poscai M. T., Kósa L. Salse A. T., Ali A., 2012: Structural evolution of the northwestern Zagros, Kurdistan Region, Iraq: Implications on oil migration. GeoArabia, Volume 17, pp.81-116.

Daniel E., 1954: Fractured reservoirs of Middle East, Bulletin of the American Association of Petroleum Geologists, Volume 38 (5), pp 774-815.

Das P. K., Baruah H., 1997: distribution of oil in India, Petroleum and Coal, (New Delhi: MD publication private limited, 1997.

Depaolo D. J., Ingram, B. L., 1985: High-resolution stratigraphy with strontium isotopes, Science 227 (4689), pp 938–941. doi:10.1126/science.227.4689.938.

Deutsche BP AG., 1989: Das Buch vom Erdöl. Reuter und Klöckner Hamburg. Fifth Edition Environment Canada / Health Canada (1994). Canadian Environment Protection Act: Priority Substances List Assessment Report: Polycyclic Aromatic Hydrocarbons.

Duissenov D., 2012: Production and Processing of High Sulfur Crude and Associated Gas, TPG4510 Petroleum Production specialization project, Darkhan.NTNU Det skapende universitet. http://www.ipt.ntnu.no/~jsg/studenter/prosjekt/2012DuissenovProsjekt.pdf

Dunnington H. V., 1958: Generation, migration, accumulation, and dissipation of oil in northern Iraq: Middle East. In: Habitat of Oil pp.1194-1251

Dunnington H. V., 1967a: Stratigraphical distribution of oil fields in the Iraq-Arabia Basin. Journ. Inst. Petrol., 53 (520), pp.129-161.

Dutton A. R., Richter B. C., Kreitler C. W., 1989: Brine discharge and salinization, Concho River Watershed, West Texas. Groundwater 27 (3). https://doi.org/10.1111/j.1745-6584.1989.tb00461.x

El- Zarka M. H., 1993: Ain Zalah Field, in Beaumont, E. A., and Foster, N. H., compilers, Structural traps VIII: Tectonic fold trap: Am. Assoc. Petrol Geol. Treatise of Petrol. Geol., Atlas of oil and gas fields, pp. 57-68.

Elderfield H., 1986: Strontium isotope stratigraphy, Palaeogeography, Palaeoclimatology, Palaeoecology 57, pp. 71– 90.

ENVI spectral library; https://www.harrisgeospatial.com/docs/THORSpectralLibraryViewer.html

Etiope G. 2015: Seepage in Field Geology and Petroleum Exploration. In: Natural Gas Seepage. Springer, Cham

Etiope G., 2009: A global dataset of onshore gas and oil seeps: a new tool for hydrocarbon exploration. Oil and Gas Business, 37, 1-10.

Falcon N.L., 1969: Problems of the relationship between surface structure and deep displacements illustrated by the Zagros Range. In: Time and place in orogeny. Spec. Publ. Geol. Soc. Lond., 3, 9-22.

Feng X., Pisula W., Müllen K., 2009: Large polycyclic aromatic hydrocarbon: synthesis and discotic organization. Pure Appl. Chem., Volume 81, No. 12, pp. 2203–2224, 2009. doi:10.1351/PAC-CON-09-07-07

Forbes, 1955: Studies in ancient technology, Leiden, volume I, pp.1955.

Gleason R.A., Tangen B.A., 2014: Brine contamination to aquatic resources from oil and gas development in the Williston Basin, United States. In: Gleason, R.A., Tangen, B.A. (Eds.), U.S. Geological Survey Scientific Investigations Report 2014–5017, pp.127.

Gonfiantini R., 1984: Report on an advisory group meeting on stable isotope reference samples for geochemical and hydrochemical investigations, Tech. rep., IAEA, Vienna.

Grantham P. J., Wakefield L. L., 1988: Variations in the sterane carbon number distributions of marine source rock derived crude oils through geologic time. Organic Geochemistry, volume 12, 1, pp.61-73.

Grove C.I., Hook S., Paylor E., 1992: Laboratory reflectance spectra of 160 mineral, 0.4 to 2.5 micrometer, Publication 92-2, Jet Propulsion Laboratory, Pasadena, CA.

Hammoshi A. S., 1972: Sulphur and Iraqi native S, National Iraqi Mineral Company, Ani press, Baghdad, Iraq (in Arabic)

Hart E., Hay J. T. C., 1974: Structure of Ain Zahah Field, Northen Iraq. AAPG Bull., 58(6), 073-981.

Head I. M., Jones M., Larter S. R., 2003: Biological activity in the deep subsurface and the origin of heavy oil, Nature, Volume 426, pp. 344–352, doi: 10.1038/nature02134

Heston H., 2015: Using chloride and bromide mass ratios and binary mixing curves to evaluate anthropogenic influences on groundwater in Lycoming and Wayne counties, Pennsylvania. GEO 546. http://www.ship.edu/uploadedFiles/Ship/Geo-ESS/Graduate/Projects/heston_project_150514.pdf

Hiederer R., Köchy M., 2011: Global Soil Organic Carbon Estimates and the Harmonized World Soil Database. European Commission Joint Research Centre Institute for Environment and Sustainability.

Hörig B., Kühn F., Oschütz F., Lehmann F., 2001: HyMap hyperspectral remote sensing to detect hydrocarbons. International Journal of Remote Sensing, Volume 22, pp.1413 –1422.

Howarth R., McArthur J., 1997: Statistics for strontium isotope stratigraphy with a look-up table version, Journal of Geology 105, pp 441- 456. doi:10.1086/515938.

Huang W., Meinschein W. G., 1979: Sterols as ecological indicators. Geochim Cosmochim Acta, Volume 43 (5), pp.739–745, doi:org/10.1016/0016-7037(79)90257-6.

Hunt J. M., 1996: Petroleum Geochemistry and Geology, 2nd Edition. W.H. Freeman and Company, New York.

Ingraham N. L., Shadel C. 1992: A comparison of the toluene distillation and vacuum/heat methods for extracting soil water for stable isotopic analysis, Journal of Hydrology 140, pp 371-387. doi: 10.1016/0022-1694(92)90249-U.

Jacob J., 2004: Deutsche Forschungsgemeinschaft: Polycyclische aromatische Kohlenwasserstoffe - Forschungsbericht; Wiley-VCH, Weinheim

Jahani S., Callot J., Letouzey J., de Lamotte D. F., 2009: The eastern termination of the Zagros Fold-and-Thrust Belt, Iran: Structures, evolution, and relationships between salt plugs, folding, and faulting. TECTONICS, Volume 28. pp.1-22.

Jassim S. Z., Al-Gailani M., 2006: Hydrocarbons. In: Jassim, S.Z. and Goff, J.C. (Eds), Geology of Iraq. Dolin, Prague and Morvian Museum, Brno, Czech Republic, pp.232-250.

Jassim S. Z., Buday, T., 2006: Units of the unstable shelf and the Zagros suture. In: S.Z. Jassim and J.C. Goff (Eds.), Geology of Iraq. Prague, Czech Republic: Dolin Brno and Brno, Czech Republic: Moravian Museum pp. 71-83.

Jassim S. Z., Goff J., 2006: Geology of Iraq, Czech Republic: Dolin Brno and Brno, Czech Republic: Moravian Museum.

Jassim S. Z., Hagopian D., Al-Hashimi H. 1986: Geological Map of Iraq 1:1,000,000 Scale Series. Sheet No. 2. Baghdad, Iraq: Iraq Geological Survey.

Jassim S. Z., Karim S., Basi M., Al-Mubarak M., Al-Munir M., 1984: The final report on the regional geological survey of Iraq. Geological Survey and Mineral Investigation (Geosurv.) unpublished report, 3. Stratigraphy. Oil Exploratioon Company Archives, Baghdad.

Jenne Mareike, 2015 Contamination of surface waters in the Kirkuk region of Iraq due to natural oil, bachelor Thesis. Institut für Angewandte Geowissenschaften Darmstadt.

Jiménez-Munt I., Fernàndez M., Saura E., Vergés J., Garcia-Castellanos D., 2012: 3-D lithospheric structure and regional/residual Bouguer anomalies in the Arabia-Eurasia collision (Iran): Geophysical Journal International, Volume 190, pp.1311–1324

Kadhim S., Nasr F., 1971: Upper Jurassic prospects. Proc. 10th Iraqi Engineering Congress. Baghdad.

Keith L. H., Telliard W. A., 1979: ES&T Special Report: Priority pollutants: I-a perspective view. Environ. Sci. Technol., 1979, Volume 13 (4), pp 416–423, doi: 10.1021/es60152a601

Kent N. W., 2010: Structures of the Kirkuk Embayment, northern Iraq: Foreland structures or Zagros Fold Belt structures? GeoArabia Volume 15 (4), pp.147-188.

Kerr J. M., McMillen S. J., Magaw R. I., Melton H. R., Naughton G., 2001: Risk-based soil screening levels for crude oil the role of polyaromatic hydrocarbons. Published in Risk-Based Decision-Making for Assessing Petroleum Impacts at Exploration and Production Sites, McMillen, S.J., R. I. Magaw, R.I., Carovillano, R. L. (Ed.), Published by the Department of Energy and the Petroleum Environmental Research Forum.

Khanaqa P. A., Al-Manmi D. A., 2011: Hydrogeochemistry and geomicrobiology of Darzila spring in Sangaw, Sulaimaniyah, NE Iraq. Iraqi Bull. Geol. Min. Volume 7 (3), pp.63–79.

Kirkuk weather station: URL: https://www.weather-forecast.com/locations/Kirkuk/forecasts/latest

Klimas A., Malisauskas A., 2008: Boron, fluoride, strontium and lithium anomalies in fresh groundwater of Lithuania, Geologija 50 (No 2(62)), pp.114 - 124. doi: 10.2478/v10056-008-0015-4

Kortum G., 1969: Reflectance Spectroscopy 3; Springer-Verlag: New York, doi: 10.1007/978-3-642-88071-1.

Kottek M., Grieser J., Beck C., Rudolf B., Rubel F. 2006: World Map of the Köppen-Geiger climate classification updated. Meteorologische Zeitschrift, Volume 15 (3) pp.259-263. doi: 10.1127/0941-2948/2006/0130

Krasny J., Al-Sam S., Jassim, S. Z., 2006: Hydrogeology of Iraq, Chapter 19. In: S.Z., Jassim and J.C., Goff (Eds.), Geology of Iraq. Dolin, Prague and Moravian Museum, Brno.

Kühn, F., Oppermann, K., Hörig, B., 2004: Hydrocarbon Index - an algorithm for hyperspectral detection of hydrocarbons. International Journal of Remote Sensing, Volume 25, pp.2467– 2473.

Kulke, H., 1994: Regional Petroleum Geology of the World, Part I: Europe and Asia.Berlin, Stuttgart: Gebrueder Borntraeger. pp. 931.

Kvenvolden K. A., Cooper C. K., 2003: Natural seepage of crude oil into the marine environment. Geo-Mar Lett, Volume 23, pp.140–146.

Lammoglia T., Filho C., 2011: Spectroscopic characterization of oils yielded from Brazilian offshore basins: Potential applications of remote sensing. Remote Sens Environ, Volume 115, pp.2525–2535.

Lane W. F., Loehr R. C., 1992: Estimating the equilibrium aqueous concentrations of polynuclear aromatic hydrocarbons in complex mixtures. Environ. Sci. Technol. Volume 26 (5), pp.983–90.

Lee L., Rao P. S. C., Okuda I., 1992: Equilibrium partitioning of polycyclic aromatic hydrocarbons from coal tar into water, Environ. Sci. Technol., 1992, Volume 26 (11), pp. 2104–2110 doi:10.1021/es00035a005

Lee, L.S., Hagwall, M., Delfino, J.J., Rao, P.S.C. (1992b). Partitioning of polycyclic aromatic hydrocarbons from diesel fuel into water. Environ. Sci. Technol., 26

Library of Congress. Kirkuk District, Iraq. Iraq Karkuk Karkūk, ca. 1932. [to 1933] Photograph. Retrieved from the Library of Congress, https://www.loc.gov/item/2002699561

Link W., 1952: Significance of oil and gas seeps in world oil exploration. Bulletin of the American Association of Petroleum Geologists, Volume 36, pp.1505–1540.

Littke R., Bayer U., Gajewski D., Nelskamp S. (Eds.) 2008: Dynamics of Complex Intracontinental Basins: the Central European Basin System, Berlin [u.a.] : Springer, pp.520. http://gfzpublic.gfz-potsdam.de/pubman/item/escidoc:238811

López-Geta J. A., Fornés J. M., Ramos G., Villarroya F. 2006: Groundwater. A natural underground resource. Environmental Education. Madrid: IGME, UNESCO and Fundación Marcelino Botín. Spain. ISBN: 84-7840-618-2, pp. 107.

Loyek D., 1998: Die Löslichkeit und Lösungskinetik von polyzyklischen aromatischen Kohlenwasserstoffen (PAK) aus der Teerphase. Institut und Museum für Geologie und Paläontologie der Universität Tübingen, Lehrstuhl für Angewandte Geologie Teutsch, G., &Einsele, G.

Macgregor D. S., 1993: Relationships between seepage, tectonics, and subsurface petroleum reserves. Marine and Petroleum Geology, Volume 10, pp.606–619.

Mackay D., Shiu W. Y., 1977: Aqueous Solubility of Polynuclear Aromatic Hydrocarbons. J. Chem. Eng.Data, 22, pp.399–409

Mahdi A., 2007: Fossils Mollusca (bivalve) from the Fatha formation of northern Iraq, Iraqi Bulletin of Geology and Mining Volume 3 (1) pp.41–53.

Majid H. A., Veizer J., 1986: Deposition and chemical diagenesis of Tertiary carbonates, Kirkuk oil field, Iraq. AAPG Bulletin, Volume 70, pp.898-913.

Manahan S. E., 2010: Environmental Chemistry. CRC Press., 9th edition, Boca Raton, FL, USA, CRC Press, 2010, pp.783, ISBN 978-1-4200-5920-5.

Marshall A. G., Rodgers R. P., 2004: Petroleomics: the next grand challenge for chemical analysis. Acc. Chem. Res. Volume 37 pp.53-59 (1), pp.53–59. doi: 10.1021/ar020177t

Mast V. A., 1985: The use of ionic mixing curves in differentiating oil field brine from natural brine in fresh water aquifer. Volume 5 (3), pp.65–69. http://dx.doi.org/10.1111/j.1745-6592.1985.tb00931.x

McArthur J. M., Howarth R. J., Shield G. A., 2012: Chapter 7: Strontium Isotope Stratigraphy. In: The Geologic Time Scale, 2012. Gredstein FM, Ogg J.G., Schmotz M.D. and Ogg G.M. Elsevier, Volume 1 of 2, pp.1144.

McClusky S., Reilinger R., Mahmoud S., Ben Sari D., Tealeb A., 2003: GPS constraints on Africa (Nubia) and Arabia plate motions. Geophysical Journal International, Volume 155, pp.126-138. https://doi.org/10.1046/j.1365-246X.2003.02023.x

McKirdy D. M., Aldridge A. K., Ypma P. J. M., 1983: A geochemical comparison of some crude oils from Pre-Ordovician carbonate rocks. Advances in Organic Geochemistry 1981, pp.99-107.

Mclean W., Jankowski J., Lavitt N., 2000: Groundwater quality and sustainability in an alluvial aquifer, Australia. In: Sililo, O., et al. (Eds.), Groundwater: Past Achievements and Future Challenges. AA Balkema, Rotterdam, pp. 567–573.

McMillen S., Kerr J., Nakles D., 2001: Composition of Crude Oils and Gas Condensates. In Risk-Based Decision-Making for Assessing Petroleum Impacts at Exploration and Production Sites, the Department of Energy and the Petroleum Environmental Research Forum USA. chapter 3.

McNutt R.H., 2001: Strontium isotopes. In: Cook, P.G., Herczeg, A.L. (Eds.), Environmental Tracers, Subsurface Hydrology. Kluwer Academic Publishers, Boston/Dordrecht/London, pp. 233–260.

McQuarrie N., 2004: Crustal scale geometry of the Zagros fold-thrust belt, Iran. Journal of Structural Geology, Volume 26, pp.519-535.

Mirnejad H., Sisakht V., Mohammadzadeh H., Amini A. H., Rostron B. J. and Haghparast G., 2011: Major, minor element chemistry and oxygen and hydrogen isotopic compositions of Marun oil-field brines, SW Iran: Source history and economic potential. Geol. J., Volume 46 (1), pp. 1–9. doi: 10.1002/gj.1226.

Mohialdeen I. M. J., Hail Hakimi M., Al-Beyati F. M., 2013: Biomarker characteristics of certain crude oils and the oil-source rock correlation for the Kurdistan oilfields, Northern Iraq. Arabian Journal of Geoscience, Volume 8, pp.507-525.

Mohialdeen I. M. J., Hail Hakimi M., Al-Beyati F. M., 2013: Geochemical and petrographic characterization of Late Jurassic-Early Cretaceous Chia Gara Formation in Northern Iraq: Palaeoenvironment and oil-generation potential. Marine and Petroleum Geology, Volume 43, pp.166-177.

Moreira L. C. J, Teixeira A. D., 2014: Laboratory Salinization of Brazilizn Alluvial Soil and the Spectral Effect of Gypsum. Remote sensing 2014, Volume 6, pp.2647–2663.

Mulder G., Olsthoorn T. N., Al-Manmi D. A. M. A., Schrama E. J. O., Smidt E. H., 2015: Identifying water mass depletion in northern Iraq observed by GRACE. Hydrol. Earth Syst. Sci., volume 19, pp.1487–1500, 2015. www.hydrol-earth-syst-sci.net/19/1487/2015/ doi:10.5194/hess-19-1487-2015

Naqishbandi S. F., Jabbar W. J., AL-Juboury A. I., in press. Hydrocarbon potential and porosity types of the Geli Khana Formation (Middle Triassic), Northern Iraq. Arabian Journal of Geosciences 10.1007/s12517-013-1258-x.

NOAA's National Climatic Data Center (NCDC), ftp://ftp.ncdc.noaa.gov/pub/data/noaa/isd-history.txt

NOC, drilling reports. internal reports. http://www.noc.oil.gov.iq/studies.htm

O'Leary D. W., Friedman J. D., Phon H. A., 1976: Lineament, Linear, Lineation: Some proposed new standards for old terms. Bulletin of the Geological Society of America, Volume 87, pp.1463 - 1469.

OPEC Annual Statistical Bulletin, 2015, p 22. http://www.opec.org.

Oslick J. S., Miller K., Feigenson M., Wright J., 1994: Oligocene-Miocene strontium isotopes: Stratigraphic revisions and correlations to an inferred glacioeustatic record, Paleoceanography Volume 9 (3), pp.427-444. doi: 10.1029/94PA00249.

Owen R. M. S., Nasr S. N., 1958: The stratigraphy of Kuwait – Basrah area. In Habitat of Oil-A Symposium, Spec. Publ. AAPG, p1252 – 1278.

Owen T., 1996: Fundamentals of UV-visible spectroscopy, Primer publication number: 12-5965-5123E, Workbook publication number 12-5967-6357E.

Palm W. U., 2002: Vorlesungsskript Organische Chemie für Umweltwissenschaftler. Universität Lüneburg Institut für Ökologie und Umweltchemie

Palmer A. N., Hill C.A., 2012: Sulfuric acid caves. In: W. White, D.C. Culver (Eds.), Encyclopedia of Caves, 2nd ed. Academic Press /Elsevier, Amsterdam, pp 810-819.

Pearlman R. S., Yalkowsky S. H., Banerjee S., 1984: Water solubility of polynuclear aromatic and heteroaromatic compounds. Journal of Physical and Chemical Reference Data, Volume 13(2), pp.555-562, doi:org/10.1063/1.555712

Perry S. L., Kruse F. A., 2011: Evidence of Hydrocarbon Seepage using Multispectral Satellite Imagery Kurdistan Iraq, American Association of Petroleum Geologists, Volume 95, pp.941-956.

Peterman Z., Stuckless J., 1992: Paleohydrological Methods and their Applications, Proc. NEA Workshop, Paris, Ch. Application of strontium and other radiogenic tracer isotopes to Paleohydrologic studies, pp 59-84.

Peterman Z., Thamke, J., Futa K., Preston T., 2012: Strontium isotope systematics of mixing groundwater and oil-field brine at Goose Lake in northeastern Montana, USA, Applied Geochemistry, Volume 27, pp.2403–2408. 10.1016/j.apgeochem.2012.08.004.

Peters K. E., Clifford C. W., Moldowan J. M., 2005: The Biomarker Guide, Volume 2, Biomarkers, and Isotopes in Petroleum Exploration and Earth History. Cambridge University Press, Cambridge, pp.700.

Peters K. E., Fraser T. H., Amris W., Rustanto B., Hermanto E., 1999: Geochemistry of crude oils from eastern Indonesia. American Association of Petroleum Geologists Bulletin Volume 83, pp.1927–1942.

Peters K. E., Moldovan J., 1993: The biomarker guide: Interpreting molecular fossils in petroleum and ancient sediments. Prentice Hall, Englewood Cliffs, pp.363.

Pitman J. K., Steinhouer D., Lewan M. D., 2004: Petroleum generation and migration in the Mesopotamian Basin and Zagros Fold Belt of Iraq: results from a basin modeling study. GeoArabia Volume 9, pp.41–72.

Pope R., Fry E., 1997: Absorption spectrum (380-700 nm) of pure water. II. Integrating cavity measurements. App. Optics 1997, Volume 36, pp.8710–8723.

Pothuluri J. V., Cerniglia C. E., 1994: Microbial metabolism of polycyclic aromatic hydrocarbons. Published. In: Biological Degradation and Bioremediation of Toxic Chemicals (Chaudhry,G.R., Ed.), Dioscorides Press, Portland, OR, pp. 92-124.

Priemon-Storer R. A., Cornillot J. L., 1985: Standard Test Method for Separation of Representative Aromatic and Nonaromatic Fractions of High Boiling Oils by Elution Chromatography. ASTM Standard D2549-85 Volume 05-02, D975-81 Vol05-01, D396-80 Vol.05-01.

Qadir F.M., 2008: Formation Evaluation of Upper Qamchuqa Reservoir, Khabbaz oil Field, Kirkuk Area, Northeastern Iraq. Ph.D. thesis, University of Sulaimani, pp.168.

Reilinger R., McClusky S., Vernant P., Lawrence S., Ergintav S., Cakmak R., Ozener H., Kadirov F., Guliev I., Stepanyan R., Nadariya M., Hahubia G., Mahmoud S., Sakr K., ArRajehi A., Paradissis D., Al-Aydrus A., Prilepin M., Guseva T., Evren E., Dmitrotsa A., Filikov S. V., Gomez F., Al-Ghazzi R., Karam G., 2006: GPS constraints on continental deformation in the Africa-Arabia-Eurasia continental collision zone and implications for the dynamics of plate interactions. J. Geophys. Res. 111, B05411.

Rengarajan T., Rajendran P., Nandakumar N., Lokeshkumar B., Rajendran P., Nishigaki I.2015: Exposure to polycyclic aromatic hydrocarbons with special focus on cancer. Asian Pac J Trop Biomed 2015, Volume 5(3) pp.182-189.

Sadiq S.N., 2008. Hydrogeochemical properties of ground water in the vicinity of Al-Hawija plain SE-Kirkuk, Iraq. J. Kirkuk Univ. Sci. Stud. Volume 3 (2).

Sadooni F., Aqrawi, A., 2000: Cretaceous Sequence Stratigraphy and Petroleum Potential of the Mesopotamian Basin, Iraq. In Alsharhan, A and Scott, B.: Middle East Models of Jurassic-Cretaceous carbonate systems, SEPM special publication, Tulsa, Oklahoma, USA. Volume 69. pp.315-334.

Sahib L. Y., Marandi A., Schüth C., 2016: Strontium isotopes as an indicator for groundwater salinity sources in the Kirkuk region, Iraq. Science of the Total Environment Volume 562, pp.935–945.

Salati S., Van Ruitenbeek F. J. A., Carranza, E. J. M., Van der Meer, F. D., Tangestani M. H. 2013: Conceptual modeling of onshore hydrocarbon seep occurrence in the Dezful Embayment, SW Iran, Marine and Petroleum Geology Volume 43, pp.102-120.

Salem F., Kaftos M., El-Ghazawi T., Gomez R., Yang R., Hyperspectral image assessment of oil-contaminated wetland. International Journal of Remote Sensing 2005, Volume 26, pp.811–821.

Saud Q. J., 2009: Hydrogeological and hydrochemical study of Kirkuk governorate, northern Iraq, Iraqi journal for geology and mining, Volume 5, pp.1-13.

Sayyab A., Kureshy A. A., 1967: The benthonic Foraminifera of the Lower Fars formation (Lower Miocene) from Shathatha, Karbala, Iraq. Bull. College of Science, Baghdad, 10, 139-149.

Scherr, K.; Aichberger, H.; Braun, R.; Loibner, A. Influence of soil fractions on microbial degradation behavior of mineral hydrocarbons. European Journal of Soil Biology, Volume 43, pp.341–350.

Schlumberger (2015). Seep. Retrieved December 28, 2015, http://www.glossary.oilfield.slb.com/Terms/s/seep.aspx

Schmidt S., 2014: Comparison of Total Organic Carbon (TOC) and Total Petroleum Hydrocarbon (TPH) content from soil samples around a seepage in NE Iraq. Bachelor Thesis. Institut für Angewandte Geowissenschaften Darmstadt.

Schneider I., Nau G., King T., Aggarwal I., 1995: Fiber-optic near infrared reflectance sensor for detection of organics in soils. Photonics Technology Letters, IEEE 1995, Volume 7, pp.87–89.

Schumacher B. A., 2002: Methods for the determination of total organic carbon (TOC) in soils and sediments. Ecological Risk Assessment Support Center 2002, pp. 1–23.

Schumacher, D, 1996: Hydrocarbon-induced alteration of soils and sediments. In D. Schumacher & M.A. Abrams (Eds.), Hydrocarbon Migration and its Near-Surface Expression. Bulletin of the American Association of Petroleum Geologists Memoir, Volume 66, pp.71-89.

Schwartz G., Ben-Dor E., Eshel G., 2012: Quantitative Analysis of Total Petroleum Hydrocarbons in Soils: Comparison between Reflectance Spectroscopy and Solvent Extraction by 3 Certified Laboratories.

Hindawi Publishing Corporation Applied and Environmental Soil Science, Volume 2012, 751956, 11. http://dx.doi.org/10.1155/2012/751956

Schwarzbauer J., Littke R., Weigelt V., 2000: Identification of specific organic contaminants for estimating the contribution of the Elbe river to the pollution of the German Bight. Organic Geochemistry Volume 31, pp.1713–1731.

Schwarzenbach R. P., Gschwend P. M., Imboden D. M., 2003: Environmental Organic Chemistry. Wileyinterscience. Second edition. Wiley-Interscience, Hoboken, NJ, 2003.

Seifert W, K., Moldowan J. M., 1978: Applications of steranes, terpanes, and monoaromatics to the maturation, migration, and source of crude oils. Geochmica et Cosmochimica Acta, Volume 42, pp.77-95.

Shand P., Darbyshire D. P. F., Love A. J., Edmunds W. M., 2009: Sr isotopes in natural waters: applications to source characterization and water–rock interaction in contrasting landscapes. Appl. Geochem. Volume 24, pp.574–583.

Sharland P. R., Archer R., Casey D. M., Davies, R. B., Hall S. H., Heward A. P., Horbury A. D., Simmons M. D., 2001: Arabian Plate Sequence Stratigraphy, GeoArabia Special Publication Volume 2, pp.371.

Shawkat G. M., 1979: The sedimentology of the lower fars formation (Miocene) of northern Iraq, Ph.D. thesis, the University of Newcastle upon Tyne.

Short N. M., Bolton J., Rocchio L., 2006: Remote Sensing Tutorial. NASA.

Simon H., 2011: Managing Oil & Gas Exploration Risk in the Kurdistan Region of Iraq. Western Zagros Resources Limited. World Independent & Junior Oil and Gas Congress, London, UK. September 26-28,2011. http://www.westernzagros.com

Sims R. C., Overcash M. R., 1983: Fate of Polynuclear Aromatic Compounds (PNAs) in Soil-Plant Systems. Residue Reviews, Volume 88, Springer-Verlag, New York

Sissakian V. K., 1993: Geological Map of Kirkuk. Quadrangle 1:250,000 Scale series. Sheet NI-38-2. Geological Map. Baghdad, Iraq: Iraq Geological Survey.

Sissakian V. K., Al-Jibouri B. S., 2012: Stratigraphy, In: Geology of the Low Folded Zone. Iraqi Bull. Geol. Min., Special Issue, No.5, pp. 63 – 132.

Sorkhabi R., 2009: Iraq: Resource Base. GeoExPro article appeared in Volume 6, No. 3.

Speight, J. G., 1999: The Chemistry and Technology of Petroleum. Marcel Dekker, New York. Third Edition.

SRTM 90m, Digital Elevation Data (srtm.csi.cgiar.org). https://www2.jpl.nasa.gov/srtm/

Tedesco S. A.,1985: Surface geochemistry in petroleum exploration. Chapman & Hall, New York, doi: 10.1007/978-1-4615-2660-5

Thomas A. N. 1952: Gach-i-turush' and associated phenomena in southwest Persia. VII Convegno Nazionale Del Metano E Del Petrolio Taormina, Section 1, preprint.

Tian Q., 2012: Study on Oil-Gas reservoir detecting methods using hyperspectral remote sensing. In Remote Sensing and Spatial Information Sciences; XXII ISPRS Congress, 25 August – 01 September 2012, Melbourne, Australia, 2012.

Tissot B. P., Welte D. H., 1984: Petroleum Formation and Occurrence. 2nd Edition, Springer-Verlag, Berlin, pp.699.

U.S. National Library of Medicine 2013: Hazardous Substances Data Bank. Retrieved December 28, 2015. http://toxnet.nlm.nih.gov/newtoxnet/hsdb.htm

UN-ESCWA and BGR (United Nations Economic and Social Commission for Western Asia; Bundesanstalt für Geowissenschaften und Rohstoffe). 2013. Inventory of Shared Water Resources in Western Asia. Beirut, Ch. 23, Taurus-Zagros, pp 544-559. https://waterinventory.org/sites/waterinventory.org/files/chapters/00-shared-water-resouces-in-western-asia-web.pdf

USGS 2017 (https://earthquake.usgs.gov/earthquakes/eventpage/us2000bmcg#executive)

Varjani S. J. Joshi R. R., Kumar, P., Senthil S., Vijay K., Kumar V., Banerjee C., Kumar R. P., 2018: Polycyclic Aromatic Hydrocarbons from Petroleum Oil Industry Activities: Effect on Human Health and Their Biodegradation. In: Varjani S., Gnansounou E., Gurunathan B., Pant D., Zakaria Z. (eds) Waste Bioremediation. Energy, Environment, and Sustainability. Springer, Singapore. https://app.dimensions.ai/details/publication/pub.1093110977

Varoujan K. S., Saffa F. A., F., 2015: GEOLOGICAL MAP OF IRAQ, SCALE 1: 1000 000, 4th EDITION, 2012. Iraqi Bulletin of Geology and Mining. Papers of the Scientific Geological Conference. Volume 11, No.1, pp. 9-16

Verma M. K., Ahlbrandt T. S., Al-Gailani M., 2004: Petroleum reserves and undiscovered resources in the total petroleum systems of Iraq: reserve growth and production implications. GeoArabia, Volume 9(3), pp.51-74.

Vinas L., Franco M. A., Soriano J. A., Gonzalez J. J., Pon J., Albaiges J. 2010: Sources and distribution of polycyclic aromatic hydrocarbons in sediments from the Spanish northern continental shelf. Assessment of spatial and temporal trends. Environ. Pollut., Volume 158, pp.1551-1560

Walrafen G. E., Pugh E., 2004: Raman combinations and stretching overtones from water, heavy water and NaCl in water at shifts to ca. 7000 cm 1. J. Solution Chem 2004, Volume 33, pp.81–97.

Wayne A., Sewell H., Deeley G., 2001: Technical Basis for Current Soil Management Levels of Total Petroleum Hydrocarbons. Shell Exploration & Production Company, Equilon Enterprises LLC. In Risk-Based Decision-Making for Assessing Petroleum Impacts at Exploration and Production Sites; McMillen, S.; Magaw, R.; R., L., Eds.; Published by the Department of Energy and the Petroleum Environmental Research Forum, chapter 2.

Wendlandt W. W., Hecht H. G., 1966: Reflectance Spectroscopy; Wiley-lnterscience: New York.

Wenger L. M., Isaksen G. H., 2002: Control of hydrocarbon seepage intensity on level of biodegradation in sea bottom sediments. Organic Geochemistry, Volume 33, pp.1277-1292.

White K. L., 1986: An overview of immunotoxicology and carcinogenic polycyclic aromatic hydrocarbons. J Environ. Sci. Health Part C: Environ. Carcino. Ecotox. Rev.2, pp. 163-202.

Winkelmann K., 2005: On the applicability of imaging spectrometry for the detection and investigation of contaminated sites with particular consideration given to the detection of fuel hydrocarbon contaminants in soil. PhD thesis, University of Cottbus, Germany.

Wu X. A., 2008: Selective Creaming: A Novel Technique to Isolate Interfacial Organics and Mineral Solids from Water-in-Oil Emulsions. Energy Fuels, Volume 22, pp. 2346–2352.

Yakovenko A., Yashin V., Kovalev A. E., Fesenko E. E., 2002: Structure of the vibrational absorption spectra of water in the visible region. Biophysics, Volume 47, pp. 891–895.

Zebari M. M., Burberry C. M. 2015: 4-d evolution of anticlines and implications for hydrocarbon exploration within the Zagros fold-thrust belt, Kurdistan region, Iraq, GeoArabia, Volume 20 (1), pp. 161-188.

Zhang G., Zou L., Shen X., Lu S., Li C., Chen H., 2009: Remote sensing detection of heavy oil through spectral enhancement techniques in the western slope zone of Songliao Basin, China, Bulletin of the American Association of Petroleum Geologists, Volume 93 (1), pp. 31-49.

Ziegler M. A., 2001: Late Permian to Holocene Paleofacies Evolution of the Arabian Plate and its Hydrocarbon Occurrences. GeoArabia, Volume 6, No. 3

Zwanziger Z., Heidrun F., 1998: Near infrared spectroscopy of fuel contaminated sand and soil. I. Preliminary results and calibration study, Journal of Near Infrared Spectroscopy, Volume 6, no. 1–4, pp. 189–197.

Appendix

Figure – App. 1: The upper red beds of the Fatha Formation in Baba Dome – Kirkuk anticline

Figure – App. 2: The seepage beds of the Fatha Formation in Baba Dome – Kirkuk anticline

Figure – App. 3: Mukdadia Formation angular unconformity south of Kirkuk anticline

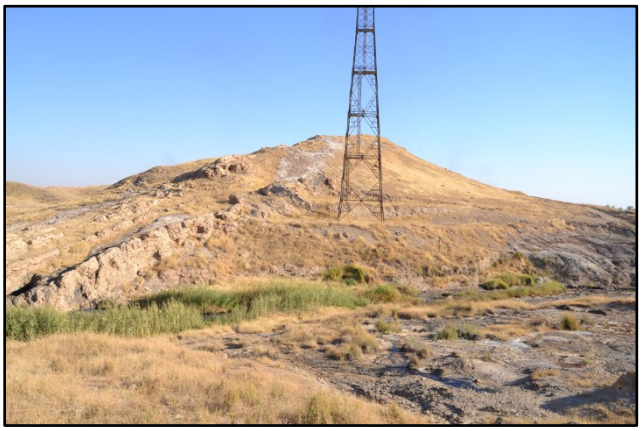

Figure – App. 4: The axis of anticline Kirkuk showing outcrops of Fatha Formation in Baba Dome

Figure – App. 5: An epigene caves in gypsum-rich layers in Fatha Formation

Figure – App. 6: Traces of sulfur at the surface within Fatha Formation in Baba Dome Kirkuk

Table App - 1: Bulk oil composition, API gravity, sulfur content. The results are separated after their oil fields and well depth, which is given with elevation starting at RTKB.

Well name	Oil field	Age - Reservoir	Depth (m)	API (°)	Sulfur (%)	SAT (%)	ARO (%)	NSO (%)	ASPH (%)
K 227	Kirkuk/ Baba	Aptian - L. Sarmord	2065	34.45	2.37	21.47	63.78	10.25	4.52
K 229	Kirkuk/ Baba	Aptian - L. Sarmord	1970	34.32	2.74	35.66	43.52	16.59	4.23
K 429	Kirkuk/ Baba	Albian - L.Qamchuqa	1450	37.46	2.32	36.07	51.1	10.2	2.65
k 218	Kirkuk/ Baba	Albian - L.Qamchuqa	1650	29.44	3.3	13.82	62.12	20.5	3.55
K 411	Kirkuk/ Baba	Albian - L.Qamchuqa	1460	37.1	2.31	42.9[1]	41.2[1]	12[1]	3.9[1]
K 334[1]	Kirkuk/ Baba	Albian - U.Qamchuqa	1142	27.8	3.13	33.7	43.2	13.5	9.5
K 337	Kirkuk/ Baba	Albian - U.Qamchuqa	1212	30.7	2.76				
K 410	Kirkuk/ Baba	Oligocene – Baba	390	34.11	2.51	34.02	41.03	20.48	4.47
k 425	Kirkuk/ Baba	Oligocene – Baba	419	31.81	2.51	32.92	52.67	13.57	5.79
k 424	Kirkuk/ Baba	Oligocene – Baba	441	34.38	2.48	31.24	52.09	12.52	4.16
K 263	Kirkuk/ Baba	Oligocene – Baba	657	34.51	2.16	33.7	47.88	16.59	1.94
K 280	Kirkuk/ Baba	Oligocene – Baba	655	34.49	2.56				
K 324	Kirkuk/ Baba	Oligocene – Baba	438	29.54	2.03				
K 412	Kirkuk/ Baba	Oligocene – Baba	390	33.52	2.76				
K 407	Kirkuk/ Baba	Oligocene - Bajawan	424	31.86	2.23	32.23	52.01	12.4	3.37
K 366	Kirkuk/ Baba	Oligocene - Bajawan	438	32.37	2.59	23.9	60.68	11	4.43
k 427	Kirkuk/ Baba	Oligocene - Bajawan	425	32.93	2.63	28.22	58.62	10.85	4.76
k 259	Kirkuk/ Baba	Oligocene - Bajawan	604	33.12	2.38				
K 371	Kirkuk/ Baba	Oligocene - Bajawan	464	34.46	2.17				
K 392	Kirkuk/ Baba	Oligocene - Bajawan	420	34.49	2.38				
K 265	Kirkuk/ Baba	Oligocene – Palani	573	35.85	2.79				
K 157	Kirkuk/ Baba	Oligocene – Palani	495	32.68	2.37				
k 353	Kirkuk/ Avanah	Eocene – Avanah	707	34.97	2.36	34.53	50.41	10.08	4.99
k 369	Kirkuk/ Avanah	Eocene – Avanah	719	34.35	2.59	28.12	56.04	12.71	3.13
k 341	Kirkuk/ Avanah	Eocene – Avanah	686	35.2	2.03	35.55	46.84	11.94	5.68
K 344	Kirkuk/ Avanah	Eocene – Avanah	709	36.02	2.42	19.74	55.44	19.51	5.32
K 345	Kirkuk/ Avanah	Eocene – Avanah	735	35.68	2.38	34.03	46.59	15.85	3.52
K 370	Kirkuk/ Avanah	Eocene – Avanah	695	33.45	3.13	32.6	51.83	12.59	2.99
K 363	Kirkuk/ Avanah	Eocene – Avanah	690	33.77	2.43	20.18	57.91	16.88	5.04
k 373	Kirkuk/ Avanah	Eocene – Avanah	736.6	35.56	2.58				
k 359	Kirkuk/ Avanah	Eocene – Avanah	669.8	34.07	2.65				
k 348	Kirkuk/ Avanah	Eocene – Avanah	685	34.77	2.62				

k 346	Kirkuk/ Avanah	Eocene – Avanah	682	35.23	2.3				
K 347	Kirkuk/ Avanah	Eocene – Avanah	710	35.86	2.56				
K 332	Kirkuk/ Avanah	Eocene – Avanah	736	34.56	2.33				
SK 614	Kirkuk/ Baba	Seepage	0						
SK 615	Kirkuk/ Baba	Seepage	0	9.09	4.50				
SK 616	Kirkuk/ Baba	Seepage	0	8.52	2.78				
bh134	Bai Hassan	Pliensbachian - Butima	1862	23.44	4.53				
bh13	Bai Hassan	Aptian - L. Sarmord	2210.4	24.74	4.36	17.41	51.65	20.58	10.91
bh96	Bai Hassan	Cenomanian - Dokan	2040	20.39	5.04	13.795	58.72	21.89	5.591
bh157	Bai Hassan	Oligocene – Baba	1496	32.64	3.11	29.63	49.49	16.38	4.51
bh29	Bai Hassan	Oligocene – Baba	1463	31.86	2.91	29.91	42.24	21.02	7.14
bh49	Bai Hassan	Oligocene – Baba	1515	30.87	3.24	15.26	57.83	21.31	5.7
bh71	Bai Hassan	Oligocene – Baba	1465	33.39	3.08				
bh88	Bai Hassan	Oligocene – Baba	1425	26.58	3.34				
bh179	Bai Hassan	Oligocene – Baba	1482	31.47	3.12				
bh132	Bai Hassan	Oligocene – Baba	1510	31.68	3.06				
bh60	Bai Hassan	Oligocene – Palani	1520	30.04	3.07	27.55	57.86	10.47	3.45
bh42	Bai Hassan	Oligocene – Palani	1537	31.94	2.92				
bh8	Bai Hassan	Eocene – Avanah	1610.8	31.44	3.02				
kz12	Khabbaz	Aptian - L. Sarmord	3058	39.61	1.40	45	41.1	13.9	6.2
kz23	Khabbaz	Albian - U.Qamchuqa	3020	31.39	2.36	34.3	53.6	12.2	4.5
kz24	Khabbaz	Albian - U.Qamchuqa	3007	31.26	2.34	24.335	62.66	11.35	1.64
kz4[2]	Khabbaz	Albian - U.Qamchuqa	3150	22.4	3.85	30.5	53.9	15.6	1.2
kz21[2]	Khabbaz	Albian - U.Qamchuqa		23.2	3.21	34.5	52.5	13	6.6
kz13	Khabbaz	Albian - U.Qamchuqa	2924.1	32.3	1.63	50	45.7	4.1	1.2
Kz18	Khabbaz	Oligocene – Baba	2346	33.41	1.84	35.83	53.7	5.24	2.14
J16	Jambur	Aptian - L. Sarmord	3501.5	43.31	1.41				
J 63	Jambur	Albian - L.Qamchuqa	3501.5	35.17	1.45	31.02	58.44	8.51	1.65
J 59	Jambur	Albian - L.Qamchuqa	3190	30.03	1.02				
J 20	Jambur	Albian - U.Qamchuqa	3237.7	36.03	1.24	36.47	53.43	7.4	1.71
J22	Jambur	Albian - U.Qamchuqa	3228	34.92	1.54	28.17	59.62	10.77	1.45
J 45	Jambur	Miocene - Srekagne	1982	37.6	1.14	40.4	47	11.2	2.3
Q 75	Qaiyarah	Miocene - Euphrates	296	11.86	7.73				
Q 73	Qaiyarah	Miocene - Euphrates	304	15.66	7.84				
Q 45	Qaiyarah	Miocene – Jeribe	237	15.13	7.48				
Q 38	Qaiyarah			15.12	7.84				
SQ 81	Qaiyarah	Seepage	0	9.89	6.45				
SQ 82	Qaiyarah	Seepage							

[1] Al-Ameri and Zumberge, 2012,[2] Qadir, 2008

Table App. 3: Appendix 1: Calculated concentrations using Raoult's law

J 16																	
		Nap	Any	Ace	Fln	Phe	Ant	Fth	Pyr	BaA	Chr	BbF	BkF	BaP	Indeno	DahA	BghiP
Mass PAH (g)		1.53E-05	7.23E-07	1.31E-06	3.08E-06	6.28E-06	0.00E+00	2.36E-07	3.72E-07	6.15E-08	3.60E-07	1.37E-07	0.00E+00	1.51E-07	1.30E-08	4.87E-08	6.21E-08
Water solubility as a subcooled liquid (mg/l)		119.4	51.4	18.2	18.1	8.3	6.4	2.1	2.7	0.34	0.45	0.04	0.02	0.15	1.67		
Molecular weight PAH (g/mol)		128	152	154	166	178	178	202	202	228	228	252	252	252	276	278	276
Molecular weight oil (g/mol)	92.7																
Mass oil (g)	0.08																
Mole fraction		1.37E-04	5.48E-06	9.82E-06	2.14E-05	4.07E-05	0.00E+00	1.35E-06	2.12E-06	3.11E-07	1.82E-06	6.27E-07	0.00E+00	6.91E-07	5.41E-08	2.02E-07	2.59E-07
Activity coefficient	1																
Raoult concentartion (mg/l)		1.64E-02	2.82E-04	1.79E-04	3.87E-04	3.38E-04	0.00E+00	2.83E-06	5.74E-06	1.06E-07	8.20E-07	2.51E-08	0.00E+00	1.04E-07	9.04E-08	2.63E-08	7.78E+00

K 411																	
		Nap	Any	Ace	Fln	Phe	Ant	Fth	Pyr	BaA	Chr	BbF	BkF	BaP	Indeno	DahA	BghiP
Mass PAH (g)		1.57E-05	1.05E-06	1.03E-06	2.95E-06	4.19E-06	0.00E+00	1.70E-07	3.02E-07	9.04E-08	1.57E-07	9.17E-08	0.00E+00	1.33E-07	1.80E-08	3.39E-08	3.81E-08
Water solubility as a subcooled liquid (mg/l)		119.4	51.4	18.2	18.1	8.3	6.4	2.1	2.7	0.34	0.45	0.04	0.02	0.15	1.67	0.13	0.03
Molecular weight PAH (g/mol)		128	152	154	166	178	178	202	202	228	228	252	252	252	276	278	276
Molecular weight oil (g/mol)	92.7																
Mass oil (g)	0.08																
Mole fraction		7.55E-06	7.32E-06	1.94E-05	2.58E-05	0.00E+00	9.24E-07	1.64E-06	4.35E-07	7.53E-07	3.99E-07	0.00E+00	5.76E-07	7.16E-08	1.33E-07	1.51E-07	
Activity coefficient	1																
Raoult concentartion (mg/l)		1.60E-02	3.88E-04	1.33E-04	3.52E-04	2.14E-04	0.00E+00	1.94E-06	4.43E-06	1.48E-07	3.39E-07	1.59E-08	0.00E+00	8.64E-08	1.20E-07	1.73E-08	4.54E-09

K324																	
		Nap	Any	Ace	Fln	Phe	Ant	Fth	Pyr	BaA	Chr	BbF	BkF	BaP	Indeno	DahA	BghiP
Mass PAH (g)		2.33E-05	5.09E-07	1.03E-06	4.15E-06	7.95E-06	0.00E+00	2.72E-07	6.66E-07	1.30E-07	5.01E-07	1.22E-07	0.00E+00	2.42E-07	2.21E-08	6.56E-08	8.16E-08
Water solubility as a subcooled liquid (mg/l)		119.4	51.4	18.2	18.1	8.3	6.4	2.1	2.7	0.34	0.45	0.04	0.02	0.15	1.67	0.13	0.03
Molecular weight PAH (g/mol)	108	128	152	154	166	178	178	202	202	228	228	252	252	252	276	278	276
Molecular weight oil (g/mol)	0.09																
Mass oil (g)																	
Mole fraction		2.26E-04	4.15E-06	8.30E-06	3.11E-05	5.54E-05	0.00E+00	1.67E-06	4.09E-06	7.10E-07	2.73E-06	6.00E-07	0.00E+00	1.19E-06	9.96E-08	2.93E-07	3.67E-07
Activity coefficient	1																
Raoult concentartion (mg/l)		2.70E-02	2.14E-04	1.51E-04	5.62E-04	4.60E-04	0.00E+00	3.52E-06	1.11E-05	2.41E-07	1.23E-06	2.40E-08	0.00E+00	1.79E-07	1.66E-07	3.81E-08	1.10E-08

bh 88																	
		Nap	Any	Ace	Fln	Phe	Ant	Fth	Pyr	BaA	Chr	BbF	BkF	BaP	Indeno	DahA	BghiP
Mass PAH (g)		1.62E-05	6.24E-07	1.05E-06	2.49E-06	5.21E-06	0.00E+00	1.87E-07	4.05E-07	1.02E-07	2.88E-07	6.94E-08	0.00E+00	1.37E-07	2.37E-08	3.84E-08	5.15E-08
Water solubility as a subcooled liquid (mg/l)		119.4	51.4	18.2	18.1	8.3	6.4	2.1	2.7	0.34	0.45	0.04	0.02	0.15	1.67	0.13	0.03
Molecular weight PAH (g/mol)	108	128	152	154	166	178	178	202	202	228	228	252	252	252	276	278	276
Molecular weight oil (g/mol)	0.09																
Mass oil (g)																	
Mole fraction		1.48E-04	4.79E-06	7.95E-06	1.75E-05	3.42E-05	0.00E+00	1.08E-06	2.34E-06	5.20E-07	1.47E-06	3.21E-07	0.00E+00	6.36E-07	1.00E-07	1.61E-07	2.18E-07
Activity coefficient	1																
Raoult concentartion (mg/l)		1.77E-02	2.46E-04	1.45E-04	3.17E-04	2.83E-04	0.00E+00	2.26E-06	6.31E-06	1.77E-07	6.62E-07	1.28E-08	0.00E+00	9.53E-08	1.67E-07	2.09E-08	6.53E-09

Q 75																	
		Nap	Any	Ace	Fln	Phe	Ant	Fth	Pyr	BaA	Chr	BbF	BkF	BaP	Indeno	DahA	BghiP
Mass PAH (g)		9.71E-06	5.34E-07	6.34E-07	1.66E-06	3.34E-06	0.00E+00	1.28E-07	3.31E-07	7.28E-08	2.36E-07	5.39E-08	0.00E+00	1.49E-07	1.07E-08	2.40E-08	7.42E-08
Water solubility as a subcooled liquid (mg/l)		119.4	51.4	18.2	18.1	8.3	6.4	2.1	2.7	0.34	0.45	0.04	0.02	0.15	1.67	0.13	0.03
Molecular weight PAH (g/mol)	135	128	152	154	166	178	178	202	202	228	228	252	252	252	276	278	276
Molecular weight oil (g/mol)	0.1																
Mass oil (g)																	
Mole fraction		1.05E-04	4.86E-06	5.70E-06	1.38E-05	2.59E-05	0.00E+00	8.75E-07	2.27E-06	4.42E-07	1.43E-06	2.96E-07	0.00E+00	8.20E-07	5.39E-08	1.20E-07	3.72E-07
Activity coefficient	1																
Raoult concentartion (mg/l)		1.25E-02	2.50E-04	1.04E-04	2.50E-04	2.15E-04	0.00E+00	1.84E-06	6.13E-06	1.50E-07	6.45E-07	1.18E-08	0.00E+00	1.23E-07	9.00E-08	1.56E-08	1.12E-08

SQ 81																	
		Nap	Any	Ace	Fln	Phe	Ant	Fth	Pyr	BaA	Chr	BbF	BkF	BaP	Indeno	DahA	BghiP
Mass PAH (g)		1.41E-06	4.68E-07	8.72E-07	1.83E-06	4.20E-06	0.00E+00	1.69E-07	4.15E-07	1.13E-07	3.18E-07	6.50E-08	0.00E+00	2.02E-07	2.00E-08	3.61E-08	6.64E-08
Water solubility as a subcooled liquid (mg/l)		119.4	51.4	18.2	18.1	8.3	6.4	2.1	2.7	0.34	0.45	0.04	0.02	0.15	1.67	0.13	0.03
Molecular weight PAH (g/mol)	135	128	152	154	166	178	178	202	202	228	228	252	252	252	276	278	276
Molecular weight oil (g/mol)	0.1																
Mass oil (g)																	
Mole fraction		1.45E-05	4.04E-06	7.43E-06	1.45E-05	3.10E-05	0.00E+00	1.10E-06	2.70E-06	6.53E-07	1.83E-06	3.39E-07	0.00E+00	1.05E-06	9.53E-08	1.70E-07	3.16E-07
Activity coefficient	1																
Raoult concentartion (mg/l)		1.73E-03	2.08E-04	1.35E-04	2.62E-04	2.57E-04	0.00E+00	2.31E-06	7.29E-06	2.22E-07	8.24E-07	1.36E-08	0.00E+00	1.58E-07	1.59E-07	2.22E-08	9.47E-09

SQ 82																	
		Nap	Any	Ace	Fln	Phe	Ant	Fth	Pyr	BaA	Chr	BbF	BkF	BaP	Indeno	DahA	BghiP
Mass PAH (g)		1.41E-06	3.03E-07	5.23E-07	1.41E-06	3.24E-06	0.00E+00	1.75E-07	4.35E-07	1.32E-07	3.19E-07	8.16E-08	0.00E+00	1.97E-07	2.78E-08	4.59E-08	7.39E-08
Water solubility as a subcooled liquid (mg/l)		119.4	51.4	18.2	18.1	8.3	6.4	2.1	2.7	0.34	0.45	0.04	0.02	0.15	1.67	0.13	0.03
Molecular weight PAH (g/mol)	135	128	152	154	166	178	178	202	202	228	228	252	252	252	276	278	276
Molecular weight oil (g/mol)	0.1																
Mass oil (g)																	
Mole fraction		1.46E-05	2.64E-06	4.50E-06	1.12E-05	2.41E-05	0.00E+00	1.15E-06	2.85E-06	7.67E-07	1.85E-06	4.29E-07	0.00E+00	1.03E-06	1.33E-07	2.19E-07	3.54E-07
Activity coefficient	1																
Raoult concentartion (mg/l)		1.74E-03	1.36E-04	8.19E-05	2.03E-04	2.00E-04	0.00E+00	2.41E-06	7.70E-06	2.61E-07	8.34E-07	1.72E-08	0.00E+00	1.55E-07	2.23E-07	2.84E-08	1.06E-08

Seep 20																	
		Nap	Any	Ace	Fln	Phe	Ant	Fth	Pyr	BaA	Chr	BbF	BkF	BaP	Indeno	DahA	BghiP
Mass PAH (g)		5.37E-08	0.00E+00	2.58E-08	2.89E-08	2.23E-07	0.00E+00	3.01E-07	7.41E-07	1.13E-07	4.57E-07	2.12E-07	0.00E+00	2.30E-07	2.97E-08	4.68E-08	1.43E-07
Water solubility as a subcooled liquid (mg/l)		119.4	51.4	18.2	18.1	8.3	6.4	2.1	2.7	0.34	0.45	0.04	0.02	0.15	1.67	0.13	0.03
Molecular weight PAH (g/mol)	135	128	152	154	166	178	178	202	202	228	228	252	252	252	276	278	276
Molecular weight oil (g/mol)	0.1																
Mass oil (g)																	
Mole fraction		5.57E-07	0.00E+00	2.22E-07	2.31E-07	1.67E-06	0.00E+00	1.98E-06	4.87E-06	6.56E-07	2.66E-06	1.12E-06	0.00E+00	1.21E-06	1.43E-07	2.24E-07	6.88E-07
Activity coefficient	1																
Raoult concentartion (mg/l)		6.66E-05	0.00E+00	4.05E-06	4.19E-06	1.38E-05	0.00E+00	4.16E-06	1.32E-05	2.23E-07	1.20E-06	4.47E-08	0.00E+00	1.82E-07	2.38E-07	2.91E-08	2.06E-08

Table App_3: The maximum, minimum and mean value of the field and analytic data from river, springs, oil field brines and groundwater - Quaternary, Bai Hassan, Mukdadia, Kirkuk area

		Na+ mg/l	K^+ mg/l	Mg^{2+} mg/l	Ca^{2+} mg/l	Cl^- mg/l	SO_4^{2-} mg/l	HCO_3 mg/l	Sr^{2+} mg/l	$Sr^{87/86}$	$\delta^{18}O$ (‰)	δ^2H (‰)	PH	EC μs/cm	Depth (m)
River n =2	Min.	6.18	1.50	6.07	16.94	5.65	29.63	41.00	0.08	0.708171	-6.57	-34.34	7.90	352.00	
	Max.	9.24	1.88	13.88	64.13	10.13	40.64	231.00	0.54	0.708182	-5.03	-29.77	8.20	410.00	
	Mean	7.71	1.69	9.98	40.54	7.89	35.14	136.00	0.31	0.708177	-5.80	-32.06	8.05	381.00	
Springs n=14	Min.	10.62	1.38	15.40	62.90	9.61	48.91	80.00	0.58	0.707885	-5.98	-32.22	7.26	413.00	
	Max.	8411.00	55.64	2875.00	1055.00	11510.50	17269.30	650.00	22.74	0.708618	3.68	12.17	8.89	19550.00	
	Mean	4210.81	28.51	1445.20	558.95	5760.06	8659.11	365.00	11.66	0.708252	-1.15	-10.03	8.08	9981.50	
Quaternary n=2	Min.	106.50	1.77	164.80	324.30	48.44	1263.00	341.00	11.22		-4.66	-24.51	7.40	2220.00	17.00
	Max.	434.00	7.66	343.20	357.70	134.30	2691.00	376.00	14.89		-4.52	-22.19	7.40	4110.00	24.00
	Mean	270.25	4.71	254.00	341.00	91.37	1977.00	358.50	13.06		-4.59	-23.35	7.40	3165.00	20.50
Bai Hassan n=35	Min.	8.82	0.41	17.85	35.87	6.06	52.65	112.00	0.86	0.708188	-6.96	-34.73	7.11	500.00	4.00
	Max.	1131.00	17.61	439.50	665.16	425.20	3581.00	391.00	19.35	0.708237	-3.30	-18.35	7.99	6440.00	167.00
	Mean	569.91	9.01	228.68	350.52	215.63	1816.83	251.50	10.10	0.708213	-5.13	-26.54	7.55	3470.00	85.50
Mukdadia n =11	Min.	22.30	0.62	22.40	37.20	9.44	48.61	121.00	1.63	0.708163	-5.12	-28.60	7.40	436.00	97.00
	Max.	955.60	4.86	317.40	421.80	787.30	2761.00	482.00	18.65	0.708226	-3.66	-20.25	7.89	6330.00	152.00
	Mean	488.95	2.74	169.90	229.50	398.37	1404.81	301.50	10.14	0.708195	-4.39	-24.42	7.65	3383.00	124.50
Oil field brine n=2	Min.	37256.00	624.80	1346.00	4996.00	68523.20	1198.00	660.00	180.60	0.707700	0.66	-29.90	6.90	155000.00	700.00
	Max.	42576.20	1740.00	1392.00	5981.00	75768.90	1400.00	850.00	300.50	0.707989	0.70	-24.60	7.30	155300.00	
	Mean	39916.10	1182.40	1369.00	5488.50	72146.05	1299.00	755.00	240.55	0.707845	0.68	-27.25	7.10	155150.00	